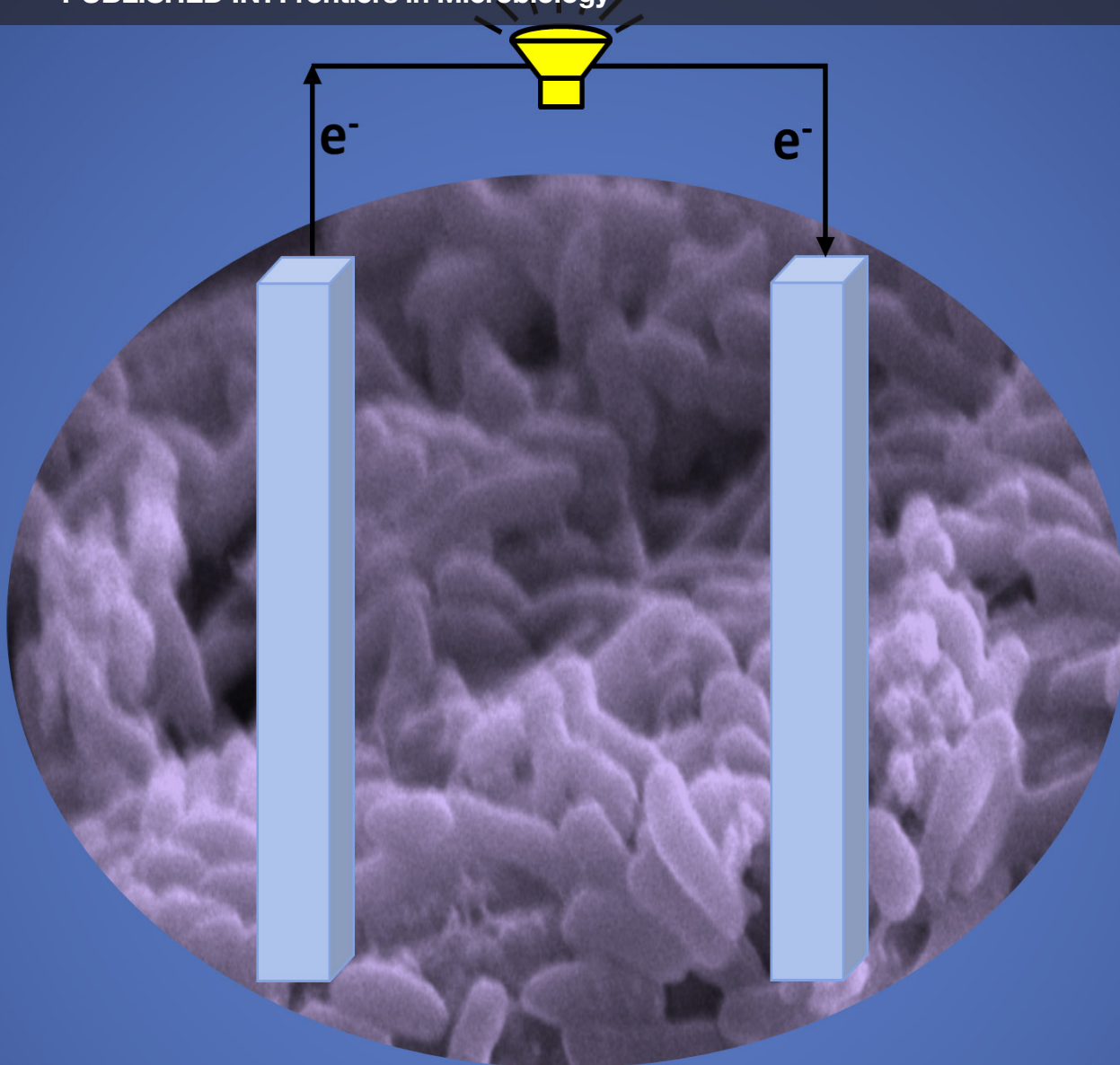# CURRENT CHALLENGES AND FUTURE PERSPECTIVES ON EMERGING BIOELECTROCHEMICAL TECHNOLOGIES

EDITED BY : Tian Zhang and Pier-Luc Tremblay
PUBLISHED IN : Frontiers in Microbiology

e⁻ e⁻

About Frontiers

Frontiers is more than just an open-access publisher of scholarly articles: it is a pioneering approach to the world of academia, radically improving the way scholarly research is managed. The grand vision of Frontiers is a world where all people have an equal opportunity to seek, share and generate knowledge. Frontiers provides immediate and permanent online open access to all its publications, but this alone is not enough to realize our grand goals.

Frontiers Journal Series

The Frontiers Journal Series is a multi-tier and interdisciplinary set of open-access, online journals, promising a paradigm shift from the current review, selection and dissemination processes in academic publishing. All Frontiers journals are driven by researchers for researchers; therefore, they constitute a service to the scholarly community. At the same time, the Frontiers Journal Series operates on a revolutionary invention, the tiered publishing system, initially addressing specific communities of scholars, and gradually climbing up to broader public understanding, thus serving the interests of the lay society, too.

Dedication to Quality

Each Frontiers article is a landmark of the highest quality, thanks to genuinely collaborative interactions between authors and review editors, who include some of the world's best academicians. Research must be certified by peers before entering a stream of knowledge that may eventually reach the public - and shape society; therefore, Frontiers only applies the most rigorous and unbiased reviews.

Frontiers revolutionizes research publishing by freely delivering the most outstanding research, evaluated with no bias from both the academic and social point of view.

By applying the most advanced information technologies, Frontiers is catapulting scholarly publishing into a new generation.

What are Frontiers Research Topics?

Frontiers Research Topics are very popular trademarks of the Frontiers Journals Series: they are collections of at least ten articles, all centered on a particular subject. With their unique mix of varied contributions from Original Research to Review Articles, Frontiers Research Topics unify the most influential researchers, the latest key findings and historical advances in a hot research area! Find out more on how to host your own Frontiers Research Topic or contribute to one as an author by contacting the Frontiers Editorial Office: **researchtopics@frontiersin.org**

CURRENT CHALLENGES AND FUTURE PERSPECTIVES ON EMERGING BIOELECTROCHEMICAL TECHNOLOGIES

Topic Editors:
Tian Zhang, Technical University of Denmark, Denmark & Wuhan University of Technology, China
Pier-Luc Tremblay, Technical University of Denmark, Denmark & Wuhan University of Technology, China
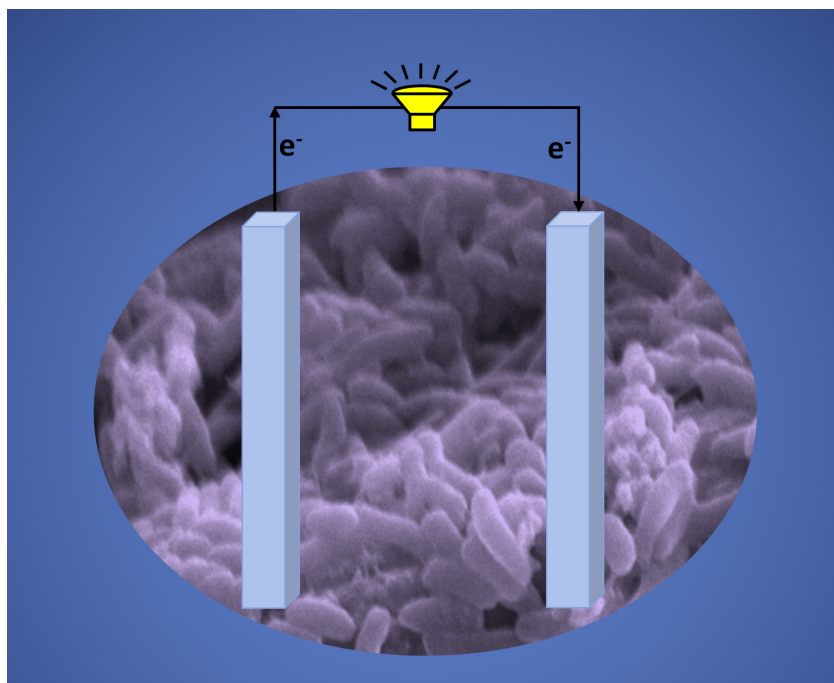
Electrodes in bioelectrochemical technologies can be used to drive bioreactions requiring an electron acceptor or an electron donor. Oxidizing bioreactions can also be coupled with reducing bioreactions in the same bioelectrochemical system.
Image by Tian Zhang

The increasing demand for energy worldwide, currently evaluated at 13 terawatts per year, has triggered a surge in research on alternative energy sources more sustainable and environmentally friendly. Bio-catalyzed electrochemical systems (BESs) are a rapidly growing biotechnology for sustainable production of bioenergy and/or value-added bioproducts using microorganisms as catalysts for bioelectrochemical reactions at the electrode surface. In the last decades, this biotechnology has been intensively studied and developed as a flexible and practical platform

for multiple applications such as electricity production, wastewater treatment, pollutants remediation, desalination and production of biogas, biofuels, or other commodities.

BESs could have a critical impact on societies in many spheres of activity and become one of the solutions to reform our petroleum-based economy. However, BESs research has so far been limited to lab scale with the notable exceptions of pilot scale microbial fuel cells for brewery and winery wastewater treatment coupled with electricity generation. In general, more knowledge has to be acquired to overcome the issues that are stymieing BESs development and commercialization. For example, it is critical to understand better microbial physiology including the mechanisms responsible for the transfer of electrons between the microbes and the electrodes to start optimizing the systems in a more rational manner. There are many BES processes and for each one of them there is a multitude of biological and electrochemical specifications to investigate and adjust such as the nature of the microbial platform, electrode materials, the reactor design, the substrate, the medium composition, and the operating conditions. The ultimate goal is to develop highly energy efficient BESs with a positive footprint on the environment while maintaining low cost and generating opportunities to create value.

BESs are complex systems developed with elements found in multiple fields of science such as microbiology, molecular biology, bioinformatics, biochemistry, electrochemistry, material science and environmental engineering. Given the high volume of research activities going on in the field of BESs today, this e-book explores the current challenges, the more recent progresses, and the future perspectives of BESs technologies. The BESs discussed here include microbial fuel cells, microbial electrolysis cells, microbial electrosynthesis cells, microbial electroremediation cells, etc.

Table of Contents

Editorial: Current Challenges and Future Perspectives on Emerging Bioelectrochemical Technologies

Tian Zhang[1,2]* and Pier-Luc Tremblay[1,2]

[1] *The Novo Nordisk Foundation Center for Biosustainability, Technical University of Denmark, Hørsholm, Denmark,* [2] *School of Chemistry, Chemical Engineering and Life Science, Wuhan University of Technology, Wuhan, China*

The Editorial on the Research Topic

Current Challenges and Future Perspectives on Emerging Bioelectrochemical Technologies

In its simplest form, bioelectrochemical systems (BESs) consist of an anode, a cathode, and a microbial catalyst (Rabaey and Rozendal, 2010). One of the attractive features of bioelectrochemical technology is that, BESs can be developed to implement anodic-based or cathodic-based bioprocesses or both at the same time. For example, pollutants can be degraded by a specialized microbial catalyst at the anode while the electrons and protons generated can be used by a biocathode to synthesize useful chemicals.

Among the notable applications of BESs, the most extensively studied is microbial fuel cell, a technology developed over the last century for the production of electrical energy from chemical substrates oxidized by a microbial catalyst at the anode (Potter, 1911; Logan and Rabaey, 2012). BESs can also be used to reduce CO_2 into methane or multicarbon chemicals including biofuels at the cathode with external electrical energy coming from renewable energy sources (Lovley and Nevin, 2013; Tremblay and Zhang). Besides greenhouse gas emissions control, one of the purposes of this application termed microbial electrosynthesis is to store electricity surplus in ready-to-use chemicals. A derived technology consists in powering a BESs reactor with solar cell for the production of chemicals thus mimicking natural photosynthesis. This approach is intensively pursued because it has the potential to have a solar-to-chemicals conversion efficiency significantly higher than traditional photosynthetic biomass-based bioprocesses (Nevin et al., 2010; Zhang, 2015). In the domain of chemicals production, BESs are also developed to electrify white biotechnologies where the substrates of the microbial catalyst are organic carbon molecules (Choi et al., 2014; Harnisch et al., 2015). In this case, BESs are employed to optimize the redox balance of production bioprocesses resulting in improved yield and profitability.

Additionally, BESs are used for environment-cleaning applications aiming for example at polishing wastewaters or at removing petroleum derivatives, heavy metals, azo dyes, and chlorinated organic compounds from contaminated sites (Logan and Rabaey, 2012; Wang et al., 2015). Employing BESs for bioremediation provides an unceasing source of electron acceptor or donor eliminating the need for costly chemical amendments. Water desalination, biosensors, H_2 production, and investigative tools to monitor biological activity are other bioelectrochemical technologies of note (Cao et al., 2009; Tremblay and Zhang).

Although BESs are versatile systems with promising features, most bioelectrochemical technologies developed until now have been restricted to lab scale. Low production rate and limited efficiency have stymied scaling up. To overcome this challenge, electroactive microbial catalysts as well as electrochemical reactor components and design must be studied in details for the development of rational optimization strategies. Furthermore, BESs are non-traditional

environments for microbes and knowledge on these systems may not be sufficient at the moment for effective optimization. This concerns particularly electron transfer mechanisms between microbes and electrodes which are central to bioelectrochemical technologies and must be well understood.

In this topic, microbe–electrode interface, electron transfer, and associated regulation mechanisms are covered with review articles and original research articles. Kracke et al. discussed in their review electron transfer in BESs performing cathodic-based bioprocesses. This article describes different electron transport hypotheses and their impact on microbial cell redox and energy levels. Kouzuma et al. focused on intracellular catabolic pathways and extracellular electron transfer (EET) in *Shewanella oneidensis*, a model bacterium for the study of EET transferring electrons to solid donors such as anode electrode. In their review, the authors elaborated on the central carbon metabolism, the electron transport chain from the cytoplasm to the final electron acceptor as well as on the involved regulation network. Dantas et al. examined EET in another important model bacterium for electron transfer to solid acceptor, *Geobacter sulfurreducens*. More specifically, the authors focused on the function and structure of multiheme c-type cytochromes in EET by discussing the considerable work done with the model periplasmic triheme c-type cytochrome PpcA. In their original research study, Alves et al. demonstrated the central role of the small tetraheme *c*-type cytochrome STC in periplasmic electron transfer during anaerobic respiration in *S. oneidensis*. Furthermore, this study showed functional redundancy between STC and the flavocytochrome *c* FccA in the electron transport chain responsible for the robustness of this pathway.

Research articles studying microbial ecosystem and physiology with bioelectrochemical tools are also presented in this topic. Ha et al. studied the impact of varying electrochemical conditions on the formation and electron transfer processes between phototrophic microbial mats and electrodes. Ishii et al. demonstrated that the Fe(II)-oxidizing bacterium *Acidithiobacillus ferrooxidans* uses electrical current as source of energy, which is a metabolism possibly involved in carbon assimilation at deep-sea vent system. Friedman et al. showed that the redox environment of a stream riparian zone can be manipulated with a poised electrode as an electron acceptor resulting in lower CH_4 emissions.

Furthermore, this topic included studies on conception and optimization of novel BES reactors for different applications. Giddings et al. analyzed the performance of a simplified microbial electrosynthesis reactor coupled with a direct power source with no separation membrane between the anode and the cathode. Rodenas Motos et al. developed a novel microbial fuel cell configuration limiting internal voltage losses in a system simultaneously generating electrical current and recovering copper. Cruz Viggi et al. proved the concept of the "oil-spill snorkel," a bioelectrochemical technology aiming at stimulating the degradation of petroleum contaminants. The "oil-spill snorkel" consists in a single electrode half-buried in sediments where it serves as electron acceptor for the biological oxidation of contaminants. The electrons then flow toward the other half of the electrode exposed in the water serving as a cathode reducing O_2.

With this topic, we presented examples of applications as well as optimization strategies developed to translate lab scale BES experiments into applicable technologies. The potential of BESs as investigative tools to study microbial physiology and ecology was also shown. Furthermore, we assembled a detailed portrait of the EET mechanisms involved in microbes–electrode interactions. BES technologies are still at an early stage of development and considerable effort must still be expanded by researchers to ensure a fruitful progression toward a bright future.

AUTHOR CONTRIBUTIONS

TZ and PT co-edited this topic and wrote this editorial.

FUNDING

REFERENCES

Cao, X., Huang, X., Liang, P., Xiao, K., Zhou, Y., Zhang, X., et al. (2009). A new method for water desalination using microbial desalination cells. *Environ. Sci. Technol.* 43, 7148–7152. doi: 10.1021/es901950j

Choi, O., Kim, T., Woo, H. M., and Um, Y. (2014). Electricity-driven metabolic shift through direct electron uptake by electroactive heterotroph *Clostridium pasteurianum*. *Sci. Rep.* 4:6961. doi: 10.1038/srep06961

Harnisch, F., Rosa, L. F. M., Kracke, F., Virdis, B., and Krömer, J. O. (2015). Electrifying white biotechnology: engineering and economic potential of electricity-driven bio-production. *ChemSusChem* 8, 758–766. doi: 10.1002/cssc.201402736

Logan, B. E., and Rabaey, K. (2012). Conversion of wastes into bioelectricity and chemicals by using microbial electrochemical technologies. *Science* 337, 686–690. doi: 10.1126/science.1217412

Lovley, D. R., and Nevin, K. P. (2013). Electrobiocommodities: powering microbial production of fuels and commodity chemicals from carbon dioxide with electricity. *Curr. Opin. Biotechnol.* 24, 385–390. doi: 10.1016/j.copbio.2013.02.012

Nevin, K. P., Woodard, T. L., Franks, A. E., Summers, Z. M., and Lovley, D. R. (2010). Microbial electrosynthesis: feeding microbes electricity to convert carbon dioxide and water to multicarbon extracellular organic compounds. *mBio* 1:e00103-10. doi: 10.1128/mBio.00103-10

Potter, M. C. (1911). Electrical effects accompanying the decomposition of organic compounds. *Proc. R. Soc. Lond. B Biol. Sci.* 84, 260–276. doi: 10.1098/rspb.1911.0073

Rabaey, K., and Rozendal, R. A. (2010). Microbial electrosynthesis—revisiting the electrical route for microbial production. *Nat. Rev. Microbiol.* 8, 706–716. doi: 10.1038/nrmicro2422

Wang, H., Luo, H., Fallgren, P. H., Jin, S., and Ren, Z. J. (2015). Bioelectrochemical system platform for sustainable environmental remediation and energy generation. *Biotechnol. Adv.* 33, 317–334. doi: 10.1016/j.biotechadv.2015.04.003

Zhang, T. (2015). More efficient together. *Science* 350, 738–739. doi: 10.1126/science.aad6452

Conflict of Interest Statement: The authors declare that the research was conducted in the absence of any commercial or financial relationships that could be construed as a potential conflict of interest.

Microbial electron transport and energy conservation – the foundation for optimizing bioelectrochemical systems

Frauke Kracke[1,2†], Igor Vassilev[1,2†] and Jens O. Krömer[1,2]*

[1] *Centre for Microbial Electrochemical Systems, The University of Queensland, Brisbane, QLD, Australia,* [2] *Advanced Water Management Centre, The University of Queensland, Brisbane, QLD, Australia*

Microbial electrochemical techniques describe a variety of emerging technologies that use electrode–bacteria interactions for biotechnology applications including the production of electricity, waste and wastewater treatment, bioremediation and the production of valuable products. Central in each application is the ability of the microbial catalyst to interact with external electron acceptors and/or donors and its metabolic properties that enable the combination of electron transport and carbon metabolism. And here also lies the key challenge. A wide range of microbes has been discovered to be able to exchange electrons with solid surfaces or mediators but only a few have been studied in depth. Especially electron transfer mechanisms from cathodes towards the microbial organism are poorly understood but are essential for many applications such as microbial electrosynthesis. We analyze the different electron transport chains that nature offers for organisms such as metal respiring bacteria and acetogens, but also standard biotechnological organisms currently used in bio-production. Special focus lies on the essential connection of redox and energy metabolism, which is often ignored when studying bioelectrochemical systems. The possibility of extracellular electron exchange at different points in each organism is discussed regarding required redox potentials and effect on cellular redox and energy levels. Key compounds such as electron carriers (e.g., cytochromes, ferredoxin, quinones, flavins) are identified and analyzed regarding their possible role in electrode–microbe interactions. This work summarizes our current knowledge on electron transport processes and uses a theoretical approach to predict the impact of different modes of transfer on the energy metabolism. As such it adds an important piece of fundamental understanding of microbial electron transport possibilities to the research community and will help to optimize and advance bioelectrochemical techniques.

Keywords: microbial electron transport, redox potential, microbial electrosynthesis, microbial fuel cell, bioelectrochemical system, bio electrochemistry, acetogenic bacteria, ATP yield

---

Abbreviations: BES, bio electrochemical system; EET, extracellular electron transport; Fd, ferredoxin; red, reduced; ox oxidized.

Introduction

The fact that some bacteria are able to transport electrons beyond their cell wall and therefore electrically interact with their environment is known for over a century (Potter, 1911). This feature can be used to develop advanced electrically enhanced bio-processes. In so called BESs the organisms interact with electrodes via the exchange of electrons, which are either supplied or removed through an external electrical circuit. The application possibilities for electrode–bacteria interactions include the production of electricity, waste and wastewater treatment, bioremediation and the production of valuable products therefore opening a wide research field (Franks, 2012; Lovley, 2012; Yang et al., 2012; Harnisch et al., 2014). Initial research mainly focused on the application of BESs for power production. In so called microbial fuel cells microbes donate electrons to electrodes and therefore generate an electrical current (Rabaey et al., 2004; Franks and Nevin, 2010; Janicek et al., 2014). Another application is presented by bioremediation of aquatic sediments and groundwater where metal-reducing microbes catalyze the transformation of organic contaminants to carbon dioxide (Williams et al., 2009; Zhang et al., 2010). Within these systems the anodic oxidation by bacteria is coupled to production of chemicals on the cathode, usually hydrogen or methane, and they are referred to as microbial electrolysis cells (Wagner et al., 2009).

In recent years another approach gets more and more attention which intends a shift in the current: the technique termed microbial electrosynthesis refers the microbial production of multi-carbon compounds in a BES under current consumption. Novel sophisticated techniques like wind turbines and photovoltaic cells enable sustainable and cheap energy production and therefore allow bringing energy consuming technologies into focus (Lovley and Nevin, 2013). Initially the term microbial electrosynthesis was used exclusively for the microbial reduction of carbon dioxide with the help of electricity (Nevin et al., 2010; Rabaey and Rozendal, 2010). But the research field was quickly widened by multiple studies that follow the same approach of optimizing microbial production by electrical enhancement from other substrates than CO_2, often referred to as electro fermentation (Kim and Kim, 1988; Emde and Schink, 1990; Shin et al., 2002; Steinbusch et al., 2009; Rabaey and Rozendal, 2010; Choi et al., 2012). Common in all studies is the aim of overcoming metabolic redox limitations by electron exchange between microbes and electrodes for increased production. In a recent metabolic modeling study, it was shown that not necessarily the degree of reduction of a product but rather the metabolic pathway that leads from the chosen substrate to the target compound decides if there is an electron surplus or demand inside the metabolic network of a cell. This was highlighted with the production of 1,4-butanediol and 2,3-butanediol from sugar. Both products have the same degree of reduction, but the different metabolic pathways employed for production will lead to different by-products and a different overall electron balance, such that in case of 2,3-butanediol a surplus of electrons needs to be balanced, while in the 1,4-butanediol

case a shortage of electron limits the theoretical yield (Kracke and Krömer, 2014). Therefore cathodic as well as anodic BES are of interest and we suggest extending the term microbial electrosynthesis to all processes that intend an electrically induced shift of carbon flow toward production of valuable chemicals.

Whether one is considering current consuming or current producing bio-processes, crucial in each application is the performance of the microbial host. The ability and especially the efficiency of the organism to exchange electrons with an electrode and connect this EET to its cellular carbon metabolism significantly influences the overall process performance. Many applications in BESs are so far restricted to lab-scale research projects as the electron transfer rates are simply too low to design a viable process scale-up (Logan and Rabaey, 2012). In order to optimize and advance bioelectrochemical techniques a more thorough understanding of possible extracellular electron exchange mechanisms in both directions is needed (Tremblay and Zhang, 2015). Especially cathodic systems and the fundamentals of electron transport towards microbes are poorly understood (Rosenbaum et al., 2011; Sydow et al., 2014). In this article we discuss the natural electron transport chains of different organisms and discuss their potential benefits and limitations if used in a BES. Special focus lies on the connection of redox and energy metabolism in each species.

Varieties of Microbial Electron Transport Chains

In microbial electron transport chains electrons are transferred from a low potential electron donor to an acceptor with more positive redox potential by redox reactions. These reactions are usually catalyzed by membrane-bound compounds that use the energy difference between donor and acceptor to establish an ion-gradient across the membrane, which in turn is used for ATP synthesis and thus converts the difference in electrical potential into chemical energy for the cell (Anraku, 1988).

In order to adapt to different environmental conditions microbes developed an enormous variety of electron transport chains (Hernandez and Newman, 2001). Important systems catalyzing these redox reactions include primary dehydrogenases that supply high energetic electrons from a donor such as NADH and usually couple electron transport to H^+ or Na^+ transport across the membrane (Anraku, 1988). Also involved in transmembrane ion-transport are membrane-localized (multi-) protein complexes such as cytochromes and terminal oxidases (reductases) that transfer electrons to a final acceptor such as oxygen, nitrate or fumarate (Hannemann et al., 2007; Vignais and Billoud, 2007; Richter et al., 2012). Most transmembrane reductases and oxidases function as ion pumps but some do not. Electron carrying co-factors such as quinones, flavines, heme, iron–sulfur clusters or copper ions also play an important role in microbial electron transport. Some of these are soluble lipophilic molecules that shuttle electrons between the relatively large enzymatic complexes inside the membrane (e.g., quinones) while others are catalytic cofactors

bound to proteins (e.g., heme groups of cytochromes; Deller et al., 2008; Dolin, 2012). There are also membrane bound complexes that use the exergonic electron bifurcation of soluble cellular redox compounds such as ferredoxin (Fd) and NADH for transmembrane ion transport and therefore establishment of a motive force across the membrane that can drive ATP synthesis (Herrmann et al., 2008; Müller et al., 2008; Schuchmann and Müller, 2012).

The achievable energy gain (Gibbs free energy, ΔG) of each electron transport chain is depending on the redox potential difference (ΔE) of all reactions between electron donor and acceptor. Some bacteria incorporate several electron transport chains, which they can use sometimes even simultaneously in order to respond to different electron acceptors and donors available in the environment (Haddock and Schairer, 1973; Anraku, 1988). Others are restricted to only one respiratory pathway (Das and Ljungdahl, 2003; Müller et al., 2008). This diversity of microbial electron transport mechanisms illustrates the complexity of the approach of bioelectrochemical techniques. In order to interfere efficiently with the redox metabolism of an organism one needs to understand the targeted site of EET and its metabolic impact.

A wide range of microbes has been discovered to be able to exchange electrons with solid surfaces (direct EET) and/or soluble mediators (indirect EET) but only a few have been studied in depth. In fact the mechanisms of electron transport that are found in different species can differ significantly from one another. Dissimilatory metal reducing bacteria are amongst the most studied being, able to "respire" insoluble metals in anaerobic environments. The model organisms *Geobacter sulfurreducens* and *Shewanella oneidensis* were studied by various research groups for decades and evidence for direct and indirect electron transfer between the organism and electrodes could be found (Bond and Lovley, 2003; Thrash and Coates, 2008; Rosenbaum et al., 2011; Ross et al., 2011). For both bacteria outer-membrane cytochromes were identified as essential compounds to enable EET (Mehta et al., 2005; Shi et al., 2007, 2009; Breuer et al., 2015). However, there are several differences in their electron transport chains, for example *Shewanella* excretes soluble electron carriers while similar compounds are missing in *Geobacter* sp. (Holmes et al., 2006; Marsili et al., 2008a). Furthermore it could be shown that the redox chains catalyzing an inward current rely on different mechanisms than current producing reactions (Dumas et al., 2008; Strycharz et al., 2008). Another group of dissimilatory metal reducing bacteria is presented by the obligate anaerobe *Thermincola*, which were also found to be capable of directly transferring electrodes to anodes (Marshall and May, 2009; Wrighton et al., 2011). Their EET mechanisms also seem to rely on cytochromes that in this case are cell-wall associated of the Gram-positive bacteria (Carlson et al., 2012). Interestingly there are also organisms such as *Clostridium ljungdahlii*, which do not have any cytochromes but were tested positive on EET (Köpke et al., 2010; Nevin et al., 2011). The exact mechanisms by which electrons are transferred between the electrode surface and the microbial metabolism still remain unclear (Patil et al., 2012; Sydow et al., 2014). Therefore we have a look at the native electron transport chains of several organisms that were studied in BESs.

An overview is given in **Table 1** and the following sections discuss the mechanisms of the presented bacteria in detail.

Specific EET in Metal Respiring Bacteria

The first microorganisms that we want to introduce and discuss belong to the group of dissimilatory metal reducing bacteria. As their name indicates, the microorganisms have the ability to interact with solid minerals, e.g., Fe(III) or Mn(IV), to obtain energy by using those minerals as electron acceptors and/or donors for their respiration process. Here a transport of electrons from a low redox potential donor to an acceptor with a higher redox potential can result in a proton gradient to drive ATP synthesis. That characteristic of breathing metals plays an important role in biogeochemical cycles and has the potential to be used in bioremediation and BES (Lovley et al., 2004; Richardson et al., 2012).
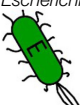
But how does the microorganisms respire insoluble metals and extract energy? This question has not been fully clarified in detail yet. In contrast to other respiration processes, where freely diffusible gas or readily soluble substances can easily enter the cell and be used as electron acceptors/donors, the major challenge for metal respiring bacteria is the interaction with the extracellular minerals, which cannot pass the cell membrane and do not have access to the periplasm nor cytoplasm. To overcome this barrier the bacteria need redox-active molecules in their outer membrane or have to excrete redox-active shuttle molecules to transfer electrons between the cellular interior and the extracellular metals (Hernandez and Newman, 2001; Hartshorne et al., 2009). There exists a great diversity of mechanisms for such electron-shuttling pathways, which is explained in more detail in the section below by describing the EET of two model organisms.

G. sulfurreducens: Branched OMCs System

The Gram-negative obligate anaerobic δ-proteobacterium *G. sulfurreducens* is used as a model organism for investigating electroactive microorganisms (Levar et al., 2012). Since its genome was sequenced it is easier to analyze the detailed molecular mechanism of EET and to construct molecular models. In its genome more than 110 genes coding for putative c-type cytochromes have been identified, which likely play an important role in the electron transport pathway of this bacterium (Methe et al., 2003). It is assumed that several multiheme c-type cytochromes enable the transport of redox equivalents between the cellular menaquinone (MQ) pool and the extracellular insoluble metals to create a proton gradient for energy conservation (Levar et al., 2012). The interaction between the cytochrome complexes in the electron transport chain is based on the redox potential of the different multiheme molecules of the cytochromes, whereby each heme has its own specific redox potential. In this way wide windows of potential ranges are created that overlap with each other and allow a bio-energetic transfer of electrons (Inoue et al., 2010; Qian et al., 2011).

Figure 1A illustrates a model of the EET mechanism with the participating proteins, which were assigned a central role. Here a diheme cytochrome c peroxidase, designated 'metal-reduction-associated cytochrome' (MacA), functions as a transmitter of

TABLE 1 | Electron transport characteristics and behavior in bioelectrochemical systems of organisms discussed in this study.

Organism	Gram staining	Key components in electron transport chain and coupling to energy conservation	Experience in BES		Important reference
			Anode	**Cathode**	
Shewanella oneidensis	−	Mtr pathway: Proton gradient created by cytochromes (c-type), soluble electron carriers and membrane bound NADH-hydrogenase; ATP via H^+-ATPase	Various studies, model organism; direct and self-mediated electron transfer	Direct use of electrons by thin biofilms for reduction of fumarate to succinate	Coursolle and Gralnick (2010), Ross et al. (2011)
Geobacter sulfurreducens	−	Branched OMCs system: Proton gradient created by cytochromes (c-, d-types), soluble electron carriers and membrane bound NADH-hydrogenase; ATP via H^+-ATPase	Various studies, model organism; generation of comparatively high current densities by direct electron transfer through biofilms	Direct use of electrons by thin biofilms for reduction of fumarate to succinate	Bond and Lovley (2003), Gregory et al. (2004)
Thermincola ferriacetica	+	Putative electron transport chain based on multiheme c-type cytochromes associated with periplasm and cell surface; ATP via H^+-ATPase	First proof of anodic current production by direct contact of a Gram-positive organism	No report	Marshall and May (2009), Parameswaran et al. (2013)
Sporomusa ovata	−	H^+ gradient via membrane-bound cytochromes (b-, c-types) and quinones; ATP via H^+-ATPase	No report	Direct use of electrons from an electrode for CO_2 reduction to acetate and 2-oxobutyrate	Nevin et al. (2010)
Moorella thermoacetica	−	H^+ gradient via membrane-bound cytochromes (b, d-type), quinones and/or Ech-complex; ATP via H^+-ATPase	No report	Direct use of electrons from an electrode for CO_2 reduction to acetate at high columbic efficiencies (>80%)	Nevin et al. (2011)
Acetobacterium woodii	+	Electron bifurcating ferredoxin reduction Na^+ gradient via membrane-bound Rnf complex (Ferredoxin:NAD^+-oxidoreductase), Membrane bound corrinoids (No cytochromes, no quinones); ATP via Na^+-ATPase	No report	*A. woodii* was shown not to be able to directly accept electrons from a cathode; however was also determined as a dominant species in a cathodic mixed culture producing acetate from CO_2 and microbial and/or electrochemically produced hydrogen	Nevin et al. (2011), Marshall et al. (2012)
Clostridium ljungdahlii	+	Electron bifurcating ferredoxin reduction H^+ gradient via membrane-bound Rnf complex (Ferredoxin:NAD^+-oxidoreductase) (No cytochromes, no quinones); ATP via H^+-ATPase	No report (however, a close relative *C. acetobutylicum* was shown to be able to oxidate acetate under current production)	Direct use of electrons from an electrode for CO_2 reduction to acetate	Logan (2009), Nevin et al. (2011)
Escherichia coli	−	H^+ gradient via membrane-bound cytochromes (a-, b-, d-, o-type) dehydrogenases, quinones, flavins (bound); ATP via H^+-ATPase	*E. coli* is able to produce current after long acclimation times without mediator, or on modified electrodes	No report	Schröder et al. (2003), Zhang et al. (2006, 2007)
Pseudomonas aeruginosa	−	H^+ gradient via membrane-bound cytochromes (a-, b-, c-, o-type), phenazines, flavines (soluble and bound), quinones and dehydrogenases; ATP via H^+-ATPase	Current production mediated by self-secreted phenazines	No report	Hernandez et al. (2004), Rabaey et al. (2005)
Corynebacterium glutamicum	+	H^+ gradient via membrane-bound cytochromes (a-, b-, c-, d-type), quinones, flavins (bound) and dehydrogenases; ATP via H^+-ATPase	No report	Increased lactic acid production with a mediator in a cathodic system	Sasaki et al. (2014)

*Colored symbols are used for microbe identification in **Figure 3**. Blue: aerobes; green: facultative anaerobes; red–yellow: obligate anaerobes.*

FIGURE 1 | Schematic image of the proposed EET of two metal respiring bacteria and their interactions with an electrode in a bioelectrochemical system. Dashed arrows indicate hypothetical electron flow and solid arrows indicate experimental proved electron flow. **(A)** Branched outer membrane cytochromes (OMCs) system of *Geobacter sulfurreducens*. Electrons can be transported between inner membrane, periplasm, outer membrane, and an electrode via a chain of cytochromes and menaquinones (MQ). Terminal OMCs can vary depending on the environmental conditions. **(B)** Unique Mtr-pathway and terminal reductases of *Shewanella oneidensis*. Quinones (Q) pass electrons to CymA or TorC, which transfer the electrons to terminal reductases or a MtrCAB complex. MtrCAB complex can interact with the electrode direct or via flavin molecules (FL).

electrons from the inner membrane to the triheme periplasmic c-type cytochrome (PpcA) in the periplasm. Following on PpcA passes the electrons to the outer membrane cytochromes, termed OMCs (e.g., OmcB, OmcC, OmcS, OmcZ), which transfer the electrons to the extracellular acceptor. The branched OMCs system is very complex and is still not fully understood. It seems that different OMCs are required to interact with different extracellular metals or electrodes (Levar et al., 2012). For example, the octaheme cytochrome OmcZ is more abundant in biofilms grown on an electrode and a deletion of *omcZ* gene leads to current decrease of more than 90% while there is no impact on the reduction of other electron acceptors as Fe(III) oxide (Nevin et al., 2009; Richter et al., 2009). The dodecaheme cytochrome OmcB and the hexaheme cytochrome OmcS are essential for Fe(III) reduction while knock-out of the *omcB* or *omcS* genes results in no or hardly any effect on current generation through biofilms grown on an anode (Kim et al., 2008; Richter et al., 2012). The proposed model reflects a greatly simplified EET mechanism. In fact the EET pathway is subjected to a complex regulatory mechanism and there exist many more homologous *omc* genes, which can replace lacking cytochromes genes in generated mutants (Kim et al., 2006; Schrott et al., 2011). For instance OmcB is important for the reduction of soluble Fe(III), but an ΔomcB mutant can express homologs such as a dodecaheme OmcC, which allows the

use of a parallel pathway to respire Fe(III) (Leang and Lovley, 2005).

In comparison to the transport of electrons to the anode, much less is known about the mechanism by which the cell takes up electrons from the cathode. Due to the reverse electron chain pathway the practicing shuttle molecules have to operate at different redox potentials. In contrast to current-generating biofilms, in current-consuming biofilms a lower expression of OMCs such as OmcZ were detected. Deletion of those associated genes, which were essential for anodic biofilms, had no impact to cathodic biofilms. In further studies it was observed, that in current-consuming biofilms a gene (GSU3274) encoding a putative monoheme c-type cytochrome was strongly expressed. Mutants lacking this gene lost their ability to take up electrons from a cathode, but did not show differences in EET to an anode. So it seems that GSU3274 plays a significant role in the EET from a cathode (Rosenbaum et al., 2011; Strycharz et al., 2011).

Geobacter sulfurreducens shows best EET performance as a biofilm grown on the electrode based on direct electron transfer. This bacterium possesses excellent biofilm formation properties and the thickness of the biofilm is linked with the amount of generated current in a linear correlation up to a certain thickness limit (Reguera et al., 2006). The transport of electrons in a multilayer biofilm to an anode can be achieved

by two combined mechanisms. One transfer way is based on secretion of non-diffusing 'mediators' (e.g., cytochromes such as OmcZ) into the biofilm matrix, which can act as electron shuttles (Richter et al., 2009). The second way depends on 'nano-wires,' which are electrically conductive appendages that enable physical connection between cells and/or cells and surface of the electrode (Reguera et al., 2006). The mechanism of the EET in such nano-wires has not been clarified yet. One model proposes that the nano-wires are pili with a metallic-like conductivity, which is based on aromatic amino acid residues within the appendages, which enable electron delocalization due to π-stacking (Malvankar et al., 2011, 2015). Another theory describes a 'superexchange' model, in which the electrons are 'hopping' along a chain of redox active proteins to the final electron acceptor (Malvankar et al., 2012; Strycharz-Glaven and Tender, 2012).

In comparison to anodic-biofilms, it was reported, that cathodic-biofilms are less-developed and much thinner (Gregory et al., 2004; Strycharz et al., 2008). The reason might be limiting redox surplus under non-autotrophic anaerobic growth conditions, which is enhanced by cathodic electron input as suggested by a recent *in silico* study (Kracke and Krömer, 2014). However, this observation needs to be studied in depth and be validated experimentally for a better understanding.

S. oneidensis: Characteristic Mtr-Pathway

The second electroactive model organism that we want to introduce and discuss its characteristic EET mechanism is the Gram-negative facultative anaerobic bacterium *S. oneidensis*. The interesting characteristic of *S. oneidensis* is its ability to utilize a great variety of inorganic and organic compounds as final electron acceptor in the absence of oxygen. As in the case for *G. sulfurreducens* that property is based on interaction of a large number of multiheme cytochromes. The sequenced genome of *S. oneidensis* shows 42 putative cytochromes, of which 80% are located in the outer membrane (Heidelberg et al., 2002; Lower et al., 2005). The first step of the electron transfer through the cell membrane is the oxidation of small electron carriers (quinols), which enable the transport of electrons between NADH-dehydrogenase and cytochromes in the inner membrane to create a proton gradient for energy conservation in form of ATP. That oxidation reaction can be catalyzed by the tetraheme cytochromes TorC and CymA, whose sequence is very similar and both are attached to the inner membrane by a single α-helix. The next link in the electron transfer chain of TorC is a periplasmic reductase TorA, which can utilize the outer membrane permeable trimethylamine *N*-oxide compound as terminal electron acceptor and reduces it to trimethoxyamphetamine (Dos Santos et al., 1998). In comparison to TorC, CymA can interact with different redox partners in the periplasm and as a consequence outer membrane-crossing molecules like sulfite can be reduced by the octaheme redox partner SirA, (Shirodkar et al., 2011) nitrite by pentaheme cytochrome NrfA, (Gao et al., 2009) nitrate by NapAB reductase (Simpson et al., 2010) and fumarate by FccA and IfcA reductase (Maier et al., 2003). Furthermore an octaheme cytochrome OTR was detected and showed *in vitro* capability of the reduction of a range of N and S oxides and oxyanions, but *in vivo* the function of OTR has not been confirmed yet (Atkinson et al., 2007).

Additionally as a metal respiring bacterium like *G. sulfurreducens*, *S. oneidensis* is able to use extracellular terminal electron acceptors, e.g., electrodes, Fe(III) and Mn(IV) (see **Figure 1B**). To overcome the outer membrane barrier the bacterium possesses a Mtr-pathway. Homologous genes for that pathway were also found in other dissimilatory metal reducing and oxidizing bacteria (Shi et al., 2012). However, *S. oneidensis* Mtr-pathway is one of the best investigated EET chains. It has been suggested that a decaheme cytochrome MtrA takes up electrons from CymA via an electron transport chain and passes them on to an extracellular decaheme cytochrome MtrC, which transfers the redox equivalents to final exogenous electron acceptors (Myers and Myers, 2000; Coursolle and Gralnick, 2010). Here MtrA, MtrC and a third element, MtrB form a complex, MtrCAB. MtrB is a porin molecule in the outer membrane and serves to organize and stabilize MtrA and MtrC to enable electron transfer. Besides MtrC a second decaheme cytochrome, OmcA was detected anchored as a lipoprotein in the outer membrane that was able to transfer electrons to exogenous electron acceptors as well (White et al., 2013; Breuer et al., 2015). In addition to the *mtrCAB* genes the genome of *S. oneidensis* encloses homologs like *mtrFDE*. The homologous cytochromes can support the EET or can partly take over the activity of the MtrCAB complex depending on the electron acceptor and the growth conditions (Coursolle and Gralnick, 2010). Likewise, the DmsABEF complex is based on homologs. Here the porin cytochrome complex DmsEF transfer the electrons to the DmsAB complex, which is then able to reduce DMSO to DMS (Gralnick et al., 2006). The periplasmic tetraheme cytochrome STC has to be mention as well, which seems to support the transfer of electrons between inner membrane and outer membrane, however, the exact mechanism is unclear (Fonseca et al., 2013). In contrast to EET to an anode, the information about taking up electrons from a cathode is limited. The interacting compounds in the cathodic process were not established yet. It was suggested due to *in vivo* studies, where electrons were provided from a graphite electrode to reduce fumarate, that an electron uptake is possible through a reverse Mtr-pathway (Ross et al., 2011).

In contrast to *G. sulfurreducens*, *S. oneidensis* shows not only the ability of direct electron transfer, but can also perform indirect electron transfer due to excretion of redox active mediators. Direct electron transfer is based on physical connection with the electrode by forming a biofilm on the surface (Marsili et al., 2008a,b) and through extensions in form of nano-wires. While *Geobacter* nano-wires are assumed to be type IV pili, for *S. oneidensis* nano-wires it was shown, that their structure is similar to outer membrane vesicles and those nano-wires can be seen as extensions of the outer membrane and periplasm that include the multiheme cytochromes responsible for EET (Pirbadian et al., 2014). In case of indirect electron transfer, *S. oneidensis* secretes flavin molecules (FL) that act as small diffusible shuttle molecules to transfer electrons between electrode and OMCs (Marsili et al., 2008a) or as bounded cofactors for OMCs (Okamoto et al., 2013). *G. sulfurreducens* is

also able to produce FL, but here the flavins are preferentially bound to the OMCs and are not mobile like free shuttle units (Okamoto et al., 2014).

Carbon Respiration of Acetogenic Bacteria

Acetogenic bacteria, short acetogens, are anaerobic organisms that are able to assimilate CO_2 or CO via the Wood–Ljungdahl pathway, also called carbonate-respiration or acetyl–CoA pathway. This autotrophic pathway offers the possibility to develop biotechnological processes that combine the usage of cheap ubiquitous substrates (i.e., syngas) with greenhouse gas reduction and therefore makes acetogens attractive hosts for biotechnology (Köpke et al., 2010; Tracy et al., 2012). This feature put the bacteria into focus of the research community trying to establish an artificial 'photo'synthesis process by using CO_2 and electrons from an electrode (Nevin et al., 2010). Acetogens are also able to utilize a great variety of heterotrophic molecules such as sugars, glycerol, and cellulose, which broadens the spectrum of possible substrates to waste streams from biodiesel industry (e.g., glycerol) or dairy industry (e.g., whey) and many more (Tracy et al., 2012). The main product is usually acetate (hence the name) but acetogens also bear the feature to naturally produce a broad spectrum of other chemicals, which are of industrial use either directly or as precursors such as ethanol, butanol, 2,3-butanediol or butyrate (Tracy et al., 2012). The mayor intermediate from carbon fixation via Wood–Ljungdahl pathway is acetyl–CoA and is linked to other metabolic pathways such as Embden–Meyerhof–Parnas pathway, therefore offering a great metabolic diversity for metabolic engineering of other production pathways.

In the Wood–Ljungdahl pathway two CO_2 molecules are merged to form one molecule Acetyl-Coenzyme-A, which is either converted to acetate or assimilated in biomass. The overall conversion of CO_2 to acetate uses one ATP (in the step of formyltetrahydrofolate synthetase) and creates one ATP by acetate kinase reaction. Therefore no net energy gain can be achieved via substrate-level phosphorylation. Since acetogens are able to grow autotrophically, the pathway must be coupled to a chemiosmotic mechanism that provides additional energy. By calculating the Gibbs free energies of each reaction in the Wood–Ljungdahl pathway a net energy benefit of about – 95 kJ/mol can be determined (Diekert and Wohlfarth, 1994). This energy could support the synthesis of 1–2 mol ATP via chemiosmosis as anaerobic bacteria require –60 to –80 kJ of free energy for the synthesis of 1 mol of ATP (Das and Ljungdahl, 2003). In recent years experimental evidence for membrane driven ATP synthesis in acetogens could be found, however, the sites and mechanisms of energy conservation differ between organisms. Over 100 different species of acetogens have been identified and despite their common feature of CO_2 assimilation via the Wood–Ljungdahl pathway they are very diverse in terms of metabolism, phylogenetics, or preferred habitat (Drake et al., 2008). The best-studied organisms belong to the genera *Acetobacterium* and *Clostridium* and include a few species with fully available genome sequences (genome published: *Moorella thermoacetica*, *Clostridium ljungdahlii*, *Clostridium carboxidivorans*, *Eubacterium limosum*; under preparation:

Acetobacterium woodii, Clostridium aceticum). Genetic and genomic tools are under intense development and promise fast advancing metabolic engineering platforms for acetogens (Lütke-Eversloh and Bahl, 2011; Lee et al., 2012; Schiel-Bengelsdorf and Dürre, 2012; Banerjee et al., 2014).

M. thermoacetica: Cytochromes or Ech-Complex?

From an energetic point of view and in regards to electron-transport properties acetogens are often divided in two groups: Na^+-gradient and H^+-gradient dependent species. *M. thermoacetica* (formerly *Clostridium thermoaceticum*) an example for the latter group was the model organism for HG Wood and LG Ljungdahl for their studies of the acetyl–CoA pathway. They identified several membrane-integrated electron carriers MQ MK-7, a flavoprotein and two b-type cytochromes that are believed to play major parts in creating a proton gradient over the membrane (Das and Ljungdahl, 2003). Later such a proton motive force that could drive ATP synthesis in *M. thermoacetica* was measured, however, which components exactly transfer protons across the membrane remains unknown (Ragsdale and Pierce, 2008). Genome studies of the organism revealed also membrane-bound components such as hydrogenases and NADH-dehydrogenase, which are known to transfer protons across the membrane in other organisms. Therefore a membrane integrated electron transport chain via these complexes with H_2 as electron donor and methylene-THF as electron acceptor is proposed (Müller and Frerichs, 2013). However, so far no experimental data supports this hypothesis. Recent studies also deliver evidence for electron-bifurcating enzymes that play important roles in electron transfer of autotrophic and heterotrophic pathways of *M. thermoacetica* (Huang et al., 2012). The soluble complex HydABC oxidizes hydrogen with simultaneous reduction of Fd and NAD^+ (Wang et al., 2013). Additionally a second soluble transhydrogenase (NfnAB) catalyzes the electron bifurcation from reduced Fd and NADH to $NADP^+$. Furthermore the genome of *M. thermoacetica* codes for a membrane-bound energy converting hydrogenase, called Ech-complex. For the methanogenic archaea *Methanosarcina mazei* the Ech-complex is responsible for establishment of a proton gradient across the membrane, which leads to the theory that could also be the case in acetogens (Welte et al., 2010; Schuchmann and Müller, 2014). This complex uses the excess energy that is freed from electron transfer from reduced Fd to H^+ to transport ions across the membrane. A very recent report states that electron stoichiometry is only balanced with involvement of the Ech-complex in energy conservation while the membrane-bound dehydrogenases and cytochromes play no major part (Schuchmann and Müller, 2014). As this hypothesis also lacks distinct experimental validation we included both theories in our summary of possible electron transport mechanisms of *M. thermoacetica* (**Figure 2A**).

A. woodii and *C. ljungdahlii*: Electron Transport without Cytochromes?

Nevin et al. (2010) reported that the electrons needed for CO_2 fixation via Wood–Ljungdahl pathway could be provided

FIGURE 2 | Schematic image of acetogenic electron transport chains and possible interactions with an electrode in a bioelectrochemical system. Dashed arrows indicate hypothetical electron and proton flow. **(A)** Electron transport mechanisms in *Moorella thermoacetica* via membrane-bound cytochromes and hydrogenases, MQ, soluble electron-bifurcating complexes (Hyd and Nfn) and proton pumping Ech-complex*; **(B)** Electron transport of *Clostridium ljungdahlii* (H^+) and *Acetobacterium woodii* (Na^+) based on membrane-bound Rnf-complex and soluble electron-bifurcating complexes (*Nfn-complex is not found in *A. woodii*). ? represents hypothetical cell-wall associated proteins that could facilitate electron transfer.

directly by an electrode, a breakthrough work in the field of bioelectrochemical techniques (Nevin et al., 2010). The acetogen *Sporomosa ovata*, a close relative to *M. thermoacetica* was able to directly accept electrons from a cathode and convert carbon dioxide to acetate and 2-oxobutyrate. Following studies showed similar abilities of other acetogens of the *Sporomosa* and *Clostridium* genera (Nevin et al., 2011). The acetogen *A. woodii*, however, was found unable to consume current and showed different behavior compared to other acetogens in Nevins experiments. *A. woodii* is an example strain for Na^+-dependent acetogens that typically lack cytochromes. It could be shown that the conversion of CO_2 to acetate via Wood–Ljungdahl pathway is coupled to the generation of a sodium gradient across the cytoplasmic membrane (Müller, 2003; Fast and Papoutsakis, 2012). Since *A. woodii* does not contain cytochromes or quinones energy conservation must be secured by a different electron transport system. In 2008 evidence for a novel membrane-bound Fd:NAD^+ oxidoreductase (Rnf complex) was reported that seems to be responsible for transmembrane Na^+ transport (Müller et al., 2008). In this complex the electrons from reduced Fd are transferred to NAD^+ to form NADH. Since the redox potential of Fd ($E^{0'}_{Fd} = -500$ to -420 mV) is more negative than that of the

NAD^+/NADH couple ($E^{0'}_{NADH} = -320$ mV), the energy surplus (equivalent to -20 to -35 kJ/mol, three to four times more than released by the Ech-complex) is available for transmembrane ion transport (Biegel et al., 2011). This sodium gradient is harvested by the Na^+-dependent F_1F_0ATP synthase of *A. woodii*. It was suggested that some steps of the Wood–Ljungdahl pathway also add to the transmembrane ion gradient. The reduction of methylene-H_4F to methyl-H_4F was discussed as a likely site since the reaction is exergonic and coupled to a corrinoid iron sulfur protein (Ragsdale and Pierce, 2008). But recent studies could identify the Rnf complex as the only membrane-bound electron transfer system and rather suggest a Fd reduction by the methylene-THF reductase (Poehlein et al., 2012).

Interestingly a similar Rnf complex was detected in *C. ljungdahlii* even though its membrane gradient is proton based, which would put the organism into the H^+-acetogen-group together with *M. thermoacetica*. However, *C. ljungdahlii* does not contain any cytochromes and therefore it seems more reasonable to categorize anaerobic homoacetogenic organisms into Ech- and Rnf-containing groups with subgroups of Na^+- and H^+- dependent species (Köpke et al., 2010; Schuchmann and Müller, 2014). It could be shown that the Rnf complex

is an electron bifurcating $Fd:NAD^+$ oxidoreductase and is essential for developing a proton gradient over the membrane under autotrophic as well as heterotrophic growth conditions (Tremblay et al., 2013). With fructose as substrate and electron donor Rnf-deficient strains were growth limited with significantly reduced ATP yields as a result of disruptions in the membrane gradient development. Autotrophic growth without Rnf complex was completely inhibited, indicating the Rnf-complex being a major if not the sole electron transport mechanism linked to energy conservation. The soluble electron bifurcating complexes HydABC and NfnAB are also found in *C. ljungdahlii* while *A. woodii* is believed to only use HydABC (Schuchmann and Müller, 2014). The proposed electron transport mechanisms for both organisms are shown in **Figure 2B**.

Other Respiratory Pathways

In the section above we introduced typical electroactive microorganisms, which were used in BES. But what about other model and/or industrial microorganisms like *Escherichia coli* and *Corynebacterium glutamicum* or pathogenic microorganisms like *Pseudomonas aeruginosa*? Can we influence/manipulate their redox and energy metabolism? In order to answer this question, it is necessary to understand their respiratory pathways.

E. coli: Model Organism with Respiratory Flexibility

The respiratory system of *E. coli* is very well known and in many studies the bacterium is used as a model for investigation of energetics and regulation of respiration. The respiratory chains show a great diversity and variability enclosing 15 primary dehydrogenases to oxidize electron donors and ten terminal reductases (or oxidases) to reduce electron acceptors (including isoenzymes; Berlyn, 1998). Those primary dehydrogenases and terminal reductases are linked by three quinones: ubiquinone ($E^{0\prime} = +110$ mV), demethyl MQ ($E^{0\prime} = +40$ mV) and MQ ($E^{0\prime} = -80$ mV). Depending on the enzymes various quantities of energy can be conserved due to the build-up of a proton gradient through proton pumps, or by arranging catalytic sites in a certain way to release the protons on opposite sides of the membrane to create a charge separation. The H^+/e^- ratios vary from 0 to 4 H^+/e^- (Unden and Bongaerts, 1997). Under aerobic conditions *E. coli* can conserve most energy by using quinol oxidases ($E^{0\prime} = +820$ mV) to reduce O_2 to H_2O. Here O_2 represses the terminal reductases of anaerobic respiration. However, in the absence of O_2, energy can be generated by nitrate reductases ($E^{0\prime} = +420$ mV), nitrite reductase ($E^{0\prime} = +360$ mV), DMSO reductase ($E^{0\prime} = +160$ mV), TMAO reductase ($E^{0\prime} = +130$ mV) or fumarate reductase ($E^{0\prime} = +30$ mV) with nitrate delivering the most energy and fumarate the least energy (Inglewod, 1983; Unden and Bongaerts, 1997; Berlyn, 1998). So depending on which level or in which step the electron chain is targeted or manipulated, the metabolism will gain more or less energy.

Furthermore it was demonstrated that *E. coli*, evolved under electrochemical tension in a microbial fuel cell, can generate current by using the electrode as an electron sink. It was proposed that the evolved cells possess the ability to excrete hydroquinone derivatives through a highly permeable outer membrane, which

act as mediators to transport the electrons between cell and electrode (Qiao et al., 2008; Qian et al., 2011). Another approach to obtain *E. coli* cells that show electro activity is via metabolic engineering, which is discussed in Section "Key Compounds in Different Electron Transport Chains."

P. aeruginosa: Secretion of Redox Carriers

Another interesting microorganism is the Gram-negative aerobic bacterium *P. aeruginosa*. It is an opportunistic pathogen, which can live in various environments due its ability to catabolize a large number of substances (Baltch and Smith, 1994). Additionally the bacterium is a good biofilm-builder and has branched respiratory chains to use oxygen as an electron acceptor, involving five oxidases (bo_3 oxidase, aa_3 oxidase, cbb_3 oxidase 1, cbb_3 oxidase 2, and cyanide-insensitive oxidase), which are adapted to the varying availability of oxygen in the different biofilm stages due to biofilm thickness (Jo et al., 2014). Preferentially *P. aeruginosa* obtains its energy from aerobic respiration; however, under anaerobic conditions the bacterium can also survive in presence of nitrate or nitrite by using reductases to reduce the N-molecules (Hassett et al., 2002).

When *P. aeruginosa* is cultivated in a microbial fuel cell, the bacterium shows an interesting behavior. Instead of oxygen, nitrate or nitrite *P. aeruginosa* can use the anode as an electron sink to generate energy for an active growth (Rabaey et al., 2005).The anode stimulates the production of phenazine derivatives, e.g., phenazine-1-carboxylic acid ($E^{0\prime} = -275$ mV), phenazine-1-carboxamide ($E^{0\prime} = -150$ mV) and procyanin ($E^{0\prime} = -32$ mV). The secreted phenazine derivatives operate as soluble mediators, which significantly enhance the electron transfer between electrode and cells, resulting in an increased current generation. In addition the diffusible phenazine derivatives enable the use of the electrode as an electron sink for cells in thick multilayer biofilms (Rabaey et al., 2005; Yang et al., 2012). Another attractive phenomenon; that in a mixed culture the secreted mediators can be use not only by *P. aeruginosa* itself, but also by other microorganism, which generally are not able to produce redox active mediators (Boon et al., 2008).

C. glutamicum: Oxygen Dependency

The third bacterium, *C. glutamicum*, is an important Gram-positive industrial microorganism, which has been widely used as a microbial cell factory for the production of various amino acids, nucleic acids and other chemicals in food, pharmaceutical, cosmetics and chemical industries (Tatsumi and Inui, 2012). *C. glutamicum* can utilize various carbon sources for energy conversion and oxygen as the preferable electron acceptor by using three oxidases. The bc_1 oxidase can take up electrons from menaquinol and pass the electrons to the aa_3 oxidase by forming a supercomplex that has a low oxygen affinity, whereas the third oxidase, a bd oxidase, has a high affinity to oxygen (Bott and Niebisch, 2003). The bacterium can also survive under anaerobic conditions in the presence of nitrate. However, the growth is very limited, because the bacterium has a nitrate reductase, but lacks enzymes to degrade the toxic product of the nitrate reductase (nitrite; Nishimura et al., 2007).

Manipulating the redox metabolism by cultivating *C. glutamicum* in a BES can result in higher yields of the target product (Sasaki et al., 2014). Experiments demonstrated that the bacterium grown under a cathodic potential ($E^{0'}$ = –600 mV) using glucose as the carbon source showed a decreased growth rate and an increased lactate yield. Here the anthraquinone 2,6-disulfonate was added to the medium as an artificial mediator to shuttle electrons between cathode and cells. The mechanisms, how the redox metabolism is influenced by the artificial mediator is still unclear (Sasaki et al., 2014).

Making the Connection: Microbe–Electrode Interaction

The previous chapter demonstrates the impressive diversity and complexity of microbial solutions for cellular electron transport. Similar to the ability to interact with many different electron donors and acceptors in the environment one can assume that microbes are also able to exchange electrons with electrodes via different cellular components and mechanisms. In order to achieve successful EET the specific characteristics of the electron transport chains of the target organism should be considered. While it is questionable if there are groups or microbes that are better adapted for EET than others it is for certain that a bio electrochemical approach is challenged by different conditions depending on the catalytic host. Organisms that feature outer membrane redox-components might be able to perform direct electron transfer with electrodes while soluble intracellular complexes such as the electron bi-furcating Nfn and Hyd complexes of acetogens are most likely only targetable via soluble mediators. For each organism the specific redox-window of its electron transport chain(s) might dictate required potentials for use in BES. The following two sections discuss key components in electron transport chains of the presented organisms and the possible metabolic impact if EET at different sites can be achieved.

Key Compounds in Different Electron Transport Chains

With **Figure 3** we created an overview of important redox-reactions that are catalyzed by the presented organisms. Actual environmental conditions in living cells differ from the standard biochemical conditions (25°C, 1 atm, pH = 7), which might influence the actual redox potentials of each couple. The potential of the proton hydrogen couple for example is −414 mV under standard conditions. In acetogenic environments, however, this potential lies closer to –350 mV as the partial hydrogen pressure is around ∼200 Pa (Müller and Frerichs, 2013). Many intracellular redox-carriers also show different redox potential than the corresponding pure compounds. The standard redox potential of Fds with one or more iron–sulfur clusters for example lies around –400 mV (Buckel and Thauer, 2013). Under physiological conditions in acetogens, however, Fds are usually >90% reduced and therefore reported to be able to catalyze reducing reactions at redox potentials as low as –500 mV (Buckel and Thauer, 2013; Hess et al., 2013). A similar effect shifts the true redox

potential of the NAD^+/NADH couple to around –280 mV as the majority of molecules (>90%) are oxidized even though the $E^{0'}$ under standard conditions is –320 mV. Very close to that of $NADP^+$/NADPH (–324 mV), which in turn is shifted to –360 mV due to the intracellular ratio of $NADP^+$/NADPH being 1/40 (Buckel and Thauer, 2013). In these cases we indicated a redox-area rather than one known midpoint potential to illustrate the potential range at which these reactions might occur inside the organisms. We allocated a fixed standard redox potential (dashed lines) or potential range for each reaction depending on availability in the literature. However the reader might want to keep in mind that environmental conditions such as pH, redox potential of the solution and specific concentrations can result in a further redox potential shift. The ion couple Fe^{3+}/Fe^{2+} as an inorganic electron acceptor/donor is a good example for how the redox potential can be influenced by environmental conditions. The midpoint potential is about +770 mV at a low pH and in the absence of precipitation. However, depending on pH, concentration and in which form iron is available the midpoint potential can vary strongly (Straub et al., 2001). For example the midpoint potential of Fe_3O_4/Fe(II) is significantly lower (–314 mV), because magnetite is a less soluble mineral. For the organic chelate complex Fe(III)-citrate/Fe(II)-citrate the solubility is higher and, respectively, the midpoint potential (+372 mV; Thamdrup, 2000; Straub et al., 2001).

Some of the listed cellular redox compounds have been shown to play a major part in electron transfer between organisms and electrodes and therefore others might as well. As discussed above direct EET in *Geobacter* and *Shewanella* can be achieved via a network of cytochromes with different midpoint potentials [e.g., PpcA: –170 mV (Lloyd et al., 2003), OmcZ: –180 mV (Inoue et al., 2010), OmcS: −212 mV (Qian et al., 2011), CymA: −200 mV, MtrA: −100 mV, MtrC: −138 mV (Firer-Sherwood et al., 2008)]. However, for a better characterization and a functional understanding of the cytochromes their wide potential windows should be considered, because the cytochromes are complex molecules not showing narrow midpoint potentials but more wide ranges of potentials suggested to be due to the multiheme molecules in the cytochromes. Each heme has its own specific redox potential and affects the potential of the neighbor hemes creating a specific wide window of potential ranges for the overall molecule (Morgado et al., 2010; Breuer et al., 2015). For example the potential windows of OmcZ, OmcS, CymA, and MtrC are from –420 to –60 mV (Inoue et al., 2010), –360 to –40 mV (Qian et al., 2011), –0.350 to –0.080 mV and –0.280 to –0 mV (Firer-Sherwood et al., 2008), respectively. It is assumed that the wide windows allow an overlapping of the redox potentials of the cytochromes in an electron transport chain and make a thermodynamic downhill process of electron transport along the chain possible. Furthermore these wide potential ranges allow the interaction with a broad spectrum of external electron acceptors and donors (Firer-Sherwood et al., 2008; Inoue et al., 2010; Breuer et al., 2015). However, the potential windows can vary depending on the environmental conditions. For the cytochromes of *S. oneidensis* it was shown that the potential windows are shifted as a function of pH. It
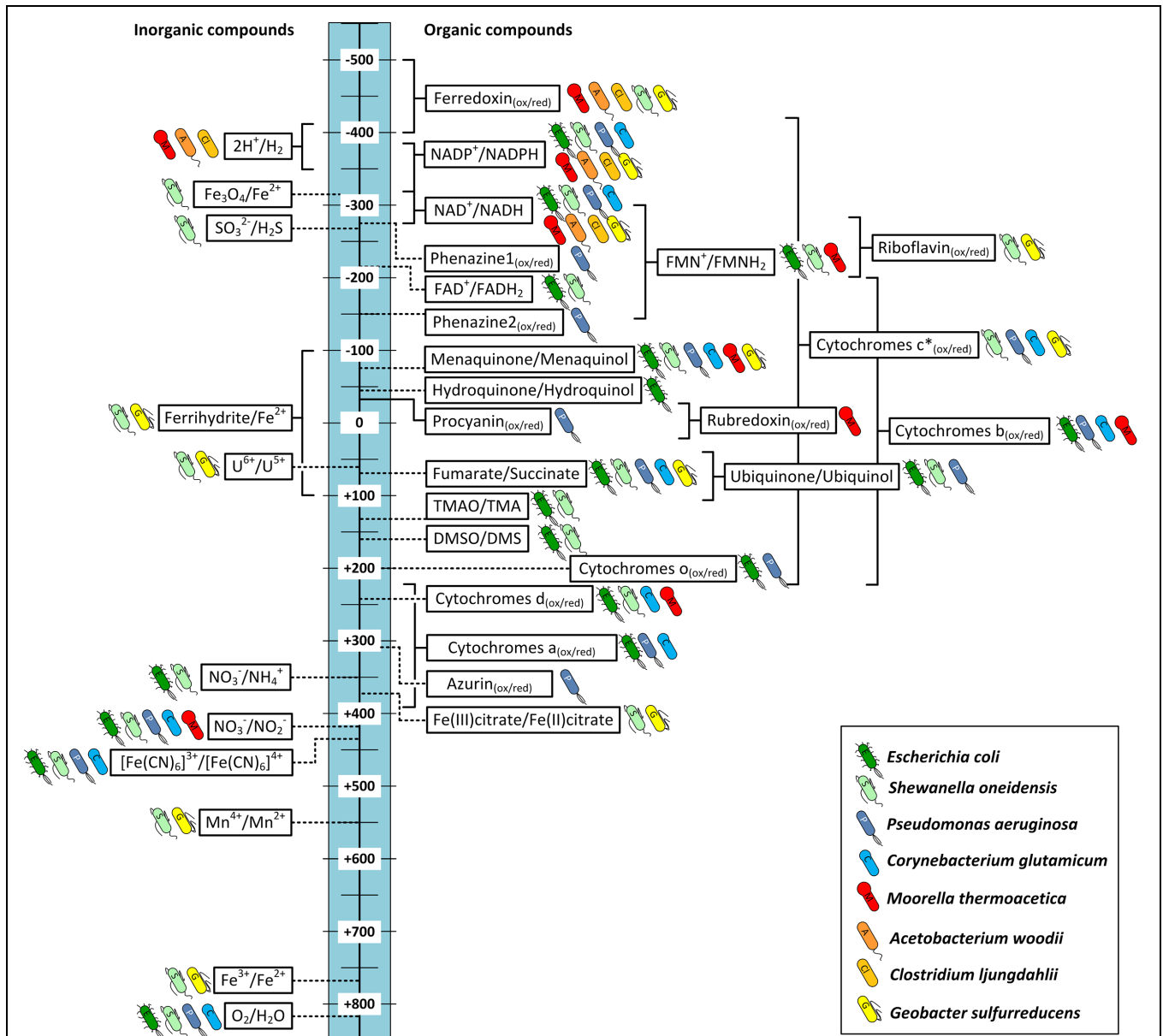
FIGURE 3 | Redox potentials of important redox reactions in electron transport chains catalyzed by the bacteria discussed in this study. Standard redox potential ($E^{0\prime}$ [mV, 25°C, pH = 7]) are indicated by dashed lines. If physiological or environmental conditions are known to shift the potential from the $E^{0\prime}$, redox windows are indicated (solid lines). The bacterial symbol behind each reaction shows the organisms that are known to catalyze the reaction naturally. Blue: aerobes; green: facultative anaerobes; red–yellow: obligate anaerobes; Phenazine1 = Phenazine-1-carboxylic acid; Phenazine2 = Phenazine-1-carboxamide. *c-type cytochromes can cover a broad range of redox potentials as indicated. Not all bacteria mentioned will cover the whole range. For detailed discussion refer to main text.

was observed that under higher pH conditions in most cases the redox potentials are shifted to more negative values (Firer-Sherwood et al., 2008). In **Figure 3** we allocated a broad potential range to c-type cytochromes based on the discussed literature and indicated all organisms that contain c-type cytochromes. However, this does not necessarily mean that all these bacteria are able to catalyze reactions in the indicated redox potential window. *G. sulfurreducens*' genome encodes for around 110 different c-type cytochromes (Methe et al., 2003), *S. oneidensis* for

42 (Heidelberg et al., 2002), and *P. aeruginosa* for 27 (Bertini et al., 2006), while *C. glutamicum* genome only encodes for a single c-type cytochrome (Bertini et al., 2006). Therefore the flexibility of the metal reducing organisms to adapt to different electron acceptors and donors is much higher.

In addition to the described cytochromes of *Geobacter* and *Shewanella* comparable complexes of other organisms might be able to perform EET via similar mechanisms. The membrane of the Gram-positive acetogen *M. thermoacetica* for example

contains b-type cytochromes that could be a possible site of interaction between electrode and organism (Pierce et al., 2008). In fact it could be shown that *M. thermoacetica* together with other cytochrome containing acetogens is able to directly use electrons from a cathode for reduction of CO_2 (Nevin et al., 2011). Interestingly the same study reports *C. ljungdahlii* is also capable of direct EET even though it is not known to be able to produce any cytochromes (see **Figures 2B** and **3**; Köpke et al., 2010). Could this electron transport rely on other membrane-bound enzymes, or be mediated by an unknown soluble molecule, or enzyme secreted by the organism? Since there is no evidence of such the actual mechanism of EET in *C. ljungdahlii* remains pure speculation to date. However, for other microbes self-excreted redox mediators are indeed an important way to exchange electrons with electrodes in both ways. *P. aeruginosa* for example produces several compounds of different redox potentials such as azurin ($E^{0\prime} = +310$ mV), procyanin ($E^{0\prime} = -31$ mV), phenazine-1-carbox amide ($E^{0\prime} = -150$ mV) and phenazine-1-carboxylic acid ($E^{0\prime} = -275$ mV). These enable the organism to adapt to different electron acceptors in the environment, including solid state electrodes (Vijgenboom et al., 1997; Rabaey et al., 2005). A very recent study of Yang et al. (2015) demonstrates that the concentration of such endogenous redox compounds can mediate electron flow in both directions and that the concentration directly correlates with achievable current densities. By heterologous expression of a synthetic flavin biosynthesis pathway from *Bacillus subtilis* in *S. oneidensis* the secreted flavin concentration could be increased ∼26 times, which increased power output as well as inward current of the organism in BES (Yang et al., 2015). Another possibility could be the secretion of whole enzymes that facilitate electron flow from the electrode surface toward organisms. In a very recent study Deutzmann et al. (2015) were the first to report evidence of this mechanism of direct EET by cell-derived free enzymes in a cathodic BES using methanogens. They could show that small surface associated enzymes such as hydrogenases and fumarate reductase were released from *Methanococcus maripaludis* cells and accumulated at the cathode surface where they catalyzed the formation of small mediating molecules such as hydrogen or formate which in turn were immediately taken up by the cells.

The location of the target site of electron transfer decides if an organism might be able to perform direct EET or if a (endogenous or exogenous) mediator is required to transport the charge across the cellular membrane. Additionally each organism can be allocated with a specific redox-potential-window in which its electron transport chains are able to operate, which is also visualized in **Figure 3**. It becomes obvious that compounds of facultative aerobe organisms such as *E. coli* and *S. oneidensis* are represented over a wide range of potentials. This visualizes the high flexibility of both organisms to adapt their electron transport chains to multiple electron donors and acceptors. *G. sulfurreducens* even though a strict anaerobe still covers an impressive range of redox potentials with its many cytochromes and the ability to use soluble metals such as iron and manganese as final electron acceptors. The rnf-complex containing acetogens *C. ljungdahlii* and *A. woodii*, however, are only able to transfer

electrons in a limited potential window as they do not contain any cytochromes and are restricted to only one way of respiration at relatively low potentials.

Transferring Electrogenic Capabilities between Bacteria

To transfer the ability of one organism that is known to interact with an electrode in a specific way to another organism, synthetic biology tools can be used. It could be shown that expressing enzymes of the Mtr pathway of *S. oneidensis* inside *E. coli* increased current production of the optimized strain (Pitts et al., 2003; Jensen et al., 2010). In 2008 researchers could show that the expression of one single enzyme from *Shewanella*'s Mtr-pathway is enough to transform *E. coli* into a metal respiring bacterium (Gescher et al., 2008). Expression of the cytoplasmic-membrane tetraheme c-type cytochrome CymA enabled the mutant strain to reduce Fe(III) and sustain growth while the native strain lacked this ability. This was independent of the presence of periplasmic or outer-membrane cytochromes for electron transfer. However, it could also be shown that activities of CymA for iron reduction were much lower in complete cells, indicating that diffusion limitations of solid state electron acceptors also play a significant role in this electron transport chain (Gescher et al., 2008). A very important follow up study was able to find evidence for a connection of this transformed electron transport to intracellular carbon flow in *E. coli* (TerAvest et al., 2014). Expression of CymA and Mtr cytochromes from *Shewanella oneidensis* in *E. coli* resulted in a strain that coupled current production to a shift in its metabolic fluxes towards more oxidized products (TerAvest et al., 2014). The possibility to design a target electron flow via artificial complexes across the outer and inner membranes and their connection to cellular redox balance and carbon flow promises many possibilities to design optimized electro active organisms. The above cited example also shows that co-expression of multiple linked enzymes can greatly enhance the electron transfer rates (TerAvest et al., 2014). Therefore the specific electron transport chains of the target organism and their possible connection to the enzymes to be introduced need to be considered when designing electro active bacteria.

Targeting Electron Transport Impacts the Cellular Energy Metabolism

The achievable energy yield of an electron transport chain is dependent on the difference in electrical potential between electron donor and acceptor. Therefore organisms that are able to respire in multiple ways will always choose available acceptors with the biggest potential difference to the donor (e.g., *E. coli* $O_2 > NO_3^- >$ fumarate). To compare energy efficiencies of different electron transport chains it is referred to the ratio of phosphate to oxygen (P/O quotient), which describes the ratio of mol ATP produced per mol oxygen reduced. The P/O ratio depends on the amount of ions that are transported across the membrane during the corresponding electron-transport chain and are available for ATP-synthesis via gradient-driven ATPase. It is also influenced by the efficiency of the specific ATPase as the amount of ions that are needed for synthesis of one mol ATP differ between organisms (Møller et al., 1996). For example the

aerobic electron transport chain of *E. coli* transports up to eight protons across the membrane with NADH as electron donor (2 e$^-$) and oxygen as final acceptor (see **Figure 4**; Unden and Bongaerts, 1997). With an ATPase that requires three protons for the conversion of one mol ADP to ATP a P/O ratio of ~2.7 is calculated (Noguchi et al., 2004).

The ATP yield is an important factor for bacterial growth and can also significantly influence production if the metabolic pathway towards the target compound requires energy. Therefore we present similar to the P/O ratio a hypothetical P/2e$^-$ ratio that reflects the ATP yield per pair of electrons transferred between the organism and an electrode in a BES. Some examples are presented in **Table 2**. The electrode can either function as electron donor (cathode) or as final electron acceptor (anode). Since the exact sites of electrode-interaction with the compounds of each electron transport chain remain unknown we assume different scenarios. In column 2 of **Table 2** the assumed site of electrode–bacteria interaction is given together with the corresponding hypothetical reaction. The P/2e$^-$ ratio is calculated based on the resulting amount of protons carried across the membrane, which are assumed to be available to drive ATP synthesis via ATPase. An example is explained in detail in the following paragraph.

Figure 4 shows a simplified image of electron transport chains in *E. coli* including possible sites of EET (dashed red arrows). As discussed above it could be shown that cytochromes of *G. sulfurreducens* are able to use electrodes as final electron acceptor. If we assume the cytochromes of *E. coli* are also

possible sites of EET we observe that the ATP yield of the electron transport chain depends on the specific cytochrome that is performing the electron transfer to the electrode. In case of cytochrome *bo* transferring electrons to an anode as final electron acceptor 8 H$^+$ are transported across the membrane (4 H$^+$ from NADH dehydrogenase and 4 H$^+$ from UQH$_2$ and cytochrome *bo*). With an ATP synthase that requires ~3 H$^+$ per ATP (Noguchi et al., 2004) this leads to a P/2e$^-$ ratio of 2.7. Running the electron transport chain with cytochrome *bd* as the final oxidase, however, leads to a P/2e$^-$ ratio of 2 as fewer protons are transferred across the membrane (6 H$^+$ in total: 4H$^+$ from NADH dehydrogenase and 2 H$^+$ from cytochrome *bd*). By including soluble redox carriers such as ubiquinones, FAD and NADH to the scenario we can address any site of *E. coli*'s electron transport chain. The observation from this theoretical exercise is to internalize that the achievable ATP yield depends on the actual site of EET. If for example electrons are drawn directly from the cellular NADH pool of *E. coli* no energy gain via chemiosmotic

FIGURE 4 | Schematic image of electron transport chains in *Escherichia coli*. NADH as electron donor via NADH dehydrogenase (NuoA-N), ubiquinone pool (UQ), succinate-dehydrogenase, and cytochromes *bd* (CydAB) and *bo* (CyoABCD). ATP is generated via F$_1$F$_0$-ATPase (3H$^+$/ATP) from the membrane proton gradient. Possible sites of interaction with an electrode are indicated with dashed arrows. For detailed discussion and references refer to main text.

TABLE 2 | Theoretical P/2e$^-$ ratios for extracellular electron transfer between electrodes and different sites in the electron transport chains of *E. coli*, *M. thermoacetica* and *C. ljungdahlii*.

Organism	Site of electron transfer	P/2e$^-$
Anodic electron transport		
E. coli[a]	Cytochrome *bo*	2.7
	Cytochrome *bd*	2
	Ubiquinone-pool (UQH$_2$ → 2e$^-$ + UQ + 2H$^+$$_{periplasm}$)	2
	FAD reduction (FADH$_2$ → 2e$^-$ + FAD$^+$ + 2H$^+$$_{cytoplasm}$)	0.6
	NADH oxidation (NADH → 2e$^-$ + NAD$^+$ + 2H$^+$$_{cytoplasm}$)	0
Cathodic electron transfer		
E. coli[a]	NADH reduction (2e$^-$ + NAD$^+$ + 2H$^+$$_{cytoplasm}$ → NADH)	2.7
	FAD reduction (2e$^-$ + FAD$^+$ + 2H$^+$$_{cytoplasm}$ → FADH$_2$)	1.3
	Ubiquinone reduction (2e$^-$ + UQ + 2H$^+$$_{cytoplasm}$ → UQH$_2$)	1.3
	Ubiquinone reduction (2e$^-$ + UQ + 2H$^+$$_{periplasm}$ → UQH$_2$)	0.6
M. thermoacetica[b,c]	Ferredoxin reduction (2e$^-$ + Fd$_{ox}$ → Fd$_{red}$)	0.75
	Hydrogen evolution (2e$^-$ + 2H$^+$$_{cytoplasm}$ → H$_2$)	0.375
	NADH reduction (2e$^-$ + NAD$^+$ → NADH)	0
C. ljungdahlii[b]	Ferredoxin reduction (2e$^-$ + Fd$_{ox}$ → Fd$_{red}$)	0.5
	Hydrogen evolution (2e$^-$ + 2H$^+$$_{cytoplasm}$ → H$_2$)	0.25
	NADH reduction (2e$^-$ + NAD$^+$ + 2H$^+$$_{cytoplasm}$ → NADH)	0

*Column 2 gives the assumed site of electron transfer including hypothetical reaction. For following reactions and references refer to the main text and **Figures 2** and **4**. The corresponding amount of protons transferred across the membrane is assumed to be available for ATP synthesis. P/2e$^-$ is mol ATP produced per pair of electrons transferred.* [a]*3 H$^+$ per ATP in ATPase,* [b]*4 H$^+$ per ATP in ATPase,* [c]*Ech-complex based electron transport chain.*
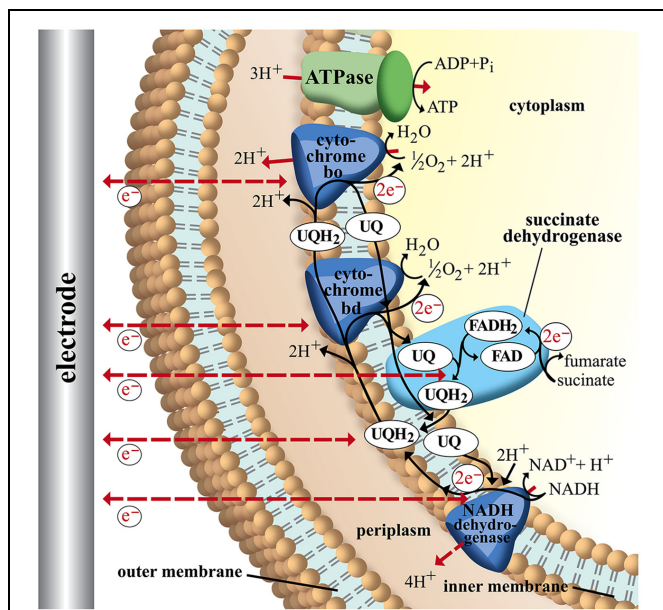
coupling is possible as no proton gradient is established (see **Figure 4**; **Table 2**).

This becomes especially crucial in regards to cathodic electron transfer where processes often aim on microbial metabolism with electrons from electrodes as sole energy and redox source (Rabaey and Rozendal, 2010; Nevin et al., 2011). As discussed in Section "Carbon Respiration of Acetogenic Bacteria" the metabolism of acetogens for example relies on ATP synthesis via membrane-based electron transport complexes. Now we can pick again an example strain and theoretically discuss metabolic impact of EET at different sites. *C. ljungdahlii* does not transfer electrons via cytochromes but was shown to interact with electrodes so we can assume EET via mediators or unknown membrane bound compounds towards its cellular redox compounds. In case electrons from a cathode would lead to hydrogen formation the organism could produce 2 mol of reduced Fd per 4 mol of H_2 via electron bifurcation in the Hyd-complex (see **Figure 2**; Buckel and Thauer, 2013). The exergonic reaction of reduced Fd and NAD^+ is used for proton translocation in the rnf complex (2 H^+/Fd_{red}) which in turn enables energy conservation via the membrane bound ATPase. With recent estimates of four protons per mol of ATP a $P/2e^-$ ratio of 0.25 is calculated (Schuchmann and Müller, 2014). If it is possible to transfer electrons from a cathode directly to Fd the ratio increases to 0.5 mol ATP per pair of electrons transferred. An electron input toward the NADH pool of the bacterium, however, would not deliver enough energy to establish a proton motive force and therefore ATP generation (see **Table 2**).

Remembering **Figure 3** one can draw the connection between required redox potential and target reaction in a specific electron transport chain of an organism to optimize the conditions for a bio electrochemical process. For a cathodic process of *C. ljungdahlii* for example the applied electrode potential needs to be at least low enough to allow hydrogen formation to enable ATP formation and therefore bacterial growth.

Conclusion

The remaining question after the presented analysis of microbial electron transport chains is: can we identify an ultimate organism for microbial electrochemical techniques? Requirements for an advantageous organism would be first of all high electro-activity. But depending on the target application different other features can be of crucial importance. Microbial electrosynthesis for example requires a strain that produces industrial relevant products preferably combined with the ability to utilize a variety of cheap substrates. Metabolic engineering tools should be available to optimize production and perform advanced strain designing. For application in bioremediation processes the ability of breaking down a wide range of organic contaminates has priority together of course with efficiency of EET. Other influencing factors are general characteristics that simplify process design such as high oxygen tolerance for anaerobes, no high risk organism, no complicated fermentation conditions such as expensive media supplements, pressurized reactor etc.

The diversity of applications for BES makes it impossible to identify one organism that features all required properties. Still for each application a specific species might outperform others. The highly flexible electron transport chains of metal respiring bacteria such as *Geobacter* and *Shewanella* make them excellent current producers over a wide range of potentials. And acetogens seem to be a very promising group of target organisms for microbial electrosynthesis with their ability to use CO_2 as sole carbon source. But our study also shows that the complexity of microbial electron transport possibilities bears many challenges for bioelectrochemical techniques. For the successful design of an electrically enhanced bio process the specific electron transport properties of the involved species needs to be considered. Environmental conditions such as applied potentials should be adjusted according to specific target sites for EET. Since these are unknown in most cases an analysis as presented in this manuscript will help to identify best- and worst-case scenarios for microbe-electrode interactions and identification of optimized windows for process parameters. Especially when looking at CO_2 as a feedstock, the available energy gain through EET will limit the feasibility of many organisms and constrain the list of feasible products. There is currently a lot of interest in microbial electrochemical technologies; however, we believe that without deeper understanding of the underlying electron transfer process development remains a trial and error exercise.

Author Contributions

FK, IV, and JK designed the study. FK and IV collected the data and drafted the manuscript. FK performed the calculations. All authors edited the manuscript and approved the final version.

Acknowledgments

References

Anraku, Y. (1988). Bacterial electron transport chains. *Annu. Rev. Biochem.* 57, 101–132. doi: 10.1146/annurev.bi.57.070188.000533

Atkinson, S. J., Mowat, C. G., Reid, G. A., and Chapman, S. K. (2007). An octaheme c-type cytochrome from *Shewanella oneidensis* can reduce nitrite and hydroxylamine. *FEBS Lett.* 581, 3805–3808. doi: 10.1016/j.febslet.2007.07.005

Baltch, A. L., and Smith, R. P. (eds). (1994). *Pseudomonas aeruginosa: Infections and Treatment.* New York, NY: Marcel Dekker, Inc.

Banerjee, A., Leang, C., Ueki, T., Nevin, K. P., and Lovley, D. R. (2014). Lactose-inducible system for metabolic engineering of *Clostridium ljungdahlii. Appl. Environ. Microbiol.* 80, 2410–2416. doi: 10.1128/AEM.03666-13

Berlyn, M. K. (1998). Linkage map of *Escherichia coli* K-10: the traditional map. *Microbiol. Mol. Biol. Rev.* 62, 814–984.

Bertini, I., Cavallaro, G., and Rosato, A. (2006). Cytochrome c: occurrence and functions. *Chem. Rev.* 106, 90–115. doi: 10.1021/cr050241v

Biegel, E., Schmidt, S., González, J., and Müller, V. (2011). Biochemistry, evolution and physiological function of the Rnf complex, a novel ion-motive electron transport complex in prokaryotes. *Cell. Mol. Life Sci.* 68, 613–634. doi: 10.1007/s00018-010-0555-8

Bond, D. R., and Lovley, D. R. (2003). Electricity production by *Geobacter sulfurreducens* attached to electrodes. *Appl. Environ. Microbiol.* 69, 1548–1555. doi: 10.1128/aem.69.3.1548-1555.2003

Boon, N., De Maeyer, K., Höfte, M., Rabaey, K., and Verstraete, W. (2008). Use of *Pseudomonas* species producing phenazine-based metabolites in the anodes of microbial fuel cells to improve electricity generation. *Appl. Microbiol. Biotechnol.* 80, 985–993. doi: 10.1007/s00253-008-1619-7

Bott, M., and Niebisch, A. (2003). The respiratory chain of *Corynebacterium glutamicum*. *J. Biotechnol.* 104, 129–153. doi: 10.1016/S0168-1656(03)00144-5

Breuer, M., Rosso, K. M., Blumberger, J., and Butt, J. N. (2015). Multi-haem cytochromes in *Shewanella oneidensis* MR-1: structures, functions and opportunities. *J. R. Soc. Interface* 12, 20141117. doi: 10.1098/rsif.2014.1117

Buckel, W., and Thauer, R. K. (2013). Energy conservation via electron bifurcating ferredoxin reduction and proton/Na+ translocating ferredoxin oxidation. *Biochim. Biophys. Acta* 1827, 94–113. doi: 10.1016/j.bbabio.2012.07.002

Carlson, H. K., Iavarone, A. T., Gorur, A., Yeo, B. S., Tran, R., Melnyk, R. A., et al. (2012). Surface multiheme c-type cytochromes from *Thermincola potens* and implications for respiratory metal reduction by Gram-positive bacteria. *Proc. Natl. Acad. Sci. U.S.A.* 109, 1702–1707. doi: 10.1073/pnas.1112905109

Choi, O., Um, Y., and Sang, B.-I. (2012). Butyrate production enhancement by *Clostridium tyrobutyricum* using electron mediators and a cathodic electron donor. *Biotechnol. Bioeng.* 109, 2494–2502. doi: 10.1002/bit.24520

Coursolle, D., and Gralnick, J. A. (2010). Modularity of the Mtr respiratory pathway of *Shewanella oneidensis* strain MR-1. *Mol. Microbiol.* 77, 995–1008. doi: 10.1111/j.1365-2958.2010.07266.x

Das, A., and Ljungdahl, L. G. (2003). "Electron-transport system in acetogens," in *Biochemistry and Physiology of Anaerobic Bacteria*, eds L. G. Ljungdahl, M. W. Adams, L. Barton, J. G. Ferry, and M. K. Johnson (New York, NY: Springer-Verlag), 191–204. doi: 10.1007/0-387-22731-8_14

Deller, S., Macheroux, P., and Sollner, S. (2008). Flavin-dependent quinone reductases. *Cell. Mol. Life Sci.* 65, 141–160. doi: 10.1007/s00018-007-7300-y

Deutzmann, J. S., Sahin, M., and Spormann, A. M. (2015). Extracellular enzymes facilitate electron uptake in biocorrosion and bioelectrosynthesis. *MBio* 6:e00496-15. doi: 10.1128/mBio.00496-15

Diekert, G., and Wohlfarth, G. (1994). Metabolism of homoacetogens. *Antonie Van Leeuwenhoek* 66, 209–221. doi: 10.1007/BF00871640

Dolin, M. (2012). Survey of microbial electron transport mechanisms. *Bacteria* 2:319.

Dos Santos, J.-P., Iobbi-Nivol, C., Couillault, C., Giordano, G., and Méjean, V. (1998). Molecular analysis of the trimethylamine N-oxide (TMAO) reductase respiratory system from a *Shewanella* species. *J. Mol. Biol.* 284, 421–433. doi: 10.1006/jmbi.1998.2155

Drake, H. L., Gößner, A. S., and Daniel, S. L. (2008). Old acetogens, new light. *Ann. N. Y. Acad. Sci.* 1125, 100–128. doi: 10.1196/annals.1419.016

Dumas, C., Basseguy, R., and Bergel, A. (2008). Microbial electrocatalysis with *Geobacter sulfurreducens* biofilm on stainless steel cathodes. *Electrochim. Acta* 53, 2494–2500. doi: 10.1016/j.electacta.2007.10.018

Emde, R., and Schink, B. (1990). Enhanced propionate formation by *Propionibacterium freudenreichii* subsp. freudenreichii in a three-electrode amperometric culture system. *Appl. Environ. Microbiol.* 56, 2771–2776.

Fast, A. G., and Papoutsakis, E. T. (2012). Stoichiometric and energetic analyses of non-photosynthetic CO2-fixation pathways to support synthetic biology strategies for production of fuels and chemicals. *Curr. Opin. Chem. Eng.* 1, 380–395. doi: 10.1016/j.coche.2012.07.005

Firer-Sherwood, M., Pulcu, G. S., and Elliott, S. J. (2008). Electrochemical interrogations of the Mtr cytochromes from *Shewanella*: opening a potential window. *J. Biol. Inorg. Chem.* 13, 849–854. doi: 10.1007/s00775-008-0398-z

Fonseca, B. M., Paquete, C. M., Neto, S. E., Pacheco, I., Soares, C. M., and Louro, R. O. (2013). Mind the gap: cytochrome interactions reveal electron pathways across the periplasm of *Shewanella oneidensis* MR-1. *Biochem. J.* 449, 101–108. doi: 10.1042/BJ20121467

Franks, A. (2012). What's current with electric microbes. *J. Bacteriol. Parasitol.* 3:e116. doi: 10.4172/2155-9597.1000e116

Franks, A. E., and Nevin, K. P. (2010). Microbial fuel cells, a current review. *Energies* 3, 899–919. doi: 10.3390/en3050899

Gao, H., Yang, Z. K., Barua, S., Reed, S. B., Romine, M. F., Nealson, K. H., et al. (2009). Reduction of nitrate in *Shewanella oneidensis* depends on atypical NAP and NRF systems with NapB as a preferred electron transport protein from CymA to NapA. *ISME J.* 3, 966–976. doi: 10.1038/ismej.2009.40

Gescher, J. S., Cordova, C. D., and Spormann, A. M. (2008). Dissimilatory iron reduction in *Escherichia coli*: identification of CymA of *Shewanella oneidensis* and NapC of *E. coli* as ferric reductases. *Mol. Microbiol.* 68, 706–719. doi: 10.1111/j.1365-2958.2008.06183.x

Gralnick, J. A., Vali, H., Lies, D. P., and Newman, D. K. (2006). Extracellular respiration of dimethyl sulfoxide by *Shewanella oneidensis* strain MR-1. *Proc. Natl. Acad. Sci. U.S.A.* 103, 4669–4674. doi: 10.1073/pnas.0505959103

Gregory, K. B., Bond, D. R., and Lovley, D. R. (2004). Graphite electrodes as electron donors for anaerobic respiration. *Environ. Microbiol.* 6, 596–604. doi: 10.1111/j.1462-2920.2004.00593.x

Haddock, B. A., and Schairer, H. U. (1973). Electron-transport chains of *Escherichia coli*. *Eur. J. Biochem.* 35, 34–45. doi: 10.1111/j.1432-1033.1973.tb02806.x

Hannemann, F., Bichet, A., Ewen, K. M., and Bernhardt, R. (2007). Cytochrome P450 systems—biological variations of electron transport chains. *Biochim. Biophys. Acta* 1770, 330–344. doi: 10.1016/j.bbagen.2006.07.017

Harnisch, F., Rosa, L. F., Kracke, F., Virdis, B., and Krömer, J. O. (2014). Electrifying white biotechnology: engineering and economic potential of electricity-driven bio-production. *ChemSusChem* 8, 758–766. doi: 10.1002/cssc.201402736

Hartshorne, R. S., Reardon, C. L., Ross, D., Nuester, J., Clarke, T. A., Gates, A. J., et al. (2009). Characterization of an electron conduit between bacteria and the extracellular environment. *Proc. Natl. Acad. Sci. U.S.A.* 106, 22169–22174. doi: 10.1073/pnas.0900086106

Hassett, D. J., Cuppoletti, J., Trapnell, B., Lymar, S. V., Rowe, J. J., Yoon, S. S., et al. (2002). Anaerobic metabolism and quorum sensing by *Pseudomonas aeruginosa* biofilms in chronically infected cystic fibrosis airways: rethinking antibiotic treatment strategies and drug targets. *Adv. Drug Del. Rev.* 54, 1425–1443. doi: 10.1016/S0169-409X(02)00152-7

Heidelberg, J. F., Paulsen, I. T., Nelson, K. E., Gaidos, E. J., Nelson, W. C., Read, T. D., et al. (2002). Genome sequence of the dissimilatory metal ion–reducing bacterium *Shewanella oneidensis*. *Nat. Biotechnol.* 20, 1118–1123. doi: 10.1038/nbt749

Hernandez, M. E., Kappler, A., and Newman, D. K. (2004). Phenazines and other redox-active antibiotics promote microbial mineral reduction. *Appl. Environ. Microbiol.* 70, 921–928. doi: 10.1128/AEM.70.2.921-928.2004

Hernandez, M., and Newman, D. (2001). Extracellular electron transfer. *Cell. Mol. Life Sci.* 58, 1562–1571. doi: 10.1007/PL00000796

Herrmann, G., Jayamani, E., Mai, G., and Buckel, W. (2008). Energy conservation via electron-transferring flavoprotein in anaerobic bacteria. *J. Bacteriol.* 190, 784–791. doi: 10.1128/JB.01422-07

Hess, V., Schuchmann, K., and Müller, V. (2013). The ferredoxin: NAD+ oxidoreductase (Rnf) from the acetogen *Acetobacterium woodii* requires Na+ and is reversibly coupled to the membrane potential. *J. Biol. Chem.* 288, 31496–31502. doi: 10.1074/jbc.M113.510255

Holmes, D. E., Chaudhuri, S. K., Nevin, K. P., Mehta, T., Methé, B. A., Liu, A., et al. (2006). Microarray and genetic analysis of electron transfer to electrodes in *Geobacter sulfurreducens*. *Environ. Microbiol.* 8, 1805–1815. doi: 10.1111/j.1462-2920.2006.01065.x

Huang, H., Wang, S., Moll, J., and Thauer, R. K. (2012). Electron bifurcation involved in the energy metabolism of the acetogenic bacterium *Moorella thermoacetica* growing on glucose or H2 plus CO2. *J. Bacteriol.* 194, 3689–3699. doi: 10.1128/JB.00385-12

Ingledew, W. J. (1983). The electron transport chain of *Escherichia coli* grown anaerobically with fumarate as terminal electron acceptor: an electron paramagnetic resonance study. *J. Gen. Microbiol.* 129, 1651–1659. doi: 10.1099/00221287-129-6-1651

Inoue, K., Qian, X., Morgado, L., Kim, B.-C., Mester, T., Izallalen, M., et al. (2010). Purification and characterization of OmcZ, an outer-surface, octaheme c-type cytochrome essential for optimal current production by *Geobacter sulfurreducens*. *Appl. Environ. Microbiol.* 76, 3999–4007. doi: 10.1128/AEM.00027-10

Janicek, A., Fan, Y., and Liu, H. (2014). Design of microbial fuel cells for practical application: a review and analysis of scale-up studies. *Biofuels* 5, 79–92. doi: 10.4155/bfs.13.69

Jensen, H. M., Albers, A. E., Malley, K. R., Londer, Y. Y., Cohen, B. E., Helms, B. A., et al. (2010). Engineering of a synthetic electron conduit in living cells. *Proc. Natl. Acad. Sci. U.S.A.* 107, 19213–19218. doi: 10.1073/pnas.1009645107

Jo, J., Price-Whelan, A., and Dietrich, L. E. (2014). An aerobic exercise: defining the roles of *Pseudomonas aeruginosa* terminal oxidases. *J. Bacteriol.* 196, 4203–4205. doi: 10.1128/JB.02336-14

Kim, B.-C., Postier, B. L., Didonato, R. J., Chaudhuri, S. K., Nevin, K. P., and Lovley, D. R. (2008). Insights into genes involved in electricity generation in *Geobacter sulfurreducens* via whole genome microarray analysis of the OmcF-deficient mutant. *Bioelectrochemistry* 73, 70–75. doi: 10.1016/j.bioelechem.2008.04.023

Kim, B.-C., Qian, X., Leang, C., Coppi, M. V., and Lovley, D. R. (2006). Two putative c-type multiheme cytochromes required for the expression of OmcB, an outer membrane protein essential for optimal Fe (III) reduction in *Geobacter sulfurreducens*. *J. Bacteriol.* 188, 3138–3142. doi: 10.1128/JB.188.8.3138-3142.2006

Kim, T. S., and Kim, B. H. (1988). Electron flow shift in *Clostridium acetobutylicum* fermentation by electrochemically introduced reducing equivalent. *Biotechnol. Lett.* 10, 123–128. doi: 10.1007/BF01024638

Köpke, M., Held, C., Hujer, S., Liesegang, H., Wiezer, A., Wollherr, A., et al. (2010). *Clostridium ljungdahlii* represents a microbial production platform based on syngas. *Proc. Natl. Acad. Sci. U.S.A.* 107, 13087–13092. doi: 10.1073/pnas.1004716107

Kracke, F., and Krömer, J. O. (2014). Identifying target processes for microbial electrosynthesis by elementary mode analysis. *BMC Bioinformatics* 15:6590. doi: 10.1186/s12859-014-0410-2

Leang, C., and Lovley, D. R. (2005). Regulation of two highly similar genes, omcB and omcC, in a 10 kb chromosomal duplication in *Geobacter sulfurreducens*. *Microbiology* 151, 1761–1767. doi: 10.1099/mic.0.27870-0

Lee, J., Jang, Y.-S., Choi, S. J., Im, J. A., Song, H., Cho, J. H., et al. (2012). Metabolic engineering of *Clostridium acetobutylicum* ATCC 824 for isopropanol-butanol-ethanol fermentation. *Appl. Environ. Microbiol.* 78, 1416–1423. doi: 10.1128/AEM.06382-11

Levar, C., Rollefson, J., and Bond, D. (2012). "Energetic and molecular constraints on the mechanism of environmental Fe (III) reduction by *Geobacter*," in *Microbial Metal Respiration*, eds J. Gescher and A. Kappler (Berlin: Springer), 29–48.

Lloyd, J., Leang, C., Hodges, M. A., Coppi, M., Cuifo, S., Methe, B., et al. (2003). Biochemical and genetic characterization of PpcA, a periplasmic c-type cytochrome in *Geobacter sulfurreducens*. *Biochem. J.* 369, 153–161. doi: 10.1042/BJ20020597

Logan, B. E. (2009). Exoelectrogenic bacteria that power microbial fuel cells. *Nat. Rev. Microbiol.* 7, 375–381. doi: 10.1038/nrmicro2113

Logan, B. E., and Rabaey, K. (2012). Conversion of wastes into bioelectricity and chemicals by using microbial electrochemical technologies. *Science* 337, 686–690. doi: 10.1126/science.1217412

Lovley, D. R. (2012). Electromicrobiology. *Annu. Rev. Microbiol.* 66, 391–409. doi: 10.1146/annurev-micro-092611-150104

Lovley, D. R., Holmes, D. E., and Nevin, K. P. (2004). Dissimilatory fe (iii) and mn (iv) reduction. *Adv. Microb. Physiol.* 49, 219–286. doi: 10.1016/s0065-2911(04)49005-5

Lovley, D. R., and Nevin, K. P. (2013). Electrobiocommodities: powering microbial production of fuels and commodity chemicals from carbon dioxide with electricity. *Curr. Opin. Biotechnol.* 24, 385–390. doi: 10.1016/j.copbio.2013.02.012

Lower, B. H., Hochella, M. F., and Lower, S. K. (2005). Putative mineral-specific proteins synthesized by a metal reducing bacterium. *Am. J. Sci.* 305, 687–710. doi: 10.2475/ajs.305.6-8.687

Lütke-Eversloh, T., and Bahl, H. (2011). Metabolic engineering of *Clostridium acetobutylicum*: recent advances to improve butanol production. *Curr. Opin. Biotechnol.* 22, 634–647. doi: 10.1016/j.copbio.2011.01.011

Maier, T. M., Myers, J. M., and Myers, C. R. (2003). Identification of the gene encoding the sole physiological fumarate reductase in *Shewanella oneidensis* MR-1. *J. Basic Microbiol.* 43, 312–327. doi: 10.1002/jobm.200390034

Malvankar, N. S., Tuominen, M. T., and Lovley, D. R. (2012). Comment on "*On Electrical Conductivity of Microbial Nanowires and Biofilms*" by S. M. Strycharz-Glaven, R. M. Snider, A. Guiseppi-Elie, and L. M. Tender, *Energy Environ. Sci.* 2011, 4, 4366. *Energy Environ. Sci.* 5, 6247–6249. doi: 10.1039/c2ee02613a

Malvankar, N. S., Vargas, M., Nevin, K. P., Franks, A. E., Leang, C., Kim, B.-C., et al. (2011). Tunable metallic-like conductivity in microbial nanowire networks. *Nat. Nanotechnol.* 6, 573–579. doi: 10.1038/nnano.2011.119

Malvankar, N. S., Vargas, M., Nevin, K., Tremblay, P.-L., Evans-Lutterodt, K., Nykypanchuk, D., et al. (2015). Structural basis for metallic-like conductivity in microbial nanowires. *MBio* 6:e00084-15. doi: 10.1128/mBio.00084-15

Marshall, C. W., and May, H. D. (2009). Electrochemical evidence of direct electrode reduction by a thermophilic gram-positive bacterium, *Thermincola ferriacetica*. *Energy Environ. Sci.* 2, 699–705. doi: 10.1039/b823237g

Marshall, C. W., Ross, D. E., Fichot, E. B., Norman, R. S., and May, H. D. (2012). Electrosynthesis of commodity chemicals by an autotrophic microbial community. *Appl. Environ. Microbiol.* 78, 8412–8420. doi: 10.1128/AEM.02401-12

Marsili, E., Baron, D. B., Shikhare, I. D., Coursolle, D., Gralnick, J. A., and Bond, D. R. (2008a). *Shewanella* secretes flavins that mediate extracellular electron transfer. *Proc. Natl. Acad. Sci. U.S.A.* 105, 3968–3973. doi: 10.1073/pnas.0710525105

Marsili, E., Rollefson, J. B., Baron, D. B., Hozalski, R. M., and Bond, D. R. (2008b). Microbial biofilm voltammetry: direct electrochemical characterization of catalytic electrode-attached biofilms. *Appl. Environ. Microbiol.* 74, 7329–7337. doi: 10.1128/AEM.00177-08

Mehta, T., Coppi, M. V., Childers, S. E., and Lovley, D. R. (2005). Outer membrane c-type cytochromes required for Fe (III) and Mn (IV) oxide reduction in *Geobacter sulfurreducens*. *Appl. Environ. Microbiol.* 71, 8634–8641. doi: 10.1128/AEM.71.12.8634-8641.2005

Methe, B., Nelson, K. E., Eisen, J., Paulsen, I., Nelson, W., Heidelberg, J., et al. (2003). Genome of *Geobacter sulfurreducens*: metal reduction in subsurface environments. *Science* 302, 1967–1969. doi: 10.1126/science.1088727

Møller, J. V., Juul, B., and Le Maire, M. (1996). Structural organization, ion transport, and energy transduction of P-type ATPases. *Biochim. Biophys. Acta Rev. Biomembr.* 1286, 1–51. doi: 10.1016/0304-4157(95)00017-8

Morgado, L., Bruix, M., Pessanha, M., Londer, Y. Y., and Salgueiro, C. A. (2010). Thermodynamic characterization of a triheme cytochrome family from *Geobacter sulfurreducens* reveals mechanistic and functional diversity. *Biophys. J.* 99, 293–301. doi: 10.1016/j.bpj.2010.04.017

Müller, V. (2003). Energy conservation in acetogenic bacteria. *Appl. Environ. Microbiol.* 69, 6345–6353. doi: 10.1128/AEM.69.11.6345-6353.2003

Müller, V., and Frerichs, J. (2013). "Acetogenic bacteria," in *Encyclopedia of Life Sciences* (Chichester: John Wiley & Sons), 1–9. doi: 10.1002/9780470015902.a0020086.pub2

Müller, V., Imkamp, F., Biegel, E., Schmidt, S., and Dilling, S. (2008). Discovery of a Ferredoxin: NAD+-Oxidoreductase (Rnf) in *Acetobacterium woodii*. *Ann. N. Y. Acad. Sci.* 1125, 137–146. doi: 10.1196/annals.1419.011

Myers, J. M., and Myers, C. R. (2000). Role of the tetraheme cytochrome CymA in anaerobic electron transport in cells of *Shewanella putrefaciens* MR-1 with normal levels of menaquinone. *J. Bacteriol.* 182, 67–75. doi: 10.1128/JB.182.1.67-75.2000

Nevin, K. P., Hensley, S. A., Franks, A. E., Summers, Z. M., Ou, J., Woodard, T. L., et al. (2011). Electrosynthesis of organic compounds from carbon dioxide is catalyzed by a diversity of acetogenic microorganisms. *Appl. Environ. Microbiol.* 77, 2882–2886. doi: 10.1128/em.02642-10

Nevin, K. P., Kim, B.-C., Glaven, R. H., Johnson, J. P., Woodard, T. L., Methé, B. A., et al. (2009). Anode biofilm transcriptomics reveals outer surface components essential for high density current production in *Geobacter sulfurreducens* fuel cells. *PLoS ONE* 4:e5628. doi: 10.1371/journal.pone.0005628

Nevin, K. P., Woodard, T. L., Franks, A. E., Summers, Z. M., and Lovley, D. R. (2010). Microbial electrosynthesis: feeding microbes electricity to convert carbon dioxide and water to multicarbon extracellular organic compounds. *MBio* 1, e00103–e00110. doi: 10.1128/mBio.00103-10

Nishimura, T., Vertès, A. A., Shinoda, Y., Inui, M., and Yukawa, H. (2007). Anaerobic growth of *Corynebacterium glutamicum* using nitrate as a terminal electron acceptor. *Appl. Microbiol. Biotechnol.* 75, 889–897. doi: 10.1007/s00253-007-0879-y

Noguchi, Y., Nakai, Y., Shimba, N., Toyosaki, H., Kawahara, Y., Sugimoto, S., et al. (2004). The energetic conversion competence of *Escherichia coli* during aerobic

respiration studied by 31P NMR using a circulating fermentation system. *J. Biochem.* 136, 509–515. doi: 10.1093/jb/mvh147

Okamoto, A., Hashimoto, K., Nealson, K. H., and Nakamura, R. (2013). Rate enhancement of bacterial extracellular electron transport involves bound flavin semiquinones. *Proc. Natl. Acad. Sci. U.S.A.* 110, 7856–7861. doi: 10.1073/pnas.1220823110

Okamoto, A., Saito, K., Inoue, K., Nealson, K. H., Hashimoto, K., and Nakamura, R. (2014). Uptake of self-secreted flavins as bound cofactors for extracellular electron transfer in *Geobacter* species. *Energy Environ. Sci.* 7, 1357–1361. doi: 10.1039/c3ee43674h

Parameswaran, P., Bry, T., Popat, S. C., Lusk, B. G., Rittmann, B. E., and Torres, C. I. (2013). Kinetic, electrochemical, and microscopic characterization of the thermophilic, anode-respiring bacterium *Thermincola ferriacetica. Environ. Sci. Technol.* 47, 4934–4940. doi: 10.1021/es400321c

Patil, S. A., Haegerhaell, C., and Gortin, L. (2012). Electron transfer mechanisms between microorganisms and electrodes in bioelectrochemical systems. *Bioanal. Rev.* 4, 159–192. doi: 10.1007/s12566-012-0033-x

Pierce, E., Xie, G., Barabote, R. D., Saunders, E., Han, C. S., Detter, J. C., et al. (2008). The complete genome sequence of *Moorella thermoacetica* (f. *Clostridium thermoaceticum*). *Environ. Microbiol.* 10, 2550–2573. doi: 10.1111/j.1462-2920.2008.01679.x

Pirbadian, S., Barchinger, S. E., Leung, K. M., Byun, H. S., Jangir, Y., Bouhenni, R. A., et al. (2014). *Shewanella oneidensis* MR-1 nanowires are outer membrane and periplasmic extensions of the extracellular electron transport components. *Proc. Natl. Acad. Sci. U.S.A.* 111, 12883–12888. doi: 10.1073/pnas.14105 51111

Pitts, K. E., Dobbin, P. S., Reyes-Ramirez, F., Thomson, A. J., Richardson, D. J., and Seward, H. E. (2003). Characterization of the *Shewanella oneidensis* MR-1 decaheme cytochrome MtrA: expression in *Escherichia coli* confers the ability to reduce soluble Fe(III) chelates. *J. Biol. Chem.* 278, 27758–27765. doi: 10.1074/jbc.M302582200

Poehlein, A., Schmidt, S., Kaster, A.-K., Goenrich, M., Vollmers, J., Thürmer, A., et al. (2012). An ancient pathway combining carbon dioxide fixation with the generation and utilization of a sodium ion gradient for ATP synthesis. *PLoS ONE* 7:e33439. doi: 10.1371/journal.pone.0033439

Potter, M. C. (1911). Electrical effects accompanying the decomposition of organic compounds. *Proc. R. Soc. Lond. B* 1911, 260–276. doi: 10.1098/rspb.191 1.0073

Qian, X., Mester, T., Morgado, L., Arakawa, T., Sharma, M. L., Inoue, K., et al. (2011). Biochemical characterization of purified OmcS, a c-type cytochrome required for insoluble Fe (III) reduction in *Geobacter sulfurreducens. Biochim. Biophys. Acta* 1807, 404–412. doi: 10.1016/j.bbabio.2011.01.003

Qiao, Y., Li, C. M., Bao, S.-J., Lu, Z., and Hong, Y. (2008). Direct electrochemistry and electrocatalytic mechanism of evolved *Escherichia coli* cells in microbial fuel cells. *Chem. Commun.* 11, 1290–1292. doi: 10.1039/b719955d

Rabaey, K., Boon, N., Höfte, M., and Verstraete, W. (2005). Microbial phenazine production enhances electron transfer in biofuel cells. *Environ. Sci. Technol.* 39, 3401–3408. doi: 10.1021/es048563o

Rabaey, K., Boon, N., Siciliano, S. D., Verhaege, M., and Verstraete, W. (2004). Biofuel cells select for microbial consortia that self-mediate electron transfer. *Appl. Environ. Microbiol.* 70, 5373–5382. doi: 10.1128/AEM.70.9.5373-5382.2004

Rabaey, K., and Rozendal, R. A. (2010). Microbial electrosynthesis—revisiting the electrical route for microbial production. *Nat. Rev. Microbiol.* 8, 706–716. doi: 10.1038/nrmicro2422

Ragsdale, S. W., and Pierce, E. (2008). Acetogenesis and the Wood–Ljungdahl pathway of CO2 fixation. *Biochim. Biophys. Acta* 1784, 1873–1898. doi: 10.1016/j.bbapap.2008.08.012

Reguera, G., Nevin, K. P., Nicoll, J. S., Covalla, S. F., Woodard, T. L., and Lovley, D. R. (2006). Biofilm and nanowire production leads to increased current in *Geobacter sulfurreducens* fuel cells. *Appl. Environ. Microbiol.* 72, 7345–7348. doi: 10.1128/AEM.01444-06

Richardson, D. J., Edwards, M. J., White, G. F., Baiden, N., Hartshorne, R. S., Fredrickson, J. K., et al. (2012). Exploring the biochemistry at the extracellular redox frontier of bacterial mineral Fe (III) respiration. *Biochem. Soc. Trans.* 40, 493–500. doi: 10.1042/BST20120018

Richter, H., Nevin, K. P., Jia, H., Lowy, D. A., Lovley, D. R., and Tender, L. M. (2009). Cyclic voltammetry of biofilms of wild type and mutant *Geobacter sulfurreducens* on fuel cell anodes indicates possible roles of OmcB, OmcZ, type

IV pili, and protons in extracellular electron transfer. *Energy Environ. Sci.* 2, 506–516. doi: 10.1039/b816647a

Richter, K., Schicklberger, M., and Gescher, J. (2012). Dissimilatory reduction of extracellular electron acceptors in anaerobic respiration. *Appl. Environ. Microbiol.* 78, 913–921. doi: 10.1128/AEM.06803-11

Rosenbaum, M., Aulenta, F., Villano, M., and Angenent, L. T. (2011). Cathodes as electron donors for microbial metabolism: which extracellular electron transfer mechanisms are involved? *Bioresour. Technol.* 102, 324–333. doi: 10.1016/j.biortech.2010.07.008

Ross, D. E., Flynn, J. M., Baron, D. B., Gralnick, J. A., and Bond, D. R. (2011). Towards electrosynthesis in *Shewanella*: energetics of reversing the Mtr pathway for reductive metabolism. *PLoS ONE* 6:e16649. doi: 10.1371/journal.pone.0016649

Sasaki, K., Tsuge, Y., Sasaki, D., and Kondo, A. (2014). Increase in lactate yield by growing *Corynebacterium glutamicum* in a bioelectrochemical reactor. *J. Biosci. Bioeng.* 117, 598–601. doi: 10.1016/j.jbiosc.2013.10.026

Schiel-Bengelsdorf, B., and Dürre, P. (2012). Pathway engineering and synthetic biology using acetogens. *FEBS Lett.* 586, 2191–2198. doi: 10.1016/j.febslet.2012.04.043

Schröder, U., Nießen, J., and Scholz, F. (2003). A generation of microbial fuel cells with current outputs boosted by more than one order of magnitude. *Angew. Chem. Int. Ed.* 42, 2880–2883. doi: 10.1002/anie.200350918

Schrott, G. D., Bonanni, P. S., Robuschi, L., Esteve-Nuñez, A., and Busalmen, J. P. (2011). Electrochemical insight into the mechanism of electron transport in biofilms of *Geobacter sulfurreducens. Electrochim. Acta* 56, 10791–10795. doi: 10.1016/j.electacta.2011.07.001

Schuchmann, K., and Müller, V. (2012). A bacterial electron-bifurcating hydrogenase. *J. Biol. Chem.* 287, 31165–31171. doi: 10.1074/jbc.M112.3 95038

Schuchmann, K., and Müller, V. (2014). Autotrophy at the thermodynamic limit of life: a model for energy conservation in acetogenic bacteria. *Nat. Rev. Microbiol.* 12, 809–821. doi: 10.1038/nrmicro3365

Shi, L., Richardson, D. J., Wang, Z., Kerisit, S. N., Rosso, K. M., Zachara, J. M., et al. (2009). The roles of outer membrane cytochromes of *Shewanella* and *Geobacter* in extracellular electron transfer. *Environ. Microbiol. Rep.* 1, 220–227. doi: 10.1111/j.1758-2229.2009.00035.x

Shi, L., Rosso, K., Zachara, J., and Fredrickson, J. (2012). Mtr extracellular electron-transfer pathways in Fe (III)-reducing or Fe (II)-oxidizing bacteria: a genomic perspective. *Biochem. Soc. Trans.* 40, 1261–1267. doi: 10.1042/BST201 20098

Shi, L., Squier, T. C., Zachara, J. M., and Fredrickson, J. K. (2007). Respiration of metal (hydr) oxides by *Shewanella* and *Geobacter*: a key role for multihaem c-type cytochromes. *Mol. Microbiol.* 65, 12–20. doi: 10.1111/j.1365-2958.2007.05783.x

Shin, H., Zeikus, J., and Jain, M. (2002). Electrically enhanced ethanol fermentation by *Clostridium thermocellum* and *Saccharomyces cerevisiae. Appl. Microbiol. Biotechnol.* 58, 476–481. doi: 10.1007/s00253-001-0923-2

Shirodkar, S., Reed, S., Romine, M., and Saffarini, D. (2011). The octahaem SirA catalyses dissimilatory sulfite reduction in *Shewanella oneidensis* MR-1. *Environ. Microbiol.* 13, 108–115. doi: 10.1111/j.1462-2920.2010.02313.x

Simpson, P. J., Richardson, D. J., and Codd, R. (2010). The periplasmic nitrate reductase in *Shewanella*: the resolution, distribution and functional implications of two NAP isoforms, NapEDABC and NapDAGHB. *Microbiology* 156, 302–312. doi: 10.1099/mic.0.034421-0

Steinbusch, K. J., Hamelers, H. V., Schaap, J. D., Kampman, C., and Buisman, C. J. (2009). Bioelectrochemical ethanol production through mediated acetate reduction by mixed cultures. *Environ. Sci. Technol.* 44, 513–517. doi: 10.1021/es902371e

Straub, K. L., Benz, M., and Schink, B. (2001). Iron metabolism in anoxic environments at near neutral pH. *FEMS Microbiol. Ecol.* 34, 181–186. doi: 10.1111/j.1574-6941.2001.tb00768.x

Strycharz, S. M., Glaven, R. H., Coppi, M. V., Gannon, S. M., Perpetua, L. A., Liu, A., et al. (2011). Gene expression and deletion analysis of mechanisms for electron transfer from electrodes to *Geobacter sulfurreducens. Bioelectrochemistry* 80, 142–150. doi: 10.1016/j.bioelechem.2010.07.005

Strycharz, S. M., Woodard, T. L., Johnson, J. P., Nevin, K. P., Sanford, R. A., Löffler, F. E., et al. (2008). Graphite electrode as a sole electron donor for reductive dechlorination of tetrachlorethene by *Geobacter lovleyi. Appl. Environ. Microbiol.* 74, 5943–5947. doi: 10.1128/AEM.00961-08

Strycharz-Glaven, S. M., and Tender, L. M. (2012). Reply to the "*Comment on 'On Electrical Conductivity of Microbial Nanowires and Biofilms*'"by N. S. Malvankar, M. T. Tuominen, and D. R. Lovley, *Energy Environ. Sci.* 2012, 5. *Energy Environ. Sci.* 5, 6250–6255. doi: 10.1039/c2ee02613a.

Sydow, A., Krieg, T., Mayer, F., Schrader, J., and Holtmann, D. (2014). Electroactive bacteria—molecular mechanisms and genetic tools. *Appl. Microbiol. Biotechnol.* 98, 8481–8495. doi: 10.1007/s00253-014-6005-z

Tatsumi, N., and Inui, M. (2012). *Corynebacterium glutamicum: Biology and Biotechnology*. Heidelberg: Springer Science & Business Media.

TerAvest, M. A., Zajdel, T. J., and Ajo-Franklin, C. M. (2014). The Mtr pathway of *Shewanella oneidensis* MR-1 couples substrate utilization to current production in *Escherichia coli*. *ChemElectroChem* 1, 1874–1879. doi: 10.1002/celc.201402194

Thamdrup, B. (2000). Bacterial manganese and iron reduction in aquatic sediments. *Adv. Microb. Ecol.* 16, 41–84. doi: 10.1007/978-1-4615-4187-5_2

Thrash, J. C., and Coates, J. D. (2008). Review: direct and indirect electrical stimulation of microbial metabolism. *Environ. Sci. Technol.* 42, 3921–3931. doi: 10.1021/es702668w

Tracy, B. P., Jones, S. W., Fast, A. G., Indurthi, D. C., and Papoutsakis, E. T. (2012). Clostridia: the importance of their exceptional substrate and metabolite diversity for biofuel and biorefinery applications. *Curr. Opin. Biotechnol.* 23, 364–381. doi: 10.1016/j.copbio.2011.10.008

Tremblay, P.-L., and Zhang, T. (2015). Electrifying microbes for the production of chemicals. *Front. Microbiol.* 6:201. doi: 10.3389/fmicb.2015.00201

Tremblay, P.-L., Zhang, T., Dar, S. A., Leang, C., and Lovley, D. R. (2013). The Rnf complex of *Clostridium ljungdahlii* is a proton-translocating ferredoxin: NAD+ oxidoreductase essential for autotrophic growth. *MBio* 4, e00406–e00412.

Unden, G., and Bongaerts, J. (1997). Alternative respiratory pathways of *Escherischia coli*: energetics and transcriptional regulation in response to electron acceptors. *Biochim. Biophys. Acta* 1320, 217–234. doi: 10.1016/S0005-2728(97)00034-0

Vignais, P. M., and Billoud, B. (2007). Occurrence, classification, and biological function of hydrogenases: an overview. *Chem. Rev.* 107, 4206–4272. doi: 10.1021/cr050196r

Vijgenboom, E., Busch, J. E., and Canters, G. W. (1997). In vivo studies disprove an obligatory role of azurin in denitrification in *Pseudomonas aeruginosa* and show that azu expression is under control of RpoS and ANR. *Microbiology* 143, 2853–2863. doi: 10.1099/00221287-143-9-2853

Wagner, R. C., Regan, J. M., Oh, S.-E., Zuo, Y., and Logan, B. E. (2009). Hydrogen and methane production from swine wastewater using microbial electrolysis cells. *Water Res.* 43, 1480–1488. doi: 10.1016/j.watres.2008.12.037

Wang, S., Huang, H., Kahnt, J., and Thauer, R. K. (2013). A reversible electron-bifurcating ferredoxin-and NAD-dependent [FeFe]-hydrogenase (HydABC) in *Moorella thermoacetica*. *J. Bacteriol.* 195, 1267–1275. doi: 10.1128/JB.02158-12

Welte, C., Krätzer, C., and Deppenmeier, U. (2010). Involvement of Ech hydrogenase in energy conservation of *Methanosarcina mazei*. *FEBS J.* 277, 3396–3403. doi: 10.1111/j.1742-4658.2010.07744.x

White, G. F., Shi, Z., Shi, L., Wang, Z., Dohnalkova, A. C., Marshall, M. J., et al. (2013). Rapid electron exchange between surface-exposed bacterial cytochromes and Fe (III) minerals. *Proc. Natl. Acad. Sci. U.S.A.* 110, 6346–6351. doi: 10.1073/pnas.1220074110

Williams, K. H., Nevin, K. P., Franks, A., Englert, A., Long, P. E., and Lovley, D. R. (2009). Electrode-based approach for monitoring in situ microbial activity during subsurface bioremediation. *Environ. Sci. Technol.* 44, 47–54. doi: 10.1021/es9017464

Wrighton, K. C., Thrash, J. C., Melnyk, R. A., Bigi, J. P., Byrne-Bailey, K. G., Remis, J. P., et al. (2011). Evidence for direct electron transfer by a gram-positive bacterium isolated from a microbial fuel cell. *Appl. Environ. Microbiol.* 77, 7633–7639. doi: 10.1128/aem.05365-11

Yang, Y., Ding, Y., Hu, Y., Cao, B., Rice, S. A., Kjelleberg, S., et al. (2015). Enhancing bidirectional electron transfer of *Shewanella oneidensis* by a synthetic flavin pathway. *ACS Synth. Biol.* doi: 10.1021/sb500331x [Epub ahead of print].

Yang, Y., Xu, M., Guo, J., and Sun, G. (2012). Bacterial extracellular electron transfer in bioelectrochemical systems. *Process Biochem.* 47, 1707–1714. doi: 10.1016/j.procbio.2012.07.032

Zhang, T., Cui, C., Chen, S., Ai, X., Yang, H., Shen, P., et al. (2006). A novel mediatorless microbial fuel cell based on direct biocatalysis of *Escherichia coli*. *Chem. Commun.* 21, 2257–2259. doi: 10.1039/b600876c

Zhang, T., Gannon, S. M., Nevin, K. P., Franks, A. E., and Lovley, D. R. (2010). Stimulating the anaerobic degradation of aromatic hydrocarbons in contaminated sediments by providing an electrode as the electron acceptor. *Environ. Microbiol.* 12, 1011–1020. doi: 10.1111/j.1462-2920.2009.02145.x

Zhang, T., Zeng, Y., Chen, S., Ai, X., and Yang, H. (2007). Improved performances of *E. coli* catalyzed microbial fuel cells with composite graphite/PTFE anodes. *Electrochem. Commun.* 9, 349–353. doi: 10.1016/j.elecom.2006.09.025

Catabolic and regulatory systems in *Shewanella oneidensis* MR-1 involved in electricity generation in microbial fuel cells

Atsushi Kouzuma, Takuya Kasai, Atsumi Hirose and Kazuya Watanabe*

School of Life Sciences, Tokyo University of Pharmacy and Life Sciences, Hachioji, Japan

Shewanella oneidensis MR-1 is a facultative anaerobe that respires using a variety of inorganic and organic compounds. MR-1 is also capable of utilizing extracellular solid materials, including anodes in microbial fuel cells (MFCs), as electron acceptors, thereby enabling electricity generation. As MFCs have the potential to generate electricity from biomass waste and wastewater, MR-1 has been extensively studied to identify the molecular systems that are involved in electricity generation in MFCs. These studies have demonstrated the importance of extracellular electron-transfer (EET) pathways that electrically connect the quinone pool in the cytoplasmic membrane to extracellular electron acceptors. Electricity generation is also dependent on intracellular catabolic pathways that oxidize electron donors, such as lactate, and regulatory systems that control the expression of genes encoding the components of catabolic and electron-transfer pathways. In addition, recent findings suggest that cell-surface polymers, e.g., exopolysaccharides, and secreted chemicals, which function as electron shuttles, are also involved in electricity generation. Despite these advances in our knowledge on the EET processes in MR-1, further efforts are necessary to fully understand the underlying intra- and extracellular molecular systems for electricity generation in MFCs. We suggest that investigating how MR-1 coordinates these systems to efficiently transfer electrons to electrodes and conserve electrochemical energy for cell proliferation is important for establishing the biological basis for MFCs.

Keywords: extracellular electron transfer, bioelectrochemical system, anaerobic respiration, transcriptional regulation, catabolic pathways

Introduction

Microbial fuel cells (MFCs) are devices that use living microbes as catalysts for the conversion of fuels, such as organic compounds, into electricity (Logan et al., 2006; Watanabe, 2008). In MFCs, electrons released by the oxidative catabolism of organic substrates in bacterial cells are transferred to extracellular electrodes, resulting in electricity generation. The natural diversity of bacterial catabolic activities provides MFCs with a great advantage over chemical fuel cells, which typically require purified reactive fuels, such as hydrogen. MFCs are able to generate electricity from a variety of organic substrates, including sugars (Rabaey et al., 2003), cellulose (Ishii et al., 2008), organic acids (Yates et al., 2012), and wastewater pollutants (Miyahara et al., 2012; Yu et al., 2012).
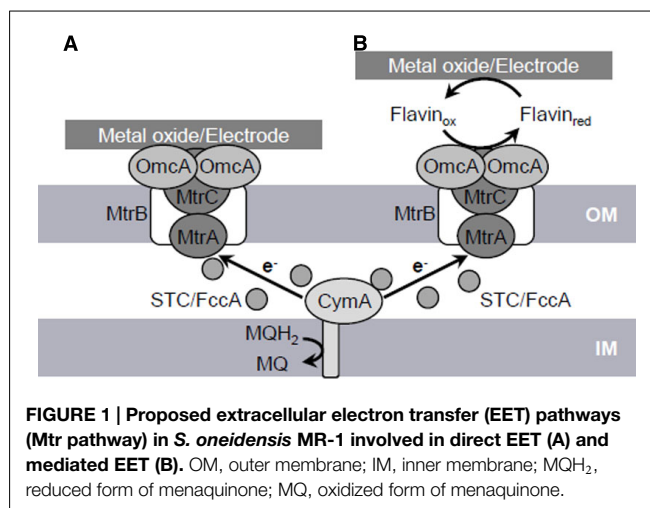
In most MFCs, bacteria, particularly those affiliated with the phylum *Proteobacteria*, mediate the transfer of electrons to anodes (Logan, 2009). These bacteria possess electron-transfer pathways that electrically connect intracellular oxidative catabolic reactions to extracellular electrodes. Certain species of dissimilatory metal-reducing bacteria (DMRB), such as members of the genus *Shewanella*, intrinsically possess such pathways (termed extracellular electron-transfer (EET) pathways), and are therefore able to use electrodes as terminal electron acceptors for respiration (electrode respiration; Shi et al., 2007). *Shewanella* species belong to the class *Gammaproteobacteria* and are widely distributed in nature, including marine, freshwater, sedimentary, and soil environments (Fredrickson et al., 2008). Members of this genus have attracted considerable recent attention due to their respiratory versatility and potential applicability to biotechnological processes, such as bioremediation (Hau and Gralnick, 2007) and MFCs (Kim et al., 1999).

Shewanella oneidensis MR-1 is the most extensively studied strain in the genus *Shewanella* due to its annotated genome sequence (Heidelberg et al., 2002), genetic accessibility, and respiratory versatility (Myers and Nealson, 1988b). This bacterium can respire using a wide variety of organic and inorganic substrates as electron acceptors, including oxygen, fumarate, nitrate, nitrite, thiosulfate, elemental sulfur, trimethylamine N-oxide, dimethyl sulfoxide (DMSO), and anthraquinone-2,6-disulfonate, as well as both soluble and solid metals such as iron, manganese, uranium, chromium, cobalt, technetium, and vanadium (Fredrickson et al., 2008). In addition, MR-1 can transfer electrons to anodes and generate electricity in MFCs without adding exogenous mediators (Kim et al., 1999). For these reasons, MR-1 is a model organism for investigating how bacteria utilize extracellular electron acceptors and generate electricity in MFCs.

The major components of the EET pathway (Mtr pathway) in MR-1 critical for electricity generation in MFCs have been identified. Intracellular catabolic pathways that produce reducing equivalents (e.g., NADH) have also been extensively studied in this species. In addition, several studies have analyzed the transcriptional regulatory systems that control catabolic and electron-transfer pathways in MR-1. In this article, we summarize the current knowledge on catabolic and regulatory systems in *S. oneidensis* MR-1 that are involved in electricity generation in MFCs. The findings from genetic and biochemical studies were reviewed to provide a detailed view of the molecular mechanisms that are directly or indirectly involved in electricity generation by MR-1.

EET Pathway

The respiration of solid metals and electrodes requires a distinct molecular pathway, i.e., the EET pathway, for transferring electrons from intracellular electron carriers (e.g., NADH and quinones), across the inner membrane (IM) and outer membrane (OM), to extracellularly located insoluble electron acceptors. Genetic and biochemical studies have identified five primary protein components, CymA, MtrA, MtrB, MtrC, and OmcA, comprising the EET pathway in *S. oneidensis* MR-1 (the Mtr

FIGURE 1 | Proposed extracellular electron transfer (EET) pathways (Mtr pathway) in *S. oneidensis* MR-1 involved in direct EET (A) and mediated EET (B). OM, outer membrane; IM, inner membrane; MQH$_2$, reduced form of menaquinone; MQ, oxidized form of menaquinone.

pathway; **Figure 1**; Shi et al., 2007). In addition, recent studies have demonstrated that the periplasmic cytochrome pool, which mainly consists of small tetraheme cytochromes (STCs; also referred to as CctA) and flavocytochrome c (FccA) proteins, is also involved in the EET process (Fonseca et al., 2012; Sturm et al., 2015). These findings indicate that the Mtr pathway serves as the major electron conduit that links the IM quinone pool to extracellular solid electron acceptors via a series of electron-transfer reactions between these component proteins.

In the Mtr pathway, EET is initiated by the transfer of electrons from the IM quinone pool to IM-anchored CymA (SO_4591). CymA is a tetraheme c-type cytochrome belonging to the NapC/NirT protein family and consists of a short N-terminal region that is anchored in the IM and a long C-terminal region that protrudes into the periplasm (Myers and Myers, 1997, 2000). The C-terminal region contains four heme-binding sites and mediate electron transfer to a decaheme c-type cytochrome, MtrA, as well as to other periplasmic respiratory proteins, including those responsible for the reduction of DMSO, fumarate, nitrate, and nitrite (Schwalb et al., 2002, 2003; Pitts et al., 2003; Gao et al., 2009; Schuetz et al., 2009).

MtrA (SO_1777) is regarded as a key protein for electron transfer to OM c-type cytochromes (OM-cyts), such as MtrC and OmcA, based on its periplasmic localization and biochemical association with MtrB and MtrC (Hartshorne et al., 2009; Schuetz et al., 2009). MtrB (SO_1776) is an OM-located β-barrel protein consisting of transmembrane β-strands and is required for metal and electrode respiration (Beliaev and Saffarini, 1998; Bretschger et al., 2007). Evidence suggests that MtrB is required for the proper localization and insertion of MtrC and OmcA into the OM (Myers and Myers, 2002). It has also been reported that MtrB forms a stable complex with MtrA and MtrC at a stoichiometry of 1:1:1 and supports electron exchange between these c-type cytochromes by serving as an OM-spanning sheath (Ross et al., 2007; Hartshorne et al., 2009). Interestingly, MtrA was detected in the periplasmic fraction of an *mtrB*-deletion strain, but is localized in the OM fraction in wild-type MR-1, indicating that MtrB supports the *in vivo* localization of MtrA to the OM, although MtrA *per se* is a soluble protein (Hartshorne et al., 2009).

The OM-cyts OmcA (SO_1779) and MtrC (SO_1778) contain 10 heme-binding sites and serve as the terminal reductases for extracellular electron acceptors in the Mtr pathway (Myers and Myers, 2003a, 2004). These OM-cyts are transported to the OM surface by the type-II protein-secretion system (Shi et al., 2008). Biochemical data indicate that OmcA and MtrC form a complex with a stoichiometry of approximately 2:1 (Shi et al., 2006). Genetic studies with MR-1 have demonstrated that current generation in MFCs and reduction rates for insoluble minerals, such as Mn(IV) and Fe(III) oxides, are decreased in single-knockout mutants of *mtrC* and *omcA* and severely impaired in a *mtrC*/*omcA* double-knockout mutant (Beliaev et al., 2001; Myers and Myers, 2001; Bretschger et al., 2007; Newton et al., 2009). In addition, Bretschger et al. (2007) reported that an *mtrC*-overexpressing strain generated 35% more current in an MFC than wild-type MR-1. These observations clearly indicate that OmcA and MtrC play crucial roles in mediating EET reactions at the OM surface. It is likely that the functions of these two OM-cyts partially overlap, as purified MtrC and OmcA proteins are both able to reduce solid Fe(III) oxides (Xiong et al., 2006; Lower et al., 2007), and the overproduction of MtrC can restore the ability of an *omcA*-deletion mutant to reduce MnO_2 (Myers and Myers, 2003b). However, several lines of evidence indicate that functional differences exist between these two OM-cyts. For instance, Lower et al. (2007) reported that OmcA shows a higher affinity toward hematite (α-Fe_2O_3) than MtrC. Furthermore, MtrC appears to play a dominant role in electron-transfer reactions to electrodes, whereas OmcA plays a preferential role in the attachment of cells to solid surfaces (Coursolle et al., 2010; Mitchell et al., 2012).
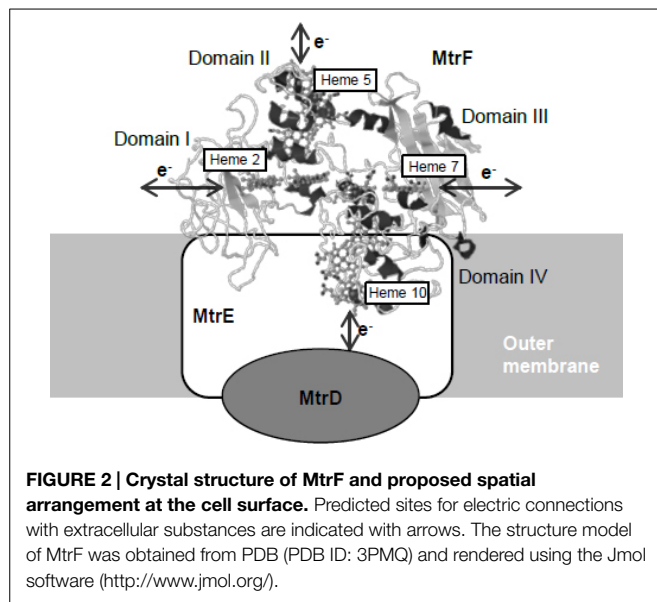
Although many studies have demonstrated that OmcA and the MtrCAB complex play key roles in the Mtr pathway, it is not yet fully understood how electrons are transferred from IM-anchored CymA across the periplasmic space, which has an average distance of 23.5 nm, to the OM components of this pathway (Dohnalkova et al., 2011). One possible explanation is that soluble electron carrier proteins diffuse through the periplasm and mediate electron transfer between CymA and OM-cyts. Consistent with this hypothesis, Fonseca et al. (2012) reported that soluble periplasmic cytochromes, STC (SO_2727) and FccA (SO_0970), interact with both CymA and MtrA with relatively large dissociation constants and thereby promote transient electron-transfer reactions between CymA and MtrA. Furthermore, Sturm et al. (2015) recently reported that the periplasmic space of MR-1 contains abundant soluble c-type cytochromes (approximately 350,000 hemes per cell), and that a double-deletion mutant of *fccA* and *stc* (*cctA*) exhibits substantial growth deficiencies on ferric iron and other soluble electron acceptors. These observations suggest that the periplasmic cytochrome pool, which mainly consists of STC and FccA, plays important roles in mediating electron transfer from CymA to OM-cyts in the Mtr pathway.

Studies have indicated that electrons are transferred from OM-cyts to electrodes via two pathways, direct electron transfer (DET) and mediated electron transfer (MET) pathways (Baron et al., 2009). In DET, electrons are directly transferred from OM-cyts to solid electron acceptors (Xiong et al., 2006; Lower et al., 2007). In contrast, MET involves the transfer of electrons from OM-cyts to distant solid electron acceptors via secreted electron-shuttle compounds, such as flavins (Marsili et al., 2008; von Canstein et al., 2008). Support for the DET process in MR-1 is based on the fact that purified OmcA and MtrC proteins strongly bind and transfer electrons to crystalline Fe(III) oxides and graphite electrodes (Xiong et al., 2006; Lower et al., 2007). Evidence for MET includes the finding that MR-1 can reduce Fe(III) oxides located at a distance from cells and without direct contact (Lies et al., 2005). In addition to this observation, von Canstein et al. (2008) and Marsili et al. (2008) demonstrated that *Shewanella* spp. secrete flavins, including riboflavin and flavin mononucleotide (FMN), which function as electron shuttles for MET. Notably, however, Coursolle et al. (2010) demonstrated that the majority (~90%) of electrons transferred to flavins are released from OmcA and MtrC, indicating that these OM-cyts are also required for MET.

Although MR-1 appears to utilize both DET and MET pathways, several lines of evidence indicate that soluble flavins are indispensable for EET under physiological conditions. For instance, Ross et al. (2009) reported that the direct reduction of insoluble metal oxides by OmcA and MtrC proceeds too slowly to explain the physiological rates of electron transfer, and that the reaction rates of these OM-cyts are markedly increased in the presence of flavins. In addition, Marsili et al. (2008) demonstrated that the accumulation of flavins in MR-1 biofilms increased the rate of electron transfer to an electrode by over threefold. Furthermore, Okamoto et al. (2013) reported that one-electron-reduced flavins bind to OM-cyts as redox cofactors, thereby enhancing the rate of electron transfer at the cell/electrode interface. Together, these studies demonstrate that flavins serve crucial functions in EET via the Mtr pathway.

The X-ray crystal structures of two OM-cyts, MtrF (MtrC homolog) and OmcA, have been resolved to date (Clarke et al., 2011; Edwards et al., 2014), and have provided insights into how electrons are transferred through these decaheme OM-cyts. Clarke et al. (2011) demonstrated that the 10 hemes in MtrF are arranged at a distance of 7 Å from each other, forming an intramolecular electron conduit with a unique "staggered cross" conformation. Based on the heme arrangement and domain configuration of MtrF, four hemes (hemes 2, 5, 7, and 10 located in domains I, II, III, and IV, respectively) that are potentially important for exchanging electrons with other molecules were identified (**Figure 2**). Heme 10 is located at the solvent-exposed terminus of the heme chain and is likely involved in receiving electrons from the MtrDE complex (an electron transfer module homologous to the MtrBA complex). In contrast, heme 5, which is located at the opposite end of the protein, is predicted to be responsible for releasing electrons to extracellular electron acceptors. Hemes 2 and 7, which are located in Greek key split β-barrel domains and contain putative FMN-binding sites (domains I and III), are regarded as possible sites for electron exchange with electron shuttles, such as flavins. Edwards et al. (2014) resolved the crystal structure of OmcA, and reported that its heme arrangement and domain configuration are similar to those of MtrF. These researchers also constructed a model structure of MtrC based on the crystal structure of MtrF, and speculated that the electrostatic surface surrounding heme 7 differ between MtrC and MtrF, suggesting that these

FIGURE 2 | Crystal structure of MtrF and proposed spatial arrangement at the cell surface. Predicted sites for electric connections with extracellular substances are indicated with arrows. The structure model of MtrF was obtained from PDB (PDB ID: 3PMQ) and rendered using the Jmol software (http://www.jmol.org/).

FIGURE 3 | Organization and proposed transcriptional mechanisms of the *mtr* genes. Two CRP-binding sites adjacent to promoters of *omcA* (P$_{omcA}$) and *mtrC* (P$_{mtrC}$) are shown (Kasai et al., 2015).

OM-cyts may differentially interact with substrates (Edwards et al., 2012).

Transcriptional Regulation of EET-Related Genes

In contrast to the extensive biochemical characterization of the Mtr pathway, limited studies have examined how MR-1 regulates EET-related genes at the transcriptional level. In the MR-1 genome, the four genes encoding the proteins comprising OM-cyts in the Mtr pathway (*omcA-mtrCAB*; the *mtr* genes) are organized in a cluster and oriented in the same direction (**Figure 3**). Transcriptional analyses of the *mtr* genes have confirmed that *mtrC*, *mtrA*, and *mtrB* are co-transcribed as an operon (Beliaev et al., 2001; Kasai et al., 2015), a finding that is consistent with the biochemical data showing that the *mtr* gene products form a complex (the MtrCAB complex) at 1:1:1 stoichiometry (Ross et al., 2007). In the *mtr* gene cluster, two different transcription start sites (and promoters) have been identified in the upstream regions of *omcA* and *mtrC* (Beliaev et al., 2001; Shao et al., 2014; Kasai et al., 2015), suggesting that *omcA* and *mtrC* are independently regulated. Previous studies have also demonstrated that a cyclic AMP (cAMP) receptor protein (CRP) and adenylate cyclase (CyaC) are essential for the transcriptional activation of the *mtr* genes (Saffarini et al., 2003; Charania et al., 2009). However, upstream signal transduction pathways involved in the cAMP/CRP-dependent transcriptional activation of the *mtr* genes remain to be elucidated.

In *Escherichia coli*, CRP is a well-known global regulator, and functions in conjugation with cAMP, which is an effector molecule of CRP and serves as a signaling molecule for the expression of numerous genes, including those involved in carbon catabolite repression (Botsford and Harman, 1992). When complexed with cAMP, CRP binds to target DNA sequences, resulting principally in the transcriptional activation of downstream genes, such as those involved in sugar metabolism
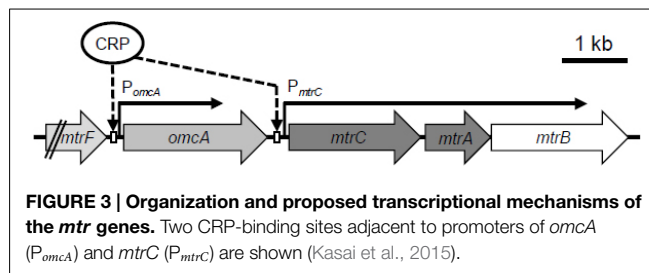
(Botsford and Harman, 1992; Hollands et al., 2007). In *Shewanella* spp., however, evidence suggests that CRP is mainly involved in the regulation of anaerobic respiration (Saffarini et al., 2003; Charania et al., 2009; Murphy et al., 2009). For example, the cAMP/CRP-dependent regulatory system is reported to be essential for regulating anaerobic arsenate reduction in *Shewanella* sp. strain ANA-3 (Murphy et al., 2009), and studies on MR-1 have revealed that CRP is required for the transcriptional activation of genes involved in the reduction of many electron acceptors, including metal oxides (*mtr*), fumarate (*fccA*), nitrate (*nap*), and DMSO (*dms*), under anaerobic conditions (Charania et al., 2009; Dong et al., 2012). Recently, Kasai et al. (2015) investigated the transcriptional mechanisms for the *mtr* genes (*omcA* and *mtrCAB*), and demonstrated that CRP directly regulates the expression of these genes by binding to the upstream regions of *omcA* and *mtrC* (**Figure 3**). Several studies have also demonstrated that expression of the *mtr* genes is up-regulated under electron acceptor-limited conditions (Beliaev et al., 2005; Teal et al., 2006; Pirbadian et al., 2014; Kasai et al., 2015), suggesting that MR-1 controls the expression of these genes in response to intracellular redox or energy status. However, the signal-sensing mechanisms underlying the regulation of the *mtr* genes remain unknown, as CRP is not considered to contain redox-sensing domains, such as PAS (Taylor and Zhulin, 1999). As the addition of cAMP to aerobic cultures of MR-1 results in significant induction of fumarate–reductase activity (Saffarini et al., 2003), intracellular cAMP concentration is likely a key determinant of the ability of MR-1 cells to reduce anaerobic electron acceptors. However, intracellular cAMP concentrations in *Shewanella* are unclear.

In addition to CRP, other transcriptional regulators may be directly or indirectly involved in the regulation of the *mtr* genes. Kasai et al. (2015) reported that the expression of *omcA* and *mtrC* is differentially regulated under different culture conditions, although the transcriptional promoters upstream of these genes (P$_{omcA}$ and P$_{mtrC}$; **Figure 3**) are both dependent on CRP. Interestingly, the researchers also found that deletion of a region upstream of the CRP-binding site of P$_{omcA}$ resulted in a significant increase in promoter activity under aerobic conditions, suggesting that a yet-unidentified regulator(s) binds to the deleted region and negatively regulates the expression of *omcA* (Kasai et al., 2015). These observations indicate that MR-1 possesses regulatory systems for tuning the composition of OM-cyts in response to changes in environmental conditions, despite that the ratio of MtrC to OmcA has been determined only under limited culture conditions (e.g., 2:1; Shi et al., 2006).

Evidence also suggests that ArcA, Fnr (also referred to as EtrA), and Fur may be involved in the transcriptional regulation of

the *mtr* genes in *Shewanella*. ArcA is a DNA-binding response regulator of the bacterial *a*erobic *r*espiration *c*ontrol (Arc) regulatory system and has been well characterized functionally in *E. coli*. The *E. coli* Arc system consists of ArcA and the sensor histidine kinase ArcB, which acts as an indirect oxygen sensor by sensing the redox state of ubiquinone and menaquinone (Georgellis et al., 2001; Malpica et al., 2004; Bekker et al., 2010). Studies have demonstrated that *S. oneidensis* MR-1 has an atypical Arc system consisting of three components, ArcS, HptA, and ArcA, and that the target genes of the MR-1 Arc system substantially differs from those of *E. coli* (Gao et al., 2008; Lassak et al., 2010, 2013). Gao et al. (2008) reported that the expression of several cytochrome *c* genes, including *cymA*, *omcA*, and *mtrC*, is significantly decreased in an *arcA*-deletion mutant of MR-1. Despite this finding, the regulation of the *mtr* genes by ArcA appears to be indirect, as consensus binding sequences for this regulator are not found in the upstream regions of *omcA* and *mtrC* (Gao et al., 2008).

*F*umarate *n*itrate-*r*eduction regulator (Fnr) is another transcriptional regulator that is reported to influence the expression of the *mtr* genes. In *E. coli*, Fnr functions as a sensory protein for environmental oxygen levels by directly reacting with oxygen through a 4Fe–4S cluster (Crack et al., 2004). Cruz-García et al. (2011) reported that the expression levels of *omcA-mtrCAB* and *cymA*, as well as other anaerobic respiratory genes, such as *nap*, *fccA*, and *dms*, are decreased in a *fnr*-deletion mutant of MR-1, suggesting that Fnr acts as a global regulator of many anaerobic catabolic processes in MR-1. However, the authors reported that the deletion of *fnr* did not significantly affect the reduction rates of Fe(III) and Mn(IV) oxides, indicating that, unlike CRP, Fnr only plays a minor role in regulation of the Mtr pathway.

Evidence also suggests that *f*erric *u*ptake *r*egulator (Fur) and intracellular iron levels affect expression of the *mtr* genes and the EET activity of *Shewanella* spp. Fur acts as a sensor for intracellular iron levels in many Gram-negative bacteria, including *E. coli* and *Shewanella* (Hantke, 2001; Wan et al., 2004). Fur complexes with ferrous iron (Fe^{2+}) and regulates the transcription of many genes, including those related to iron uptake and homeostasis (Griggs and Konisky, 1989; Andrews et al., 2003). Considering that large amounts of iron are required for the synthesis of decaheme OM-cyts, it is reasonable to speculate that expression of the *mtr* genes is responsive to intracellular iron concentrations. In support of this assumption, a previous study reported that *mtr*-gene expression was repressed by iron depletion and induced by iron repletion (Yang et al., 2009). In addition, Kouzuma et al. (2012) also demonstrated that iron uptake supported by siderophore synthesis enhances transcription of the *mtr* genes under Mn(IV)-reducing conditions, suggesting that the intracellular iron concentration is a key determinant of the expression levels of the *mtr* genes. Furthermore, Yang et al. (2013) reported that Fur is involved in the regulation of *mtr* homologs in *S. piezotolerans* WP3 by directly binding to the upstream region of an *omcA* homolog (swp3277). In MR-1, the deletion of the *fur* gene decreases *mtr*-gene expression, and a putative Fur-binding site is located upstream of *omcA* (Wan et al., 2004). However, a subsequent study indicated that regulation of the *mtr* genes in

MR-1 is iron responsive but Fur independent, as the transcription of these genes is repressed by iron depletion, even in a *fur*-deletion mutant (Yang et al., 2008). Thus, additional studies are required for elucidating the signal-transduction mechanisms underlying the iron-responsive transcription of the *mtr* genes in MR-1.

The above-mentioned studies indicate that, although the cAMP/CRP-dependent regulatory system plays a direct role in *mtr*-gene regulation, the transcription of these genes is also affected by other regulatory systems. However, it remains to be elucidated how these regulatory systems conjunctively influence the regulation of the Mtr pathway. Gao et al. (2010) have reported in MR-1 that ArcA represses *fnr* and its own transcription and that Fnr also represses *arcA* transcription, indicating that these two regulatory genes are interactively controlled. In addition, the authors have also found that the expression of *crp* is independent of ArcA and Fnr, although it is currently unclear how *crp* is regulated in *Shewanella*. Further investigation is therefore necessary to identify and fully understand the complex environmental-sensing and regulatory networks that regulate the Mtr pathway in MR-1.

Extracellular EET Components

The synthesis and secretion of electron shuttles, such as riboflavin and FMN, are important for EET by *Shewanella* cells. Previous studies have demonstrated that riboflavin and FMN are secreted at concentrations between 250 nM and 1 μM in cultures of MR-1 and other *Shewanella* strains (Marsili et al., 2008; von Canstein et al., 2008; Coursolle et al., 2010), and it is reasonable to speculate that *Shewanella* possesses specific molecular mechanisms for extracellular secretion of flavins. Covington et al. (2010) isolated a MR-1 mutant with decreased ability to secrete riboflavin and FMN, and found that the disruption of *ushA*, which encodes a putative 5′-nucleotidase, resulted in the accumulation of flavin adenine dinucleotide (FAD) in the culture supernatant, along with decreased levels of FMN and riboflavin. Since UshA was located to the periplasmic space and was shown to catalyze the hydrolysis of FAD to FMN (Covington et al., 2010), MR-1 appears to secrete FAD into the periplasm, where it is then hydrolyzed to FMN by UshA. The synthesized FMN likely diffuses through OM pores into the extracellular space and mediates electron-transfer reactions between OM-cyts and extracellular electron acceptors. Riboflavin appears to be produced by the spontaneous hydrolysis of FMN (Covington et al., 2010), and may also contribute to EET reactions.

Studies on MR-1 have also revealed the involvement of other extracellular components in the transfer of electrons to solid metals and electrodes. For example, Gorby et al. (2006) and El-Naggar et al. (2010) reported that, under O_2-limited conditions, MR-1 produces conductive pilus-like structures (referred to as nanowires) that appear to be involved in the reduction of solid Fe(III) oxides and electricity generation in MFCs. MtrC and OmcA were also shown to be required for not only the EET activity of MR-1 cells, but also for the conductivity of nanowires (Gorby et al., 2006; El-Naggar et al., 2010). Consistent with these observations, Pirbadian et al. (2014) recently demonstrated that MR-1 nanowires are not pilus-based structures, but rather,

extensions of the OM and periplasm that include OM-cyts. Interestingly, these authors also provided evidence suggesting that nanowire filaments are formed from chains of membrane vesicles released from MR-1 cells (Pirbadian et al., 2014).

Cell-surface polysaccharides (CSPs) and other biofilm-related components are also reported to influence the EET activity of MR-1. For example, Kouzuma et al. (2010) reported that a mutant deficient in a CSP biosynthesis gene, SO_3177, generated 1.5-fold higher current than wild-type MR-1 in an MFC. In addition, the SO_3177-deficient mutant (ΔSO_3177) also formed larger colonies with a rough surface and exhibited an enhanced ability to adhere to graphite electrodes. Notably, the surface of ΔSO_3177 cells was more hydrophobic than that of wild-type MR-1 cells, suggesting that cell surface hydrophobicity influences the adhesiveness of MR-1 cells to graphite electrodes and current generation in MFCs (Kouzuma et al., 2010). Altered current generation has also been observed for several transposon- (Tn-) insertion mutants of MR-1, including those with Tn insertion in a putative pilus biosynthesis gene (SO_3350) and a gene with unknown function (SO_4704; Tajima et al., 2011). More recently, Kouzuma et al. (2014) identified a Tn-insertion mutant of MR-1 with distinct colony morphology and high current-generating ability. DNA-microarray analyses of this mutant revealed that a number of genes, including those involved in CPS biosynthesis and biofilm formation, were differentially expressed compared to wild-type MR-1, also suggesting the importance of cell-surface structures for current generation by MR-1.

Lactate and Pyruvate Metabolism

Carbon catabolism is comprised a series of enzymatic reactions, in which reducing equivalents, such as NADH, formate, and reduced quinones, are produced from the oxidation of organic matter. The generated reducing equivalents must be removed from the cell for the catabolic reactions to proceed. In MR-1, these reducing equivalents are utilized for the transfer electrons to extracellular electron acceptors via the EET pathway. As can be seen from the main catabolic pathways in MR-1 (**Figure 4**), this strain prefers to catabolize low-molecular-weight organic acids, including lactate and pyruvate (Myers and Nealson, 1988a,b; Scott and Nealson, 1994; Serres and Riley, 2006). MR-1 is able to utilize either D- or L-lactate stereoisomers under both aerobic and anaerobic conditions (Pinchuk et al., 2009). In many aerobic bacteria, the oxidation of lactate to pyruvate is catalyzed by membrane-bound respiratory D- and L-lactate dehydrogenases (D- and L-LDH) that use oxidized quinones as electron acceptors (Kohn and Kaback, 1973; Futai and Kimura, 1977; Ma et al., 2007). Although no homologs of previously characterized bacterial respiratory D- and L-LDHs are present in the MR-1 genome or any other sequenced genome of *Shewanella* spp., a study using a comparative genomic approach identified a MR-1 gene cluster (SO_1522 to SO_1588) consisting of a putative lactate permease gene [*lldP* (SO_1522)] and candidate LDH genes for oxidative lactate utilization (Pinchuk et al., 2009). The putative D-LDH gene [*dld-II* (SO_1521)] is a distant homolog of FAD-dependent LDH in yeast, whereas L-LDH is predicted to be comprised three subunits encoded by *lldEFG* (SO_1520 to SO_1518). Genetic and
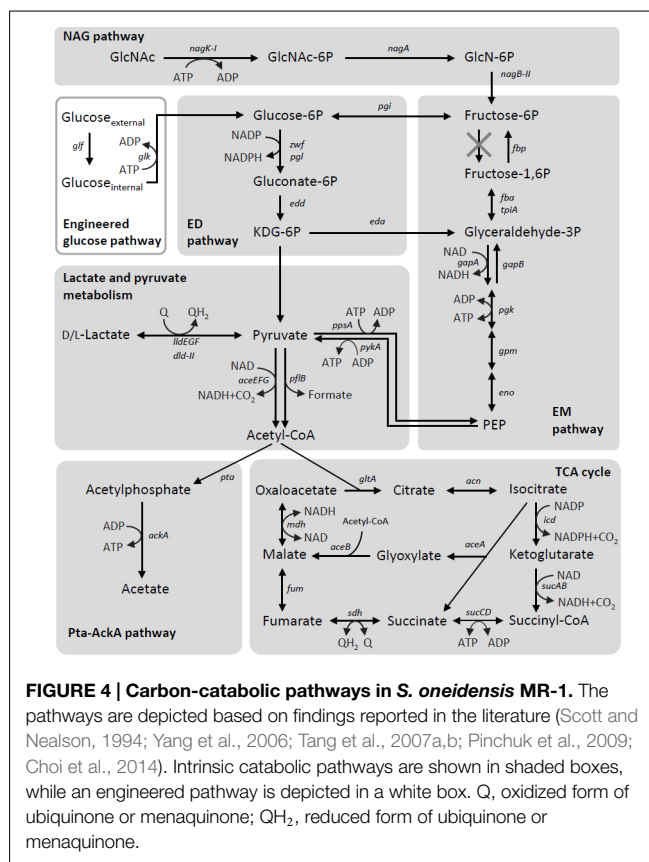
FIGURE 4 | Carbon-catabolic pathways in *S. oneidensis* MR-1. The pathways are depicted based on findings reported in the literature (Scott and Nealson, 1994; Yang et al., 2006; Tang et al., 2007a,b; Pinchuk et al., 2009; Choi et al., 2014). Intrinsic catabolic pathways are shown in shaded boxes, while an engineered pathway is depicted in a white box. Q, oxidized form of ubiquinone or menaquinone; QH₂, reduced form of ubiquinone or menaquinone.

biochemical characterization confirmed that *dld*-II and *lldEFG* encode functional D- and L-LDHs, respectively (Pinchuk et al., 2009). Although these enzymes represent novel types of bacterial LDHs, the results from comparative genomic analysis suggest that homologs of Dld-II and LldEFG are present not only in *Shewanella* and its close relatives, but also in diverse bacteria, including members of *Alphaproteobacteria* and *Betaproteobacteria* (Pinchuk et al., 2009). Notably, although MR-1 utilizes both D- and L-lactate as energy sources, Brutinel and Gralnick (2012) have reported that this strain preferentially utilizes D-lactate, likely due to the inhibition of L-lactate utilization by D-lactate. However, the molecular mechanisms underlying this inhibitory effect remain to be elucidated. These researchers also demonstrated that LlpR (L-*l*actate-*p*ositive regulator, SO_3460) is required for L-lactate utilization by MR-1, although the regulatory mechanisms, including the role of LlpR, in the transcription of LDH genes have not yet been determined.

The end products from lactate metabolism in MR-1 are determined by the growth conditions (Scott and Nealson, 1994; Tang et al., 2007a,b). Under fully aerobic conditions, MR-1 utilizes the complete TCA cycle and therefore does not produce any metabolites from lactate other than CO₂, because the pyruvate produced from lactate is completely oxidized into CO₂ (Tang et al., 2007a). In contrast, under anaerobic conditions, including electricity-generating conditions, MR-1 produces acetate as the main metabolite from lactate (Tang et al., 2007a; Lanthier et al., 2008), mainly due to the decreased activity of enzymes involved in acetate oxidation and the TCA cycle (Scott and

Nealson, 1994). Under these conditions, MR-1 appears to obtain a substantial portion of ATP by substrate-level phosphorylation in the phosphotransacetylase-acetate kinase (Pta-AckA) pathway (Scott and Nealson, 1994; Tang et al., 2007a; Hunt et al., 2010; **Figure 4**). In this pathway, pyruvate is oxidized by the pyruvate dehydrogenase (PDH) complex [*aceEFG* (SO_0424 to SO_0426)] and/or pyruvate formate-lyase [*pflB* (SO_2912)], resulting in the formation of acetyl-CoA and CO_2 or formate, respectively (Pinchuk et al., 2011). The conversion of acetyl-CoA to acetate is catalyzed by acetyltransferase [*pta* (SO_2916)] and acetate kinase [*ackA* (SO_2915)], where ATP is synthesized by substrate-level phosphorylation (Scott and Nealson, 1994; Tang et al., 2007a). As *ack*- and *pta*-deletion mutants of MR-1 are unable to grow on lactate as the sole electron donor and fumarate or Fe(III) citrate as the electron acceptor (Hunt et al., 2010), the Pta-AckA pathway appears to have a crucial role in anaerobic lactate utilization by MR-1.

Sugar Metabolism

Although glucose is an important source of carbon and energy for diverse heterotrophs, and is often used as a growth substrate in various biotechnology processes, including bioelectrochemical systems (Pham et al., 2003; Logan and Regan, 2006), *S. oneidensis* MR-1 lacks a complete glycolytic pathway and is therefore unable to grow on glucose (Myers and Nealson, 1988a; Serres and Riley, 2006; Rodionov et al., 2010). Of the two main pathways for bacterial glucose catabolism, the Embden–Meyerhof–Parnas (EMP) and Entner–Doudoroff (ED) pathways (**Figure 4**), the genome of MR-1 has been shown to code for all of the enzymes needed to reconstruct the ED pathway (Rodionov et al., 2010). The EMP pathway of MR-1 is incomplete, as the genome lacks the gene encoding 6-phosphofructokinase, a key enzyme in this pathway (**Figure 4**; Serres and Riley, 2006; Rodionov et al., 2010), and a glucose/galactose transporter (GluP, SO_2214) is not functional as a result of a frameshift mutation (Romine et al., 2008; Rodionov et al., 2010). In addition, because a glucokinase gene (*glk*) is also not encoded in the genome, MR-1 is unable to catabolize glucose. Although MR-1 has a complete set of genes encoding the phosphoenolpyruvate (PEP):glucose phosphotransferase system (PTS^{Glc}; *ptsHI-crr* and *ptsG*), it is known that this system does not support growth on glucose via the ED pathway, as this glycolytic pathway cannot produce a sufficient amount of PEP for the phosphotransferase reaction (Rodionov et al., 2010). However, MR-1 is capable of growing on *N*-acetylglucosamine using the NAG and ED pathways under aerobic and electrode-respiring conditions (**Figure 4**; Yang et al., 2006; Rodionov et al., 2010).

An interesting feature of *S. oneidensis* MR-1 is that spontaneous mutants able to grow on glucose relatively easily arise, after culture media are supplemented with glucose under aerobic conditions. Biffinger et al. (2008, 2009) showed that glucose was utilized for current generation by *S. oneidensis* after a relatively long adaptation period, when oxygen was supplied to MFCs. Howard et al. (2012) reported that, when exposed to glucose under aerobic conditions, MR-1 gained relatively frequently the ability to utilize glucose. Unfortunately, it remains not to be identified how these mutants gained the ability to catabolize glucose. On the other

hand, it is also shown that the introduction of glucose facilitator (*glf*) and glucokinase (*glk*) genes of *Zymomonas mobilis* allowed MR-1 to generate current using glucose as the electron donor in MFC (the engineered glucose pathway in **Figure 4**) (Choi et al., 2014).

TCA Cycle and its Regulation

The metal-reducing and current-generating bacteria identified to date preferentially utilize low-molecular-weight organic acids, such as lactate and acetate, as carbon and energy sources. As these organic acids are catabolized via the TCA cycle, the metabolic activity of this pathway is an important factor determining the EET activity of current-generating bacteria. *Geobacter* spp. are capable of completely oxidizing acetate to CO_2 under metal-reducing and current-generating conditions (Lovley and Phillips, 1988; Bond and Lovley, 2003). In contrast, MR-1 does not appear to utilize the complete TCA cycle during anaerobic respiration and current generation, as several key genes involved in the TCA cycle, including those encoding the 2-oxoglutarate dehydrogenase complex (*sucAB*), are not sufficiently expressed under anaerobic conditions (Scott and Nealson, 1994; Beliaev et al., 2005; Tang et al., 2007a). When MR-1 catabolizes one lactate molecule without utilizing the TCA cycle, one NADH and one formate are released through the partial oxidation of lactate to acetyl-CoA (**Figure 4**). These metabolites correspond to a total of four electrons, which are one third of the electrons released by the complete oxidation of lactate via the TCA cycle. The low Coulombic efficiencies that are observed in lactate-fed *Shewanella* MFCs are likely attributable to this low recovery of electrons. Newton et al. (2009) reported that the Coulombic efficiencies of lactate-fed air-cathode MFCs inoculated with *S. loihica* PV-4 and *S. oneidensis* MR-1 were 26% and 16%, respectively, as calculated based on the total coulombs produced by the complete oxidation of lactate to CO_2. In addition, substantial amounts of organic acids, predominantly acetate, were accumulated in the electrolyte of both the PV-4 and MR-1 MFCs, suggesting that the TCA cycle is only partially functional in the *Shewanella* MFCs. However, Matsuda et al. (2013) found that the TCA-cycle activity in *S. loihica* PV-4 cells could be modified by changing the electrode potential of the electrochemical cells. Grobbler et al. (2015) also reported the electrode potential-dependent induction of TCA cycle enzymes in electrochemically active biofilms of MR-1. Taken together, these findings suggest that both the extracellular and intracellular redox states are key determinants controlling the TCA-cycle activity in *Shewanella* cells, although the underlying molecular mechanisms remain to be elucidated.

Several studies have indicated that the regulatory systems for the TCA cycle genes of *Shewanella* are distinct from those of *E. coli*. In *E. coli*, many genes involved in the TCA cycle are regulated by the Arc two-component regulatory system (Liu and De Wulf, 2004). Under anaerobic conditions, the kinase activity of sensor kinase ArcB is activated by reduced quinones, and phosphorylated ArcA represses target TCA cycle genes, including those encoding citrate synthase (*gltA*), isocitrate dehydrogenase (*icdA*), succinate dehydrogenase (*sdhABCD*), and malate dehydrogenase (*mdh*, Liu and De Wulf, 2004). However, transcriptome

analyses of MR-1 have revealed that these TCA cycle genes are not regulated by the Arc system (Gao et al., 2008). It has also been reported that although a few TCA cycle genes in *E. coli*, including *acnA* and *sdhABCD*, are regulated by Fur and the related small RNA, RyhB (Massé and Gottesman, 2002), the corresponding genes in MR-1 are not under the control of the Fur/RyhB-dependent regulatory system (Yang et al., 2010). Further studies are therefore needed to elucidate the regulatory mechanisms for TCA cycle genes in MR-1.

Conclusion

MR-1 is an extensively studied model organism for understanding the genetics and biochemistry of bacterial EET and electricity generation in MFCs. Current knowledge on the mechanisms by which bacteria generate electricity in MFCs has largely been obtained from studies performed on MR-1. As described in this article, studies have revealed that many cellular components that are directly and/or indirectly involved in bacterial electricity generation have been identified. However, relatively limited information is available concerning how these components cooperatively work for efficiently generating electricity and conserving energy. As available evidence suggests that the EET pathway is regulated by the level of cAMP, which is an indicator of the cellular energetic states (Charania et al., 2009; Kasai et al., 2015), the EET activity appears to be linked to energy conservation. However, further studies are necessary to determine how cAMP levels are controlled in MR-1 cells. As the intracellular energetic and redox states are two major parameters influencing the global regulation of various cellular activities, future studies addressing how global regulatory systems operate in MR-1 to coordinate catabolic and electron-transfer pathways are needed. As MR-1 is a representative environmental bacterium that thrives in changing environments, such studies are expected to provide useful insights into understanding bacterial lifestyles in the natural environment.

References

Andrews, S. C., Robinson, A. K., and Rodríguez-Quiñones, F. (2003). Bacterial iron homeostasis. *FEMS Microbiol. Rev.* 27, 215–237. doi: 10.1016/S0168-6445(03)00055-X

Baron, D., LaBelle, E., Coursolle, D., Gralnick, J. A., and Bond, D. R. (2009). Electrochemical measurement of electron transfer kinetics by *Shewanella oneidensis* MR-1. *J. Biol. Chem.* 284, 28865–28873. doi: 10.1074/jbc.M109.043455

Bekker, M., Alexeeva, S., Laan, W., Sawers, G., De Mattos, J. T., and Hellingwerf, K. (2010). The ArcBA two-component system of *Escherichia coli* is regulated by the redox state of both the ubiquinone and the menaquinone pool. *J. Bacteriol.* 192, 746–754. doi: 10.1128/JB.01156-09

Beliaev, A. S., Klingeman, D. M., Klappenbach, J. A., Wu, L., Romine, M. F., Tiedje, J. M., et al. (2005). Global transcriptome analysis of *Shewanella oneidensis* MR-1 exposed to different terminal electron acceptors. *J. Bacteriol.* 187, 7138–7145. doi: 10.1128/JB.187.20.7138-7145.2005

Beliaev, A. S., and Saffarini, D. A. (1998). *Shewanella putrefaciens* mtrB encodes an outer membrane protein required for Fe(III) and Mn(IV) reduction. *J. Bacteriol.* 180, 6292–6297.

Beliaev, A. S., Saffarini, D. A., McLaughlin, J. L., and Hunnicutt, D. (2001). MtrC, an outer membrane decahaem c cytochrome required for metal reduction in *Shewanella putrefaciens* MR-1. *Mol. Microbiol.* 39, 722–730. doi: 10.1046/j.1365-2958.2001.02257.x

Biffinger, J. C., Byrd, J. N., Dudley, B. L., and Ringeisen, B. R. (2008). Oxygen exposure promotes fuel diversity for *Shewanella oneidensis* microbial fuel cells. *Biosens. Bioelectron.* 23, 820–826. doi: 10.1016/j.bios.2007.08.021

Biffinger, J. C., Ray, R., Little, B. J., Fitzgerald, L. A., Ribbens, M., Finkel, S. E., et al. (2009). Simultaneous analysis of physiological and electrical output changes in an operating microbial fuel cell with *Shewanella oneidensis*. *Biotechnol. Bioeng.* 103, 524–531. doi: 10.1002/bit.22266

Bond, D. R., and Lovley, D. R. (2003). Electricity production by *Geobacter sulfurreducens* attached to electrodes. *Appl. Environ. Microbiol.* 69, 1548–1555. doi: 10.1128/AEM.69.3.1548-1555.2003

Botsford, J. L., and Harman, J. G. (1992). Cyclic AMP in prokaryotes. *Microbiol. Rev.* 56, 100–122.

Bretschger, O., Obraztsova, A., Sturm, C. A., Chang, I. S., Gorby, Y. A., Reed, S. B., et al. (2007). Current production and metal oxide reduction by *Shewanella oneidensis* MR-1 wild type and mutants. *Appl. Environ. Microbiol.* 73, 7003–7012. doi: 10.1128/AEM.01087-07

Brutinel, E. D., and Gralnick, J. A. (2012). Preferential utilization of D-lactate by *Shewanella oneidensis*. *Appl. Environ. Microbiol.* 78, 8474–8476. doi: 10.1128/AEM.02183-12

Charania, M. A., Brockman, K. L., Zhang, Y., Banerjee, A., Pinchuk, G. E., Fredrickson, J. K., et al. (2009). Involvement of a membrane-bound class III adenylate cyclase in regulation of anaerobic respiration in *Shewanella oneidensis* MR-1. *J. Bacteriol.* 191, 4298–4306. doi: 10.1128/JB.01829-08

Choi, D., Lee, S. B., Kim, S., Min, B., Choi, I.-G., and Chang, I. S. (2014). Metabolically engineered glucose-utilizing *Shewanella* strains under anaerobic conditions. *Bioresour. Technol.* 154, 59–66. doi: 10.1016/j.biortech.2013.12.025

Clarke, T. A., Edwards, M. J., Gates, A. J., Hall, A., White, G. F., Bradley, J., et al. (2011). Structure of a bacterial cell surface decaheme electron conduit. *Proc. Natl. Acad. Sci. U.S.A.* 108, 9384–9389. doi: 10.1073/pnas.1017200108

Coursolle, D., Baron, D. B., Bond, D. R., and Gralnick, J. A. (2010). The Mtr respiratory pathway is essential for reducing flavins and electrodes in *Shewanella oneidensis*. *J. Bacteriol.* 192, 467–474. doi: 10.1128/JB.00925-09

Covington, E. D., Gelbmann, C. B., Kotloski, N. J., and Gralnick, J. A. (2010). An essential role for UshA in processing of extracellular flavin electron shuttles by *Shewanella oneidensis*. *Mol. Microbiol.* 78, 519–532. doi: 10.1111/j.1365-2958.2010.07353.x

Crack, J., Green, J., and Thomson, A. J. (2004). Mechanism of oxygen sensing by the bacterial transcription factor fumarate-nitrate reduction (FNR). *J. Biol. Chem.* 279, 9278–9286. doi: 10.1074/jbc.M309878200

Cruz-García, C., Murray, A. E., Rodrigues, J. L. M., Gralnick, J. A., McCue, L. A., Romine, M. F., et al. (2011). Fnr (EtrA) acts as a fine-tuning regulator of anaerobic metabolism in *Shewanella oneidensis* MR-1. *BMC Microbiol.* 11:64. doi: 10.1186/1471-2180-11-64

Dohnalkova, A. C., Marshall, M. J., Arey, B. W., Williams, K. H., Buck, E. C., and Fredrickson, J. K. (2011). Imaging hydrated microbial extracellular polymers: comparative analysis by electron microscopy. *Appl. Environ. Microbiol.* 77, 1254–1262. doi: 10.1128/AEM.02001-10

Dong, Y., Wang, J., Fu, H., Zhou, G., Shi, M., and Gao, H. (2012). A Crp-dependent two-component system regulates nitrate and nitrite respiration in *Shewanella oneidensis*. *PLoS ONE* 7:e51643. doi: 10.1371/journal.pone.0051643

Edwards, M. J., Baiden, N. A., Johs, A., Tomanicek, S. J., Liang, L., Shi, L., et al. (2014). The X-ray crystal structure of *Shewanella oneidensis* OmcA reveals new insight at the microbe–mineral interface. *FEBS Lett.* 588, 1886–1890. doi: 10.1016/j.febslet.2014.04.013

Edwards, M. J., Fredrickson, J. K., Zachara, J. M., Richardson, D. J., and Clarke, T. A. (2012). Analysis of structural MtrC models based on homology with the crystal structure of MtrF. *Biochem. Soc. Trans.* 40, 1181–1185. doi: 10.1042/BST20120132

El-Naggar, M. Y., Wanger, G., Leung, K. M., Yuzvinsky, T. D., Southam, G., Yang, J., et al. (2010). Electrical transport along bacterial nanowires from *Shewanella oneidensis* MR-1. *Proc. Natl. Acad. Sci. U.S.A.* 107, 18127–18131. doi: 10.1073/pnas.1004880107

Fonseca, B., Paquete, C., Neto, S., Pacheco, I., Soares, C., and Louro, R. (2012). Mind the gap: cytochrome interactions reveal electron pathways across the periplasm of *Shewanella oneidensis* MR-1. *Biochem. J.* 108, 101–108. doi: 10.1042/BJ20121467

Fredrickson, J. K., Romine, M. F., Beliaev, A. S., Auchtung, J. M., Driscoll, M. E., Gardner, T. S., et al. (2008). Towards environmental systems biology of *Shewanella*. *Nat. Rev. Microbiol.* 6, 592–603. doi: 10.1038/nrmicro1947

Futai, M., and Kimura, H. (1977). Inducible membrane-bound l-lactate dehydrogenase from *Escherichia coli*. Purification and properties. *J. Biol. Chem.* 252, 5820–5827.

Gao, H., Wang, X., Yang, Z. K., Chen, J., Liang, Y., Chen, H., et al. (2010). Physiological roles of ArcA, Crp, and EtrA and their interactive control on aerobic and anaerobic respiration in *Shewanella oneidensis*. *PLoS ONE* 5:e15295. doi: 10.1371/journal.pone.0015295

Gao, H., Wang, X., Yang, Z. K., Palzkill, T., and Zhou, J. (2008). Probing regulon of ArcA in *Shewanella oneidensis* MR-1 by integrated genomic analyses. *BMC Genomics* 9:42. doi: 10.1186/1471-2164-9-42

Gao, H., Yang, Z. K., Barua, S., Reed, S. B., Romine, M. F., Nealson, K. H., et al. (2009). Reduction of nitrate in *Shewanella oneidensi*s depends on atypical NAP and NRF systems with NapB as a preferred electron transport protein from CymA to NapA. *ISME J.* 3, 966–976. doi: 10.1038/ismej.2009.40

Georgellis, D., Kwon, O., and Lin, E. C. (2001). Quinones as the redox signal for the arc two-component system of bacteria. *Science* 292, 2314–2316. doi: 10.1126/science.1059361

Gorby, Y. A., Yanina, S., McLean, J. S., Rosso, K. M., Moyles, D., Dohnalkova, A., et al. (2006). Electrically conductive bacterial nanowires produced by *Shewanella oneidensis* strain MR-1 and other microorganisms. *Proc. Natl. Acad. Sci. U.S.A.* 103, 11358–11363. doi: 10.1073/pnas.0604517103

Griggs, D. W., and Konisky, J. (1989). Mechanism for iron-regulated transcription of the *Escherichia coli* cir gene: metal-dependent binding of fur protein to the promoters. *J. Bacteriol.* 171, 1048–1052.

Grobbler, C., Virdis, B., Nouwens, A., Harnisch, F., Rabaey, K., and Bond, P. L. (2015). Use of SWATH mass spectrometry for quantitative proteomic investigation of *Shewanella oneidensis* MR-1 biofilms grown on graphite cloth electrodes. *Syst. Appl. Microbiol.* 38, 135–139. doi: 10.1016/j.syapm.2014.11.007

Hantke, K. (2001). Iron and metal regulation in bacteria. *Curr. Opin. Microbiol.* 4, 172–177. doi: 10.1016/S1369-5274(00)00184-3

Hartshorne, R. S., Reardon, C. L., Ross, D., Nuester, J., Clarke, T. A., Gates, A. J., et al. (2009). Characterization of an electron conduit between bacteria and the extracellular environment. *Proc. Natl. Acad. Sci. U.S.A.* 106, 22169–22174. doi: 10.1073/pnas.0900086106

Hau, H. H., and Gralnick, J. A. (2007). Ecology and biotechnology of the genus *Shewanella*. *Annu. Rev. Microbiol.* 61, 237–258. doi: 10.1146/annurev.micro.61.080706.093257

Heidelberg, J. F., Paulsen, I. T., Nelson, K. E., Gaidos, E. J., Nelson, W. C., Read, T. D., et al. (2002). Genome sequence of the dissimilatory metal ion-reducing bacterium *Shewanella oneidensis*. *Nat. Biotechnol.* 20, 1118–1123. doi: 10.1038/nbt749

Hollands, K., Busby, S. J. W., and Lloyd, G. S. (2007). New targets for the cyclic AMP receptor protein in the *Escherichia coli* K-12 genome. *FEMS Microbiol. Lett.* 274, 89–94. doi: 10.1111/j.1574-6968.2007.00826.x

Howard, E. C., Hamdan, L. J., Lizewski, S. E., and Ringeisen, B. R. (2012). High frequency of glucose-utilizing mutants in *Shewanella oneidensis* MR-1. *FEMS Microbiol. Lett.* 327, 9–14. doi: 10.1111/j.1574-6968.2011.02450.x

Hunt, K. A., Flynn, J. M., Naranjo, B., Shikhare, I. D., and Gralnick, J. A. (2010). Substrate-level phosphorylation is the primary source of energy conservation during anaerobic respiration of *Shewanella oneidensis* strain MR-1. *J. Bacteriol.* 192, 3345–3351. doi: 10.1128/JB.00090-10

Ishii, S., Shimoyama, T., Hotta, Y., and Watanabe, K. (2008). Characterization of a filamentous biofilm community established in a cellulose-fed microbial fuel cell. *BMC Microbiol.* 8:6. doi: 10.1186/1471-2180-8-6

Kasai, T., Kouzuma, A., Nojiri, H., and Watanabe, K. (2015). Transcriptional mechanisms for differential expression of outer membrane cytochrome genes omcA and mtrC in *Shewanella oneidensis* MR-1. *BMC Microbiol.* 15:68. doi: 10.1186/s12866-015-0406-8

Kim, B. H., Kim, H. J., Hyun, M. S., and Park, D. H. (1999). Direct electrode reaction of Fe(III)-reducing bacterium, *Shewanella putrefaciens*. *J. Microbiol. Biotechnol.* 9, 127–131.

Kohn, L. D., and Kaback, H. R. (1973). Mechanisms of active transport in isolated bacterial membrane vesicles. XV. Purification and properties of the membrane-bound D-lactate dehydrogenase from *Escherichia coli*. *J. Biol. Chem.* 248, 7012–7017.

Kouzuma, A., Hashimoto, K., and Watanabe, K. (2012). Roles of siderophore in manganese-oxide reduction by *Shewanella oneidensis* MR-1. *FEMS Microbiol. Lett.* 326, 91–98. doi: 10.1111/j.1574-6968.2011.02444.x

Kouzuma, A., Meng, X.-Y., Kimura, N., Hashimoto, K., and Watanabe, K. (2010). Disruption of the putative cell surface polysaccharide biosynthesis gene SO3177 in *Shewanella oneidensis* MR-1 enhances adhesion to electrodes and current generation in microbial fuel cells. *Appl. Environ. Microbiol.* 76, 4151–4157. doi: 10.1128/AEM.00117-10

Kouzuma, A., Oba, H., Tajima, N., Hashimoto, K., and Watanabe, K. (2014). Electrochemical selection and characterization of a high current-generating *Shewanella oneidensis* mutant with altered cell-surface morphology and biofilm-related gene expression. *BMC Microbiol.* 14:190. doi: 10.1186/1471-2180-14-190

Lanthier, M., Gregory, K. B., and Lovley, D. R. (2008). Growth with high planktonic biomass in *Shewanella oneidensis* fuel cells. *FEMS Microbiol. Lett.* 278, 29–35. doi: 10.1111/j.1574-6968.2007.00964.x

Lassak, J., Bubendorfer, S., and Thormann, K. M. (2013). Domain analysis of ArcS, the hybrid sensor kinase of the *Shewanella oneidensis* MR-1 Arc two-component system, reveals functional differentiation of its two receiver domains. *J. Bacteriol.* 195, 482–492. doi: 10.1128/JB.01715-12

Lassak, J., Henche, A. L., Binnenkade, L., and Thormann, K. M. (2010). ArcS, the cognate sensor kinase in an atypical Arc system of *Shewanella oneidensis* MR-1. *Appl. Environ. Microbiol.* 76, 3263–3274. doi: 10.1128/AEM.00512-10

Lies, D. P., Hernandez, M. E., Kappler, A., Mielke, R. E., Gralnick, J. A., and Newman, D. K. (2005). *Shewanella oneidensis* MR-1 uses overlapping pathways for iron reduction at a distance and by direct contact under conditions relevant for biofilms. *Appl. Environ. Microbiol.* 71, 4414–4426. doi: 10.1128/AEM.71.8.4414-4426.2005

Liu, X., and De Wulf, P. (2004). Probing the ArcA-P modulon of *Escherichia coli* by whole genome transcriptional analysis and sequence recognition profiling. *J. Biol. Chem.* 279, 12588–12597. doi: 10.1074/jbc.M313454200

Logan, B. E., Hamelers, B., Rozendal, R., Schröder, U., Keller, J., Freguia, S. et al. (2006). Microbial fuel cells: methodology and technology. *Environ. Sci. Technol.* 40, 5181–5192. doi: 10.1021/es0605016

Logan, B. E. (2009). Exoelectrogenic bacteria that power microbial fuel cells. *Nat. Rev. Microbiol.* 7, 375–381. doi: 10.1038/nrmicro2113

Logan, B. E., and Regan, J. M. (2006). Electricity-producing bacterial communities in microbial fuel cells. *Trends Microbiol.* 14, 512–518. doi: 10.1016/j.tim.2006.10.003

Lovley, D. R., and Phillips, E. J. (1988). Novel mode of microbial energy metabolism: organic carbon oxidation coupled to dissimilatory reduction of iron or manganese. *Appl. Environ. Microbiol.* 54, 1472–1480.

Lower, B. H., Shi, L., Yongsunthon, R., Droubay, T. C., McCready, D. E., and Lower, S. K. (2007). Specific bonds between an iron oxide surface and outer membrane cytochromes MtrC and OmcA from *Shewanella oneidensis* MR-1. *J. Bacteriol.* 189, 4944–4952. doi: 10.1128/JB.01518-06

Ma, C., Gao, C., Qiu, J., Hao, J., Liu, W., Wang, A., et al. (2007). Membrane-bound l- and D-lactate dehydrogenase activities of a newly isolated *Pseudomonas stutzeri* strain. *Appl. Microbiol. Biotechnol.* 77, 91–98. doi: 10.1007/s00253-007-1132-4

Malpica, R., Franco, B., Rodriguez, C., Kwon, O., and Georgellis, D. (2004). Identification of a quinone-sensitive redox switch in the ArcB sensor kinase. *Proc. Natl. Acad. Sci. U.S.A.* 101, 13318–13323. doi: 10.1073/pnas.0403064101

Marsili, E., Baron, D. B., Shikhare, I. D., Coursolle, D., Gralnick, J. A., and Bond, D. R. (2008). *Shewanella* secretes flavins that mediate extracellular electron transfer. *Proc. Natl. Acad. Sci. U.S.A.* 105, 3968–3973. doi: 10.1073/pnas.0710525105

Massé, E., and Gottesman, S. (2002). A small RNA regulates the expression of genes involved in iron metabolism in *Escherichia coli*. *Proc. Natl. Acad. Sci. U.S.A.* 99, 4620–4625. doi: 10.1073/pnas.032066599

Matsuda, S., Liu, H., Kouzuma, A., Watanabe, K., Hashimoto, K., and Nakanishi, S. (2013). Electrochemical gating of tricarboxylic acid cycle in electricity-producing bacterial cells of *Shewanella*. *PLoS ONE* 8:e72901. doi: 10.1371/journal.pone.0072901

Mitchell, A. C., Peterson, L., Reardon, C. L., Reed, S. B., Culley, D. E., Romine, M. R., et al. (2012). Role of outer membrane c-type cytochromes MtrC and OmcA in *Shewanella oneidensis* MR-1 cell production, accumulation, and detachment during respiration on hematite. *Geobiology* 10, 355–370. doi: 10.1111/j.1472-4669.2012.00321.x

Miyahara, M., Hashimoto, K., and Watanabe, K. (2012). Use of cassette-electrode microbial fuel cell for wastewater treatment. *J. Biosci. Bioeng.* 115, 176–181. doi: 10.1016/j.jbiosc.2012.09.003

Murphy, J. N., Durbin, K. J., and Saltikov, C. W. (2009). Functional roles of arcA, etrA, cyclic AMP (cAMP)-cAMP receptor protein, and cya in the arsenate respiration pathway in *Shewanella* sp. *strain ANA-3*. *J. Bacteriol.* 191, 1035–1043. doi: 10.1128/JB.01293-08

Myers, C. R., and Myers, J. M. (1997). Cloning and sequence of cymA, a gene encoding a tetraheme cytochrome c required for reduction of iron(III), fumarate, and nitrate by *Shewanella putrefaciens* MR-1. *J. Bacteriol.* 179, 1143–1152.

Myers, C. R., and Myers, J. M. (2002). MtrB is required for proper incorporation of the cytochromes OmcA and OmcB into the outer membrane of *Shewanella putrefaciens* MR-1. *Appl. Environ. Microbiol.* 68, 5585–5594. doi: 10.1128/AEM.68.11.5585-5594.2002

Myers, C. R., and Myers, J. M. (2003a). Cell surface exposure of the outer membrane cytochromes of *Shewanella oneidensis* MR-1. *Lett. Appl. Microbiol.* 37, 254–258. doi: 10.1046/j.1472-765X.2003.01389.x

Myers, J. M., and Myers, C. R. (2003b). Overlapping role of the outer membrane cytochromes of *Shewanella oneidensis* MR-1 in the reduction of manganese(IV) oxide. *Lett. Appl. Microbiol.* 37, 21–25. doi: 10.1046/j.1472-765X.2003.01338.x

Myers, C. R., and Myers, J. M. (2004). The outer membrane cytochromes of *Shewanella oneidensis* MR-1 are lipoproteins. *Lett. Appl. Microbiol.* 39, 466–470. doi: 10.1111/j.1472-765X.2004.01611.x

Myers, C. R., and Nealson, K. H. (1988a). Bacterial manganese reduction and growth with manganese oxide as the sole electron acceptor. *Science* 240, 1319–1321. doi: 10.1126/science.240.4857.1319

Myers, C. R., and Nealson, K. H. (1988b). Microbial reduction of manganese oxides—interactions with iron and sulfur. *Geochim. Cosmochim. Acta* 52, 2727–2732. doi: 10.1016/0016-7037(88)90041-5

Myers, J. M., and Myers, C. R. (2000). Role of the tetraheme cytochrome CymA in anaerobic electron transport in cells of *Shewanella putrefaciens* MR-1 with normal levels of menaquinone. *J. Bacteriol.* 182, 67–75. doi: 10.1128/JB.182.1.67-75.2000

Myers, J. M., and Myers, C. R. (2001). Role for outer membrane cytochromes OmcA and OmcB of *Shewanella putrefaciens* MR-1 in reduction of manganese dioxide. *Appl. Environ. Microbiol.* 67, 260–269. doi: 10.1128/AEM.67.1.260-269.2001

Newton, G. J., Mori, S., Nakamura, R., Hashimoto, K., and Watanabe, K. (2009). Analyses of current-generating mechanisms of *Shewanella loihica* PV-4 and *Shewanella oneidensis* MR-1 in microbial fuel cells. *Appl. Environ. Microbiol.* 75, 7674–7681. doi: 10.1128/AEM.01142-09

Okamoto, A., Hashimoto, K., Nealson, K. H., and Nakamura, R. (2013). Rate enhancement of bacterial extracellular electron transport involves bound flavin semiquinones. *Proc. Natl. Acad. Sci. U.S.A.* 110, 7856–7861. doi: 10.1073/pnas.1220823110

Pham, C. A., Jung, S. J., Phung, N. T., Lee, J., Chang, I. S., Kim, B. H., et al. (2003). A novel electrochemically active and Fe(III)-reducing bacterium phylogenetically related to *Aeromonas hydrophila*, isolated from a microbial fuel cell. *FEMS Microbiol. Lett.* 223, 129–134. doi: 10.1016/S0378-1097(03)00354-9

Pinchuk, G. E., Geydebrekht, O. V, Hill, E. A., Reed, J. L., Konopka, A. E., Beliaev, A. S., and Fredrickson, J. K. (2011). Pyruvate and lactate metabolism by *Shewanella oneidensis* MR-1 under fermentation, oxygen limitation, and fumarate respiration conditions. *Appl. Environ. Microbiol.* 77, 8234–8240. doi: 10.1128/AEM.05382-11

Pinchuk, G. E., Rodionov, D. A., Yang, C., Li, X., Osterman, A. L., Dervyn, E., et al. (2009). Genomic reconstruction of *Shewanella oneidensis* MR-1 metabolism reveals a previously uncharacterized machinery for lactate utilization. *Proc. Natl. Acad. Sci. U.S.A.* 106, 2874–2879. doi: 10.1073/pnas.0806798106

Pirbadian, S., Barchinger, S. E., Leung, K. M., Byun, H. S., Jangir, Y., Bouhenni, R. A., et al. (2014). *Shewanella oneidensis* MR-1 nanowires are outer membrane and periplasmic extensions of the extracellular electron transport components. *Proc. Natl. Acad. Sci. U.S.A.* 111, 1–6. doi: 10.1073/pnas.1410551111

Pitts, K. E., Dobbin, P. S., Reyes-Ramirez, F., Thomson, A. J., Richardson, D. J., and Seward, H. E. (2003). Characterization of the *Shewanella oneidensis* MR-1 decaheme cytochrome MtrA: expression in *Escherichia coli* confers the ability to reduce soluble Fe(III) chelates. *J. Biol. Chem.* 278, 27758–27765. doi: 10.1074/jbc.M302582200

Rabaey, K., Lissens, G., Siciliano, S. D., and Verstraete, W. (2003). A microbial fuel cell capable of converting glucose to electricity at high rate and efficiency. *Biotechnol. Lett.* 25, 1531–1535. doi: 10.1023/A:1025484009367

Rodionov, D. A., Yang, C., Li, X., Rodionova, I. A., Wang, Y., Obraztsova, A. Y., et al. (2010). Genomic encyclopedia of sugar utilization pathways in the *Shewanella* genus. *BMC Genomics* 11:494. doi: 10.1186/1471-2164-11-494

Romine, M. F., Carlson, T. S., Norbeck, A. D., McCue, L. A., and Lipton, M. S. (2008). Identification of mobile elements and pseudogenes in the *Shewanella oneidensis* MR-1 genome. *Appl. Environ. Microbiol.* 74, 3257–3265. doi: 10.1128/AEM.02720-07

Ross, D. E., Brantley, S. L., and Tien, M. (2009). Kinetic characterization of OmcA and MtrC, terminal reductases involved in respiratory electron transfer for dissimilatory iron reduction in *Shewanella oneidensis* MR-1. *Appl. Environ. Microbiol.* 75, 5218–5226. doi: 10.1128/AEM.00544-09

Ross, D. E., Ruebush, S. S., Brantley, S. L., Hartshorne, R. S., Clarke, T. A., Richardson, D. J., et al. (2007). Characterization of protein–protein interactions involved in iron reduction by *Shewanella oneidensis* MR-1. *Appl. Environ. Microbiol.* 73, 5797–5808. doi: 10.1128/AEM.00146-07

Saffarini, D. A., Schultz, R., and Beliaev, A. (2003). Involvement of cyclic AMP (cAMP) and cAMP receptor protein in anaerobic respiration of *Shewanella oneidensis*. *J. Bacteriol.* 185, 3668–3671. doi: 10.1128/JB.185.12.3668-3671.2003

Schuetz, B., Schicklberger, M., Kuermann, J., Spormann, A. M., and Gescher, J. (2009). Periplasmic electron transfer via the c-type cytochromes MtrA and FccA of *Shewanella oneidensis* MR-1. *Appl. Environ. Microbiol.* 75, 7789–7796. doi: 10.1128/AEM.01834-09

Schwalb, C., Chapman, S. K., and Reid, G. A. (2002). The membrane-bound tetrahaem c-type cytochrome CymA interacts directly with the soluble fumarate reductase in *Shewanella*. *Biochem. Soc. Trans.* 30, 658–662. doi: 10.1042/BST0300658

Schwalb, C., Chapman, S. K., and Reid, G. A. (2003). The tetraheme cytochrome CymA is required for anaerobic respiration with dimethyl sulfoxide and nitrite in *Shewanella oneidensis*. *Biochemistry* 42, 9491–9497. doi: 10.1021/bi034456f

Scott, J. H., and Nealson, K. H. (1994). A biochemical study of the intermediary carbon metabolism of *Shewanella putrefaciens*. *J. Bacteriol.* 176, 3408–3411.

Serres, M. H., and Riley, M. (2006). Genomic analysis of carbon source metabolism of *Shewanella oneidensis* MR-1: predictions versus experiments. *J. Bacteriol.* 188, 4601–4609. doi: 10.1128/JB.01787-05

Shao, W., Price, M. N., Deutschbauer, A. M., Romine, M. F., and Arkin, A. P. (2014). Conservation of transcription start sites within genes across a bacterial genus. *mBio* 5, e01398–14. doi: 10.1128/mBio.01398-14

Shi, L., Chen, B., Wang, Z., Elias, D. A., Mayer, M. U., Gorby, Y. A., et al. (2006). Isolation of a high-affinity functional protein complex between OmcA and MtrC: two outer membrane decaheme c-type cytochromes of *Shewanella oneidensis* MR-1. *J. Bacteriol.* 188, 4705–4714. doi: 10.1128/JB.01966-05

Shi, L., Deng, S., Marshall, M. J., Wang, Z., Kennedy, D. W., Dohnalkova, A. C., et al. (2008). Direct involvement of type II secretion system in extracellular translocation of *Shewanella oneidensis* outer membrane cytochromes MtrC and OmcA. *J. Bacteriol.* 190, 5512–5516. doi: 10.1128/JB.00514-08

Shi, L., Squier, T. C., Zachara, J. M., and Fredrickson, J. K. (2007). Respiration of metal (hydr)oxides by *Shewanella* and *Geobacter*: a key role for multihaem c-type cytochromes. *Mol. Microbiol.* 65, 12–20. doi: 10.1111/j.1365-2958.2007.05783.x

Sturm, G., Richter, K., Doetsch, A., Heide, H., Louro, R. O., and Gescher, J. (2015). A dynamic periplasmic electron transfer network enables respiratory flexibility beyond a thermodynamic regulatory regime. *ISME J.* 1–10. doi: 10.1038/ismej.2014.264

Tajima, N., Kouzuma, A., Hashimoto, K., and Watanabe, K. (2011). Selection of *Shewanella oneidensis* MR-1 gene-knockout mutants that adapt to an electrode-respiring condition. *Biosci. Biotechnol. Biochem.* 75, 2229–2233. doi: 10.1271/bbb.110539

Tang, Y. J., Hwang, J. S., Wemmer, D. E., and Keasling, J. D. (2007a). *Shewanella oneidensis* MR-1 fluxome under various oxygen conditions. *Appl. Environ. Microbiol.* 73, 718–729. doi: 10.1128/AEM.01532-06

Tang, Y. J., Meadows, A. L., Kirby, J., and Keasling, J. D. (2007b). Anaerobic central metabolic pathways in *Shewanella oneidensis* MR-1 reinterpreted in the light of isotopic metabolite labeling. *J. Bacteriol.* 189, 894–901. doi: 10.1128/JB.00926-06

Taylor, B. L., and Zhulin, I. B. (1999). PAS domains: internal sensors of oxygen, redox potential, and light. *Microbiol. Mol. Biol. Rev.* 63, 479–506.

Teal, T. K., Lies, D. P., Wold, B. J., and Newman, D. K. (2006). Spatiometabolic stratification of *Shewanella oneidensis* biofilms. *Appl. Environ. Microbiol.* 72, 7324–7330. doi: 10.1128/AEM.01163-06

von Canstein, H., Ogawa, J., Shimizu, S., and Lloyd, J. R. (2008). Secretion of flavins by *Shewanella* species and their role in extracellular electron transfer. *Appl. Environ. Microbiol.* 74, 615–623. doi: 10.1128/AEM.01387-07

Wan, X. F., VerBerkmoes, N. C., McCue, L. A., Stanek, D., Connelly, H., Hauser, L. J., et al. (2004). Transcriptomic and proteomic characterization of the Fur modulon in the metal-reducing bacterium *Shewanella oneidensis*. *J. Bacteriol.* 186, 8385–8400. doi: 10.1128/JB.186.24.8385-8400.2004

Watanabe, K. (2008). Recent developments in microbial fuel cell technologies for sustainable bioenergy. *J. Biosci. Bioeng.* 106, 528–536. doi: 10.1263/jbb.106.528

Xiong, Y., Shi, L., Chen, B., Mayer, M. U., Lower, B. H., Londer, Y., et al. (2006). High-affinity binding and direct electron transfer to solid metals by the *Shewanella oneidensis* MR-1 outer membrane c-type cytochrome OmcA. *J. Am. Chem. Soc.* 128, 13978–13979. doi: 10.1021/ja063526d

Yang, C., Rodionov, D. A., Li, X., Laikova, O. N., Gelfand, M. S., Zagnitko, O. P., et al. (2006). Comparative genomics and experimental characterization of *N*-acetylglucosamine utilization pathway of *Shewanella oneidensis*. *J. Biol. Chem.* 281, 29872–29885. doi: 10.1074/jbc.M605052200

Yang, X.-W., He, Y., Xu, J., Xiao, X., and Wang, F.-P. (2013). The regulatory role of ferric uptake regulator (Fur) during anaerobic respiration of *Shewanella piezotolerans* WP3. *PLoS ONE* 8:e75588. doi: 10.1371/journal.pone.0075588

Yang, Y., Harris, D. P., Luo, F., Xiong, W., Joachimiak, M., Wu, L., et al. (2009). Snapshot of iron response in *Shewanella oneidensis* by gene network reconstruction. *BMC Genomics* 10:131. doi: 10.1186/1471-2164-10-131

Yang, Y., Harris, D. P., Luo, F., Wu, L., Parsons, A. B., Palumbo, A. V., and Zhou, J. (2008). Characterization of the *Shewanella oneidensis* Fur gene: roles in iron and acid tolerance response. *BMC Genomics* 9(Suppl. 1), S11. doi: 10.1186/1471-2164-9-S1-S11

Yang, Y., McCue, L. A., Parsons, A. B., Feng, S., and Zhou, J. (2010). The tricarboxylic acid cycle in *Shewanella oneidensis* is independent of Fur and RyhB control. *BMC Microbiol.* 10:264. doi: 10.1186/1471-2180-10-264

Yates, M. D., Kiely, P. D., Call, D. F., Rismani-Yazdi, H., Bibby, K., Peccia, J., et al. (2012). Convergent development of anodic bacterial communities in microbial fuel cells. *ISME J.* 6, 2002–2013. doi: 10.1038/ismej.2012.42

Yu, J., Seon, J., Park, Y., Cho, S., and Lee, T. (2012). Electricity generation and microbial community in a submerged-exchangeable microbial fuel cell system for low-strength domestic wastewater treatment. *Biores. Technol.* 117, 172–179. doi: 10.1016/j.biortech.2012.04.078

Rational engineering of *Geobacter sulfurreducens* electron transfer components: a foundation for building improved *Geobacter*-based bioelectrochemical technologies

Joana M. Dantas[1‡], Leonor Morgado[1†‡], Muktak Aklujkar[2], Marta Bruix[3], Yuri Y. Londer[4], Marianne Schiffer[4], P. Raj Pokkuluri[4] and Carlos A. Salgueiro[1]*

[1] Research Unit on Applied Molecular Biosciences (UCIBIO), Rede de Química e Tecnologia, Departamento de Química, Faculdade de Ciências e Tecnologia, Universidade Nova de Lisboa, Caparica, Portugal, [2] Department of Biological Sciences, Towson University, Towson, MD, USA, [3] Departamento de Química Física Biológica, Instituto de Química-Física "Rocasolano", Consejo Superior de Investigaciones Científicas, Madrid, Spain, [4] Biosciences Division, Argonne National Laboratory, Lemont, IL, USA

Multiheme cytochromes have been implicated in *Geobacter sulfurreducens* extracellular electron transfer (EET). These proteins are potential targets to improve EET and enhance bioremediation and electrical current production by *G. sulfurreducens*. However, the functional characterization of multiheme cytochromes is particularly complex due to the co-existence of several microstates in solution, connecting the fully reduced and fully oxidized states. Over the last decade, new strategies have been developed to characterize multiheme redox proteins functionally and structurally. These strategies were used to reveal the functional mechanism of *G. sulfurreducens* multiheme cytochromes and also to identify key residues in these proteins for EET. In previous studies, we set the foundations for enhancement of the EET abilities of *G. sulfurreducens* by characterizing a family of five triheme cytochromes (PpcA-E). These periplasmic cytochromes are implicated in electron transfer between the oxidative reactions of metabolism in the cytoplasm and the reduction of extracellular terminal electron acceptors at the cell's outer surface. The results obtained suggested that PpcA can couple e^-/H^+ transfer, a property that might contribute to the proton electrochemical gradient across the cytoplasmic membrane for metabolic energy production. The structural and functional properties of PpcA were characterized in detail and used for rational design of a family of 23 single site PpcA mutants. In this review, we summarize the functional characterization of the native and mutant proteins. Mutants that retain the mechanistic features of PpcA and adopt preferential e^-/H^+ transfer pathways at lower reduction potential values compared to the wild-type protein were selected for *in vivo* studies as the best candidates to increase the electron transfer rate of *G. sulfurreducens*. For the first time *G. sulfurreducens* strains have been manipulated by the introduction of mutant forms of essential proteins with the aim to develop and improve bioelectrochemical technologies.

Keywords: *Geobacter*, cytochrome *c*, multiheme, extracellular electron transfer, *Geobacter* mutant strains

Introduction

Biological processes have the potential to promote sustainable energy strategies and to deal with environmental contamination. The hallmark physiological characteristic of the *Geobacteraceae* family of bacteria is their ability to oxidize organic compounds completely to carbon dioxide with the concomitant reduction of various extracellular electron acceptors. These include the reduction of Fe(III) and Mn(IV) oxides, as well as the reduction of soluble U(VI) to insoluble U(IV). The latter process can be utilized for immobilization of uranium to prevent contamination of ground-water (Lovley et al., 1987, 1991; Lovley and Phillips, 1988). *Geobacter* species are also being explored to generate electricity from waste organic matter using electrodes as electron acceptors in microbial fuel cells (Nevin et al., 2008; Yi et al., 2009). The natural abundance of *Geobacter* species in distinct environments and their capability to perform extracellular electron transfer (EET) to reduce toxic/radioactive metals and to convert renewable biomass into electricity prompted their selection as target bacteria for practical biotechnological applications in the areas of bioremediation, bioenergy and biofuel production.

Geobacter sulfurreducens has 111 genes for *c*-type cytochromes, most of which contain multiple hemes (Methé et al., 2003). Gene knockout and proteomic studies identified several *c*-type multiheme cytochromes that participate in EET pathways. These include the inner-membrane heptaheme cytochrome ImcH, the five periplasmic triheme cytochromes of the PpcA family (PpcA-E) and several outer membrane cytochromes (Leang et al., 2003; Lloyd et al., 2003; Methé et al., 2003; Mehta et al., 2005; Holmes et al., 2006; Shelobolina et al., 2007; Ding et al., 2008; Kim and Lovley, 2008; Kim et al., 2008; Nevin et al., 2009; Levar et al., 2014; Liu et al., 2014; Smith et al., 2014). One methodology to develop and improve the bioremediation and electricity production capabilities of *Geobacter* species is to perform rational engineering of the relevant proteins for EET.

G. sulfurreducens expresses various periplasmic cytochromes (Lloyd et al., 2003; Ding et al., 2006) that occupy a strategic position to function as a capacitor (Esteve-Núñez et al., 2008) and control electron flow toward outer membrane components. Therefore, PpcA family cytochromes are in the front line as potential targets to develop mutant strains rationally designed to increase the respiratory rate of *Geobacter*. In order to achieve this goal, it is first necessary to obtain detailed structural and functional data for the targeted electron transfer components. However, the presence of several heme groups in multiheme cytochromes makes the determination of their solution structures difficult (Morgado et al., 2010b). In addition, the co-existence of several microstates connecting the fully reduced and oxidized states complicates the characterization of the individual redox centers and, therefore, of the functional mechanisms of multiheme cytochromes.

In this report, we review the technological and methodological improvements that have contributed to the functional and

structural characterization of *G. sulfurreducens* multiheme cytochromes, using the PpcA family as a model. The structures of all these cytochromes in the oxidized state were determined by protein crystallography (Pokkuluri et al., 2004b, 2010). The solution structure of PpcA was determined in the reduced state by nuclear magnetic resonance (NMR) (Morgado et al., 2012b). The functional mechanisms of PpcA family cytochromes showed that the highly abundant PpcA can couple e^-/H^+ transfer and might contribute to the generation of a proton electrochemical gradient across the cytoplasmic membrane within the physiological ranges of pH and redox potential for *G. sulfurreducens* (Morgado et al., 2010a, 2012a). The well-established structural and functional properties of PpcA were used to design a set of 23 PpcA mutants as a first step toward improving the EET capabilities of *G. sulfurreducens*. The results obtained from the characterization of these mutants are also described in this review. Finally, we report the successful engineering of *G. sulfurreducens* strains to express selected PpcA mutants, a procedure that establishes a foundation for future evaluation of these strains in EET.

Methodological Improvements to Assist the Solution Structural Characterization of Multiheme Cytochromes

Structural determination is a crucial step in understanding the functional mechanisms of proteins with multiple redox centers. NMR spectroscopy enables the determination of protein structures in similar conditions to their physiological environment, providing information about the protein's internal motions and interactions with its redox partners in solution. However, the numerous proton-containing groups of the hemes in cytochromes and the magnetic properties of the heme iron, particularly in the oxidized state, complicate the assignment of the NMR signals (Morgado et al., 2010b; Paixão et al., 2010). Advances in protein expression protocols have contributed to increase the expression yields for mature multiheme cytochromes (Londer et al., 2002, 2005, 2006; Pokkuluri et al., 2004a; Shi et al., 2005) and, concomitantly, to overcome the traditional difficulties associated with the determination of solution structures using natural abundance samples. This rendered the isotopic labeling of multiheme cytochromes much more cost-effective (Fernandes et al., 2008), facilitated the NMR signal assignment procedure and provided the foundations to identify redox partners and map their interacting regions (Dantas et al., 2014). A methodology that enables the isotopic labeling of multiheme cytochromes exclusively in their redox centers was recently reported (Fonseca et al., 2012b) and is expected to be a valuable tool in the assignment of heme signals in very large multiheme cytochromes for which the overlap of signals in the NMR spectra is severe.

The isotopic labeling protocol described by Fernandes et al. (2008) was used to produce ^{15}N- and $^{13}C,^{15}N$-labeled PpcA family cytochromes (Morgado et al., 2010b, 2011, 2012b; Dantas et al., 2015b) and allowed us to obtain in a cost-effective manner proteins labeled in their polypeptide chains with the correct folding and post-translational incorporation of heme groups.

A strategy that simplifies the assignment of the NMR signals of multiheme cytochromes, developed by Morgado and co-workers (Morgado et al., 2010b), combines the analysis of ^{1}H,^{13}C HSQC (heteronuclear single-quantum coherence) NMR spectra obtained for an un-labeled sample and for a sample labeled exclusively in its polypeptide chain. A simple comparison of these spectra allows a straightforward discrimination between the heme and the polypeptide chain signals and is illustrated for PpcA in **Figure 1**.

Taking advantage of the methodologies described above, the NMR fingerprints, including heme proton signals and protein backbone and side-chain NH signals, were identified for the PpcA family cytochromes in both oxidized and reduced forms (Morgado et al., 2011; Dantas et al., 2014, 2015b). Chemical shift perturbation measurements on these fingerprints can quickly provide valuable information for investigation of EET respiratory mechanisms in *G. sulfurreducens*. Such investigations can involve protein-protein and protein-ligand interactions studies to survey and identify electron transfer between redox partners and establish foundations to engineer modified redox proteins for various applications. An example is provided for chemical shift perturbation studies carried out on PpcA at increasing concentrations of the humic substance analog anthraquinone-2,6-disulfonate (AQDS) (**Figure 2**). These studies showed that PpcA interacts with oxidized or reduced AQDS in the positively charged surface near heme IV (Dantas et al., 2014). When

complemented with kinetic experiments, bidirectional electron transfer between PpcA and the humic substance analog was revealed for the first time. Such behavior might confer a selective advantage to *G. sulfurreducens*, which can modulate its energy metabolism according to the redox state of the humic substances available in the environment (Dantas et al., 2014). However, the precise mechanisms underlying the reduction of humic substances by *G. sulfurreducens* are still under debate. Lloyd et al. (2003) suggested that PpcA may transfer electrons directly to AQDS or humic materials that are able to traverse the outer membrane. On the other hand, Voordeckers et al. (2010) showed that the simultaneous deletion of genes coding for outer-membrane cytochromes OmcB, OmcS, OmcT, OmcE, and OmcZ yielded to a complete inhibition of AQDS reduction. Under the hypothesis that AQDS or humic substances are unable to access the periplasmic space of *G. sulfurreducens*, the interaction studies between AQDS and PpcA should be envisioned as working models (Dantas et al., 2014, 2015a). These models are even more relevant as no structural data are currently available for any of the outer membrane cytochromes mentioned above.

Isotopically labeled PpcA samples were also used to assist the determination of its solution structures in the oxidized and reduced states (Morgado et al., 2012b). Structural data are crucial to establish structure-function relationships, and therefore to optimize the rational design of electron transfer complexes that

FIGURE 1 | 2D ^{1}H,^{13}C HSQC NMR spectra of oxidized PpcA (pH 5.5 and 298 K). The spectra correspond to PpcA samples: labeled (^{13}C/^{15}N) exclusively in its polypeptide chain (black contours) and unlabeled sample (red contours). The red contours that are not overlapped with black contours correspond to the heme signals. The inset represents the lowest energy

NMR solution structure of PpcA (PDB code 2LDO, Morgado et al., 2012b). The peptide chain and the hemes are colored gray and red, respectively. The hemes are numbered I, III and IV, a designation that derives from the superimposition of the hemes of PpcA and other cytochromes c_7 with those of the structurally homologous tetraheme cytochromes c_3.

FIGURE 2 | Overlay of 2D ^{1}H,^{15}N HSQC NMR spectra of ^{15}N-enriched oxidized (A) and reduced PpcA (B) in the presence of increasing amounts of the humic substance analog AQDS. The assignments of NH signals are indicated. In the spectra the amount of AQDS increases from blue to orange contours. The insets show the surface map of significantly perturbed residues in PpcA (PDB code, 2LDO, Morgado et al., 2012b) upon binding of AQDS. The chemical shift perturbation increases from yellow (small) to red (large). Heme IV is shown in red and hemes I and III are shown in black. The molecular surfaces were generated in PyMOL (Wl, 2002).

can improve the efficiency of microbial fuel cells and other *G. sulfurreducens* -based biotechnological applications (see below).

Thermodynamic Characterization of Multiheme Cytochromes

The reduction potential of a monoheme cytochrome can be obtained directly by the application of the Nernst equation, where

n is the number of electrons involved in the reaction:

$$E = E^0 + \frac{RT}{nF} ln \frac{[ox]}{[red]} \tag{1}$$

In this case, only the fully reduced and oxidized states co-exist in solution and the e_{app}-value (i.e., the point at which the oxidized and reduced fractions are equal) corresponds to the reduction potential of the heme group. This is illustrated in **Figure 3**

FIGURE 3 | Electronic distribution scheme for monoheme (OmcF) and triheme (PpcA) cytochromes showing the possible microstates in each situation. The inner circles represent heme groups, which can either be reduced (red circles) or oxidized (white circles). The microstates are grouped according to the number of oxidized hemes in each oxidation stage, connected by consecutive one-electron redox steps. P_{0H} and P_0 represent the reduced protonated and deprotonated microstates, respectively. P_{ijkH} and P_{ijk}, indicate, respectively, the protonated and deprotonated

microstates, where *i*, *j*, and *k* represent the heme(s) that are oxidized in that particular microstate. In the lower panels potentiometric redox titrations followed by visible spectroscopy of OmcF and PpcA (pH 7) are indicated. Solid lines indicate the result of the fits for the Nernst equation (OmcF) and for a model of three consecutive reversible redox steps between the different oxidation stages (PpcA) (Morgado et al., 2008; Pokkuluri et al., 2009). The structures of OmcF (PDB code, 3CU4, Pokkuluri et al., 2009) and PpcA (PDB code, 2LDO, Morgado et al., 2012b) are represented in the inset.

for monoheme cytochrome OmcF from *G. sulfurreducens*. The fitting of Equation (1) to the data obtained from potentiometric redox titrations followed by visible spectroscopy for OmcF yielded an e_{app}-value of +180 mV. On the other hand, redox titrations by potentiometric or electrochemical methods for multiheme cytochromes typically describe the whole-protein macroscopic redox behavior because the techniques cannot discriminate the reduction potentials of the individual redox centers. To illustrate this aspect, a potentiometric redox titration obtained for the triheme cytochrome PpcA is also represented in **Figure 3**. The experimental data can be fitted to a model

that considers sequential midpoint reduction potentials for each center (Turner et al., 1996). However, this model is purely macroscopic and the reduction potentials obtained from the fitting ($E_1 = -171$ mV; $E_2 = -119$ mV; $E_3 = -60$ mV), designated macroscopic reduction potentials, cannot be formally assigned to any specific heme in the protein. This is a consequence of the co-existence of several microstates in solution connecting the reduced and oxidized states. **Figure 3** illustrates the microstates for a triheme cytochrome with one redox-Bohr center. In this case, the 16 microstates can be grouped according to the number of oxidized hemes in four macroscopic

oxidation stages linked by successive one-electron reductions. For multiheme cytochromes containing higher numbers of hemes (N) and redox-Bohr centers (NB), the distribution can be easily scaled up. The total number of microstates and oxidation stages would be given by $2^N(NB + 1)$ and $N + 1$, respectively. The microstates are interrelated by a set of Nernst equations and the mathematical formalism underlying the thermodynamic model that permits determination of the redox properties of the heme groups was first derived by Turner et al. (1996).

In addition to the pH of the solution (redox-Bohr interactions), the reduction potential of the hemes in multiheme cytochromes can be modulated by redox interactions with neighboring hemes, which can become quite significant when iron-iron distances are very short (Fonseca et al., 2012a). Therefore, for a triheme cytochrome the simplest model to describe the energy of the microstates over the full range of pH and solution potential, taking as reference the fully reduced and protonated protein, requires consideration of 10 parameters: the three energies of oxidation of the hemes (reduction potentials), the pK_a of the redox-Bohr center, and six two-center interaction energies (three heme–heme and three redox-Bohr). In order to achieve this it is necessary to monitor the oxidation profile of each heme at different pH values by NMR and complement this information with the data obtained from potentiometric redox titrations monitored by visible spectroscopy, as described by Turner et al. (1996).
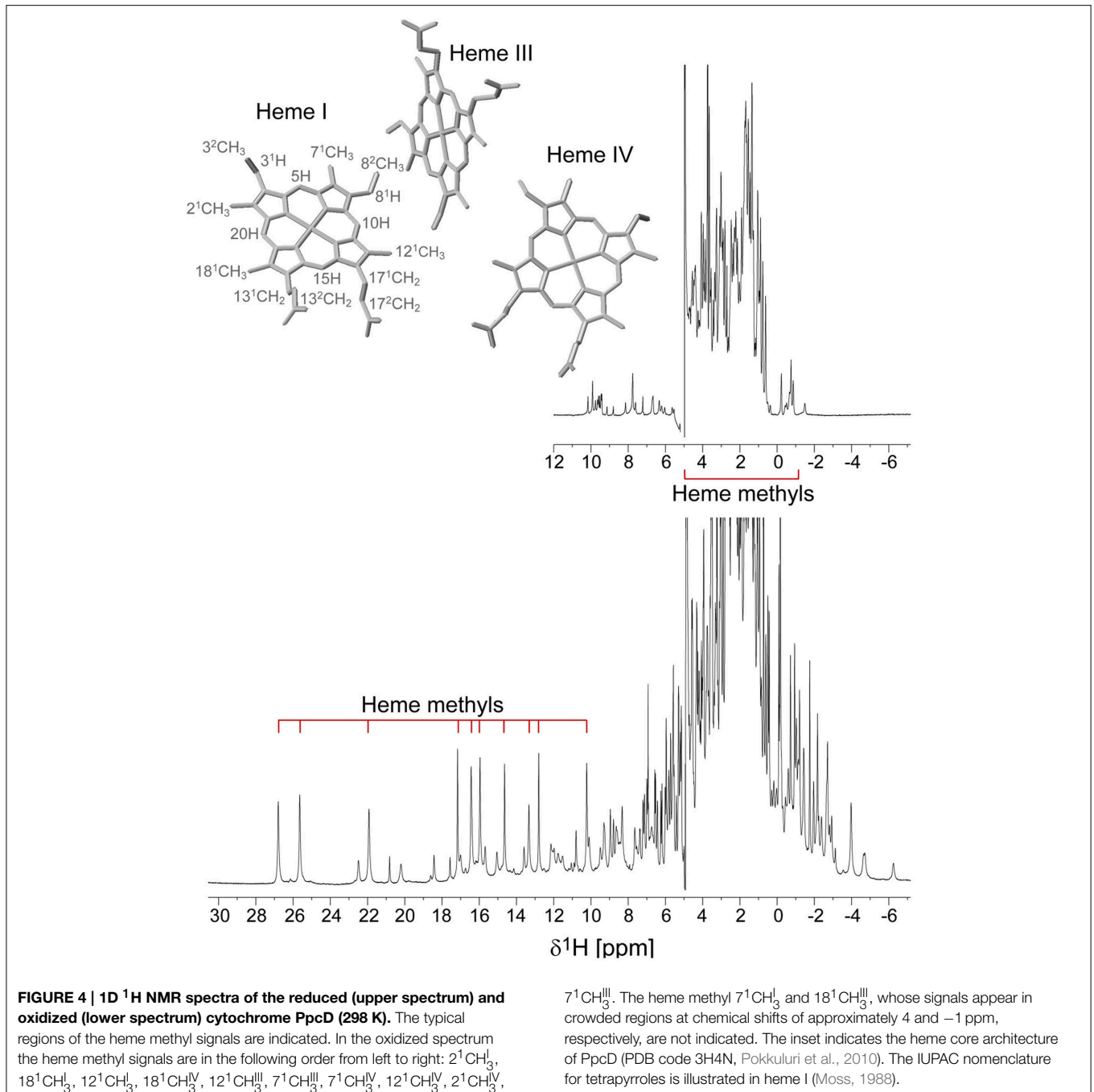
Thermodynamic Characterization of PpcA Family Cytochromes from *G. sulfurreducens*

The PpcA family cytochromes contain between 70 and 75 amino acids and three *c*-type hemes axially co-ordinated by two histidine residues (Pokkuluri et al., 2004b, 2010; Morgado et al., 2012b). The hemes are low spin in both diamagnetic ($S = 0$) reduced state and paramagnetic ($S = 1/2$) oxidized state (Morgado et al., 2010c; Dantas et al., 2011). These features are convenient in that they provide well-resolved ^1H NMR spectra in both states. NMR explores the highly distinct features of the low-spin heme signals in the diamagnetic and paramagnetic forms. In the diamagnetic form, the chemical shifts of the heme substituents are dominated by the porphyrin ring-current effects and, therefore, appear in well-defined regions of the ^1H NMR spectra (**Figure 4**) (Morgado et al., 2007, 2008, 2010a). In contrast, in the oxidized form the unpaired electron of each heme iron exerts significant paramagnetic shifts on the heme signals. Consequently, the same heme signals are differently affected by the paramagnetic centers, have different levels of broadening and are spread over the entire spectral width (**Figure 4**) (Morgado et al., 2010c; Dantas et al., 2011). As illustrated in **Figure 4**, the heme methyl signals are typically shifted to higher ppm values as the oxidation of the proteins progresses and, therefore, are ideal candidates to monitor the stepwise oxidation of the individual hemes throughout the different oxidation stages (see **Figure 3**). The heme methyl chemical shifts are proportional to the oxidized fraction of a particular heme, and therefore contain information

about the redox properties of each heme (Morgado et al., 2010a). However, in order to probe the stepwise oxidation of the hemes, it is necessary to meet conditions of fast intramolecular electron exchange (between the different microstates within the same oxidation stage) and slow intermolecular electron exchange (between different oxidation stages) on the NMR timescale (Morgado et al., 2008). Slower intermolecular electron exchange can be favored by decreasing the temperature, decreasing the sample concentration or increasing the ionic strength of the solution. Earlier studies aiming to monitor the stepwise oxidation of the hemes in cytochrome PpcA were carried out at relatively high ionic strength (500 mM) and using a NMR spectrometer operating at 500 MHz (Pessanha et al., 2006). However, signal broadness was observed for the connectivities between the heme methyl signals in the different oxidation stages (**Figure 5**). The use of high-magnetic-field NMR spectrometers equipped with cryoprobes is an excellent example of how progress in the NMR technology has contributed to the detailed characterization of multiheme cytochromes (Morgado et al., 2010a). This equipment permitted the use of less concentrated samples (as low as 70 μM) and low ionic strength solutions, favoring the slow intermolecular electron exchange regime between the different oxidation stages. Under these new experimental conditions, well-resolved 2D-exchange NMR spectroscopy (EXSY) spectra were obtained for PpcA family cytochromes (**Figure 5**). The stepwise oxidation of the hemes monitored by NMR experiments carried out in the conditions mentioned above, combined with data obtained from potentiometric redox titrations, allowed us to determine with higher precision the detailed redox properties of PpcA family cytochromes (Morgado et al., 2010a). The only exception was in the case of PpcC, which presented different conformations at intermediate stages of oxidation, leading to a splitting and an excessive broadening of the NMR signals, making it impossible to follow the oxidation profile of the individual hemes (Morgado et al., 2007).

Functional Mechanisms of PpcA Family Cytochromes

The thermodynamic parameters obtained for the aforementioned cytochromes in the fully reduced and protonated state showed that the heme reduction potentials are negative, differ from each other, and cover different functional ranges (**Table 1**). These reduction potentials are strongly modulated by redox interactions amongst the three hemes (covering a range of 3–46 mV) and by redox-Bohr interactions between the hemes and a redox-Bohr center (2 to −58 mV), which was identified as heme IV propionate P_{13} (Morgado et al., 2008, 2012b). The positive values of the redox interactions indicate that the oxidation of a particular heme renders the oxidation of its neighbors more difficult, whereas the typically negative values observed for the redox-Bohr interactions show that the oxidation of the hemes facilitates the deprotonation of the redox-Bohr center and *vice versa*. Consequently, during the redox cycle of the protein the affinity of each redox center for electrons is tuned by the oxidation states of neighboring hemes

FIGURE 4 | 1D ^{1}H NMR spectra of the reduced (upper spectrum) and oxidized (lower spectrum) cytochrome PpcD (298 K). The typical regions of the heme methyl signals are indicated. In the oxidized spectrum the heme methyl signals are in the following order from left to right: $2^1CH_3^I$, $18^1CH_3^I$, $12^1CH_3^I$, $18^1CH_3^{IV}$, $12^1CH_3^{III}$, $7^1CH_3^{III}$, $7^1CH_3^{IV}$, $12^1CH_3^{IV}$, $2^1CH_3^{IV}$, $7^1CH_3^{III}$. The heme methyl $7^1CH_3^I$ and $18^1CH_3^{III}$, whose signals appear in crowded regions at chemical shifts of approximately 4 and −1 ppm, respectively, are not indicated. The inset indicates the heme core architecture of PpcD (PDB code 3H4N, Pokkuluri et al., 2010). The IUPAC nomenclature for tetrapyrroles is illustrated in heme I (Moss, 1988).

and by the pH, such that their apparent midpoint reduction potentials (e_{app}) are different compared to the values for the fully reduced and protonated protein. The e_{app}-values for the heme groups of PpcA, PpcB, PpcD, and PpcE at physiological pH are indicated in **Figure 6A**. The contribution of each microstate in each oxidation stage (see **Figure 3**) can also be determined from the thermodynamic parameters listed in **Table 1**. The results clearly showed that PpcA and PpcD have dominant microstates during the redox cycle of the proteins (**Figure 6B**). In the case of PpcA, oxidation stages 0 and 1 are dominated by the forms

P_{0H} and P_{1H}, respectively, in which the redox-Bohr center is kept protonated. Stage 2 is dominated by the oxidation of heme IV and deprotonation of the redox-Bohr center (P_{14}), which remains deprotonated in stage 3 (P_{134}). Therefore, a route is defined for the electrons within PpcA: $P_{0H} \rightarrow P_{1H} \rightarrow P_{14} \rightarrow P_{134}$. In the case of PpcD, a different profile for electron transfer is observed that favors a proton-coupled $2e^-$ transfer step between oxidation stages 0 and 2: $P_{0H} \rightarrow P_{14} \rightarrow P_{134}$. In the case of PpcB and PpcE, several microstates are significantly populated in oxidation stages 1 and 2, and therefore no preferential pathway
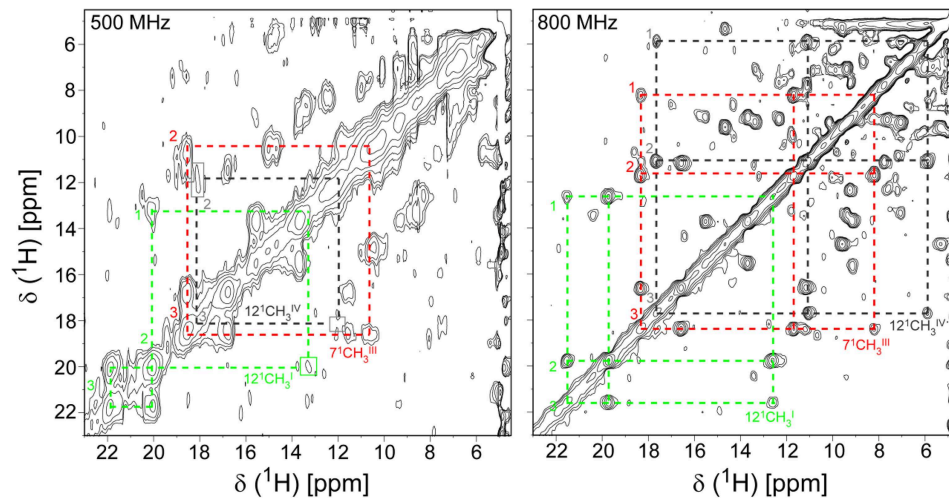
FIGURE 5 | Expansions of 2D EXSY NMR spectra of PpcA acquired at 500 MHz (500 mM ionic strength) and 800 MHz (250 mM ionic strength), at different levels of oxidation (288 K and pH 6). Cross-peaks resulting from intermolecular electron transfer across the oxidation stages 1–3 are indicated by dashed lines for the hemes $12^1CH_3^I$ (green), $7^1CH_3^{III}$ (red), and $12^1CH_3^{IV}$ (black). Signals connecting oxidation stage 1 are not visible at 500 MHz due the poor quality of this spectrum. Roman and Arabic numbers indicate the hemes and the oxidation stages, respectively. In order to prevent overcrowding of the figure, the 2D EXSY NMR spectra with cross-peaks to oxidation stage 0 are not shown.

TABLE 1 | Thermodynamic parameters for PpcA, PpcB, PpcD, and PpcE (Morgado et al., 2010a).

Cytochrome	Energy (meV)			
	Heme I	Heme III	Heme IV	Redox-Bohr center
PpcA				
Heme I	**−154 (5)**	27 (2)	16 (3)	−32 (4)
Heme III		**−138 (5)**	41 (3)	−31 (4)
Heme IV			**−125 (5)**	−58 (4)
Redox-Bohr center				**495 (8)**
PpcB				
Heme I	**−150 (3)**	17 (2)	8 (2)	−16 (4)
Heme III		**−166 (3)**	32 (2)	−9 (4)
Heme IV			**−125 (3)**	−38 (4)
Redox-Bohr center				**426 (8)**
PpcD				
Heme I	**−156 (6)**	46 (3)	3 (4)	−28 (6)
Heme III		**−139 (6)**	14 (4)	−23 (6)
Heme IV			**−149 (6)**	−53 (6)
Redox-Bohr center				**501 (8)**
PpcE				
Heme I	**−167 (4)**	27 (3)	5 (3)	−12 (4)
Heme III		**−175 (4)**	22 (3)	2 (4)
Heme IV			**−116 (5)**	−13 (4)
Redox-Bohr center				**445 (10)**

All energies are reported in meV, with standard errors given in parentheses. For each cytochrome, the fully reduced and protonated protein was taken as reference. Diagonal values (in bold) correspond to oxidation energies of the hemes and deprotonating energy of the redox-Bohr center. Off-diagonal values are the redox (heme–heme) and redox-Bohr (heme–proton) interaction energies.

for electron transfer can be established. For further details on the fractional contribution of each microstate in each oxidation stage see Morgado et al. (2010a). The different functional mechanisms shown by the four periplasmic cytochromes indicate that they have evolved to perform different functions in the cell and illustrate how proteins with closely related structures can specifically fine-tune the properties of their redox centers.

Rational Design of PpcA Mutant Forms

PpcA is the most abundant cytochrome in *G. sulfurreducens* during growth on soluble and insoluble iron, and is most likely a reservoir of electrons destined for the outer surface (Ding et al., 2008). Therefore, it plays a crucial role by bridging electron transfer from cytoplasmic oxidation reactions to the reduction of extracellular terminal electron acceptors. The redox-Bohr effect in PpcA observed under physiologically relevant conditions, the magnitude of which is the highest amongst the PpcA family members (see **Table 2**), might implicate this protein in the e^-/H^+ coupling mechanisms that sustain cellular growth. In addition, structural data were obtained for this cytochrome in both oxidized and reduced forms (Pokkuluri et al., 2004b, 2010; Morgado et al., 2012b). For these reasons, PpcA was selected for rational design of mutant proteins, an essential step toward engineering variants of *G. sulfurreducens* with increased respiratory rates. A set of 23 PpcA-mutants was produced, following the protein expression and purification protocols previously described for the wild-type (Londer et al., 2002; Fernandes et al., 2008). The designed mutants covered sites in different regions of the protein and included: (i) conserved residues amongst PpcA family members located in the region of heme III (V13A, V13I, V13S, and V13T) and between hemes I and III (F15Y, F15W, and F15L); (ii) a residue M58 that was hypothesized to control the solvent accessibility of heme III (M58S; M58D; M58N, M58K) and (iii) lysine residues located
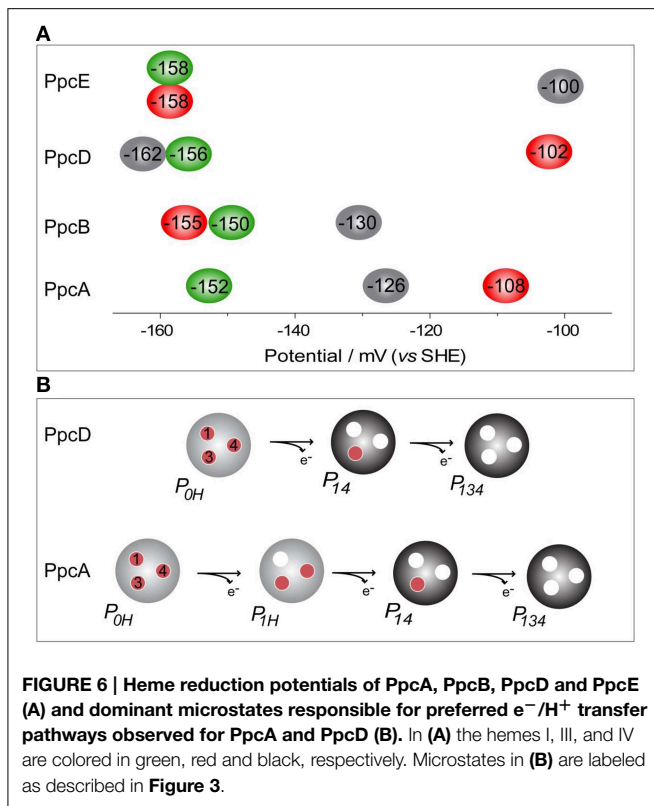
FIGURE 6 | Heme reduction potentials of PpcA, PpcB, PpcD and PpcE (A) and dominant microstates responsible for preferred e⁻/H⁺ transfer pathways observed for PpcA and PpcD (B). In (A) the hemes I, III, and IV are colored in green, red and black, respectively. Microstates in (B) are labeled as described in **Figure 3**.

FIGURE 7 | Spatial location of residues mutated in PpcA solution structure (PDB code, 2LDO, Morgado et al., 2012b). The PpcA polypeptide chain (gray) is shown as Cα ribbon and heme groups (red). The side-chain of K9, K18, K22, K43, K52, and K60 (green); V13 and F15 (orange); M58 (blue) are represented as stick drawings.

TABLE 2 | Macroscopic pK_a-values of the redox-Bohr center for PpcA, PpcB, PpcD, and PpcE in the reduced (pK_{red}) and oxidized states (pK_{ox}) (Morgado et al., 2010a).

	PpcA	PpcB	PpcD	PpcE
pK_{red}	8.6	7.4	8.7	7.7
pK_{ox}	6.5	6.3	6.9	7.4
$\Delta pK_a (pK_{red} - pK_{ox})$	2.1	1.1	1.8	0.3

near the hemes: K18 (near heme I), K22 (between hemes I and III), K60 (near heme III) and K9, K43 and K52 (near heme IV). In the last group of mutants, each lysine was substituted by glutamine and glutamic acid. The spatial location of each replaced residue is illustrated using the solution structure of PpcA (**Figure 7**).

Impact of the Mutations on the Global Fold and Heme Core of the Proteins

For each protein, the impact of the mutations on the global fold and heme core was probed by comparing the dispersion of both the heme proton and the polypeptide NH signals in 2D ¹H-NOESY and ¹H,¹⁵N-HSQC NMR spectra, respectively (Dantas et al., 2012; Morgado et al., 2013, 2014). For all the mutants, the protein global fold and heme core were conserved and changes in the chemical shifts were only observed for residues in the vicinity of the mutant site. It was possible to determine the heme oxidation profiles for 19 mutants (**Table 3**).
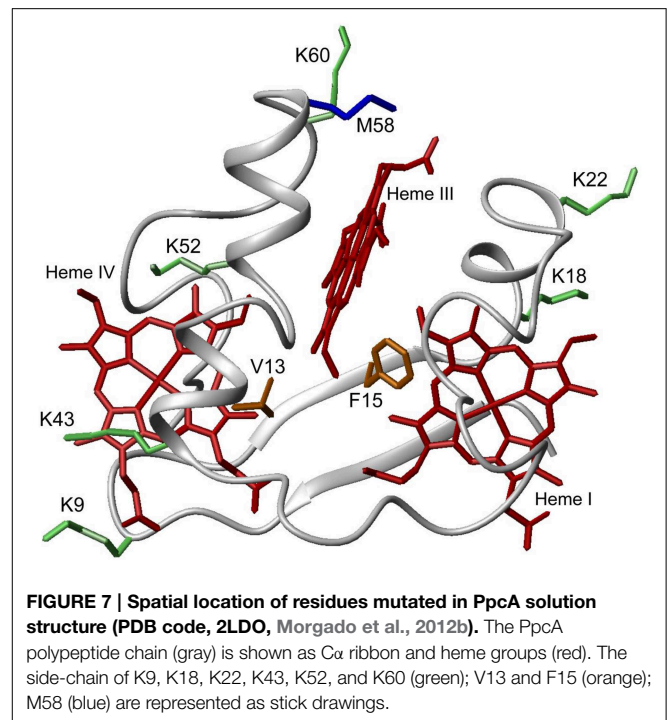
On contrary, signal broadening was observed in the case of mutants F15W, F15Y, V13S, and V13T (Pessanha et al., 2004; Dantas et al., 2012), very likely due to the co-existence of more than one protein conformation in solution (Dantas et al., 2012), which impairs our ability to monitor the stepwise oxidation of the hemes. This suggests that the location of some residues in the 3D structure of the protein imposes severe constraints on the nature of the amino acids by which they can be replaced.

Impact of the Mutations on the Relative Heme Oxidation Profile

The redox-Bohr effect observed for PpcA showed that the heme oxidation fractions are modulated by the solution pH in the range 6–8 (Pessanha et al., 2006; Morgado et al., 2008, 2010a). Therefore, a survey of the heme oxidation profiles for each mutant was carried out at pH 6 and 8, as described for the wild-type cytochrome (Dantas et al., 2012; Morgado et al., 2013, 2014). This strategy allowed us to identify and select the mutants with considerable differences in their heme oxidation profiles compared to the wild-type for further detailed thermodynamic characterization. Comparison of the heme oxidation fractions, at both pH values, showed that the heme oxidation profiles were only slightly altered for V13A, V13I, M58S, K9, K18, and K22 mutants, whereas those for F15L, M58D/N/K, K43, K52, and K60 were significantly changed (**Table 3**). Therefore, the latter group of mutants was selected for detailed functional characterization (Dantas et al., 2012; Morgado et al., 2013, 2014). In addition, M58S was selected as an example from the former group of mutants and a detailed characterization was carried out on it

TABLE 3 | Variation of heme oxidation fractions of PpcA mutants *vs.* the native cytochrome (pH 6 and 8) at intermediate oxidation stages (S_1 and S_2) (Dantas et al., 2012; Morgado et al., 2013, 2014).

Protein	Oxidation fraction relative to PpcA (%)											
	Heme I				Heme III				Heme IV			
	6		8		6		8		6		8	
	S_1	S_2	S_1	S_2	S_1	S_2	S_1	S_2	S_1	S_2	S_1	S_2
V13A	−11	−9	−9	−9	+7	+3	+7	+7	+4	+5	+9	+4
V13I	+3	+2	+1	+2	−5	−5	−4	−6	+2	+3	+4	+4
F15L	−16	−4	−13	−8	+16	+19	+16	+22	−5	−16	−8	−15
M58S	+1	0	0	+1	−4	−4	−4	−4	+2	+3	+4	+2
M58D	−8	−3	−8	−5	+8	+9	+9	+11	−1	−6	−1	−6
M58N	+13	+6	+7	+9	−20	−29	−15	−25	+8	+22	+11	+16
M58K	+11	+4	+6	+7	−17	−24	−15	−22	+7	+19	+9	+14
K9Q	0	0	+1	0	+1	+1	+1	+2	0	−1	−2	−2
K9E	−3	−2	−2	−1	−1	−5	−2	−4	+4	+7	+1	+6
K18Q	+3	+2	+2	+1	−1	+2	0	+2	−2	−4	−2	−3
K18E	+6	+3	+6	+2	−2	+4	0	+4	−4	−6	−6	−5
K22Q	−3	−1	−1	−1	+3	+2	+3	+3	0	−1	0	−1
K22E	−4	−1	−4	−2	+5	+6	+6	+8	−1	−5	−2	−5
K43Q	−5	−3	−6	−2	−1	−8	−2	−6	+7	+10	+9	+7
K43E	−20	−7	−22	−5	−9	−24	−11	−16	+30	+31	+34	+20
K52Q	−19	−8	−23	−6	−10	−24	−12	−16	+29	+31	+36	+20
K52E	−19	−7	−29	−10	−7	−23	−11	−13	+29	+28	+38	+21
K60Q	−8	−2	−7	−5	+12	+12	+14	+16	−3	−9	−7	−10
K60E	−13	−3	−14	−9	+18	+17	+26	+28	−4	−13	−11	−17

to confirm that mutants showing no significant variation of their heme oxidation profiles displayed similar thermodynamic parameters and functional mechanisms compared to the wild-type.

Impact of the Mutations on the Heme Oxidation Order at Physiological pH

The detailed thermodynamic characterization of F15L, M58, K43, K52, and K60 mutants was carried out as previously described for the wild-type protein (Dantas et al., 2012; Morgado et al., 2013, 2014). The heme reduction potentials of these mutants are indicated in **Table 4**. As expected, the heme reduction potentials of the M58S mutant are similar to those of the wild-type cytochrome. However, considerable changes in the heme reduction potentials were observed for the other mutant proteins. In the case of the lysine mutants (K43, K52, and K60) the e_{app}-values of the most affected hemes are smaller compared to the wild-type, as expected from the replacement of a positive charge in their vicinity. Similarly, the inclusion of a negative charge at position 58 is expected to stabilize the oxidized form of the nearest heme (heme III) by lowering its reduction potential. The opposite effect is expected by the introduction of a positive charge in the same position (M58K). All these effects can be rationalized on a purely electrostatic basis. On the other hand, the changes caused by the neutral leucine and asparagine side chains at

positions 15 and 58, respectively, cannot be understood in purely electrostatic terms and were attributed to structural changes in the vicinity of heme III (Dantas et al., 2012, 2013; Morgado et al., 2013). With a few exceptions (K43Q, M58K/N), the changes observed in the heme reduction potentials also altered the oxidation order of the heme groups, compared to the wild-type (**Table 4**).
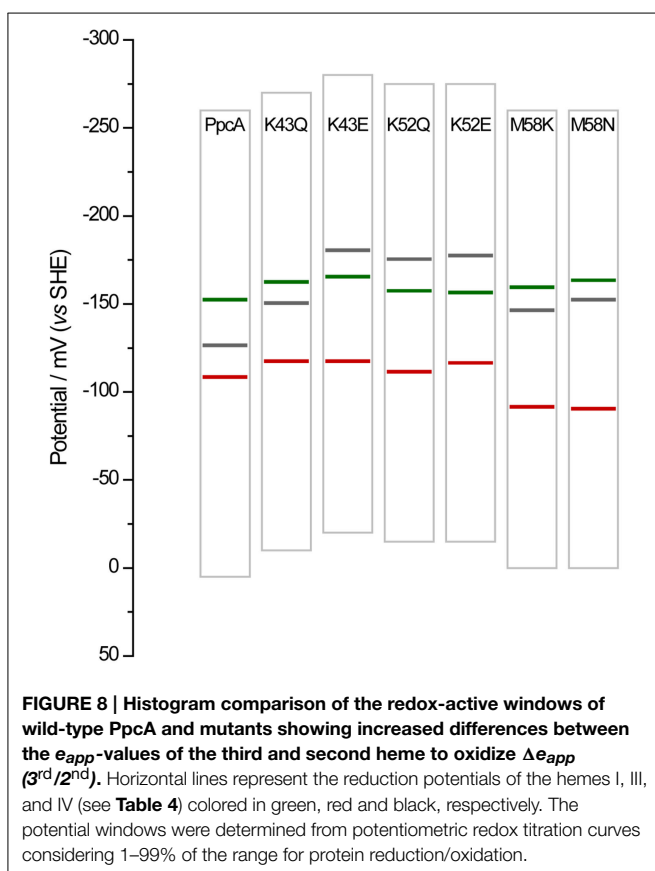
Impact of the Mutated Residues on the Functional Mechanism of PpcA

As described above, the oxidation profile of the redox centers is highly dependent on the nature of the side-chains at positions 15, 43, 52, 58, and 60. Thus, to evaluate the effect of each mutation upon the PpcA functional mechanism, the relative contributions of the 16 possible microstates were also determined (Dantas et al., 2012; Morgado et al., 2013, 2014). This information is summarized in **Table 4** together with the data obtained for PpcA family cytochromes. As mentioned above, for PpcA a coherent e^-/H^+ transfer was established: $P_{0H} \rightarrow P_{1H} \rightarrow P_{14} \rightarrow P_{134}$. In the mutant proteins different scenarios were observed. For K60, M58D and F15L mutants, lowering of the e_{app} of heme III brings the midpoint reduction potential values of all the heme groups closer and favors the oxidation of heme III at earlier oxidation stages in a way that it is no longer the last heme to oxidize. Therefore, two microstates (P_{1H} and P_{3H}) dominated the first

TABLE 4 | Comparison of the results obtained from the thermodynamic characterization of PpcA mutants at pH 7.5 (Dantas et al., 2012; Morgado et al., 2013, 2014).

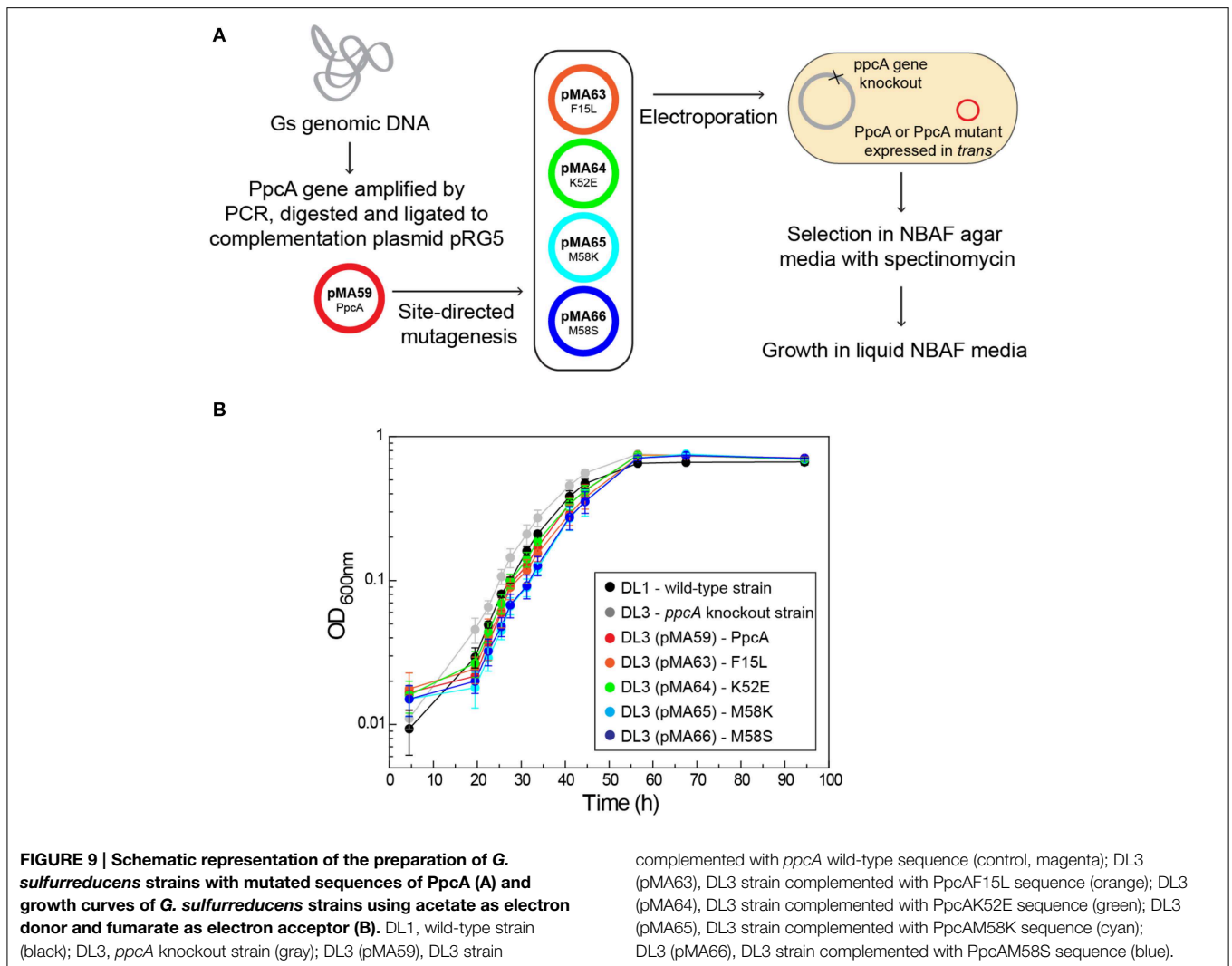| Protein	e_{app} (mV)			Order of heme oxidation	Δe_{app} (mV) ($2^{nd}/1^{st}$)	Δe_{app} (mV) ($3^{rd}/2^{nd}$)	Electron transfer pathway
	Heme I	Heme III	Heme IV				
PpcA	−152	−108	−126	I-IV-III	26	18	$P_{0H} \rightarrow P_{1H} \rightarrow P_{14} \rightarrow P_{134}$
K43Q	−162	−117	−150	I-IV-III	12	33	$P_{0H} \rightarrow (P_{1H}) \rightarrow P_{14} \rightarrow P_{134}$
K43E	−165	−117	−180	IV-I-III	15	48	$P_{0H} \rightarrow P_{14} \rightarrow P_{134}$
K52Q	−157	−111	−175	IV-I-III	18	46	$P_{0H} \rightarrow P_{14} \rightarrow P_{134}$
K52E	−156	−116	−177	IV-I-III	21	40	$P_{0H} \rightarrow P_{14} \rightarrow P_{134}$
K60Q	−161	−143	−134	I-III-IV	18	9	No preferential pathway
K60E	−145	−146	−119	(III,I)-IV	1	26	No preferential pathway
M58S	−159	−110	−139	I-IV-III	20	29	$P_{0H} \rightarrow P_{1H} \rightarrow P_{14} \rightarrow P_{134}$
M58D	−160	−139	−140	I-(III,IV)	20	1	No preferential pathway
M58K	−159	−91	−146	I-IV-III	13	55	$P_{0H} \rightarrow P_{14} \rightarrow P_{134}$
M58N	−163	−90	−152	I-IV-III	11	62	$P_{0H} \rightarrow P_{14} \rightarrow P_{134}$
F15L	−155	−146	−125	I-III-IV	6	24	No preferential pathway
PpcB	−150	−155	−130	(III,I)-IV	5	20	No preferential pathway
PpcD	−156	−102	−162	IV-I-III	6	54	$P_{0H} \rightarrow P_{14} \rightarrow P_{134}$
PpcE	−158	−158	−100	(III,I)-IV	0	58	No preferential pathway

For comparison the values previously obtained for PpcA, PpcB, PpcD, and PpcE (Morgado et al., 2010a) were also included. Δe_{app} ($2^{nd}/1^{st}$) is the difference between the e_{app}-values of the second and the first heme to be oxidized. Δe_{app} ($3^{rd}/2^{nd}$) is the difference between the e_{app}-values of the third and second heme to be oxidized.

FIGURE 8 | Histogram comparison of the redox-active windows of wild-type PpcA and mutants showing increased differences between the e_{app}-values of the third and second heme to oxidize Δe_{app} ($3^{rd}/2^{nd}$). Horizontal lines represent the reduction potentials of the hemes I, III, and IV (see **Table 4**) colored in green, red and black, respectively. The potential windows were determined from potentiometric redox titration curves considering 1–99% of the range for protein reduction/oxidation.

removal of a positively charged side-chain either at position 43 or at 52 contributes to stabilization of the oxidized form and lowers heme IV e_{app}-values, so that it becomes the first one to oxidize, followed by heme I (**Table 4**). In these mutants, the oxidation stage 0 is also dominated by the protonated form P_{0H}, as in PpcA, but the contributions of microstates in oxidation stage 1 are overcome by that of P_{14} (microstate with hemes I and IV oxidized—see **Figure 3**). Thus, a different preferential route for electrons is established, favoring a proton-coupled $2e^-$ transfer step between oxidation stages 0 and 2: $P_{0H} \rightarrow P_{14} \rightarrow P_{134}$, as observed for PpcD (**Table 4**). The same preferential electron transfer route is observed for M58K/N mutants. However, in this case, this is achieved by the concerted effect of increasing the reduction potential of heme III and decreasing that of heme IV (**Table 4**). Taking these observations together, it is clear that residues F15, K43, K52, M58, and K60 modulate the reduction potential of their closest hemes, which in turn controls the microscopic redox states that can be accessed during the redox cycle of the proteins.

Overall, the detailed study of this group of mutants suggests that the reduction potential of heme III, relative to the other two hemes, seems to be crucial in enabling these proteins to couple electron transfer with deprotonation of the redox-Bohr center. Indeed, preferential e^-/H^+ pathways are established only when heme III is the last one to oxidize (higher e_{app}-value), which is reinforced by a higher separation between the e_{app}-values of the second and third hemes to oxidize (see **Table 4**). However, the pathway varies with the separation between the e_{app}-values of heme III and its predecessor in the order of oxidation (**Table 4**). In the case of PpcA such separation was 18 mV and the route for electron transfer was: $P_{0H} \rightarrow P_{1H} \rightarrow P_{14} \rightarrow P_{134}$. In the case of K43Q the same route was observed but with slightly higher separation between the e_{app}-values (33 mV

oxidation stage and, thus, no preferential pathway for electron transfer is observed for this set of mutants (Morgado et al., 2014). On the other hand, in the case of K43 and K52 mutants, the

FIGURE 9 | Schematic representation of the preparation of *G. sulfurreducens* strains with mutated sequences of PpcA (A) and growth curves of *G. sulfurreducens* strains using acetate as electron donor and fumarate as electron acceptor (B). DL1, wild-type strain (black); DL3, *ppcA* knockout strain (gray); DL3 (pMA59), DL3 strain complemented with *ppcA* wild-type sequence (control, magenta); DL3 (pMA63), DL3 strain complemented with PpcAF15L sequence (orange); DL3 (pMA64), DL3 strain complemented with PpcAK52E sequence (green); DL3 (pMA65), DL3 strain complemented with PpcAM58K sequence (cyan); DL3 (pMA66), DL3 strain complemented with PpcAM58S sequence (blue).

vs. 18 mV in the wild-type). Finally, in K43E, K52Q/E, and M58N/K the higher separation between the e_{app}-values of heme III and its predecessor led to a significant contribution of the microstate P_{14} so that a different preferred route for electrons was observed: $P_{0H} \rightarrow P_{14} \rightarrow P_{134}$. It is important to note that this preferential route is independent of the order of oxidation of the first hemes (I-IV or IV-I). The impact of the changes in heme redox potentials, heme-heme interactions and redox-Bohr interactions on the behavior of the redox centers is summarized in **Figure 8**. The more negative values of the heme redox potentials compared to PpcA indicate that the functional working potential ranges in the mutants are shifted to lower redox potential ranges by preserving the concerted e^-/H^+ transfer and energy transduction features of the wild-type protein. This would thermodynamically favor the reduction of downstream redox partners and might have an impact in increasing the efficiency of the *G. sulfurreducens* respiratory chain. As shown above, this can be achieved by the rational design of mutants in the region of heme III or heme IV that lead to the modulation of their reduction potential values.

PpcA Mutant Strains of *G. sulfurreducens*

The functional characterization of a large family of PpcA mutants provided a foundation to evaluate the effect that some of these mutants, when incorporated in *G. sulfurreducens*, would have on the electron transfer capabilities of this organism. Previous studies with a *G. sulfurreducens* strain with the *ppcA* gene knocked out showed that the growth with fumarate as an electron acceptor was not affected, but the growth rate significantly decreased when Fe(III) citrate was used as an electron acceptor (Lloyd et al., 2003). The ability to grow with Fe(III) was restored when PpcA was expressed in *trans* from a complementation plasmid. Taking into account the results obtained for the functional mechanisms of PpcA mutants, four mutants were selected for *in vivo* studies in *G. sulfurreducens*: (i) F15L that disrupts the preferential e^-/H^+ transfer pathway observed for PpcA; (ii) M58S, which conserves the functional mechanism observed for the wild-type; (iii) K52E and M58K, both of which favor a proton-coupled $2e^-$ transfer step but with different order of heme oxidation: IV-I-III and I-IV-III, respectively, at lower

redox potential (see **Table 4** and **Figure 8**). The *G. sulfurreducens* strains carrying the selected PpcA mutants were constructed using published protocols (Lloyd et al., 2003; Kim et al., 2005) and their viability was evaluated (**Figure 9**). The next step will be to study their growth in media with different electron acceptors, such as Fe(III) citrate and Fe(III) oxides. This work is currently underway.

Outlook

In summary, the detailed analysis of PpcA mutants enabled us to learn the principles by which the individual redox properties of the hemes control the e$^-$/H$^+$ transfer pathways in multiheme cytochromes. It is expected that introduction of the mutations associated with preferential e$^-$/H$^+$ transfer pathways at lower reduction potential values in *G. sulfurreducens* cells will improve the bacterium's electron transfer rate, resulting in increased biomass yield. These features can be further explored to test the effect of *G. sulfurreducens* mutants on the efficiency of microbial fuel cells. In principle, this knowledge will enable us to design mutants of other cytochromes to achieve a specific desired functional pathway for any given biotechnological application.

References

Dantas, J. M., Kokhan, O., Pokkuluri, P. R., and Salgueiro, C. A. (2015a). Molecular interaction studies revealed the bifunctional behavior of triheme cytochrome PpcA from *Geobacter sulfurreducens* toward the redox active analog of humic substances. *Biochim. Biophys. Acta* 1847, 1129–1138. doi: 10.1016/j.bbabio.2015.06.004

Dantas, J. M., Morgado, L., Catarino, T., Kokhan, O., Raj Pokkuluri, P., and Salgueiro, C. A. (2014). Evidence for interaction between the triheme cytochrome PpcA from *Geobacter sulfurreducens* and anthrahydroquinone-2,6-disulfonate, an analog of the redox active components of humic substances. *Biochim. Biophys. Acta* 1837, 750–760. doi: 10.1016/j.bbabio.2014.02.004

Dantas, J. M., Morgado, L., Londer, Y. Y., Fernandes, A. P., Louro, R. O., Pokkuluri, P. R., et al. (2012). Pivotal role of the strictly conserved aromatic residue F15 in the cytochrome c_7 family. *J. Biol. Inorg. Chem.* 17, 11–24. doi: 10.1007/s00775-011-0821-8

Dantas, J. M., Morgado, L., Pokkuluri, P. R., Turner, D. L., and Salgueiro, C. A. (2013). Solution structure of a mutant of the triheme cytochrome PpcA from *Geobacter sulfurreducens* sheds light on the role of the conserved aromatic residue F15. *Biochim. Biophys. Acta* 1827, 484–492. doi: 10.1016/j.bbabio.2012.12.008

Dantas, J. M., Salgueiro, C. A., and Bruix, M. (2015b). Backbone, side chain and heme resonance assignments of the triheme cytochrome PpcD from *Geobacter sulfurreducens*. *Biomol. NMR Assign.* 9, 211–214. doi: 10.1007/s12104-014-9576-9

Dantas, J. M., Saraiva, I. H., Morgado, L., Silva, M. A., Schiffer, M., Salgueiro, C. A., et al. (2011). Orientation of the axial ligands and magnetic properties of the hemes in the cytochrome c_7 family from *Geobacter sulfurreducens* determined by paramagnetic NMR. *Dalton Trans.* 40, 12713–12718. doi: 10.1039/c1dt10975h

Ding, Y. H., Hixson, K. K., Aklujkar, M. A., Lipton, M. S., Smith, R. D., Lovley, D. R., et al. (2008). Proteome of *Geobacter sulfurreducens* grown with Fe(III) oxide or Fe(III) citrate as the electron acceptor. *Biochim. Biophys. Acta* 1784, 1935–1941. doi: 10.1016/j.bbapap.2008.06.011

Ding, Y. H., Hixson, K. K., Giometti, C. S., Stanley, A., Esteve-Núñez, A., Khare, T., et al. (2006). The proteome of dissimilatory metal-reducing microorganism *Geobacter sulfurreducens* under various growth conditions. *Biochim. Biophys. Acta* 1764, 1198–1206. doi: 10.1016/j.bbapap.2006.04.017

Esteve-Núñez, A., Sosnik, J., Visconti, P., and Lovley, D. R. (2008). Fluorescent properties of *c*-type cytochromes reveal their potential role as an extracytoplasmic electron sink in *Geobacter sulfurreducens*. *Environ. Microbiol.* 10, 497–505. doi: 10.1111/j.1462-2920.2007.01470.x

Fernandes, A. P., Couto, I., Morgado, L., Londer, Y. Y., and Salgueiro, C. A. (2008). Isotopic labeling of *c*-type multiheme cytochromes overexpressed in *E. coli*. *Protein Expr. Purif.* 59, 182–188. doi: 10.1016/j.pep.2008.02.001

Fonseca, B. M., Paquete, C. M., Salgueiro, C. A., and Louro, R. O. (2012a). The role of intramolecular interactions in the functional control of multiheme cytochromes *c*. *FEBS Lett.* 586, 504–509. doi: 10.1016/j.febslet.2011.08.019

Fonseca, B. M., Tien, M., Rivera, M., Shi, L., and Louro, R. O. (2012b). Efficient and selective isotopic labeling of hemes to facilitate the study of multiheme proteins. *Biotechniques* 1–7. doi: 10.2144/000113859

Holmes, D. E., Chaudhuri, S. K., Nevin, K. P., Mehta, T., Methé, B. A., Liu, A., et al. (2006). Microarray and genetic analysis of electron transfer to electrodes in *Geobacter sulfurreducens*. *Environ. Microbiol.* 8, 1805–1815. doi: 10.1111/j.1462-2920.2006.01065.x

Kim, B. C., Leang, C., Ding, Y. H., Glaven, R. H., Coppi, M. V., and Lovley, D. R. (2005). OmcF, a putative monoheme outer membrane cytochrome required for the expression of other outer membrane cytochromes in *Geobacter sulfurreducens*. *J. Bacteriol.* 187, 4505–4513. doi: 10.1128/JB.187.13.4505-4513.2005

Kim, B. C., and Lovley, D. R. (2008). Investigation of direct vs. indirect involvement of the *c*-type cytochrome MacA in Fe(III) reduction by *Geobacter sulfurreducens*. *FEMS Microbiol. Lett.* 286, 39–44. doi: 10.1111/j.1574-6968.2008.01252.x

Kim, B. C., Postier, B. L., Didonato, R. J., Chaudhuri, S. K., Nevin, K. P., and Lovley, D. R. (2008). Insights into genes involved in electricity generation in *Geobacter sulfurreducens* via whole genome microarray analysis of the OmcF-deficient mutant. *Bioelectrochemistry* 73, 70–75. doi: 10.1016/j.bioelechem.2008.04.023

Leang, C., Coppi, M. V., and Lovley, D. R. (2003). OmcB, a *c*-type polyheme cytochrome, involved in Fe(III) reduction in *Geobacter sulfurreducens*. *J. Bacteriol.* 185, 2096–2103. doi: 10.1128/JB.185.7.2096-2103.2003

Levar, C. E., Chan, C. H., Mehta-Kolte, M. G., and Bond, D. R. (2014). An inner membrane cytochrome required only for reduction of high redox potential extracellular electron acceptors. *MBio* 5, e02034. doi: 10.1128/mBio.02034-14

Liu, Y., Wang, Z., Liu, J., Levar, C., Edwards, M. J., Babauta, J. T., et al. (2014). A trans-outer membrane porin-cytochrome protein complex for extracellular electron transfer by *Geobacter sulfurreducens* PCA. *Environ. Microbiol. Rep.* 6, 776–785. doi: 10.1111/1758-2229.12204

Lloyd, J. R., Leang, C., Hodges Myerson, A. L., Coppi, M. V., Ciufo, S., Methe, B., et al. (2003). Biochemical and genetic characterization of PpcA, a periplasmic *c*-type cytochrome in *Geobacter sulfurreducens*. *Biochem. J.* 369, 153–161. doi: 10.1042/BJ20020597

Londer, Y. Y., Pokkuluri, P. R., Erickson, J., Orshonsky, V., and Schiffer, M. (2005). Heterologous expression of hexaheme fragments of a multidomain cytochrome from *Geobacter sulfurreducens* representing a novel class of cytochromes *c*. *Protein Expr. Purif.* 39, 254–260. doi: 10.1016/j.pep.2004.10.015

Londer, Y. Y., Pokkuluri, P. R., Orshonsky, V., Orshonsky, L., and Schiffer, M. (2006). Heterologous expression of dodecaheme "nanowire" cytochromes *c* from *Geobacter sulfurreducens*. *Protein Expr. Purif.* 47, 241–248. doi: 10.1016/j.pep.2005.11.017

Londer, Y. Y., Pokkuluri, P. R., Tiede, D. M., and Schiffer, M. (2002). Production and preliminary characterization of a recombinant triheme cytochrome *c₇* from *Geobacter sulfurreducens* in *Escherichia coli*. *Biochim. Biophys. Acta* 1554, 202–211. doi: 10.1016/S0005-2728(02)00244-X

Lovley, D. R., Philips, E. J. P., Gorby, Y. A., and Landa, E. R. (1991). Microbial reduction of uranium. *Nature* 350, 413–416. doi: 10.1038/350413a0

Lovley, D. R., and Phillips, E. J. (1988). Novel mode of microbial energy metabolism: organic carbon oxidation coupled to dissimilatory reduction of iron or manganese. *Appl. Environ. Microbiol.* 54, 1472–1480.

Lovley, D. R., Stolz, J. F., Nord,. G. L. Jr., and Philips, E. J. P. (1987). Anaerobic production of magnetite by a dissimilatory iron-reducing microorganism. *Nature* 330, 252–254. doi: 10.1038/330252a0

Mehta, T., Coppi, M. V., Childers, S. E., and Lovley, D. R. (2005). Outer membrane *c*-type cytochromes required for Fe(III) and Mn(IV) oxide reduction in *Geobacter sulfurreducens*. *Appl. Environ. Microbiol.* 71, 8634–8641. doi: 10.1128/AEM.71.12.8634-8641.2005

Methé, B. A., Nelson, K. E., Eisen, J. A., Paulsen, I. T., Nelson, W., Heidelberg, J. F., et al. (2003). Genome of *Geobacter sulfurreducens*: metal reduction in subsurface environments. *Science* 302, 1967–1969. doi: 10.1126/science.1088727

Morgado, L., Bruix, M., Londer, Y. Y., Pokkuluri, P. R., Schiffer, M., and Salgueiro, C. A. (2007). Redox-linked conformational changes of a multiheme cytochrome from *Geobacter sulfurreducens*. *Biochem. Biophys. Res. Commun.* 360, 194–198. doi: 10.1016/j.bbrc.2007.06.026

Morgado, L., Bruix, M., Orshonsky, V., Londer, Y. Y., Duke, N. E., Yang, X., et al. (2008). Structural insights into the modulation of the redox properties of two *Geobacter sulfurreducens* homologous triheme cytochromes. *Biochim. Biophys. Acta* 1777, 1157–1165. doi: 10.1016/j.bbabio.2008.04.043

Morgado, L., Bruix, M., Pessanha, M., Londer, Y. Y., and Salgueiro, C. A. (2010a). Thermodynamic characterization of a triheme cytochrome family from *Geobacter sulfurreducens* reveals mechanistic and functional diversity. *Biophys. J.* 99, 293–301. doi: 10.1016/j.bpj.2010.04.017

Morgado, L., Dantas, J. M., Bruix, M., Londer, Y. Y., and Salgueiro, C. A. (2012a). Fine tuning of redox networks on multiheme cytochromes from *Geobacter sulfurreducens* drives physiological electron/proton energy transduction. *Bioinorg. Chem. Appl.* 2012, 1–9. doi: 10.1155/2012/298739

Morgado, L., Dantas, J. M., Simoes, T., Londer, Y. Y., Pokkuluri, P. R., and Salgueiro, C. A. (2013). Role of Met(58) in the regulation of electron/proton transfer in trihaem cytochrome PpcA from *Geobacter sulfurreducens*. *Biosci. Rep.* 33, 11–22. doi: 10.1042/BSR20120086

Morgado, L., Fernandes, A. P., Londer, Y. Y., Bruix, M., and Salgueiro, C. A. (2010b). One simple step in the identification of the cofactors signals, one giant leap for the solution structure determination of multiheme proteins. *Biochem. Biophys. Res. Commun.* 393, 466–470. doi: 10.1016/j.bbrc.2010.02.024

Morgado, L., Lourenço, S., Londer, Y. Y., Schiffer, M., Pokkuluri, P. R., and Salgueiro, C. (2014). Dissecting the functional role of key residues in triheme cytochrome PpcA: a path to rational design of *G. sulfurreducens* strains with enhanced electron transfer capabilities. *PLoS ONE* 9:e105566. doi: 10.1371/journal.pone.0105566

Morgado, L., Paixão, V. B., Salgueiro, C. A., and Bruix, M. (2011). Backbone, side chain and heme resonance assignments of the triheme cytochrome PpcA from *Geobacter sulfurreducens*. *Biomol. NMR Assign.* 5, 113–116. doi: 10.1007/s12104-010-9280-3

Morgado, L., Paixão, V. B., Schiffer, M., Pokkuluri, P. R., Bruix, M., and Salgueiro, C. A. (2012b). Revealing the structural origin of the redox-Bohr effect: the first solution structure of a cytochrome from *Geobacter sulfurreducens*. *Biochem. J.* 441, 179–187. doi: 10.1042/BJ20111103

Morgado, L., Saraiva, I. H., Louro, R. O., and Salgueiro, C. A. (2010c). Orientation of the axial ligands and magnetic properties of the hemes in the triheme ferricytochrome PpcA from *G. sulfurreducens* determined by paramagnetic NMR. *FEBS Lett.* 584, 3442–3445. doi: 10.1016/j.febslet.2010.06.043

Moss, G. P. (1988). Nomenclature of tetrapyrroles. Recommendations 1986 IUPAC-IUB joint commission on biochemical nomenclature (JCBN). *Eur. J. Biochem.* 178, 277–328. doi: 10.1111/j.1432-1033.1988.tb14453.x

Nevin, K. P., Kim, B. C., Glaven, R. H., Johnson, J. P., Woodard, T. L., Methe, B. A., et al. (2009). Anode biofilm transcriptomics reveals outer surface components essential for high density current production in *Geobacter sulfurreducens* fuel cells. *PLoS ONE* 4:e5628. doi: 10.1371/journal.pone.0005628

Nevin, K. P., Richter, H., Covalla, S. F., Johnson, J. P., Woodard, T. L., Orloff, A. L., et al. (2008). Power output and columbic efficiencies from biofilms of *Geobacter sulfurreducens* comparable to mixed community microbial fuel cells. *Environ. Microbiol.* 10, 2505–2514. doi: 10.1111/j.1462-2920.2008.01675.x

Paixão, V. B., Vis, H., and Turner, D. L. (2010). Redox linked conformational changes in cytochrome *c₃* from *Desulfovibrio desulfuricans* ATCC 27774. *Biochemistry* 49, 9620–9629. doi: 10.1021/bi101237w

Pessanha, M., Londer, Y. Y., Long, W. C., Erickson, J., Pokkuluri, P. R., Schiffer, M., et al. (2004). Redox characterization of *Geobacter sulfurreducens* cytochrome *c₇*: physiological relevance of the conserved residue F15 probed by site-specific mutagenesis. *Biochemistry* 43, 9909–9917. doi: 10.1021/bi0492859

Pessanha, M., Morgado, L., Louro, R. O., Londer, Y. Y., Pokkuluri, P. R., Schiffer, M., et al. (2006). Thermodynamic characterization of triheme cytochrome PpcA from *Geobacter sulfurreducens*: evidence for a role played in e^-/H^+ energy transduction. *Biochemistry* 45, 13910–13917. doi: 10.1021/bi061394v

Pokkuluri, P. R., Londer, Y. Y., Duke, N. E., Erickson, J., Pessanha, M., Salgueiro, C. A., et al. (2004a). Structure of a novel *c₇*-type three-heme cytochrome domain from a multidomain cytochrome *c* polymer. *Protein. Sci.* 13, 1684–1692. doi: 10.1110/ps.04626204

Pokkuluri, P. R., Londer, Y. Y., Duke, N. E., Long, W. C., and Schiffer, M. (2004b). Family of cytochrome *c₇*-type proteins from *Geobacter sulfurreducens*: structure of one cytochrome *c₇* at 1.45 Å resolution. *Biochemistry* 43, 849–859. doi: 10.1021/bi0301439

Pokkuluri, P. R., Londer, Y. Y., Wood, S. J., Duke, N. E., Morgado, L., Salgueiro, C. A., et al. (2009). Outer membrane cytochrome *c*, OmcF, from *Geobacter sulfurreducens*: high structural similarity to an algal cytochrome *c₆*. *Proteins* 74, 266–270. doi: 10.1002/prot.22260

Pokkuluri, P. R., Londer, Y. Y., Yang, X., Duke, N. E., Erickson, J., Orshonsky, V., et al. (2010). Structural characterization of a family of cytochromes *c₇* involved in Fe(III) respiration by *Geobacter sulfurreducens*. *Biochim. Biophys. Acta* 1797, 222–232. doi: 10.1016/j.bbabio.2009.10.007

Shelobolina, E. S., Coppi, M. V., Korenevsky, A. A., Didonato, L. N., Sullivan, S. A., Konishi, H., et al. (2007). Importance of *c*-type cytochromes for U(VI) reduction by *Geobacter sulfurreducens*. *BMC Microbiol.* 7:16. doi: 10.1186/1471-2180-7-16

Shi, L., Lin, J. T., Markillie, L. M., Squier, T. C., and Hooker, B. S. (2005). Overexpression of multi-heme *c*-type cytochromes. *Biotechniques* 38, 297–299. doi: 10.2144/05382PT01

Smith, J. A., Tremblay, P. L., Shrestha, P. M., Snoeyenbos-West, O. L., Franks, A. E., Nevin, K. P., et al. (2014). Going wireless: Fe(III) oxide reduction without pili by *Geobacter sulfurreducens* strain JS-1. *Appl. Environ. Microbiol.* 80, 4331–4340. doi: 10.1128/AEM.01122-14

Turner, D. L., Salgueiro, C. A., Catarino, T., Legall, J., and Xavier, A. V. (1996). NMR studies of cooperativity in the tetrahaem cytochrome *c₃* from *Desulfovibrio vulgaris*. *Eur. J. Biochem.* 241, 723–731. doi: 10.1111/j.1432-1033.1996.00723.x

Voordeckers, J. W., Kim, B. C., Izallalen, M., and Lovley, D. R. (2010). Role of *Geobacter sulfurreducens* outer surface *c*-type cytochromes in reduction of soil humic acid and anthraquinone-2,6-disulfonate. *Appl. Environ. Microbiol.* 76, 2371–2375. doi: 10.1128/AEM.0 2250-09

Wl, D. (2002). *The PyMOL Molecular Graphics System*. Available online at: http://www.pymol.org

Yi, H., Nevin, K. P., Kim, B. C., Franks, A. E., Klimes, A., Tender, L. M., et al. (2009). Selection of a variant of *Geobacter sulfurreducens* with enhanced capacity for current production in microbial fuel cells. *Biosens. Bioelectron.* 24, 3498–3503. doi: 10.1016/j.bios.2009.05.004

Conflict of Interest Statement: The authors declare that the research was conducted in the absence of any commercial or financial relationships that could be construed as a potential conflict of interest.

frontiers
in Microbiology

Characterization of the periplasmic redox network that sustains the versatile anaerobic metabolism of *Shewanella oneidensis* MR-1

Mónica N. Alves, Sónia E. Neto, Alexandra S. Alves, Bruno M. Fonseca, Afonso Carrêlo, Isabel Pacheco, Catarina M. Paquete, Cláudio M. Soares and Ricardo O. Louro*

Inorganic Biochemistry and NMR Laboratory, Instituto de Tecnologia Química e Biológica António Xavier, Universidade Nova de Lisboa, Oeiras, Portugal

The versatile anaerobic metabolism of the Gram-negative bacterium *Shewanella oneidensis* MR-1 (SOMR-1) relies on a multitude of redox proteins found in its periplasm. Most are multiheme cytochromes that carry electrons to terminal reductases of insoluble electron acceptors located at the cell surface, or *bona fide* terminal reductases of soluble electron acceptors. In this study, the interaction network of several multiheme cytochromes was explored by a combination of NMR spectroscopy, activity assays followed by UV-visible spectroscopy and comparison of surface electrostatic potentials. From these data the small tetraheme cytochrome (STC) emerges as the main periplasmic redox shuttle in SOMR-1. It accepts electrons from CymA and distributes them to a number of terminal oxidoreductases involved in the respiration of various compounds. STC is also involved in the electron transfer pathway to reduce nitrite by interaction with the octaheme tetrathionate reductase (OTR), but not with cytochrome *c* nitrite reductase (ccNiR). In the main pathway leading the metal respiration STC pairs with flavocytochrome *c* (FccA), the other major periplasmic cytochrome, which provides redundancy in this important pathway. The data reveals that the two proteins compete for the binding site at the surface of MtrA, the decaheme cytochrome inserted on the periplasmic side of the MtrCAB–OmcA outer-membrane complex. However, this is not observed for the MtrA homologues. Indeed, neither STC nor FccA interact with MtrD, the best replacement for MtrA, and only STC is able to interact with the decaheme cytochrome DmsE of the outer-membrane complex DmsEFABGH. Overall, these results shown that STC plays a central role in the anaerobic respiratory metabolism of SOMR-1. Nonetheless, the trans-periplasmic electron transfer chain is functionally resilient as a consequence of redundancies that arise from the presence of alternative pathways that bypass/compete with STC.

Keywords: dissociation constant, electron transfer, electrostatics, extracellular respiration, paramagnetic NMR, periplasmic cytochromes, *Shewanella oneidensis* MR-1

Abbreviations: SOMR-1, *Shewanella oneidensis* MR-1; MFC, microbial fuel cell; STC, small tetraheme cytochrome; FccA, flavocytochrome *c*; OTR, octaheme tetrathionate reductase; ccNiR, Cytochrome *c* nitrite reductase.

Introduction

Shewanella oneidensis MR-1 is a Gram-negative bacterium that can use a wide range of terminal electron acceptors in the absence of oxygen, including fumarate, nitrite, nitrate, trimethylamine oxide (TMAO), dimethyl sulfoxide (DMSO), sulfur compounds and a variety of metal compounds including radionuclides (Myers and Nealson, 1988; Nealson and Saffarini, 1994; Myers and Myers, 2000; Gralnick and Newman, 2007; Burns and DiChristina, 2009). This metabolic versatility has made SOMR-1 a target of biotechnological research for the development of novel bioremediation processes and generation of electricity in MFC (Lovley, 2006; Logan and Rabaey, 2012). Electron transfer from SOMR-1 to extracellular substrates relies on the conduction of electrons from the cytoplasm to the cell surface via a periplasmic network of redox proteins dominated by *c*-type cytochromes (Heidelberg et al., 2002; Hau and Gralnick, 2007). With the exception of thiosulfate and TMAO reduction, all forms of anaerobic respiration described in SOMR-1 are routed via the tetraheme *c*-type cytochrome CymA, anchored to the inner membrane of the cell (Myers and Myers, 1997; Saffarini et al., 2002). This protein collects electrons from the menaquinone pool in the cytoplasmic membrane and distributes them among periplasmic proteins. These proteins can be either terminal reductases or periplasmic redox shuttles that transfer electrons to outer-membrane reductases (Myers and Myers, 1997; Saffarini et al., 2002; Schwalb et al., 2003). Nevertheless, the detailed organization of the trans-periplasmic redox network remains to be completely elucidated (Hartshorne et al., 2009). In anaerobic conditions, the most abundant periplasmic *c*-type cytochromes in SOMR-1 are the STC and the FccA (Tsapin et al., 2001). It was recently shown that both STC and FccA can accept electrons from CymA and transfer them to outer-membrane metal reductases, which lead to the identification of two independent redox pathways across the periplasm (Fonseca et al., 2013). Although this finding confirmed the functional redundancy already observed for other multiheme cytochromes (Coursolle and Gralnick, 2010; Richardson et al., 2012), the physiological reason for this is still unknown. One of the most explored and well described anaerobic respiratory pathways in SOMR-1 is Fe(III) reduction, which involves the outer membrane MtrCAB–OmcA complex (Myers and Nealson, 1988; Myers and Myers, 1997, 2000; Pitts et al., 2003). However, less is known about the periplasmic electron transfer network that delivers electrons to the homologous complexes, MtrDEF and DmsEFABGH. While the DmsEFABGH complex is responsible for the extracellular respiration of DMSO, the specific physiological function of MtrDEF is still unclear. It appears to play a similar role to MtrCAB–OmcA complex because of their high similarity (Fredrickson et al., 2008; Coursolle and Gralnick, 2010).

Another important respiratory process carried out by SOMR-1 is the conversion of nitrogen compounds to ammonia (Myers and Nealson, 1988; Nealson and Saffarini, 1994). This respiratory pathway involves the OTR and the cytochrome *c* nitrite reductase (ccNiR). OTR is described as an efficient nitrite and hydroxylamine reductase and ccNiR catalyzes the reduction of nitrite (Einsle et al., 2002; Atkinson et al., 2007). It

was previously demonstrated that CymA is essential for nitrite reduction (Schwalb et al., 2003), but nothing is known about the routes of electron transfer to OTR and ccNiR. In order to determine if STC and FccA mediate the electron transfer from CymA to the outer-membrane complexes MtrDEF and DmsEFABGH, protein interactions studied by Nuclear magnetic resonance (NMR) and UV-visible spectroscopy were performed. NMR spectroscopy together with protein electrostatic surface potential calculations was also used to explore the ability of STC and FccA transfer electrons to OTR and ccNiR (Mowat et al., 2004; Youngblut et al., 2012). These results showed that the functional redundancy between STC and FccA appears to be restricted to the interaction with the MtrCAB–OmcA complex. Furthermore, the data showed that STC plays the major role in connecting CymA with the DmsEFABGH complex and OTR, but is not involved in interactions neither with ccNiR nor with MtrD.

Materials and Methods

Cloning and Expression of the Genes of Interest

The vectors containing *dmsE* and *mtrD* genes were kindly provided by Dr. Liang Shi from the Pacific Northwest National Laboratory (Richland, WA, U.S.A.). A stop codon was inserted at the 3′ end of each gene, allowing the removal of the V5 epitope and the 6xHis-tag sequence at the C-terminus of the proteins. The lack of these sequences eliminated concerns about proper folding of the protein in the presence of the 6xHis-tag at the C-terminus. The cloning vector pHSG298 (Takara Bio), containing the *ccnir* gene with the wild-type N-terminal signal peptide replaced by the signal peptide from the SOMR-1 protein STC, was gently provided by Dr. Sean J. Elliott from Boston University. The *otr* gene was amplified from genomic DNA of SOMR-1 and cloned into the pBAD202/D-TOPO vector following the instructions from the supplier (pBAD202 directional TOPO Expression Invitrogen KIT) and according to the work of Shi et al. (2005). The primers used are reported in **Table 1**.

Bacterial Strains and Growth Conditions

Shewanella oneidensis JG207 strain (knockout strain of the *fccA* gene), kindly provided by Prof. Dr. Johannes Gescher from Karlsruher Institut für Technologie (Karlsruher, Germany), was transformed with the vector containing the *otr* gene. The vectors containing the *dmsE* and *mtrD* genes were separately transformed in SOMR-1. *S. oneidensis* cells were grown at 30°C in Terrific Broth (TB) containing 50 μg/ml kanamycin in 5 l Erlenmeyer flasks containing 2 l of medium and 1:100 inoculum volume, at 130 rev./min. Protein expression was induced by addition of L-arabinose: 1 mM (for the strains over-expressing DmsE and OTR) and 2 mM (for the strain over-expressing MtrD) after 6–8 h of growth. After induction, cells continued to grow for 16 h, until harvesting. Bacterial cells were harvested by centrifugation at 11,325 *g* for 10 min, at 4°C. In this study the strain SOMR-1 was used to express ccNiR employing the growth conditions previously reported in the literature (Judd et al., 2012). The vectors, strains and growth conditions to express MtrA, STC,

Primer	Sequence (5′-3′)
DmsE_Stop_Forw	GCGGCAGCAATTTTGCCCGTTGAGGCGAGCTCAAGCTTGAAGGTAAGCC
DmsE_Stop_Rev	GGCTTACCTTCAAGCTTGAGCTCGCCTCAACGGGCAAAATTGCTGCCGC
MtrD_Stop_Forw	AAGTTGCTGCAGAGATAAGGCGAGCTCAAGCTTGA
MtrD_Stop_Rev	TCAAGCTTGAGCTCGCCTTATCTCTGCAGCAACTT
OTR_Stop_Forw	CACCTAAGAAGGAGATATACATCCCATGAA
OTR_Stop_Rev	TTATTGCTTATGTTTAGGGCCTTGTTTGTT

FccA, and CymA were as previously described (Fonseca et al., 2009, 2013).

Protein Purification

The cell pellets were resuspended in 20 mM Tris-HCl (pH 7.6) containing protease inhibitor cocktail (Roche) and DNase I (Sigma). The disruption of the cells was achieved by a passage through a French Press at 1000 psi. Membranes and cell debris were removed by centrifugation at 219,000 g for 1 h, at 4°C, and the supernatant containing the soluble protein fraction was dialyzed overnight against 4 l of 20 mM Tris-HCl (pH 7.6). These fractions were concentrated in ultrafiltration cells, using a 10 kDa cut-off membrane. The fractions containing each of the target proteins were loaded onto a diethylaminoethyl (DEAE) column (GE Healthcare) pre-equilibrated with 20 mM Tris-HCl (pH 7.6). A gradient from 0 to 1 M NaCl was applied. The fractions containing MtrD were eluted at 150 mM NaCl, while DmsE and OTR were eluted at 200 mM NaCl. The fractions containing DmsE and MtrD were concentrated and loaded onto a HTP (hydroxyapatite) column (Bio-Rad Laboratories) pre-equilibrated with 10 mM potassium phosphate buffer (pH 7.6) and gradient from 10 mM to 1 M. DmsE and MtrD were eluted at 100 and 150 mM of potassium phosphate buffer (pH 7.6), respectively. The final purification step used a Superdex 75 column (GE Healthcare) pre-equilibrated with 20 mM potassium phosphate buffer (pH 7.6) and 100 mM NaCl. The fraction resulting from the DEAE column containing OTR was concentrated and loaded onto a Q-Sepharose column (GE Healthcare) previously equilibrated with 20 mM Tris-HCl (pH 7.6). A salt gradient from 0 to 1 M NaCl was applied and this protein was eluted at 150 mM NaCl. The fraction containing OTR was concentrated and loaded onto a HTP column pre-equilibrated with 10 mM potassium phosphate buffer (pH 7.6). A gradient from 10 mM to 1 M of potassium phosphate buffer (pH 7.6) was applied, and pure OTR was eluted at 100 mM. The purification of STC, FccA, CymA, and ccNiR cytochromes was performed as described in the literature (Judd et al., 2012; Fonseca et al., 2013). The recombinant TEV protease was removed from the fraction containing ccNiR using a Superdex 75 column pre-equilibrated with 20 mM potassium phosphate buffer (pH 7.6) with 150 mM KCl. All the chromatographic fractions were analyzed by SDS/PAGE stained for heme proteins (Francis and Becker, 1984) and by UV-visible spectroscopy to select those containing the target proteins. Proteins were considered pure when having an absorbance ratio Soret Peak/A280nm higher than 3.5, and when showing a single band in Coomassie staining

SDS/PAGE gels. The identity of DmsE, MtrD, and OTR was confirmed by mass spectrometry and N-terminal sequencing.

NMR Sample Preparation and Titrations

Stock samples of DmsE, MtrD, OTR, ccNiR, STC, and FccA in 20 mM potassium phosphate (pH 7.6) with an ionic strength of 100 mM (adjusted by addition of potassium chloride) were lyophilized and dissolved in ^{2}H$_2$O (99.9 atom%, Spectra Stable Isotopes). NMR spectra obtained before and after lyophilization were identical, demonstrating that the proteins were not affected by this procedure. The protein concentration was determined by UV-visible spectroscopy using ε_{410nm} of 125,000 M^{-1}cm^{-1} per heme for the oxidized state of the protein (Massey, 1959; Hartshorne et al., 2007). Samples containing 50 or 100 µM of STC and FccA were titrated against increasing concentrations of DmsE, MtrD, OTR, and ccNiR. The competition titration was performed with a sample of MtrA (50 µM) incubated with sufficient amount of FccA to have at least 90% of MtrA bound to FccA. Subsequently, increasing amounts of STC were added to the NMR tube, in order to detect any perturbation in STC signals. ^{1}H-1D-NMR spectra were recorded after each addition. The chemical shifts of the signals corresponding to the methyl substituents of the hemes of STC and FccA were measured in each spectrum. These signals have been previously assigned to specific hemes in the structure, allowing the identification of the docking sites with its redox partners (Fonseca et al., 2009; Pessanha et al., 2009).

Nuclear magnetic resonance experiments were performed at 25°C on a Bruker Avance II spectrometer operating at 500 MHz equipped with a TXI probe. The proton spectra were calibrated using the water signal as an internal reference (Banci et al., 1995).

Data Analysis and Binding Affinities

Chemical shift perturbations equal to or larger than 0.025 ppm were considered significant (Diaz-Moreno et al., 2005b). The chemical shift perturbations ($\Delta\delta_{bind}$) of the NMR signals from a cytochrome resulting from the complex formation with another cytochrome were plotted against the molar ratio (R) of [CytB]/[CytA]. The data were fitted using least squares minimization to a 1:1 binding model using equations (1) and (2) (Worrall et al., 2003):

$$\Delta\delta_{bind} = \frac{1}{2}\Delta\delta_{bind}^{\infty}(A - \sqrt{(A^2 - 4R)})\qquad(1)$$

$$A = 1 + R + \frac{K_d([Cyt_A]_0 R + [Cyt_B]_0)}{[Cyt_A]_0[Cyt_B]_0}\qquad(2)$$

where $\Delta\delta_{bind}^{\infty}$ is the maximal chemical shift perturbation of the NMR signals resulting from the complex formation between Cyt_A and Cyt_B, K_d is the dissociation constant, $[Cyt_A]_0$ is the initial concentration of Cyt_A and $[Cyt_B]_0$ is the stock concentration of Cyt_B. When several methyl signals belonging to an individual heme were visible, the data obtained for all methyls were used to define the dissociation constant. Experimental uncertainty was estimated from the spectral resolution of the NMR data acquired.

Spectroscopic Assay of Interprotein Electron Transfer

Electron transfer involving FccA from SOMR-1 was measured spectrophotometrically inside an anaerobic chamber using an UV–visible spectrophotometer (Shimadzu model UV-1800) to collect spectra in the range of 300–800 nm as previously described. Briefly, an approximate final concentration of 1 μM of each target protein was prepared in a 1 ml cuvette. Dilutions were made from stock solutions of DmsE, MtrD, OTR, ccNiR, and FccA in degassed 20 mM potassium phosphate buffer (pH 7.6) with 100 mM KCl. Each protein was reduced by addition of small amounts of a concentrated solution of sodium dithionite. The absorbance was monitored at 314 nm to avoid excess of reducing agent. Fumarate was added to the reduced protein solutions to a final concentration of ∼1 mM. Only when no change was observed in absorbance at 552 nm, the reaction would be initiated by the addition of 1 nM FccA. The spectral changes were monitored over time. Experiments were performed with constant stirring and the temperature was kept at 25°C using an external thermostatic bath.

Protein Electrostatic Surface Potential Calculations

The structures of ccNiR (PDB code 3UBR; Youngblut et al., 2012) and the OTR (PDB code 1SP3; Mowat et al., 2004), were used to calculate the electrostatic potential at the surface of both proteins. Both proteins were set in their fully oxidized states, which were the experimental conditions used to study their interactions. The GROMOS 43A1 force field (Scott et al., 1999) was used to set the partial charges of the proteins and co-factors. The MEAD package (Bashford and Karplus, 1990), which solves the Poisson–Boltzmann equation for a system, was used to calculate the electrostatic potentials. The ionic strength used was 0 mM and the internal and external dielectric constants were set at 2 and 80, respectively. The electrostatic potential was mapped at the surface of the proteins using PyMOL (DeLano, 2003).
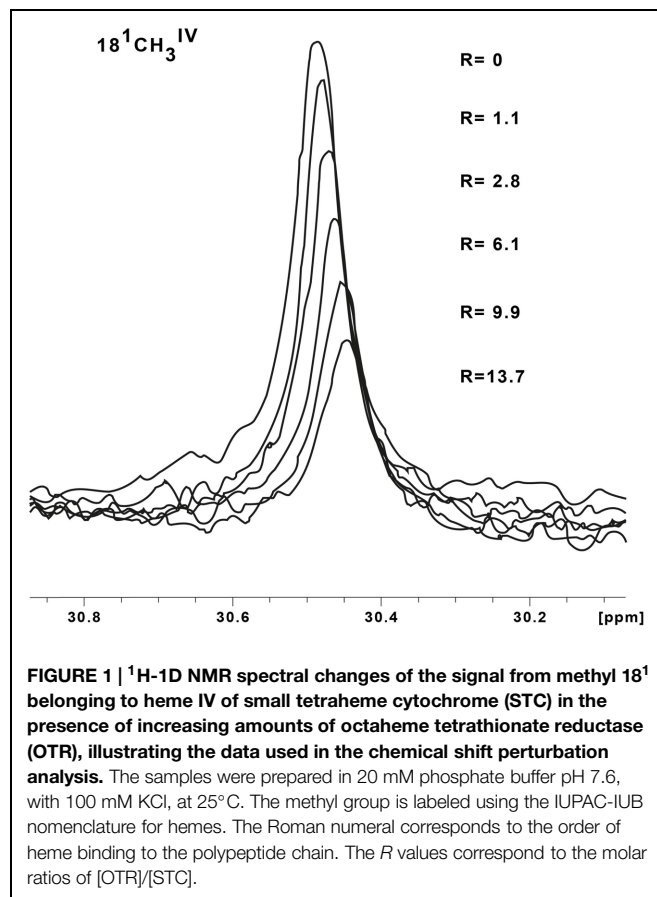
Results

NMR Titrations and Binding Affinities

For electron transfer to occur at physiologically relevant rates between two cytochromes, the heme groups of donor and acceptor must be in close proximity (Zhang et al., 2008; Gray and Winkler, 2010). Therefore, when multiheme cytochromes bind in a configuration that is relevant for interprotein electron transfer, NMR spectroscopy can be used to detect this binding

through observation of changes in the chemical shifts of signals belonging to the hemes near to the binding sites (Fonseca et al., 2013). This technique is thus highly suited to study interactions between the redox proteins found in the periplasmic space of SOMR-1, revealing the detailed organization of its trans-periplasmic redox network. **Figure 1** illustrates spectral changes for the 18^1 methyl signal (IUPAC-IUB nomenclature) from heme IV ($18^1CH_3^{IV}$) of STC in the presence of increasing amounts of OTR.

Chemical shift perturbations of the STC and FccA signals, resulting from binding to putative redox partners, were plotted against the molar ratio of redox partner:STC and redox partner:FccA (**Figure 2**). All the periplasmic pairs of proteins tested and K_d values of proteins that showed interactions are reported in **Table 2**. In some cases, such as the signals of the 2^1 methyl of heme III or the 18^1 methyl of hemes II and IV of STC during interaction with DmsE, the chemical shift perturbation of their signals is smaller than 0.025 ppm. These are therefore of insufficient magnitude for a confident estimation of binding parameters as indicated in the Section "Materials and Methods" and were not used in the calculations. The K_d values calculated are typical of weakly transient interactions as reported for other cytochromes (Diaz-Moreno et al., 2005a; Perkins et al., 2010; Bashir et al., 2011; Meschi et al., 2011; Fonseca et al., 2013).
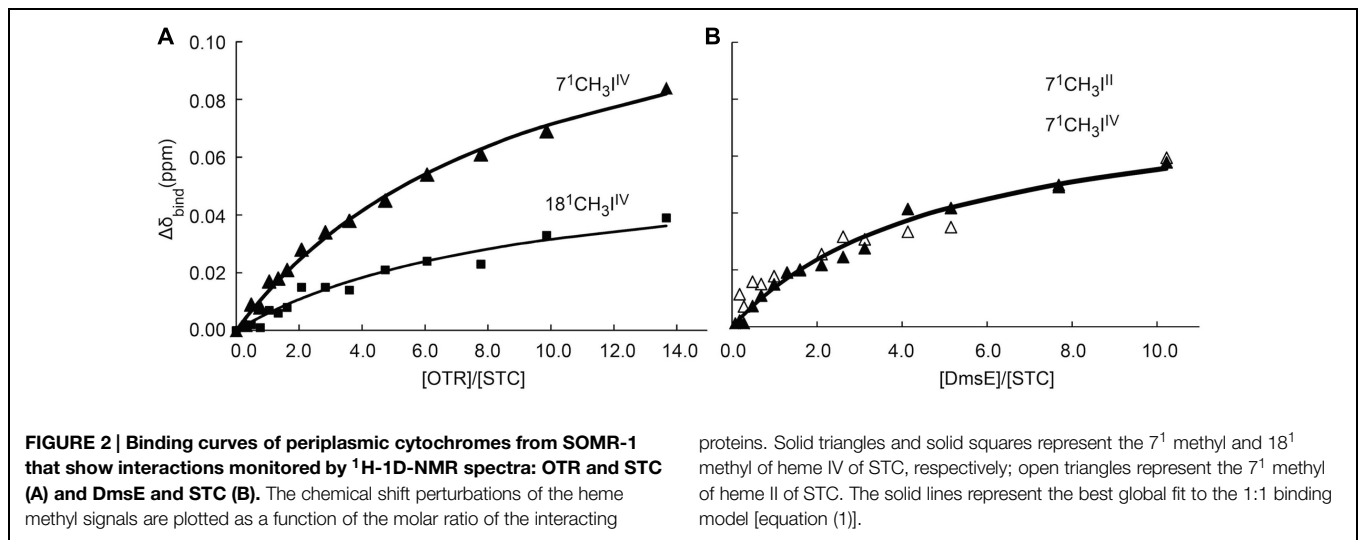

FIGURE 1 | ^{1}H-1D NMR spectral changes of the signal from methyl 18^1 belonging to heme IV of small tetraheme cytochrome (STC) in the presence of increasing amounts of octaheme tetrathionate reductase (OTR), illustrating the data used in the chemical shift perturbation analysis. The samples were prepared in 20 mM phosphate buffer pH 7.6, with 100 mM KCl, at 25°C. The methyl group is labeled using the IUPAC-IUB nomenclature for hemes. The Roman numeral corresponds to the order of heme binding to the polypeptide chain. The *R* values correspond to the molar ratios of [OTR]/[STC].

FIGURE 2 | Binding curves of periplasmic cytochromes from SOMR-1 that show interactions monitored by ^{1}H-1D-NMR spectra: OTR and STC (A) and DmsE and STC (B). The chemical shift perturbations of the heme methyl signals are plotted as a function of the molar ratio of the interacting proteins. Solid triangles and solid squares represent the 7^1 methyl and 18^1 methyl of heme IV of STC, respectively; open triangles represent the 7^1 methyl of heme II of STC. The solid lines represent the best global fit to the 1:1 binding model [equation (1)].

TABLE 2 | Pairwise interactions tested for cytochromes found in the periplasm of SOMR-1.

Cytochrome Complex	K_d (μM)	Docking Site
FccA and MtrA	35 (14)	Heme II
FccA and DmsE	–	
FccA and MtrD	–	
FccA and OTR	–	
FccA and ccNiR	–	
STC and MtrA	572 (5)	Heme IV
STC and DmsE	783 (227)	Hemes II, III, and IV
STC and MtrD	–	
STC and OTR	1600 (400)	Heme IV
STC and ccNiR	–	

The "–" symbol indicates no interaction detected. Values in parenthesis are standard errors obtained from the diagonal of the covariance matrix arising from the fitting of the binding model to the experimental data.
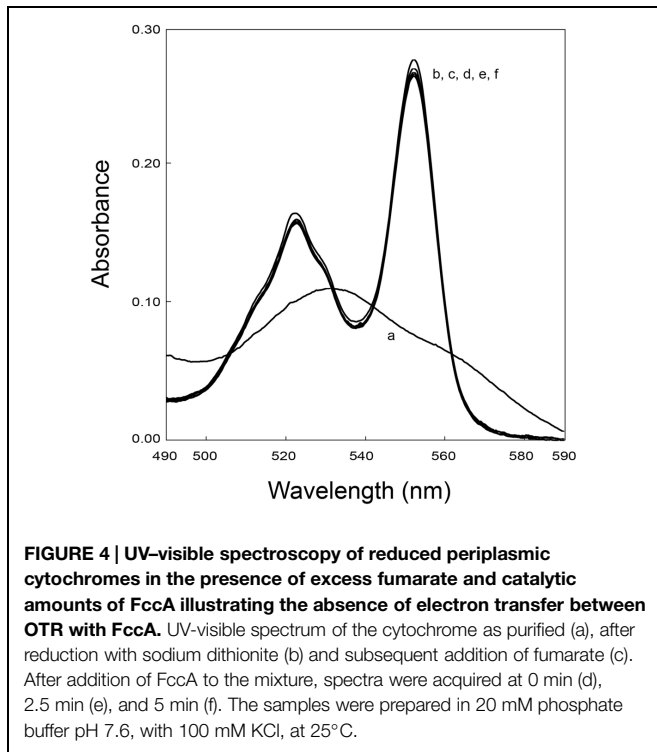
Previous studies showed that both STC and FccA interact with the decaheme cytochrome MtrA and that the affinity between FccA and MtrA is much stronger than the affinity between STC and MtrA (Fonseca et al., 2013). Given that the three-dimensional structure of MtrA is not yet available, a competition binding assay monitored by ^{1}H-1D-NMR was performed to study the docking place of STC and FccA with MtrA. In conditions where more than 90% of MtrA is bound to FccA, the chemical shift of the STC signals are not perturbed when the molar ratio of MtrA:STC is changed (**Figure 3**). This result shows that the presence of FccA bound to MtrA prevents the interaction between MtrA and STC, suggesting that the binding of STC and FccA at the surface of MtrA occurs in the same place or in close proximity.

The inverse competition binding assay with MtrA saturated with bound STC in the presence of increasing amounts of FccA added to the sample is not experimentally feasible. To reach more than 90% saturation of a sample with 50 μM of MtrA with STC would require concentrations of STC above 5 mM. Likewise, a similar experiment exploring the interactions of STC and FccA with CymA, another key protein for which a structure has not been reported in the literature, is not also
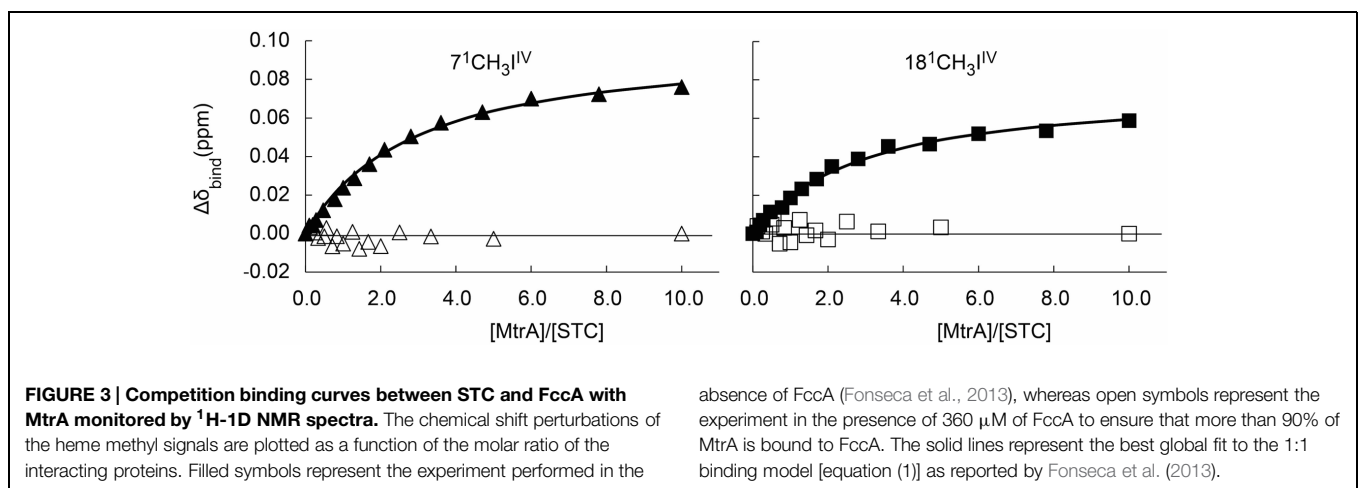
FIGURE 3 | Competition binding curves between STC and FccA with MtrA monitored by ^{1}H-1D NMR spectra. The chemical shift perturbations of the heme methyl signals are plotted as a function of the molar ratio of the interacting proteins. Filled symbols represent the experiment performed in the absence of FccA (Fonseca et al., 2013), whereas open symbols represent the experiment in the presence of 360 μM of FccA to ensure that more than 90% of MtrA is bound to FccA. The solid lines represent the best global fit to the 1:1 binding model [equation (1)] as reported by Fonseca et al. (2013).

FIGURE 4 | UV–visible spectroscopy of reduced periplasmic cytochromes in the presence of excess fumarate and catalytic amounts of FccA illustrating the absence of electron transfer between OTR with FccA. UV-visible spectrum of the cytochrome as purified (a), after reduction with sodium dithionite (b) and subsequent addition of fumarate (c). After addition of FccA to the mixture, spectra were acquired at 0 min (d), 2.5 min (e), and 5 min (f). The samples were prepared in 20 mM phosphate buffer pH 7.6, with 100 mM KCl, at 25°C.

require concentrations of STC and FccA of 2.2 and 3.5 mM, respectively.

Spectroscopic Assay of Interprotein Electron Transfer

UV-visible experiments were performed to confirm the interaction data obtained from NMR experiments involving FccA. The fumarate reductase activity of FccA was used to measure the re-oxidation of possible partner cytochromes. These experiments showed that FccA cannot re-oxidize MtrD, DmsE, OTR, and ccNiR (**Figure 4**), which is in agreement with the data obtained from NMR titrations.

Electrostatic Calculations

The electrostatic potential at the surfaces of the enzymes ccNiR and OTR were calculated using the same procedure as previously used for STC and FccA (Fonseca et al., 2013). OTR presents an overall negative surface, with the exception of two regions, one near heme II (the catalytic heme) and the other one near heme VIII. In the case of ccNiR, the surface potential does not show a clear cut trend as in the case of OTR, with the exception of the region near heme I, which is the catalytic heme. The region around this heme is strongly negative (**Figure 5**).

Discussion

The electron transfer pathways of the SOMR-1 to reduce Fe(III), DMSO, fumarate and nitrite are established by a variety of multiheme *c*-type cytochromes located at the inner membrane, periplasm and outer membrane. Biochemical studies

experimentally feasible. The large dissociation constants reported for the interaction between STC and CymA or FccA and CymA (Fonseca et al., 2013) mean that achieving more than 90% saturation of 50 μM CymA with any of the partners would

FIGURE 5 | Electrostatic potential mapping on the protein's surface of (A) OTR (PDB code 1S3P) and (B) ccNiR (PDB code 3UBR) from SOMR-1. Electrostatic potentials were calculated considering a fully oxidized state for these cytochromes. The Roman numerals correspond to the order of heme binding motifs in the polypeptide chain.

showed that all of these routes have the common feature of being initiated by the oxidation of the quinone pool at the inner-membrane by the tetraheme *c*-type cytochrome, CymA (Schwalb et al., 2003; Marritt et al., 2012). The detailed understanding of the organization of the trans-periplasmic redox network has been compounded by two factors: spectroscopic signatures of *c*-type cytochromes are often overlapping or identical (Firer-Sherwood et al., 2011), and they form low-affinity complexes with fast dissociation rates (Crowley and Ubbink, 2003; Rudolph, 2007; Abresch et al., 2009). Nevertheless, recent studies have demonstrated that NMR spectroscopy is an effective technique to identify transient interactions between redox partners by monitoring the perturbation of the chemical shifts of heme signals (Fonseca et al., 2013). This method does not disturb the protein conformation because it is a soluble assay. Furthermore, it has the unique advantage of allowing the determination of docking regions between redox partners when resonance assignments of the interacting proteins are available.

A previous study revealed that STC and FccA can independently mediate electron transfer between CymA and MtrA leading to extracellular electron transfer (Fonseca et al., 2013). Since the three-dimensional structure of MtrA was only characterized at low resolution using SAXS (Firer-Sherwood et al., 2011), the docking with its redox partners STC and FccA cannot be modeled at this point. Notwithstanding, in this work the interaction of STC and FccA with MtrA was further characterized by a competition binding assay between STC and FccA. It revealed that these two proteins bind MtrA in the same or at least closely related locations, given that saturation of MtrA with FccA prevents the binding of STC.

This study also reveals that STC interacts transiently with DmsE and that the signals of hemes II, III, and IV are perturbed. Clearly, the interaction between STC and DmsE is different from that between STC and MtrA, which affects only signals of the heme IV of STC. Given the bracket shape of the structure of STC, if one considers the hemes ordered sequentially from top to bottom it can be envisaged that interaction with DmsE occurs via the lower external face of the bracket (Supplementary Figure S1).

The genome of SOMR-1 contains three homologues of the MtrCAB–OmcA complex, the MtrDEF complex, the DmsEFABGH complex and the complex coded by the genes SO_4357-62. Studies involving MtrA knockout strains showed that two of these complexes constitute alternative routes of

electron flow to Fe(III) respiration (Coursolle and Gralnick, 2010). MtrA can be functionally replaced in ferric citrate reduction in the order MtrD > DmsE (Coursolle and Gralnick, 2012). Despite the high homology of SO4360 with MtrA, this decaheme cytochrome cannot functionally replace MtrA and requires its own porin SO4359 to function in metal reduction (Schicklberger et al., 2013). This hierarchy in the capacity for functional replacement of MtrA matches the sequence homology among these decaheme cytochromes (**Table 3**) but does not match the observed interactions with the major trans-periplasmic redox shuttles. MtrA interacts with STC and FccA that compete for the same binding site on the surface of MtrA. DmsE interacts with STC but not FccA, and MtrD does not interact with STC or FccA. Altogether, these data give strong indications that the dominant factor in the capacity of other periplasmic decaheme cytochromes to functionally replace MtrA is the matching with the MtrB porin to establish contact with the outer-membrane MtrC cytochrome, since neither STC nor FccA interact with MtrD.

Studies recently published by Sturm et al. (2015) showed that single mutants of STC and FccA have only minor phenotypic changes in their ability to reduce DMSO. However, the double mutant strain is unable to grow using this electron acceptor (Sturm et al., 2015). Those results suggest that both STC and FccA have a key role in the respiration of DMSO in SOMR-1 and the data reported in this work indicates that FccA does not interact directly with DmsE.
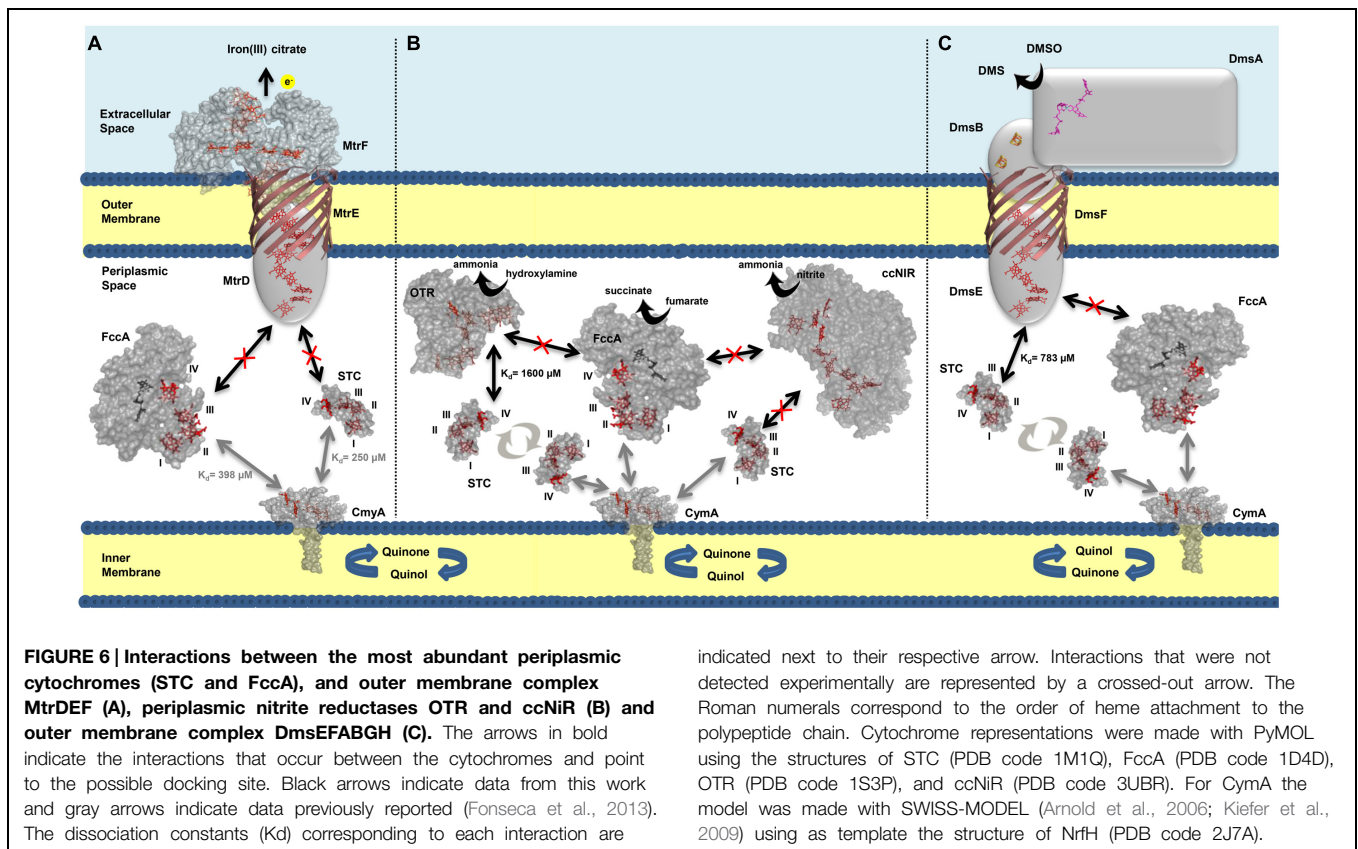
In this study, interactions involving two major terminal reductases involved in pathways for dissimilatory nitrate ammonification of SOMR-1, ccNiR, and OTR, were also explored (Berks et al., 1995; Simon, 2002; Einsle and Kroneck, 2004). While the pentaheme ccNiR catalyzes the reduction of nitrite (NO_2^-) to ammonium (NH_4^+), the octaheme OTR can reduce nitrite (NO_2^-) and hydroxylamine (NH_2OH), as well as the sulfur compound tetrathionate ($S_4O_6^{2-}$) (Atkinson et al., 2007). The results showed that heme IV of STC is perturbed upon interaction with OTR. The region around heme IV of STC displays the strongest negative surface, making it a good candidate to interact with OTR that displays positively charged potentials in various regions of its surface (**Figure 5**). By contrast, no interaction was observed between ccNiR and STC or FccA. The surface of ccNiR is predominantly weakly negative with a strongly negative region near the catalytic center, therefore discouraging interactions with the negatively charged STC or heme domain of FccA. This result is also consistent with a previous study showing that both wild-type SOMR-1 and the $\Delta stc \Delta fccA$ mutant strain reduce nitrite at similar rates (Sturm et al., 2015).

Interestingly, all protein–protein interactions reported between STC and its putative physiological partners involve heme IV (Fonseca et al., 2013). Given that to perform its function of shuttling electrons between redox partners STC needs to charge and discharge, clearly this protein does not operate as a molecular wire. It functions more like an electronic cul-de-sac that forces electrons to enter and leave the cytochrome by the same heme. This enables *Shewanella* to transfer electrons in a controlled and efficient manner (maximum of four electrons can be transferred by STC) to specific proteins in the periplasmic

TABLE 3 | Sequence identity matrix for the periplasmic decaheme cytochromes from SOMR-1.

	MtrA	MtrD	DmsE	SO4360
MtrA	100	72	69	54
MtrD	++	100	60	49
DmsE	+		100	51
SO4360	−			100

Sequences of the four decaheme cytochromes were retrieved from Pubmed-NCBI database and aligned using the Clustal 2.1 Multiple Sequence Alignment website. Values are presented in percentage. Below the diagonal is an indication of the relative ability to functionally replace MtrA according to Coursolle and Gralnick (2010).

FIGURE 6 | Interactions between the most abundant periplasmic cytochromes (STC and FccA), and outer membrane complex MtrDEF (A), periplasmic nitrite reductases OTR and ccNiR (B) and outer membrane complex DmsEFABGH (C). The arrows in bold indicate the interactions that occur between the cytochromes and point to the possible docking site. Black arrows indicate data from this work and gray arrows indicate data previously reported (Fonseca et al., 2013). The dissociation constants (Kd) corresponding to each interaction are indicated next to their respective arrow. Interactions that were not detected experimentally are represented by a crossed-out arrow. The Roman numerals correspond to the order of heme attachment to the polypeptide chain. Cytochrome representations were made with PyMOL using the structures of STC (PDB code 1M1Q), FccA (PDB code 1D4D), OTR (PDB code 1S3P), and ccNiR (PDB code 3UBR). For CymA the model was made with SWISS-MODEL (Arnold et al., 2006; Kiefer et al., 2009) using as template the structure of NrfH (PDB code 2J7A).

space, rather than transfer randomly to any protein that may interact with STC. This minimizes the risk of diverting electrons to side redox pathways and production of radical species.

Conclusion

We have elucidated the organization of the multi-branched periplasmic respiratory network of SOMR-1. NMR studies revealed that STC not only contributes to extracellular respiration of metals via interaction with MtrCAB–OmcA, but also to the reduction of nitrogen compounds and DMSO by interacting with OTR and DmsE, respectively (**Figure 6**). These results demonstrate that STC is a promiscuous periplasmic electron shuttle with a variety of redox partners. Notwithstanding, STC is clearly selective in the mode of interaction with its multiple partners that always appears to involve the participation of heme IV. Interestingly, in contrast to STC, no interaction was observed between FccA with MtrD, DmsE, OTR, and ccNiR. These results contrast with the functional redundancy that FccA provides for STC revealed by delayed or no growth with ferric citrate, DMSO or nitrite as electron acceptors (Sturm et al., 2015) in double deletion mutant studies. Further studies will reveal whether the differences arise from different metabolic regulation in the mutant strains or if FccA interacts indirectly with partners in those metabolic pathways.

Supplementary Material

The Supplementary Material for this article can be found online at: http://journal.frontiersin.org/article/10.3389/fmicb.2015.00665

References

Abresch, E. C., Gong, X. M., Paddock, M. L., and Okamura, M. Y. (2009). Electron transfer from cytochrome c(2) to the reaction center: a transition state model for ionic strength effects due to neutral mutations. *Biochemistry* 48, 11390–11398. doi: 10.1021/bi901332t

Arnold, K., Bordoli, L., Kopp, J., and Schwede, T. (2006). The SWISS-MODEL workspace: a web-based environment for protein structure homology modelling. *Bioinformatics* 22, 195–201. doi: 10.1093/bioinformatics/bti770

Atkinson, S. J., Mowat, C. G., Reid, G. A., and Chapman, S. K. (2007). An octaheme c-type cytochrome from *Shewanella oneidensis* can reduce nitrite and hydroxylamine. *FEBS Lett.* 581, 3805–3808. doi: 10.1016/j.febslet.2007.07.005

Banci, L., Pierattelli, R., and Turner, D. L. (1995). Determination of haem electronic structure in cytochrome b5 and metcyanomyoglobin. *Eur. J. Biochem.* 232, 522–527. doi: 10.1111/j.1432-1033.1995.522zz.x

Bashford, D., and Karplus, M. (1990). pKa's of ionizable groups in proteins: atomic detail from a continuum electrostatic model. *Biochemistry* 29, 10219–10225. doi: 10.1021/bi00496a010

Bashir, Q., Scanu, S., and Ubbink, M. (2011). Dynamics in electron transfer protein complexes. *FEBS J.* 278, 1391–1400. doi: 10.1111/j.1742-4658.2011.08062.x

Berks, B. C., Ferguson, S. J., Moir, J. W., and Richardson, D. J. (1995). Enzymes and associated electron transport systems that catalyse the respiratory reduction of nitrogen oxides and oxyanions. *Biochim. Biophys. Acta* 1232, 97–173. doi: 10.1016/0005-2728(95)00092-5

Burns, J. L., and DiChristina, T. J. (2009). Anaerobic respiration of elemental sulfur and thiosulfate by *Shewanella oneidensis* MR-1 requires psrA, a homolog of the phsA gene of *Salmonella enterica* serovar typhimurium LT2. *Appl. Environ. Microbiol.* 75, 5209–5217. doi: 10.1128/AEM.00888-09

Coursolle, D., and Gralnick, J. A. (2010). Modularity of the Mtr respiratory pathway of *Shewanella oneidensis* strain MR-1. *Mol. Microbiol.* 77, 995–1008. doi: 10.1111/j.1365-2958.2010.07266.x

Coursolle, D., and Gralnick, J. A. (2012). Reconstruction of extracellular respiratory pathways for Iron(III) reduction in *Shewanella oneidensis* strain MR-1. *Front. Microbiol.* 3:56. doi: 10.3389/fmicb.2012.00056

Crowley, P. B., and Ubbink, M. (2003). Close encounters of the transient kind: protein interactions in the photosynthetic redox chain investigated by NMR spectroscopy. *Acc. Chem. Res.* 36, 723–730. doi: 10.1021/ar0200955

DeLano, W. L. (2003). *The PyMOL Molecular Graphics System*. San Carlos, CA: DeLano Scientific LLC.

Diaz-Moreno, I., Diaz-Quintana, A., Molina-Heredia, F. P., Nieto, P. M., Hansson, O., De la Rosa, M. A., et al. (2005a). NMR analysis of the transient complex between membrane photosystem I and soluble cytochrome c6. *J. Biol. Chem.* 280, 7925–7931. doi: 10.1074/jbc.M412422200

Diaz-Moreno, I., Diaz-Quintana, A., Ubbink, M., and De la Rosa, M. A. (2005b). An NMR-based docking model for the physiological transient complex between cytochrome f and cytochrome c6. *FEBS Lett.* 579, 2891–2896. doi: 10.1016/j.febslet.2005.04.031

Einsle, O., and Kroneck, P. M. (2004). Structural basis of denitrification. *Biol. Chem.* 385, 875–883. doi: 10.1515/BC.2004.115

Einsle, O., Messerschmidt, A., Huber, R., Kroneck, P. M., and Neese, F. (2002). Mechanism of the six-electron reduction of nitrite to ammonia by cytochrome c nitrite reductase. *J. Am. Chem. Soc.* 124, 11737–11745. doi: 10.1021/ja0206487

Firer-Sherwood, M. A., Bewley, K. D., Mock, J. Y., and Elliott, S. J. (2011). Tools for resolving complexity in the electron transfer networks of multiheme cytochromes c. *Metallomics* 3, 344–348. doi: 10.1039/c0mt00097c

Fonseca, B. M., Paquete, C. M., Neto, S. E., Pacheco, I., Soares, C. M., and Louro, R. O. (2013). Mind the gap: cytochrome interactions reveal electron pathways across the periplasm of *Shewanella oneidensis* MR-1. *Biochem. J.* 449, 101–108. doi: 10.1042/BJ20121467

Fonseca, B. M., Saraiva, I. H., Paquete, C. M., Soares, C. M., Pacheco, I., Salgueiro, C. A., et al. (2009). The tetraheme cytochrome from *Shewanella oneidensis* MR-1 shows thermodynamic bias for functional specificity of the hemes. *J. Biol. Inorg. Chem.* 14, 375–385. doi: 10.1007/s00775-008-0455-7

Francis, R. T. Jr., and Becker, R. R. (1984). Specific indication of hemoproteins in polyacrylamide gels using a double-staining process. *Anal. Biochem.* 136, 509–514. doi: 10.1016/0003-2697(84)90253-7

Fredrickson, J. K., Romine, M. F., Beliaev, A. S., Auchtung, J. M., Driscoll, M. E., Gardner, T. S., et al. (2008). Towards environmental systems biology of *Shewanella*. *Nat. Rev. Microbiol.* 6, 592–603. doi: 10.1038/nrmicro1947

Gralnick, J. A., and Newman, D. K. (2007). Extracellular respiration. *Mol. Microbiol.* 65, 1–11. doi: 10.1111/j.1365-2958.2007.05778.x

Gray, H. B., and Winkler, J. R. (2010). Electron flow through metalloproteins. *Biochim. Biophys. Acta* 1797, 1563–1572. doi: 10.1016/j.bbabio.2010.05.001

Hartshorne, R. S., Jepson, B. N., Clarke, T. A., Field, S. J., Fredrickson, J., Zachara, J., et al. (2007). Characterization of *Shewanella oneidensis* MtrC: a cell-surface decaheme cytochrome involved in respiratory electron transport to extracellular electron acceptors. *J. Biol. Inorg. Chem.* 12, 1083–1094. doi: 10.1007/s00775-007-0278-y

Hartshorne, R. S., Reardon, C. L., Ross, D., Nuester, J., Clarke, T. A., and Gates, A. J. (2009). Characterization of an electron conduit between bacteria and the extracellular environment. *Proc. Natl. Acad. Sci. U.S.A.* 106, 22169–22174. doi: 10.1073/pnas.0900086106

Hau, H. H., and Gralnick, J. A. (2007). Ecology and biotechnology of the genus *Shewanella*. *Annu. Rev. Microbiol.* 61, 237–258. doi: 10.1146/annurev.micro.61.080706.093257

Heidelberg, J. F., Paulsen, I. T., Nelson, K. E., Gaidos, E. J., Nelson, W. C., Read, T. D., et al. (2002). Genome sequence of the dissimilatory metal ion-reducing bacterium *Shewanella oneidensis*. *Nat. Biotechnol.* 20, 1118–1123. doi: 10.1038/nbt749

Judd, E. T., Youngblut, M., Pacheco, A. A., and Elliott, S. J. (2012). Direct electrochemistry of *Shewanella oneidensis* cytochrome c nitrite reductase: evidence of interactions across the dimeric interface. *Biochemistry* 51, 10175–10185. doi: 10.1021/bi3011708

Kiefer, F., Arnold, K., Kunzli, M., Bordoli, L., and Schwede, T. (2009). The SWISS-MODEL repository and associated resources. *Nucleic Acids Res.* 37, D387–D392. doi: 10.1093/nar/gkn750

Logan, B. E., and Rabaey, K. (2012). Conversion of wastes into bioelectricity and chemicals by using microbial electrochemical technologies. *Science* 337, 686–690. doi: 10.1126/science.1217412

Lovley, D. R. (2006). Bug juice: harvesting electricity with microorganisms. *Nat. Rev. Microbiol.* 4, 497–508. doi: 10.1038/nrmicro1442

Marritt, S. J., Lowe, T. G., Bye, J., McMillan, D. G., Shi, L., Fredrickson, J., et al. (2012). A functional description of CymA, an electron-transfer hub supporting anaerobic respiratory flexibility in *Shewanella*. *Biochem. J.* 444, 465–474. doi: 10.1042/BJ20120197

Massey, V. (1959). The microestimation of succinate and the extinction coefficient of cytochrome c. *Biochim. Biophys. Acta* 34, 255–256. doi: 10.1016/0006-3002(59)90259-8

Meschi, F., Wiertz, F., Klauss, L., Blok, A., Ludwig, B., Merli, A., et al. (2011). Efficient electron transfer in a protein network lacking specific interactions. *J. Am. Chem. Soc.* 133, 16861–16867. doi: 10.1021/ja205043f

Mowat, C. G., Rothery, E., Miles, C. S., McIver, L., Doherty, M. K., Drewette, K., et al. (2004). Octaheme tetrathionate reductase is a respiratory enzyme with novel heme ligation. *Nat. Struct. Mol. Biol.* 11, 1023–1024. doi: 10.1038/nsmb827

Myers, C. R., and Myers, J. M. (1997). Isolation and characterization of a transposon mutant of *Shewanella putrefaciens* MR-1 deficient in fumarate reductase. *Lett. Appl. Microbiol.* 25, 162–168. doi: 10.1046/j.1472-765X.1997.00196.x

Myers, C. R., and Nealson, K. H. (1988). Bacterial manganese reduction and growth with manganese oxide as the sole electron acceptor. *Science* 240, 1319–1321. doi: 10.1126/science.240.4857.1319

Myers, J. M., and Myers, C. R. (2000). Role of the tetraheme cytochrome CymA in anaerobic electron transport in cells of *Shewanella putrefaciens* MR-1 with normal levels of menaquinone. *J. Bacteriol.* 182, 67–75. doi: 10.1128/JB.182.1.67-75.2000

Nealson, K. H., and Saffarini, D. (1994). Iron and manganese in anaerobic respiration: environmental significance, physiology, and regulation. *Annu. Rev. Microbiol.* 48, 311–343. doi: 10.1146/annurev.mi.48.100194.001523

Perkins, J. R., Diboun, I., Dessailly, B. H., Lees, J. G., and Orengo, C. (2010). Transient protein-protein interactions: structural, functional, and network properties. *Structure* 18, 1233–1243. doi: 10.1016/j.str.2010.08.007

Pessanha, M., Rothery, E. L., Miles, C. S., Reid, G. A., Chapman, S. K., Louro, R. O., et al. (2009). Tuning of functional heme reduction potentials in

Shewanella fumarate reductases. *Biochim. Biophys. Acta* 1787, 113–120. doi: 10.1016/j.bbabio.2008.11.007

Pitts, K. E., Dobbin, P. S., Reyes-Ramirez, F., Thomson, A. J., Richardson, D. J., and Seward, H. E. (2003). Characterization of the *Shewanella oneidensis* MR-1 decaheme cytochrome MtrA: expression in *Escherichia coli* confers the ability to reduce soluble Fe(III) chelates. *J. Biol. Chem.* 278, 27758–27765. doi: 10.1074/jbc.M302582200

Richardson, D. J., Butt, J. N., Fredrickson, J. K., Zachara, J. M., Shi, L., Edwards, M. J., et al. (2012). The "porin-cytochrome" model for microbe-to-mineral electron transfer. *Mol. Microbiol.* 85, 201–212. doi: 10.1111/j.1365-2958.2012.08088.x

Rudolph, J. (2007). Inhibiting transient protein-protein interactions: lessons from the Cdc25 protein tyrosine phosphatases. *Nat. Rev. Cancer* 7, 202–211. doi: 10.1038/nrc2087

Saffarini, D. A., Blumerman, S. L., and Mansoorabadi, K. J. (2002). Role of menaquinones in Fe(III) reduction by membrane fractions of *Shewanella putrefaciens*. *J. Bacteriol.* 184, 846–848. doi: 10.1128/JB.184.3.846-848.2002

Schicklberger, M., Sturm, G., and Gescher, J. (2013). Genomic plasticity enables a secondary electron transport pathway in *Shewanella oneidensis*. *Appl. Environ. Microbiol.* 79, 1150–1159. doi: 10.1128/AEM.03556-12

Schwalb, C., Chapman, S. K., and Reid, G. A. (2003). The tetraheme cytochrome CymA is required for anaerobic respiration with dimethyl sulfoxide and nitrite in *Shewanella oneidensis*. *Biochemistry* 42, 9491–9497. doi: 10.1021/bi034456f

Scott, W., Hünenberger, P., Tironi, I., Mark, A., Billeter, S., Fennen, J., et al. (1999). The GROMOS biomolecular simulation program package. *J. Phys. Chem. A* 103, 3596–3607. doi: 10.1021/jp984217f

Shi, L., Lin, J. T., Markillie, L. M., Squier, T. C., and Hooker, B. S. (2005). Overexpression of multi-heme C-type cytochromes. *Biotechniques* 38, 297–299. doi: 10.2144/05382PT01

Simon, J. (2002). Enzymology and bioenergetics of respiratory nitrite ammonification. *FEMS Microbiol. Rev.* 26, 285–309. doi: 10.1111/j.1574-6976.2002.tb00616.x

Sturm, G., Richter, K., Doetsch, A., Heide, H., Louro, R. O., and Gescher, J. (2015). A dynamic periplasmic electron transfer network enables respiratory flexibility beyond a thermodynamic regulatory regime. *ISME J.* doi: 10.1038/ismej.2014.264 [Epub ahead of print].

Tsapin, A. I., Vandenberghe, I., Nealson, K. H., Scott, J. H., Meyer, T. E., Cusanovich, M. A., et al. (2001). Identification of a small tetraheme cytochrome c and a flavocytochrome c as two of the principal soluble cytochromes c in *Shewanella oneidensis* strain MR1. *Appl. Environ. Microbiol.* 67, 3236–3244. doi: 10.1128/AEM.67.7.3236-3244.2001

Worrall, J. A., Reinle, W., Bernhardt, R., and Ubbink, M. (2003). Transient protein interactions studied by NMR spectroscopy: the case of cytochrome C and adrenodoxin. *Biochemistry* 42, 7068–7076. doi: 10.1021/bi0342968

Youngblut, M., Judd, E. T., Srajer, V., Sayyed, B., Goelzer, T., Elliott, S. J., et al. (2012). Laue crystal structure of *Shewanella oneidensis* cytochrome c nitrite reductase from a high-yield expression system. *J. Biol. Inorg. Chem.* 17, 647–662. doi: 10.1007/s00775-012-0885-0

Zhang, H., Chobot, S. E., Osyczka, A., Wraight, C. A., Dutton, P. L., and Moser, C. C. (2008). Quinone and non-quinone redox couples in Complex III. *J. Bioenerg. Biomembr.* 40, 493–499. doi: 10.1007/s10863-008-9174-6

Regulation of electron transfer processes affects phototrophic mat structure and activity

Phuc T. Ha[1], Ryan S. Renslow[2], Erhan Atci[1], Patrick N. Reardon[2], Stephen R. Lindemann[3], James K. Fredrickson[3], Douglas R. Call[4] and Haluk Beyenal[1]*

[1] The Gene and Linda Voiland School of Chemical Engineering and Bioengineering, Washington State University, Pullman, WA, USA, [2] Environmental Molecular Sciences Laboratory, Pacific Northwest National Laboratory, Richland, WA, USA, [3] Biological Sciences Division, Pacific Northwest National Laboratory, Richland, WA, USA, [4] Paul G. Allen School for Global Animal Health, Washington State University, Pullman, WA, USA

Phototrophic microbial mats are among the most diverse ecosystems in nature. These systems undergo daily cycles in redox potential caused by variations in light energy input and metabolic interactions among the microbial species. In this work, solid electrodes with controlled potentials were placed under mats to study the electron transfer processes between the electrode and the microbial mat. The phototrophic microbial mat was harvested from Hot Lake, a hypersaline, epsomitic lake located near Oroville (Washington, USA). We operated two reactors: graphite electrodes were polarized at potentials of -700 mV$_{Ag/AgCl}$ [cathodic (CAT) mat system] and $+300$ mV$_{Ag/AgCl}$ [anodic (AN) mat system] and the electron transfer rates between the electrode and mat were monitored. We observed a diel cycle of electron transfer rates for both AN and CAT mat systems. Interestingly, the CAT mats generated the highest reducing current at the same time points that the AN mats showed the highest oxidizing current. To characterize the physicochemical factors influencing electron transfer processes, we measured depth profiles of dissolved oxygen (DO) and sulfide in the mats using microelectrodes. We further demonstrated that the mat-to-electrode and electrode-to-mat electron transfer rates were light- and temperature-dependent. Using nuclear magnetic resonance (NMR) imaging, we determined that the electrode potential regulated the diffusivity and porosity of the microbial mats. Both porosity and diffusivity were higher in the CAT mats than in the AN mats. We also used NMR spectroscopy for high-resolution quantitative metabolite analysis and found that the CAT mats had significantly higher concentrations of osmoprotectants such as betaine and trehalose. Subsequently, we performed amplicon sequencing across the V4 region of the 16S rRNA gene of incubated mats to understand the impact of electrode potential on microbial community structure. These data suggested that variation in the electrochemical conditions under which mats were generated significantly impacted the relative abundances of mat members and mat metabolism.

Keywords: electron transfer, Hot Lake, microbial mats, current, microelectrodes, mat structure, metabolite analysis, microbial community

Introduction

Phototrophic microbial mats are remarkable self-sustaining natural ecosystems, being composed of highly interactive species that completely cycle energy and elements within them (Guerrero et al., 2002; Des Marais, 2003; Bender and Phillips, 2004). These systems undergo daily cycling of redox potential caused by variations in light energy input and metabolic interactions among the microbial species (Frund and Cohen, 1992; Burow et al., 2012). Light also drives mat structure and activity by providing a diverse energy spectrum to sustain photosynthesis in photosynthetic microorganisms, which fix carbon and produce organic materials needed by other microorganisms in the community. Numerous studies have characterized the variations in physicochemical parameters, the elemental cycles, and the diversity and interactions of the microbial community members within the mat (Des Marais, 1995; Decker et al., 2005; van der Meer et al., 2005; Burow et al., 2012; Lindemann et al., 2013; Pages et al., 2014). Mat systems provide an excellent ecological model that can be used to investigate how microbial populations associate and interact as well as how electrons are used for energy transfer (Guerrero et al., 2002; Babauta et al., 2014). In this ecological model, electrons have to be transferred to convert and carry captured light energy to the deeper layers of the mat. The mat structure, inclusive of its physical structure and pore distribution, may play a critical role in these mass and energy transport processes (Moran et al., 2014). Therefore, it is critical to understand the effects of electron transfer processes on mat structure and activity. Energy transfer in a microbial mat starts with light energy being absorbed in the photic zone of the mat, which allows fixation of carbon dioxide by photoautotrophs. This energy transfer is mediated by diverse processes, such as the synthesis of organic compounds (e.g., carbohydrates) and their diffusion to deeper, and frequently hypoxic, strata of the mat where they may be consumed by fermenters and/or sulfate reducers (Paerl et al., 2000). Many of these reactions involve extracellular electron transfer processes, which can occur either directly or through electron carriers (mediators). We hypothesized that regulating the electron transfer processes in a mat system would, in turn, change its structure and activity. "Structure" refers to the physical structure or architecture of the mat, and "activity" refers to the metabolites and energy exchanged by the mat. According to our previous work and other work in the literature, electron transfer processes can be controlled by controlling the potential of an inert solid electrode and using it as an electron donor or acceptor in a biological system (Renslow et al., 2013).

Use of polarized electrodes to study electron transfer by microorganisms has become an important tool for filling the knowledge gap about microbial electrochemical activities (Rabaey et al., 2007). This technique offers a unique strategy for controlling the activity of a microbial population by accepting or donating electrons from/to the local environment. The measured electron transfer rate can be used to interpret the response of microbial activities to the perturbation of electron transfer processes. Some microbial species respond by altering their metabolism, activating a defense mechanism, or reducing their growth rates. Other microbial species benefit because of their ability to transfer or accept electrons from the electrodes (Babauta et al., 2014). Thus, by increasing the metabolic activities of certain species present near the electrode surface, the electrode potential will not only select the species enriched on it but also regulate the structure, activity, and composition of the local microbial community. To the best of our knowledge, the responses of mat structure, activity, and electron transfer rates when solid electrodes are employed to accept or donate electrons have not yet been quantified.

The goal of this work is to characterize the response of a microbial mat to a solid electron acceptor and a donor. The phototrophic microbial mats used in this study were derived from Hot Lake, a hypersaline, epsomitic lake located near Oroville (Washington, USA). The seasonal characteristics of mat and lake conditions were described detail by Lindemann et al. (2013). The electrodes were placed at the bottom of the mat to create the mat electrochemical systems. The electrodes that provided electrons to the mat were polarized at -700 mV$_{Ag/AgCl}$ (hereafter called the "CAT mat"). The ones that worked as an electron sink were polarized at $+300$ mV$_{Ag/AgCl}$ (hereafter called the "AN mat"). The electron transfer rates from mat-to-electrode and from electrode-to-mat were continuously monitored. We quantified the diel cycling of AN and CAT mats. To understand the factors affecting the diel cycle, (1) we examined the influences of temperature and light condition, separately, to electron transfer rate; (2) we used microelectrodes to measure the depth profiles of hydrogen sulfide and oxygen concentrations; and (3) we introduced acetate and sulfide into AN and CAT mats and quantified their influence on electron transfer rates, separately. To understand how AN or CAT processes regulate mat structure and activity, we used nuclear magnetic resonance (NMR) imaging for morphology and NMR metabolite analysis to quantify the activity of the mats. Finally, we employed amplicon sequencing across the V4 region of the 16S gene to determine the effect of electrochemical regime upon mat community structure.
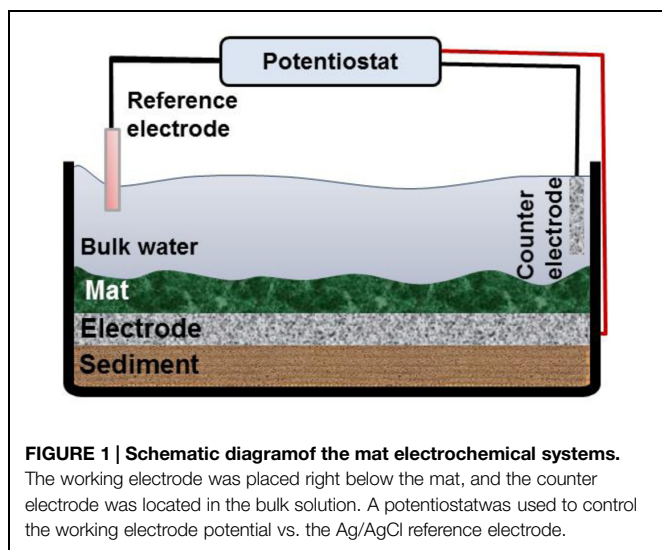
Materials and Methods

Field Site and Sample Collection

Hot Lake is located near Oroville, North Washington, CO, USA. Photosynthetic microbial mats and Hot Lake water were sampled on June 6th and September 26th, 2014. Each mat sample was between 1.5 and 2 cm in depth and about 200 cm^2 in size. The samples were kept in petri dishes and placed in a cold ice box when carried to our laboratory at Washington State University, Pullman, WA, USA. Upon arrival, the mat was paced in glass jars and covered with Hot Lake water from the field site. Mats were kept under natural solar conditions and at room temperature for 2 days before being transferred to the mat electrochemical systems.

Construction of Mat Electrochemical Systems and Current Monitoring

We used an acrylic aquarium with a working volume of 1.5 L to construct the mat electrochemical systems. The reactors

FIGURE 1 | Schematic diagram of the mat electrochemical systems.
The working electrode was placed right below the mat, and the counter electrode was located in the bulk solution. A potentiostat was used to control the working electrode potential vs. the Ag/AgCl reference electrode.

mimicked the lake condition without flow (**Figure 1**). For each reactor, approximately 3 cm of sediment was added to the bottom of the reactor. Then the hollow polycarbonate plate on which the graphite cloth electrode (2.5c m × 2.5 cm) was embedded was placed on top of the sediment. The mat was carefully placed on top of the electrode. The electrode placed under the mat was used as the working electrode. The counter electrode was constructed by attaching another piece of graphite cloth (2.5 cm × 2.5 cm) to a hollow plastic dish and placing it in the water phase of the reactor. Ti wire was woven into each electrode and secured with nylon bolts. The part of the Ti wire that was exposed to Hot Lake water was covered by marine sealant and inserted into a sealed silicon tube. During operation of the reactor, deionized (DI) water was added periodically to maintain the water level and salinity in the reactor. All the reactors were operated under natural solar conditions: they were incubated near a laboratory window. For some experiments, the reactors were moved to an incubator or to a water bath with controlled temperature, as described in the relevant sections.

A 6-channel custom-built potentiostat was used to control the desired potential of the working electrodes under the mat (Renslow et al., 2011). The custom-made Ag/AgCl reference electrodes were used ($\sim +210$ mV vs. SHE). We operated reactors in which the graphite electrodes were polarized at potentials of -700 mV$_{Ag/AgCl}$ (CAT mat) and $+300$ mV$_{Ag/AgCl}$ (AN mat). These potentials are in the range that was previously used to enrich AN and CAT communities in bioelectrochemical systems (Wagner et al., 2010; Tremblay and Zhang, 2015). Moreover, due to the presence of sulfide in the mat we polarized cathode at lower potential than the redox potential of sulfide ($E^o_{H2S/So} = -490$ mV$_{Ag/AgCl}$) to prevent the deposition of elemental sulfur on the electrode. We also operated a mat system under open circuit condition as the control mat [open circuit potential (OCP) mat]. Two technical replicates with two biological replicates were performed for all experiments.

Effects of Light Intensity, Temperature and Electron Donor/Acceptor Addition on the Mat

To examine the effects of light/dark conditions with AN and CAT currents, we operated our mat systems in an incubator. An incandescent light bulb was used as the light (light intensity of 6.4 ± 0.2 μmol/m^2/s). The temperature was maintained by the incubator at the same value as under the light ($22.5 \pm 1°$C). To examine the effect of temperature on current, the mat electrochemical systems were placed in a temperature-controlled water bath. The water bath was covered to prevent light penetration when needed. The effects of acetate and sulfide on the electron transfer process were examined by carefully injecting 2 mL of 1 M acetate solution or 0.3 mL of 0.1 M Na$_2$S.9H$_2$O solution into the bottom of the mat. The mat systems were operated under constant light (6.4 ± 0.2 μmol/m^2/s) and stable temperature ($22.5 \pm 1°$C) to minimize the acetate and sulfide production by the mat itself.

Dissolved Oxygen and H$_2$S Microelectrodes and Measurements

The DO microelectrodes were constructed according to the procedure described by Lewandowski and Beyenal (2014). The final tip diameter of the DO microelectrodes was ~ 15 μm. A Keithley 6517 A electrometer/high-resistance meter was used as both the voltage source and an ammeter. The DO microelectrodes were polarized to -800 mV$_{Ag/AgCl}$ during the operation. Prior to use, the DO microelectrodes were calibrated using two-point calibration: in the air-saturated solution and in Na$_2$SO$_3$ solution (zero oxygen concentration). Microelectrode movements were administered using a Mercury Step motor controller PI M-230.10S Part No. M23010SX (Physik Instrumente, Auburn, MA, USA). Each microelectrode was positioned ~ 2000 μm above the mat surface and stepped down in 50-μm increments using a custom microprofiler. For the DO profiles, the measurements were taken in the air first (~ 1 mm) and in the bulk above the mat (~ 1 mm) until the microelectrode touched the mat surface; then ~ 3 mm of profile was measured in the mat. Before the DO profiles were measured, some of the bulk liquid above the mat was discharged.

The hydrogen sulfide microelectrodes were constructed and operated according to Jeroschewski et al. (1996). The hydrogen sulfide microelectrodes had tip diameters of ~ 20 μm. A Gamry Interface 1000TM potentiostat (Gamry® Instruments, Warminster, PA, USA) was used to polarize the hydrogen peroxide microelectrodes at $+100$ mV against a Pt counter electrode. The microelectrode was calibrated in standard solutions of various hydrogen sulfide concentrations prepared by dissolving Na$_2$S in anoxic phosphate buffer (16 mM, pH 7). The response of the microelectrodes was linear in the range of hydrogen sulfide concentrations from 0 to 570 μM. The hydrogen sulfide microelectrode was placed ~ 1 mm above the mat surface, and the microelectrode was stepped down in 1-mm increments through 13 mm of the mat thickness using the manual control. After the depth profiles were measured, the microelectrode was left at the 13-mm depth to monitor the hydrogen sulfide concentration over 24 h. Each

microelectrode used in the measurements was also calibrated for verification after the measurements. A Zeiss Stemi 2000 stereomicroscope was used to determine the locations of the microelectrode tip and the mat surface during all microelectrode experiments.

Morphology Analysis using NMR Micro-Imaging

Pulsed-field gradient NMR (PFG-NMR) was used to observe mat morphology and determine intra-mat porosity and diffusion coefficients. The techniques used were similar to those of Renslow et al. (2013). The details of the NMR imaging techniques and full method descriptions are provided in the Supplementary Information. Briefly, the NMR imaging experiments were conducted at 500.40 MHz for proton (1H) detection using a 89-mm-wide bore 11.7-T magnet with a Bruker Avance III digital NMR spectrometer and ParaVision 5.1 imaging software (Bruker Instruments, Billerica, MA, USA). Each mat sample was placed in a 15-mm NMR tube on a support bed of 2% agar gel. Experiments performed included 2D magnetic resonance imaging (mic_flash), diffusion tensor imaging for determining diffusion coefficients (DtiStandard; Renslow et al., 2013), and chemical shift selective imaging for generating porosity measurements.

Metabolite Analysis using NMR Spectroscopy

Sections of microbial mat were dissected out such that the full thickness of the mat was retained. Mat samples were frozen at $-80°C$ immediately following dissection and lyophilized before their dry weight was measured. Dried samples were coarsely ground in glass vials using a small metal spatula. Metabolite extraction was performed using a 1:1:1 volume of water:methanol:chloroform. Ice cold solvents were sequentially added to the samples in the order listed. Samples were allowed to extract and phase separate at $-20°C$ for $\sim$24 h. Samples were spun at $4000 \times g$ for 10 min, and the hydrophilic supernatant was removed. Samples were spun again at $20800 \times g$ for 10 min, and 1 mL of supernatant was retained. The retained samples were dried under vacuum in a speedvac overnight. Dried samples were dissolved in 50 mM sodium phosphate at pH 7, with 10% D_2O, 448 uM DSS, and 10 mM imidazole.

Nuclear magnetic resonance spectroscopy was carried out using an Agilent VNMRS 600 MHz (proton frequency) spectrometer equipped with a cryogenically cooled HCN triple resonance probe. One-dimensional NOESY experiments were performed using the following parameters, 28896 complex points (acquisition time of 4 s), a recycle delay of 1 s, a sweep width of 12 ppm and 512 scans per experiment for a total acquisition time of $\sim$48 min per sample. The temperature was held constant at 25°C. The NMR spectra were Fourier transformed, phased, baseline corrected and apodized (0.5-Hz line broadening) using nmrPipe. Spectra were referenced to DSS at 0 ppm. Data were imported into Chenomx NMR Suite (Chenomx, Inc., Edmonton, AB, Canada) for subsequent metabolic profiling. Profiling was carried out independently by two operators to reduce operator bias. The DSS internal standard was used to determine metabolite concentrations.

Imidazole peaks were used to correct for pH differences. The raw data in varian format is submitted as Supplemental Information.

Community Structure Analysis using 16S rRNA Sequencing

Mat community structure changes were examined using 16S rRNA amplicon sequencing. Two samples of mat ($\sim$4 cm^2) were collected for each condition: (OCP, AN and CAT). These samples were further subdivided into nine subsamples. Genomic DNA (gDNA) was extracted as described in Lindemann et al. (2013) with the following modifications: prior to extraction, samples were washed three times with washing buffer containing 0.5 M EDTA and 0.55 M NaCl at pH 8.0 and suspended in lysis buffer (50 mM Tris/25 mM EDTA pH 8.0). Samples were then transferred to Lysing Matrix E tube (MP Biomedicals, Santa Ana, CA, USA) and beat for 2 min. After centrifugation (16,000 rpm for 90 s) the aqueous portions were incubated at 85° C for 5 min to inactivate native nucleases and slowly cooled to 37°C. Chemical lysis then was initiated by adding 70 µl of 10% SDS and proteinase K to the final concentration of 0.2 mg/ml prior to incubation at 56°C for 1 h. Subseqently, 100 µl of NaCl 5 M and 100 µl of CTAB/NaCl solution were added to samples and incubated at 65°C for 10 min. Post-lysis, DNA was extracted with phenol-chloroform-isoamyl alcohol (25:24:1) and then chloroform-isoamyl alcohol (24:1) before being treated with RNAase (10 µg) at 37°C for 30 min. DNA was precipitated with addition of 1:10 vol of sodium acetate 3 M (pH 5.5) and ice-cold 100% ethanol, washed in 70% ethanol, dried and resuspended in TE buffer (10 mM Tris-HCl at pH 8.0, 1 mM EDTA). Similarly, gDNA was extracted from fresh mats harvested at Hot Lake at the same time as those used in incubation studies but immediately frozen in 2.3 M sucrose and held at $-80°C$ prior to extraction. gDNA was amplified and sequenced as described previously (Caporaso et al., 2012). Briefly, the V4 region of the 16S rRNA gene was amplified using primers 515F and 806R with 0–3 random bases and the Illumina sequencing primer binding site (Caporaso et al., 2011) and amplicons were sequenced on an Illumina MiSeq using MiSeq Reagent Kit MS-102-2001 {[v2 chemistry over 500 total cycles (2 × 250); Illumina, San Diego, CA, USA]}. Sequences were demultiplexed and processed using mothur v. 1.34.1 (Schloss et al., 2009) according to the MiSeq SOP (http://mothur.org/wiki/MiSeq_SOP, accessed 7/6/15) except for the following modifications: (1) sequences were aligned against a SILVA reference alignment to which full-length 16S clones from Hot Lake had been added (Lindemann et al., 2013), and (2) only sequences that could not be placed within any of the domains of life were removed using remove.lineage(taxon = unknown). Sequences were clustered using a 0.03 average neighbor cutoff using cluster.split at the Order level (taxlevel = 4) and subsampled to 6283 sequences per sample; all samples containing fewer sequences were discarded from the analysis. Bray–Curtis dissimilarity (Bray and Curtis, 1957) was calculated for all pairwise combinations of samples using dist.shared (calc = braycurtis) and a neighbor-joining dendrogram was constructed using the tree.shared() command.

FIGURE 2 | Electron transfer rates (A) from the microbial mat to the electrode in the anodic (AN) mat and **(B)** from the electrode to the microbial mat in the cathodic (CAT) mat. Both systems showed the cyclic fluctuation of current which is also referred to as the diel cycle.
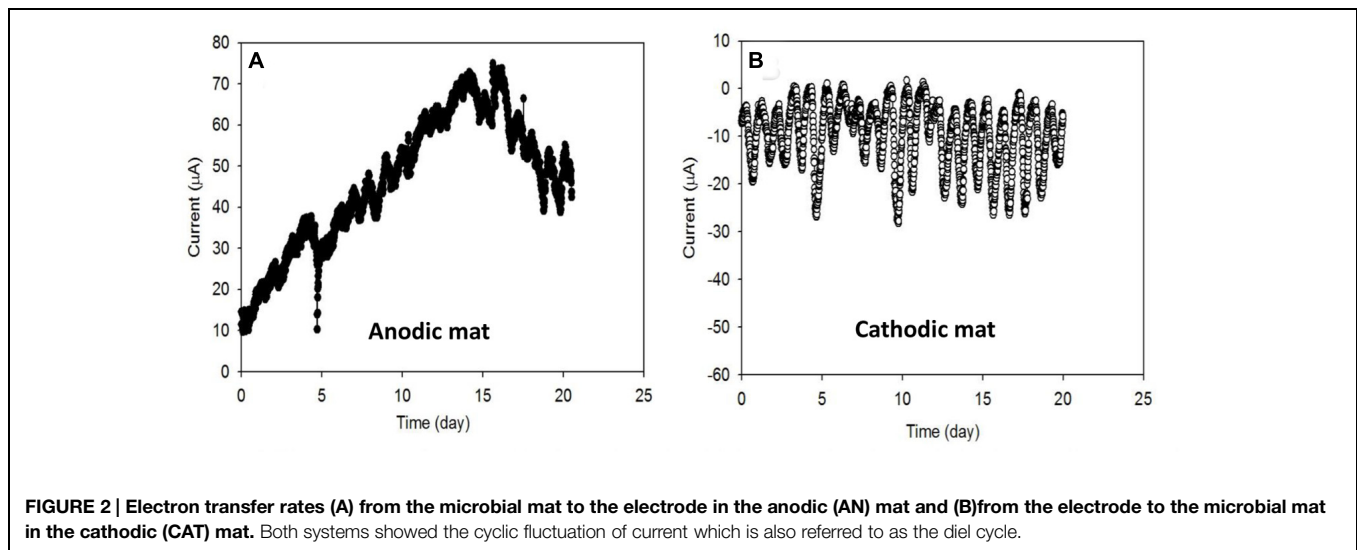
Results and Discussion

Electron Transfer Rates in Anodic and Cathodic Mat Systems

Current generated from AN and CAT mats over the first 20 days under ambient light conditions is shown in **Figure 2**. Increasing AN current over time (**Figure 2A**) indicated that electrons were transferred from the mat to the solid electrode during the first 15 days. The current generation started immediately after the electrode was polarized. It developed in the range from 10 μA to about 70 μA with cyclic fluctuation. We hypothesized that these electrons may be transferred to the anode either (1) through direct sulfide oxidation (Rabaey et al., 2006; Babauta et al., 2014) and/or (2) through microbial exogenous electron transfer (Lovley, 2008; Logan, 2009). In the first case, the abiotic oxidation of sulfide generates electrons and elemental sulfur is deposited on the electrode (Rabaey et al., 2006). Sulfide is commonly produced in phototrophic mats by sulfate-reducing bacteria. Because the sulfate concentration in the Hot Lake environment is extremely high, ranging from ∼200 mM to 1.8 M (Lindemann et al., 2013), the rate of sulfide production depends on the availability of substrates for sulfate reducers such as H_2 and acetate. In the case of exogenous electron transfer, electrogenic bacteria act as a catalyst which oxidizes substrates and transfers electrons to the electrode. The rate of electron transfer is governed by the enrichment of the electrogens and the concentration of the available substrates in the mat. Thus, in both cases the current generated by an AN microbial mat is regulated by substrate availability at the bottom of the mat.

A recent study reported that green sulfur bacteria were a dominant population on a polarized AN microelectrode (Babauta et al., 2013). Sulfur cycling in combination with the activities of green sulfur bacteria was hypothesized to be the cause for the cycling of current. In another study, Badalamenti et al. (2013) used a large-size graphite electrode to enrich AN biofilm from a microbial mat inoculum (Badalamenti et al., 2013). The authors found that the phototrophically enriched anode biofilms

were dominated by green sulfur bacteria. These bacteria were reported to have the ability to respire on electrodes. Thus, it is possible that the phototrophic community is also involved in the current production from our AN mat.

We also observed that the negative current generation from the CAT mat started immediately after the electrode was polarized (**Figure 2B**). Like the AN condition, mat under CAT conditions showed cyclic current fluctuations. Among the cycles, the lowest current ranged from approximately −0 μA to approximately −5 μA while the highest ranged from about −10 μA to about −30 μA. The generation of negative current indicates the consumption of electrons from the solid electrode by the mat. These electrons could be consumed by (1) an abiotic oxidant such as oxygen or (2) biocathodic microbes (Lovley and Nevin, 2011; Rosenbaum et al., 2011). In the first case, the current would be controlled by the DO concentration near the electrode surface. Oxygen is generated in the mat during the day by oxygenic phototrophs in the illuminated zone near the surface. Thus, the abiotic CAT current will be ultimately governed by photosynthetic activity and the diffusion of the oxygen through the mat. In the latter case, the current would be governed by the enrichment of microbes that are capable of using the electrode as an electron source for their metabolism.

In the literature, CAT current has been obtained from mixed CAT cultures enriched from wastewater (Marshall et al., 2012), activated sludge (Su et al., 2013), freshwater (Babauta et al., 2013), and pure bacterial cultures (Gregory et al., 2004; Nevin et al., 2011; Ueki et al., 2014). Our study demonstrates that CAT current can also be generated by the phototrophic mat community. Microbes that can potentially consume electrons from solid electrodes include methanogens (Villano et al., 2010), acetogens (Nevin et al., 2011), phototrophs (Bose et al., 2014) and oxygen reducers (Clauwaert et al., 2007; Debuy et al., 2015).

Diel Cycle of Cathodic and Anodic Current

To understand the reasons for the cyclic fluctuation seen during the development of AN and CAT current, we superimposed
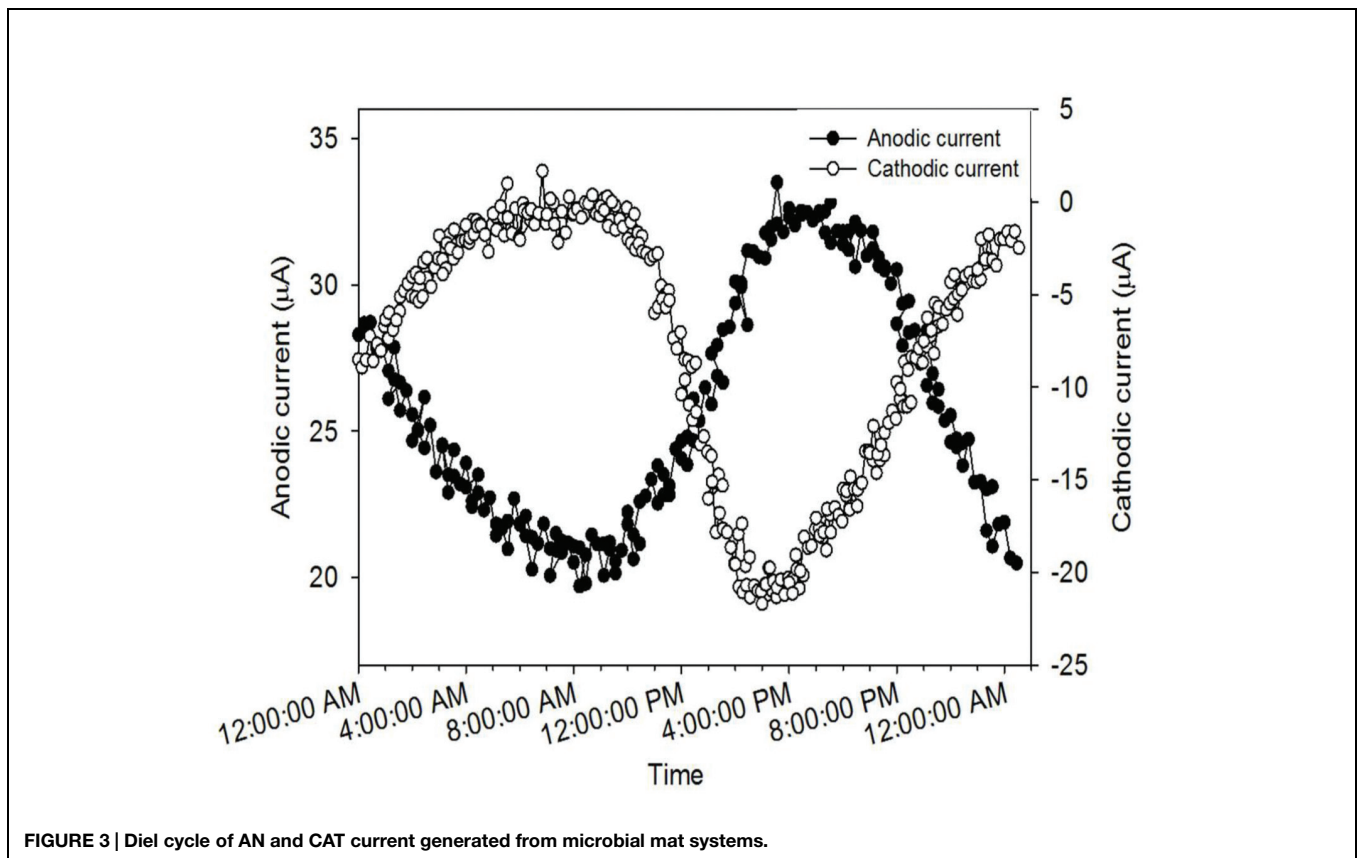
FIGURE 3 | Diel cycle of AN and CAT current generated from microbial mat systems.

individual cycles of each current as a function of time. **Figure 3** shows that both AN and CAT current followed an oscillating pattern in tandem with the diel cycle. It is known that phototrophic mats generally undergo a diel cycling of redox potential and speciation of redox-active elements caused by diel variations in light intensity and temperature and hence metabolic interactions among the microbial species (Finke and Jorgensen, 2008; Burow et al., 2012). Thus, the diel cycling of our current is likely to have been caused by these diel variations.

Interestingly, the lowest and highest points in the diel cycles of AN and CAT current occurred at the same time (**Figure 3**). The minimum values of AN and CAT current both occurred at about 8:00 a.m. (20 μA for AN current and −1 μA for CAT current). Similarly, the AN mat generated its highest current (33 μA) simultaneously with the CAT mat generating its highest current (−22 μA), at around 4:00 p.m. Thus, the CAT mat achieved its highest reducing potential at the same time that the AN mat achieved its highest oxidizing potential. The similarity in diel pattern suggested that the CAT and AN mat currents were governed by the same factors. However, the contrary redox characteristics of the two mat systems indicated that (1) there was an element or a microbial group in the mat that could function as both electron donor and electron acceptor to/from a solid electrode or (2) the characteristic of the mat was changed by the polarized potential of the solid electrode.

Effect of Temperature on Electron Transfer Process

Under natural conditions, temperature and light intensity co-vary. Therefore, to isolate the effect of temperature change on the current, we operated the system in the dark. The AN and CAT currents were compared with the maximum current obtained at 4:00 p.m. from the closest diel cycle. At that time, the temperature was about $21.3 \pm 0.2°C$.

Figure 4 shows that in the dark the AN current increased as temperature increased. This agrees with the observations made when the system was operated under diel temperature changes (Supplementary Figure S1). The current was highest at 4:00 p.m., when the temperature reached a maximum value of about 23°C. The effect of temperature on AN current may be due to an increase of chemical and biological activities that contribute electrons to the electrode. Because of the temperature dependence, we believe that the decrease of AN current after 15 days of operation under ambient temperature (**Figure 2A**) was caused by temperature differences owing to seasonal change.

In the dark with a constant temperature, the CAT current did not oscillate as was observed under diel cycling. Despite an increasing temperature, the current was significantly lower than the maximum obtained during diel cycling (at 4:00 p.m.; −15 μA vs. > −3.5 μA). Although the CAT current also increased with increasing temperature the change was not significant compared with the difference under a diel temperature change (Supplementary Figure S2). This suggests that the temperature
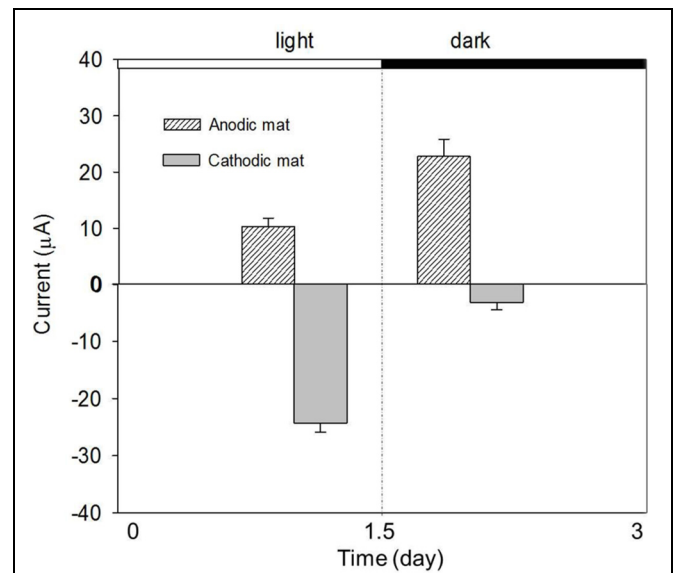
FIGURE 4 | Performance of AN and CAT currents at various temperatures. The currents were compared with the maximum current obtained at 4:00 p.m. under the diel condition.

FIGURE 5 | Performance of AN and CAT currents with a change of light condition. The AN and CAT mats showed opposite responses to the change of light condition.
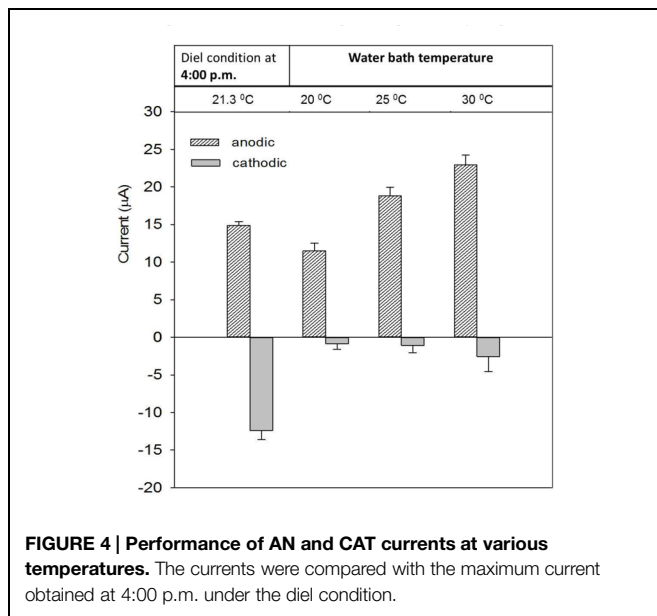
change was not the main factor governing the diel cycling of CAT current.

Effect of Light Energy on Electron Transfer Processes

The effect of the light on the AN and CAT currents was further investigated under constant temperature. **Figure 5** shows the currents obtained from the AN and CAT mats under light and dark conditions. Both the AN and the CAT current changed in response to light. The AN current increased when the system was operated in the dark (10–23 μA). In contrast, the CAT current was higher in the light than in the dark (−23 μA vs. −2.5 μA). Thus, the two exhibit an opposite responses to light.

Because of the association of light intensity and temperature, our recorded diel temperature showed that the highest temperature was reached when the light intensity was highest (at 4:00 p.m.). Thus, it is clear from the diel cycle that the highest AN current occurred when the highest light intensity was presented to the mat (**Figure 3**). This is the opposite of the observation in **Figure 5**, in which the AN current was higher in the dark than in the light. The increase of AN current during the dark might be because: when illuminated, phototrophic microbes will convert light energy to chemical energy typically stored in organic polymers such as glycogen and in the dark depolymerized to form monomers that fermented to easily respired compounds such as H_2 and acetate. These compounds will diffuse through the mat (Des Marais, 2003; Burow et al., 2012). Fermentation products could increase sulfide production from sulfate reduction which, in consequence, increase the current caused by sulfide oxidation on electrode. Fermentation products could also be used as substrates for electrogenic bacteria which use the electrode as an electron acceptor. Thus, the inconsistency between the behavior of AN current in light/dark tests and that observed during the diel cycle suggests that a diffusion process may control the transport of fermentation products from the phototrophic layer to the bottom of the AN mat. Therefore, the highest AN current was delayed from the darkest time in the diel cycle.

The significant increase of CAT current in the light reveals that electron consumption in a CAT mat is light-dependent (**Figure 5**). This is consistent with the observation from diel cycle results in which the CAT current was highest when the highest light intensity was present. The light-dependent behavior of CAT current also explains why the CAT current in the dark was lower than that obtained at 4:00 p.m. in the diel condition in spite of increased temperature at this time (**Figure 4**). One hypothesis to explain this is that the CAT current was caused by the abiotic reduction of oxygen by electrode which diffused from the aerobic phototrophic layer. If this is the case, oxygen must have diffused through the mat fast enough that the CAT current cycle synchronized with the light intensity cycle.

Effect of Sulfide and Acetate Additions on the Electron Transfer Process

As previously mentioned, AN current is regulated by the availability of an electron source in the surrounding environment. In this experiment, we examined the response of current to two different electron sources: sulfide and acetate. Acetate is a common end product of fermentation while sulfide is a common product of anaerobic respiration in phototrophic mats (Grotzschel et al., 2002).

Figure 6A shows that the AN current increased immediately after an injection of sodium sulfide (5 mg). However, the current decreased quickly to the background value, indicating that sulfide was rapidly oxidized in this system. Since sulfide is normally produced from sulfate reduction in a microbial mat, these results
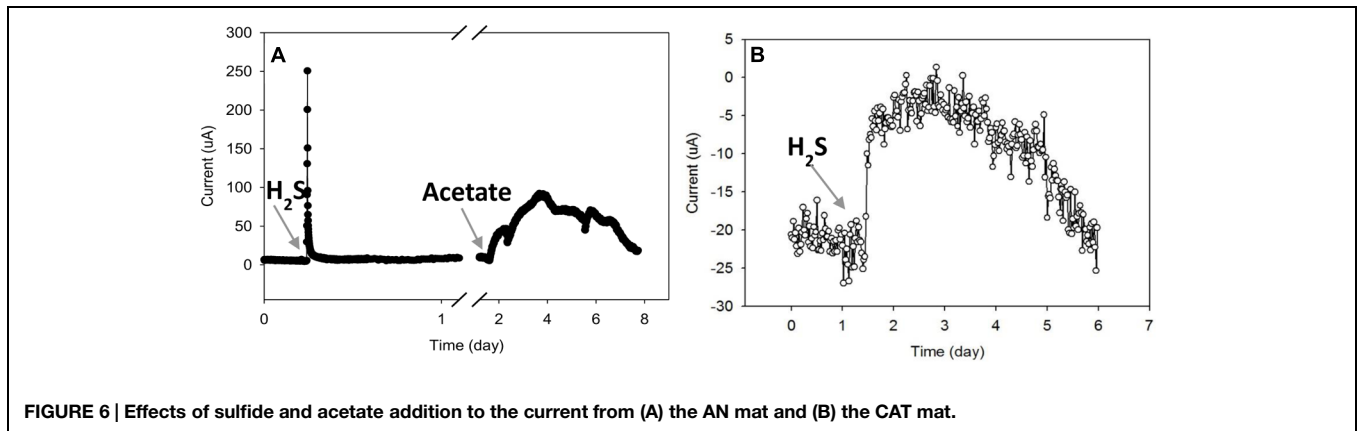
FIGURE 6 | Effects of sulfide and acetate addition to the current from (A) the AN mat and (B) the CAT mat.
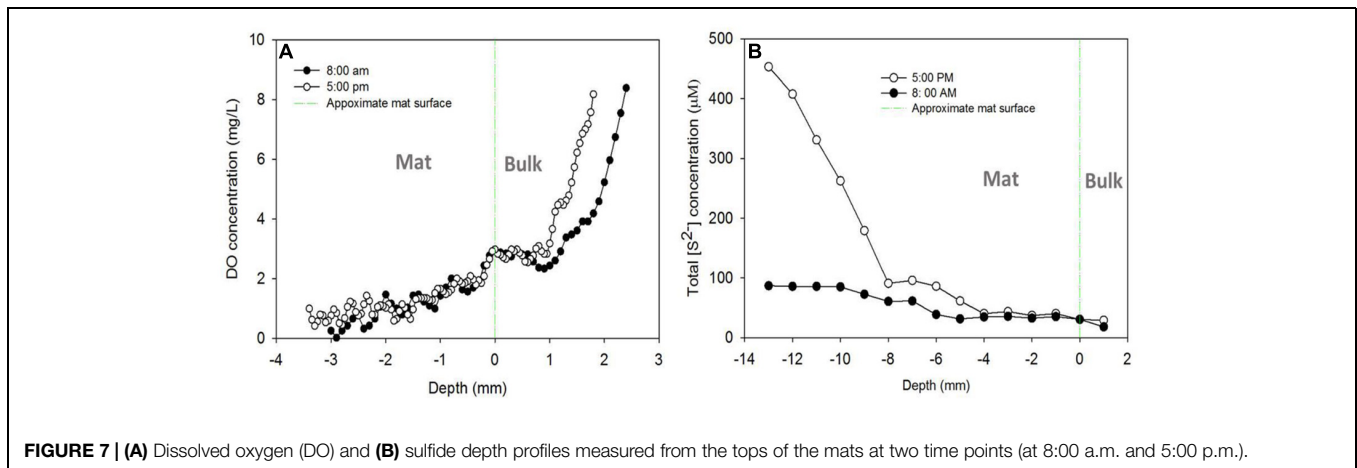

FIGURE 7 | (A) Dissolved oxygen (DO) and (B) sulfide depth profiles measured from the tops of the mats at two time points (at 8:00 a.m. and 5:00 p.m.).
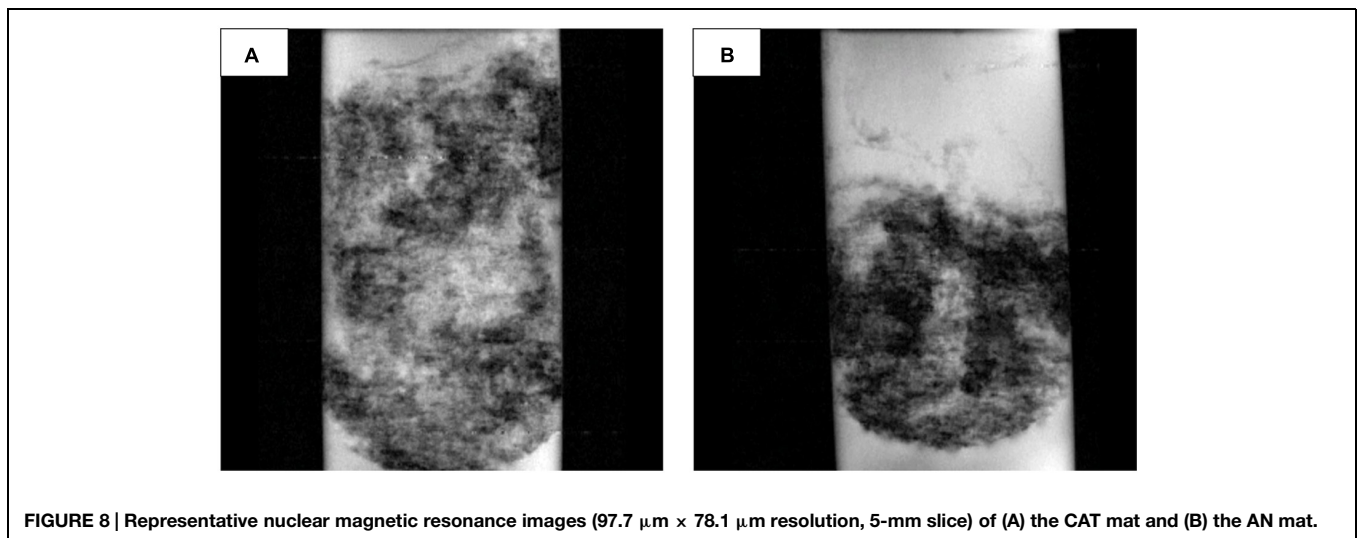

FIGURE 8 | Representative nuclear magnetic resonance images (97.7 μm $\times$ 78.1 μm resolution, 5-mm slice) of (A) the CAT mat and (B) the AN mat.

demonstrate that sulfide could be abiotically oxidized by the AN electrode.

The AN current slowly increased after acetate was added (**Figure 6A**). After about 1.5 days, the current reached a maximum value of about 30 μA, then slowly decreased during the next 4 days. The gradual increasing and decreasing of AN

current after acetate addition indicates that biological processes were likely involved in current generation from acetate. Acetate addition probably increased the rate of sulfate reduction at the bottom of the mat; the produced sulfide could then be oxidized on the electrode surface, driving increases in current. In addition, acetate could be used as a substrate for electrode-respiring

microbes which can transfer electrons to an electrode. Thus the increase in AN current due to acetate addition may occur by both biotic and abiotic mechanisms.

The addition of the same amount of acetate (0.2 mmol) to the CAT mat did not alter current (data not shown). However, the CAT current decreased when sulfide was added (**Figure 6B**). If the CAT current was due to direct oxygen reduction on the electrode, it is possible that the introduction of sulfide reduced the oxygen available at the electrode, decreasing the current. Sulfide at high concentration is known to inhibitory or toxic to microbial metabolism including anaerobic and aerobic bacteria (Karhadkar et al., 1987; Chen et al., 2008). If these microbes are involved in the CAT current generation, it is possible that sulfide inhibited the consumption of electrons.

Oxygen and Sulfide Profiles in the Mats over the Diel Cycle

Figures 7A,B shows the DO and sulfide depth profiles measured from the tops of the mats at two time points (at 8:00 a.m. and 5:00 p.m.) during a diel cycle. We tried to measure the profiles at time points close to when the current peaks occurred, as shown in **Figure 3**. Similar DO profiles were obtained from AN mat (**Figure 7A**) and CAT mat (data not shown). The DO profile suggests that the oxygen concentration inside the mat decreased with the depth. At 3.5 mm bellow the mat surface, the DO concentration was close to zero, both for the 8:00 a.m. and 5:00 p.m. measurements. Since the thickness of the mat used in this study was 1.5–2 cm, this suggests that the environment surrounding the electrodes, which were placed at the bottom of the mat, was anoxic. To further confirm that the CAT electrode was in an anoxic environment, we switched the electrode potential of the cathode from -700 mV vs. Ag/AgCl to $+300$ mV vs. Ag/AgCl (i.e., to an AN condition). This switch occurred at about 4:00 p.m, when CAT current was highest (Supplementary Figure S2). Positive current (AN current) was immediately generated; suggesting that an anoxic condition at the bottom of the mat, therefore allowed electrons transfer to the electrode.

Figure 7B shows the change in total sulfide concentration in the mat with depth for different measurement times. The sulfide concentration increased with the depth for both 8:00 a.m. and 5:00 p.m. measurements. However, at 8:00 a.m. the increase was only 3.6-fold, from 25 μM at the surface of the mat to about 90 μM at a depth of 1.3 cm. In contrast to the profile observed at 8:00 a.m., sulfide concentration increased significantly with the depth at 5:00 p.m. The total sulfide concentration at 1.3 cm beneath the mat surface was about 18 times higher than that observed at the surface, and about 5 times higher than that obtained at the same depth at 8:00 a.m. (460 μM vs 90 μM). This sulfide profile is similar to a previous observation in a different mat (van der Meer et al., 2005; Pages et al., 2014)

Since the sulfide concentration continued to increase with depth, we left the sulfide microelectrode near the colonized electrode (at 13 mm below the mat surface) to measure sulfide concentration over the diel cycle. The diel sulfide profile shown in Supplementary Figure S3 aligns well with the oscillation of AN and CAT currents discussed above (**Figure 3**), in which

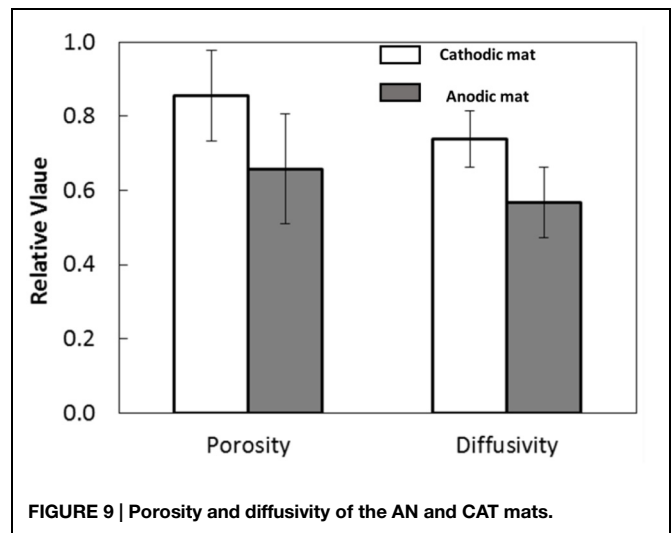FIGURE 9 | Porosity and diffusivity of the AN and CAT mats.

TABLE 1 | Percent increase and average approximate concentration increase of primary metabolites with significant and consistently higher concentrations in the cathodic (CAT) mat than in the anodic (AN) mat.

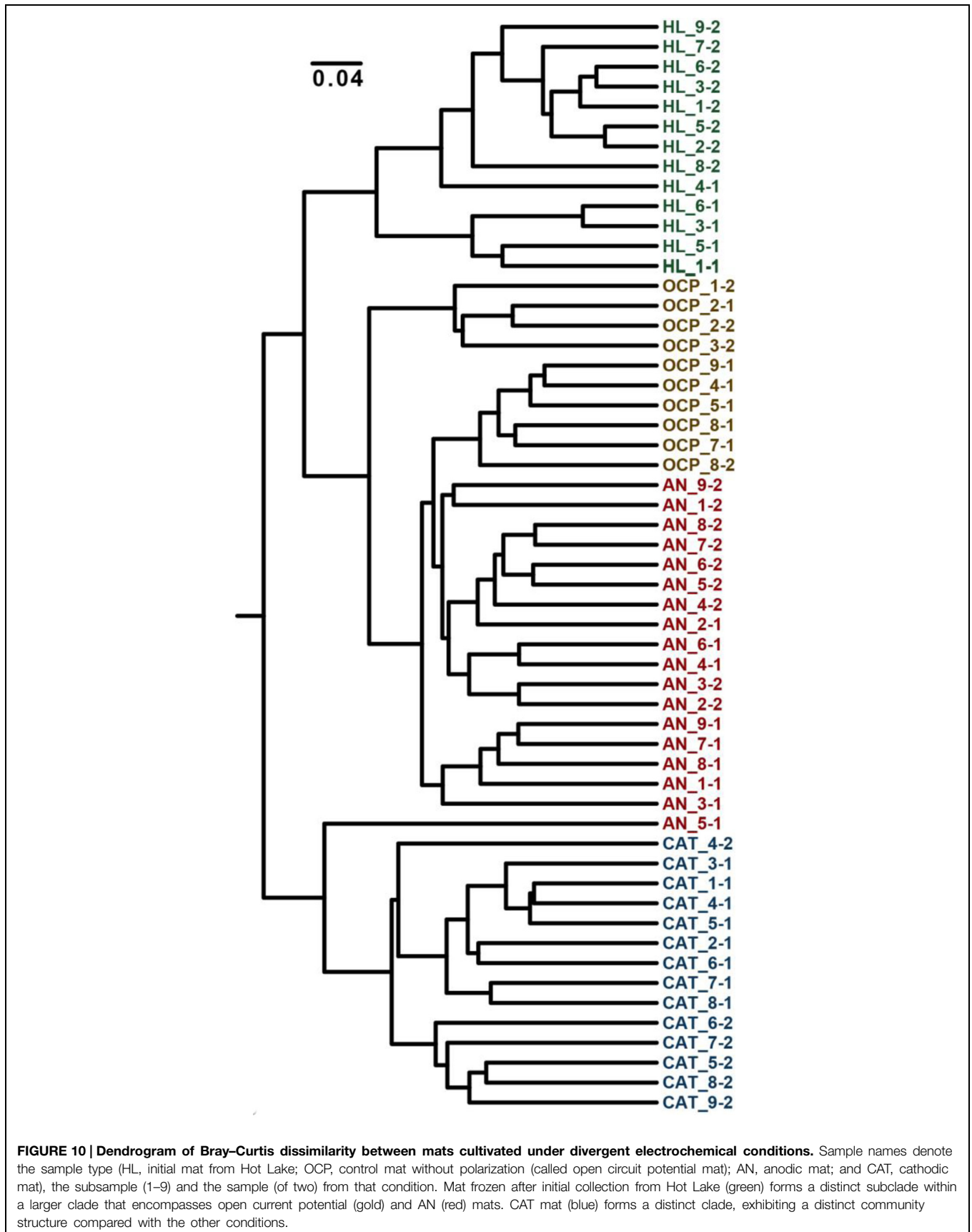|	June 6th collected mat	September 26th collected mat	Ave. Approx. Increase in CAT mat
Trehalose	52.7%	162.3%	+439 μg/g
Betaine	58.8%	80.5%	+26 μg/g
Glutamate	35.1%	64.7%	+17 μg/g
Oxypurinol	143.4%	113.4%	+18 μg/g

the currents reached a maximum level around 5:00 p.m. and a minimum at about 8:00 a.m. This suggests that the electron transfer processes between the electrode and the mat have a strong relationship with the sulfur cycling in the mat.

Microbial Mat Morphology and Structural Change under Different Polarized Conditions

Nuclear magnetic resonance imaging analysis showed that the internal architecture of the CAT mat system was very different from the AN mat (**Figure 8**). The darker regions in **Figure 8** qualitatively represent denser biomass and regions with less porosity. The CAT mat had dispersed biomass, and therefore was thicker and more porous than the more compact AN mat. These results corroborate the visible and tactile form of the mat samples during the harvesting period.

Nuclear magnetic resonance imaging showed that the quantitative porosity and diffusion coefficients were higher in the CAT mat than in the AN mat (P-value < 0.0001; **Figure 9**). These structural differences may have resulted from changes in microbial community composition selected under the different electrochemical conditions. Thus, this result indicates that the electrode potential regulated the development of the mat, leading to differences in morphology and structure.

The higher porosity and lower density of biomass of the CAT mat promote relatively rapid oxygen diffusion through the CAT mat, resulting in higher current. However, **Figure 2B** shows that

FIGURE 10 | Dendrogram of Bray–Curtis dissimilarity between mats cultivated under divergent electrochemical conditions. Sample names denote the sample type (HL, initial mat from Hot Lake; OCP, control mat without polarization (called open circuit potential mat); AN, anodic mat; and CAT, cathodic mat), the subsample (1–9) and the sample (of two) from that condition. Mat frozen after initial collection from Hot Lake (green) forms a distinct subclade within a larger clade that encompasses open current potential (gold) and AN (red) mats. CAT mat (blue) forms a distinct clade, exhibiting a distinct community structure compared with the other conditions.

the CAT mat was able to generate current from the initiation of the experiment, when the mat had a structure similar to that of the original sample as well as to that of the mat used in the AN system. This suggests that the electron-consuming processes in the CAT system were active in the native mat and not solely caused by the increasing porosity and diffusion coefficient of the mat.

We further used NMR spectroscopy for quantitative metabolite analysis of mat samples from our AN and CAT mats. The results were compared with data obtained from the control mat, which developed under OCP condition (OCP mat). The concentrations of major metabolites detected in the microbial mats under AN and CAT conditions are shown in Supplementary Table S1. Generally, most of the significant metabolites (with concentration >10 ug/g sample) were found at higher concentrations in the CAT mat than in the AN mat (**Table 1**). The metabolite analysis results also showed that the AN mat and OCP mat were relatively similar while the CAT mat were clearly distinguished from the other mat samples (Supplementary Table S1).

Most of the significant metabolites—trehalose, betaine, and glutamate—are known osmolytes. Trehalose is known to be a stress molecule, protecting cells from injuries imposed by high osmolarity, heat, oxidation, and salinity (Purvis et al., 2005; Reina-Bueno et al., 2012). Similar functions have been found for betaine (McNeil et al., 1999; Kapfhammer et al., 2005) and glutamate (Feehily and Karatzas, 2013). Glutamate is also involved in the bacterial response to acid stress. Thus, the significantly higher concentrations of these compounds in the CAT mat may indicate that the CAT potential (−700 mV vs. Ag/AgCl) caused stress to the mat which led to a high response of the microbial mat community. It is possible that the addition of electrons from electrode to the mat alleviated the energy limitations allowing the mat to maintain large carbon pools of osmolytes. It is possible that some microorganisms in the mat such as acetogens and anaerobic phototrophs used electrons from the electrode to drive carbon fixations which also increased the total carbon available to the mat.

Community Structure Changes due to Electrochemical Potential

Analysis of the community structure of mats revealed that variation in the electrochemical conditions under which mats were generated significantly impacted the relative abundances of mat community members (**Figure 10**). Average within-treatment Bray–Curtis dissimilarity was 0.367 (with a pooled *SD* of 0.106) compared with 0.501 (*SD* = 0.130) for all pairwise combinations. All incubated samples were significantly different from the original mat, indicating a strong effect of electrode-based cultivation on community composition. This result was expected, considering the significant differences in environmental conditions between the field and laboratory cultivation conditions. Mat incubated under OCP formed a broad clade with AN mat; suggesting the additional effect of the anode exerted only modest impacts on microbial community structure beyond the general effects of cultivation. These data agree with the relatively small differences in

mat metabolites observed between mat cultivated without polarization (OCP condition) and AN condition (Supplementary Table S1). Furthermore, this subclade was more similar to the original mat than were the CAT mats. In contrast, apart from one outlying sample of the AN mats, CAT mats formed a clade distinct from the initial, OCP, and AN mats. These community structure data are consistent with our metabolite analysis results that suggested greater changes in CAT mat metabolism compared with OCP and AN mat (Supplementary Table S1). Although it is not possible to determine whether changes in metabolism or community structure lead the CAT mat phenotype, our data strongly suggest that donation of electrons via a solid electrode is capable of strongly altering phototrophic mat morphology, community composition, and metabolic function.

Conclusion

We quantified the diel variations of electron transfer rates to and from the solid electrode in the mat electrochemical systems. We observed the diel cycling of current in which the lowest and highest magnitudes of AN current occurred simultaneously with those of CAT current. We also characterized the influence of physicochemical conditions (temperature, light, sulfide, and DO gradients) within the phototrophic mat upon electron transfer processes. AN current was higher in the dark and it increased with temperature. In contrast, CAT current increased with the illumination but did not change significantly with increased temperature. Comparing the behavior of AN current under constant light and dark conditions vs. diel-cycling mats revealed that AN current reached maximum under photic conditions under diel cycling conditions but was greater under constant dark conditions. This suggested diffusion control of the fermentable substrates from the photic layer to the bottom of the AN mat. We propose that the generated diel cycle data can be used to develop model of energy flow in the mat to predict diffusion controls. DO and sulfide gradients over diel cycle suggested that the current cycles of CAT and AN mats related to sulfur cycling in the mat. The congruence of community structure data with metabolite profiles suggested that variation in the electrochemical conditions under which mats were generated significantly impacted the relative abundances of mat members and mat metabolism. It remains unclear whether the electron transfer to and from the electrode to the mat was mediated by microbial metabolism of selectively enriched community on the electrode or was caused by abiotic reactions on electrode. These findings suggest that it is possible to electrochemically regulate the morphology, community composition, and activities of phototrophic mats and may represent a new paradigm for designing and manipulating microbial communities (Fredrickson, 2015).

Acknowledgments

Supplementary Material

The Supplementary Material for this article can be found online at: http://journal.frontiersin.org/article/10.3389/fmicb.2015.00909

References

Babauta, J. T., Atci, E., Ha, P. T., Lindemann, S. R., Ewing, T., Call, D. R., et al. (2014). Localized electron transfer rates and microelectrode-based enrichment of microbial communities within a phototrophic microbial mat. *Front. Microbiol.* 5:11. doi: 10.3389/fmicb.2014.00011

Babauta, J. T., Nguyen, H. D., Istanbullu, O., and Beyenal, H. (2013). Microscale gradients of oxygen, hydrogen peroxide, and ph in freshwater cathodic biofilms. *Chemsuschem* 6, 1252–1261. doi: 10.1002/cssc.201300019

Badalamenti, J. P., Torres, C. I., and Krajmalnik-Brown, R. (2013). Light-responsive current generation by phototrophically enriched anode biofilms dominated by green sulfur bacteria. *Biotechnol. Bioeng.* 110, 1020–1027. doi: 10.1002/bit.24779

Bender, J., and Phillips, P. (2004). Microbial mats for multiple applications in aquaculture and bioremediation. *Bioresour. Technol.* 94, 229–238. doi: 10.1016/j.biortech.2003.12.016

Bose, A., Gardel, E. J., Vidoudez, C., Parra, E. A., and Girguis, P. R. (2014). Electron uptake by iron-oxidizing phototrophic bacteria. *Nat. Commun.* 5:3391. doi: 10.1038/ncomms4391

Bray, J. R., and Curtis, J. T. (1957). An ordination of the upland forest communities of southern wisconsin. *Ecol. Monogr.* 27, 326–349. doi: 10.2307/1942268

Burow, L. C., Woebken, D., Bebout, B. M., McMurdie, P. J., Singer, S. W., Pett-Ridge, J., et al. (2012). Hydrogen production in photosynthetic microbial mats in the Elkhorn Slough estuary. *Monterey Bay. ISME J.* 6, 863–874. doi: 10.1038/ismej.2011.142

Caporaso, J. G., Lauber, C. L., Walters, W. A., Berg-Lyons, D., Huntley, J., Fierer, N., et al. (2012). Ultra-high-throughput microbial community analysis on the Illumina HiSeq and MiSeq platforms. *ISME J.* 6, 1621–1624. doi: 10.1038/ismej.2012.8

Caporaso, J. G., Lauber, C. L., Walters, W. A., Berg-Lyons, D., Lozupone, C. A., Turnbaugh, P. J., et al. (2011). Global patterns of 16S rRNA diversity at a depth of millions of sequences per sample. *Proc. Natl. Acad. Sci. U.S.A.* 108, 4516–4522. doi: 10.1073/pnas.1000080107

Chen, Y., Cheng, J. J., and Creamer, K. S. (2008). Inhibition of anaerobic digestion process: a review. *Bioresour. Technol.* 99, 4044–4064. doi: 10.1016/j.biortech.2007.01.057

Clauwaert, P., Van der Ha, D., Boon, N., Verbeken, K., Verhaege, M., Rabaey, K., et al. (2007). Open air biocathode enables effective electricity generation with microbial fuel cells. *Environ. Sci. Technol.* 41, 7564–7569. doi: 10.1021/es0709831

Debuy, S., Pecastaings, S., Bergel, A., and Erable, B. (2015). Oxygen-reducing biocathodes designed with pure cultures of microbial strains isolated from seawater biofilms. *Int. Biodeterior. Biodegradation* 103, 16–22. doi: 10.1016/j.ibiod.2015.03.028

Decker, K. L. M., Potterb, C. S., Beboutc, B. M., Des Maraisc, D. J., Carpenterd, S., Discipulo, M., et al. (2005). Mathematical simulation of the diel O, S, and C biogeochemistry of a hypersaline microbial mat. *Fems Microbiol. Ecol.* 52, 377–395. doi: 10.1016/j.femsec.2004.12.005

Des Marais, D. J. (1995). The biogeochemistry of hypersaline microbial mats. *Adv. Microb. Ecol.* 14, 251–274. doi: 10.1007/978-1-4684-7724-5_6

Des Marais, D. J. (2003). Biogeochemistry of hypersaline microbial mats illustrates the dynamics of modern microbial ecosystems and the early evolution of the biosphere. *Biol. Bull-Us* 204, 160–167. doi: 10.2307/1543552

Feehily, C., and Karatzas, K. A. G. (2013). Role of glutamate metabolism in bacterial responses towards acid and other stresses. *J. Appl. Microbiol.* 114, 11–24. doi: 10.1111/j.1365-2672.2012.05434.x

Finke, N., and Jorgensen, B. B. (2008). Response of fermentation and sulfate reduction to experimental temperature changes in temperate and Arctic marine sediments. *ISME J.* 2, 815–829. doi: 10.1038/ISMEJ.2008.20

Fredrickson, J. K. (2015). ECOLOGY. Ecological communities by design. *Science* 348, 1425–1427. doi: 10.1126/science.aab0946

Frund, C., and Cohen, Y. (1992). Diurnal cycles of sulfate reduction under oxic conditions in cyanobacterial mats. *Appl. Environ. Microb.* 58, 70–77.

Gregory, K. B., Bond, D. R., and Lovley, D. R. (2004). Graphite electrodes as electron donors for anaerobic respiration. *Environ. Microbiol.* 6, 596–604. doi: 10.1111/j.1462-2920.2004.00593.x

Grotzschel, S., Abed, R. M. M., and de Beer, D. (2002). Metabolic shifts in hypersaline microbial mats upon addition of organic substrates. *Environ. Microbiol.* 4, 683–695. doi: 10.1046/j.1462-2920.2002.00356.x

Guerrero, R., Piqueras, M., and Berlanga, M. (2002). Microbial mats and the search for minimal ecosystems. *Int. Microbiol.* 5, 177–188. doi: 10.1007/s10123-002-0094-8

Jeroschewski, P., Steuckart, C., and Kuhl, M. (1996). An amperometric microsensor for the determination of H2S in aquatic environments. *Anal. Chem.* 68, 4351–4357. doi: 10.1021/ac960091b

Kapfhammer, D., Karatan, E., Pflughoeft, K. J., and Watnick, P. I. (2005). Role for glycine betaine transport in *Vibrio cholerae* osmoadaptation and biofilm formation within microbial communities. *Appl. Environ. Microbiol.* 71, 3840–3847. doi: 10.1128/AEM.71.7.3840-3847.2005

Karhadkar, P. P., Audic, J. M., Faup, G. M., and Khanna, P. (1987). Sulfide and sulfate inhibition of methanogenesis. *Water Res.* 21, 1061–1066. doi: 10.1016/0043-1354(87)90027-3

Lewandowski, Z., and Beyenal, H. (2014). *Fundamentals of Biofilm Research.* Abingdon: Taylor & Francis.

Lindemann, S. R., Moran, J. J., Stegen, J. C., Renslow, R. S., Hutchison, J. R., Cole, J. K., et al. (2013). The epsomitic phototrophic microbial mat of Hot Lake, Washington: community structural responses to seasonal cycling. *Front. Microbiol.* 4:323. doi: 10.3389/fmicb.2013.00323

Logan, B. E. (2009). Exoelectrogenic bacteria that power microbial fuel cells. *Nat. Rev. Microbiol.* 7, 375–381. doi: 10.1038/nrmicro2113

Lovley, D. R. (2008). The microbe electric: conversion of organic matter to electricity. *Curr. Opin. Biotech* 19, 564–571. doi: 10.1016/j.copbio.2008.10.005

Lovley, D. R., and Nevin, K. P. (2011). A shift in the current: new applications and concepts for microbe-electrode electron exchange. *Curr. Opin. Biotech.* 22, 441–448. doi: 10.1016/j.copbio.2011.01.009

Marshall, C. W., Ross, D. E., Fichot, E. B., Norman, R. S., and May, H. D. (2012). Electrosynthesis of commodity chemicals by an autotrophic microbial community. *Appl. Environ. Microb.* 78, 8412–8420. doi: 10.1128/AEM.02401-12

McNeil, S. D., Nuccio, M. L., and Hanson, A. D. (1999). Betaines and related osmoprotectants. Targets for metabolic engineering of stress resistance. *Plant Physiol.* 120, 945–949. doi: 10.1104/pp.120.4.945

Moran, J. J., Doll, C. G., Bernstein, H. C., Renslow, R. S., Cory, A. B., Hutchison, J. R., et al. (2014). Spatially tracking C-13-labelled substrate (bicarbonate) accumulation in microbial communities using laser ablation isotope ratio

mass spectrometry. *Environ. Microbiol. Rep.* 6, 786–791. doi: 10.1111/1758-2229.12211

Nevin, K. P., Hensley, S. A., Franks, A. E., Summers, Z. M., Ou, J., Woodard, T. L., et al. (2011). Electrosynthesis of organic compounds from carbon dioxide is catalyzed by a diversity of acetogenic microorganisms. *Appl. Environ. Microb.* 77, 2882–2886. doi: 10.1128/AEM.02642-10

Paerl, H. W., Pinckney, J. L., and Steppe, T. F. (2000). Cyanobacterial–bacterial mat consortia: examining the functional unit of microbial survival and growth in extreme environments. *Environ. Microbiol.* 2, 11–26. doi: 10.1046/j.1462-2920.2000.00071.x

Pages, A., Welshb, D. T., Teasdaleb, P. R., Gricea, K., Vacherc, M., Bennettb, W. W., et al. (2014). Diel fluctuations in solute distributions and biogeochemical cycling in a hypersaline microbial mat from Shark Bay. WA. *Mar. Chem.* 167, 102–112. doi: 10.1016/j.marchem.2014.05.003

Purvis, J. E., Yomano, L. P., and Ingram, L. O. (2005). Enhanced trehalose production improves growth of *Escherichia coli* under osmotic stress. *Appl. Environ. Microb.* 71, 3761–3769. doi: 10.1128/AEM.71.7.3761-3769.2005

Rabaey, K., Rodríguez, J., Blackall, L. L., Keller, J., Gross, P., Batstone, D., et al. (2007). Microbial ecology meets electrochemistry: electricity-driven and driving communities. *ISME J.* 1, 9–18. doi: 10.1038/ismej.2007.4

Rabaey, K., Van de Sompel, K., Maignien, L., Boon, N., Aelterman, P., Clauwaert, P., et al. (2006). Microbial fuel cells for sulfide removal. *Environ. Sci. Technol.* 40, 5218–5224. doi: 10.1021/es060382u

Reina-Bueno, M., Argandoña, M., Salvador, M., Rodríguez-Moya, J., Iglesias-Guerra, F., Csonka, L. N., et al. (2012). Role of trehalose in salinity and temperature tolerance in the model halophilic bacterium chromohalobacter salexigens. *PLoS ONE* 7:e33587. doi: 10.1371/journal.pone.0033587

Renslow, R., Babauta, J., Kuprat, A., Schenk, J., Ivory, C., Fredrickson, J., et al. (2013). Modeling biofilms with dual extracellular electron transfer mechanisms. *Phys. Chem. Chem. Phys.* 15, 19262–19283. doi: 10.1039/c3cp53759e

Renslow, R., Donovan, C., Shim, M., Babauta, J., Nannapaneni, S., Schenk, J., et al. (2011). Oxygen reduction kinetics on graphite cathodes in sediment microbial fuel cells. *Phys. Chem. Chem. Phys.* 13, 21573–21584. doi: 10.1039/c1cp23200b

Rosenbaum, M., Aulenta, F., Villano, M., and Angenent, L. T. (2011). Cathodes as electron donors for microbial metabolism: which extracellular electron transfer mechanisms are involved? *Bioresour. Technol.* 102, 324–333. doi: 10.1016/j.biortech.2010.07.008

Schloss, P. D., Westcott, S. L., Ryabin, T., Hall, J. R., Hartmann, M., Hollister, E. B., et al. (2009). Introducing mothur: open-Source, platform-independent, community-supported software for describing and comparing microbial communities. *Appl. Environ. Microb.* 75, 7537–7541. doi: 10.1128/AEM.01541-09

Su, M., Jiang, Y., and Li, D. (2013). Production of acetate from carbon dioxide in bioelectrochemical systems based on autotrophic mixed culture. *J. Microbiol. Biotechnol.* 23, 1140–1146. doi: 10.4014/jmb.1304.04039

Tremblay, P. L., and Zhang, T. (2015). Electrifying microbes for the production of chemicals. *Front. Microbiol.* 6:201. doi: 10.3389/fmicb.2015.00201

Ueki, T., Nevin, K. P., Woodard, T. L., and Lovley, D. R. (2014). Converting carbon dioxide to butyrate with an engineered strain of *Clostridium ljungdahlii*. *MBio* 5:e1636-14. doi: 10.1128/mBio.01636-14

van der Meer, M. T. J., Schouten, S., Bateson, M. M., Nübel, U., Wieland, A., Kühl, M., et al. (2005). Diel variations in carbon metabolism by green nonsulfur-like bacteria in alkaline siliceous hot spring microbial mats from Yellowstone National Park. *Appl. Environ. Microb.* 71, 3978–3986. doi: 10.1128/AEM.71.7.3978-3986.2005

Villano, M., Aulenta, F., Ciucci, C., Ferri, T., Giuliano, A., and Majone, M. (2010). Bioelectrochemical reduction of CO2 to CH4 via direct and indirect extracellular electron transfer by a hydrogenophilic methanogenic culture. *Bioresour. Technol.* 101, 3085–3090. doi: 10.1016/j.biortech.2009.12.077

Wagner, R. C., Call, D. F., and Logan, B. E. (2010). Optimal set anode potentials vary in bioelectrochemical systems. *Environ. Sci. Technol.* 44, 6036–6041. doi: 10.1021/es101013e

From chemolithoautotrophs to electrolithoautotrophs: CO_2 fixation by Fe(II)-oxidizing bacteria coupled with direct uptake of electrons from solid electron sources

Takumi Ishii[1], Satoshi Kawaichi[2], Hirotaka Nakagawa[1], Kazuhito Hashimoto[1]* and Ryuhei Nakamura[2]*

[1] Department of Applied Chemistry, School of Engineering, The University of Tokyo, Tokyo, Japan, [2] Biofunctional Catalyst Research Team, RIKEN Center for Sustainable Resource Science, Saitama, Japan

At deep-sea vent systems, hydrothermal emissions rich in reductive chemicals replace solar energy as fuels to support microbial carbon assimilation. Until recently, all the microbial components at vent systems have been assumed to be fostered by the primary production of chemolithoautotrophs; however, both the laboratory and on-site studies demonstrated electrical current generation at vent systems and have suggested that a portion of microbial carbon assimilation is stimulated by the direct uptake of electrons from electrically conductive minerals. Here we show that chemolithoautotrophic Fe(II)-oxidizing bacterium, *Acidithiobacillus ferrooxidans,* switches the electron source for carbon assimilation from diffusible Fe^{2+} ions to an electrode under the condition that electrical current is the only source of energy and electrons. Site-specific marking of a cytochrome aa3 complex (aa3 complex) and a cytochrome bc1 complex (bc1 complex) in viable cells demonstrated that the electrons taken directly from an electrode are used for O_2 reduction via a down-hill pathway, which generates proton motive force that is used for pushing the electrons to NAD^+ through a bc1 complex. Activation of carbon dioxide fixation by a direct electron uptake was also confirmed by the clear potential dependency of cell growth. These results reveal a previously unknown bioenergetic versatility of Fe(II)-oxidizing bacteria to use solid electron sources and will help with understanding carbon assimilation of microbial components living in electronically conductive chimney habitats.

Keywords: extracellular electron transfer, hydrothermal vents, iron oxidizing bacteria, carbon assimilation, electrolithoautotrophy

Introduction

Chemolithoautotrophs are a class of organisms that conserve their energy, electrons, and carbon from inorganic chemical sources. As opposed to phototrophs that harvest energy from the sun, they are able to synthesize their own organic molecules from the fixation of carbon dioxide under the complete absence of solar radiation. The discovery of deep-sea hydrothermal vents has revealed the physiologically and phylogenetically diverse life around the vents

(Takai and Horikoshi, 1999; Reysenbach and Shock, 2002; Takai et al., 2013), and the existence of chemolithoautotroph-dependent ecosystems has sparked interest in determining the unexplored bioenergetic underpinnings of their energy yielding and carbon assimilation metabolisms (Takai et al., 2006; Baaske et al., 2007; Martin et al., 2008; Meierhenrich et al., 2010; Nakamura et al., 2010; Sander and Koschinsky, 2011; Girguis and Holden, 2012; Sievert and Vetriani, 2012; Yamamoto et al., 2013).

In such deep-vent systems, the hydrothermal fluids abundant with reductive chemicals such as H_2, H_2S, and Fe^{2+} are formed through high-temperature seawater-rock interaction (Takai and Horikoshi, 1999; Reysenbach and Shock, 2002; Takai et al., 2013). Considering that chemolithoautotrophs are able to conserve energy by coupling oxidation of the reductive hydrothermal fluid and reduction of the oxidative sea water containing sulfate, nitrate, and oxygen, etc., it is generally believed that nearly all microbial populations and ecosystems around deep-sea hydrothermal vents are fostered by existing diffusible reductive chemicals as energy and electron sources (Baaske et al., 2007; Sander and Koschinsky, 2011). While the validity of this conceptual framework has been well established, important details regarding the bioenergetics of microbial energy yield from geothermal sources remain open to question (Nakamura et al., 2010; Girguis and Holden, 2012; Sievert and Vetriani, 2012; Yamamoto et al., 2013; Yamaguchi et al., 2014).

Noteworthy, a recent finding of geo-electrical current generation across a wall of black-smoker chimney pointed to "electrical current flow" as a new way of energy transport from hydrothermal fluid to seawater (Nakamura et al., 2010; Yamamoto et al., 2013). Since electrical current is triggered by different redox potential of spatially segregated two redox couples, energetics that underpins energy transport to microbial niches profoundly differs from the commonly accepted notion of mass transfer, that is, energy propagation is driven by diffusion and convection of soluble reductive molecules (Baaske et al., 2007; Sander and Koschinsky, 2011). Moreover, other important findings (Nealson and Saffarini, 1994; Myers and Myers, 1997; Newman and Kolter, 2000; Gorby et al., 2006; Fredrickson et al., 2008; Marsili et al., 2008; Nakamura et al., 2009, 2013; Coursolle et al., 2010; Lovley, 2012; Mogi et al., 2013; Okamoto et al., 2013, 2014; Bose et al., 2014) of microbial extracellular electron transfer to/from metallic and/or semiconductive minerals have encouraged us to propose "electrolithoautotrophs" as the third type of microbial energy yielding metabolisms which can utilize carbon dioxide to synthesize organic matters by using electrons directly taken from solid-inorganic electron donors. According to these findings, here we propose a hypothesis that not only the diffusible reductive compounds, but also the high-energy electrons directly transported from the inner hydrothermal fluid through mineral conduit, may serve as a primary energy source for microbial ecosystems in the deep ocean (Nakamura et al., 2010; Yamamoto et al., 2013).

To examine the validity of the hypothetical metabolic pathway for electrolithoautotrophic carbon assimilation, herein we cultivated the chemolithoautotrophic Fe(II)-oxidizing bacterium, *Acidithiobacillus ferrooxidans,* in Fe^{2+}-ions free electrochemical reactors. Using site-specific chemical marking for intracellular

electron-transfer chains involved in carbon assimilation, we demonstrate the previously unaccounted ability of an Fe(II)-oxidizing bacterium to switch the metabolic mode from chemosynthesis to hypothetical electrolithoautotrophic carbon assimilation under the conditions that electrical current is the only source of energy and electrons for their carbon assimilation.

Materials and Methods

Cell Preparation

Acidithiobacillus ferrooxidans (ATCC23270) was cultured in DSMZ medium 882 (132 mg L^{-1} $(NH_4)_2SO_4$, 53 mg L^{-1} $MgCl_26H_2O$, 27 mg L^{-1} KH_2PO_4, 147 mg L^{-1} $CaCl_22H_2O$, and trace elements) supplemented with ferrous iron (66 mM) as an electron source and incubated aerobically at 30°C with shaking at 150 rpm in Erlenmeyer flask (volume of medium: 150 mL). The pH of solutions was adjusted to 1.8 using 5 M H_2SO_4. Subsequently, the culture was centrifuged at 15000 rpm for 10 min, and the pelleted cells were washed vigorously with a fresh medium at pH 1.8. This process was repeated more than three times to remove soluble Fe^{2+} ions and insoluble iron oxides from the cell culture prior to being used for electrochemical experiments.

Electrochemical Measurements

A single-chamber three-electrode system equipped with the working electrode on the bottom surface of the reactor was used for the electrochemical analysis of intact cells. A conducting glass substrate [fluorine-doped tin oxide (FTO)-coated glass electrode, resistance: 20 Ω/square, size: 30 mm × 30 mm; SPD Laboratory, Inc.] was used as the working electrode. The reference and counter electrodes were Ag/AgCl (KCl sat.) and a platinum wire, respectively. An air-exposed DSMZ medium 882 was used as an electrolyte. The pH of solutions was adjusted to 1.8 using 5 M H_2SO_4. The head space of the reactor was purged with air which is the source of N_2, O_2, and CO_2.

Chemical Marking Experiments

Coordination of CO to heme proteins in living cells was carried out by bubbling the cell suspension of *A. ferrooxidans* with CO gas for 10 min in the electrochemical reactor (Shibanuma et al., 2011). For the photocurrent measurements, a 1000-w Xe lamp (Ushio) equipped with a monochromator with a band width of 10 nm was used as an excitation source to irradiate light from the bottom of the electrochemical cell. For the inhibitor experiment of a bc1 complex, 1 v/v % Antimycin A solubilized in methanol was added in the electrochemical reactor. The final concentration of Antimycin A was 100 μM.

Results and Discussion

Branched Electron-Transfer Chain of *A. ferrooxidans*

The electron transfer pathways spanning from the outer to inner-membrane of *A. ferrooxidans* has been extensively studied and
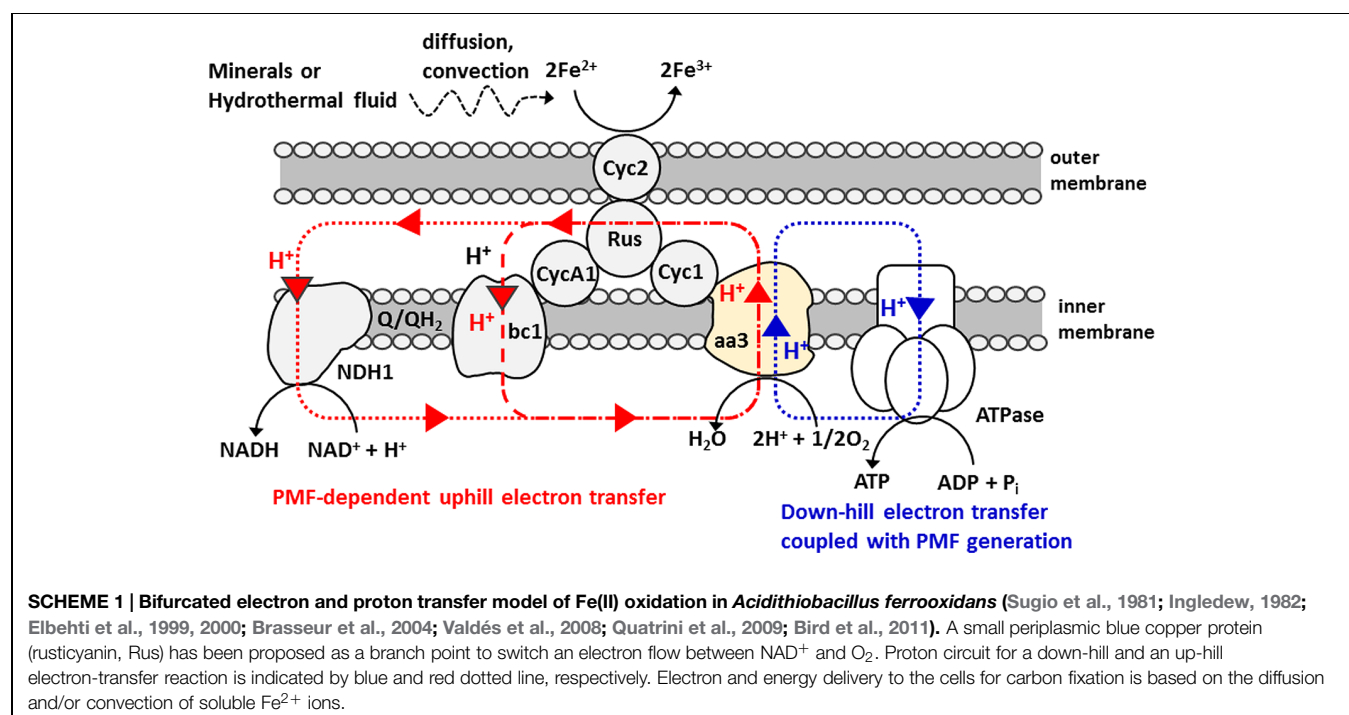
the bifurcated chain composed of "down-hill (exergonic)" and "up-hill (endergonic)" pathways has been identified (**Scheme 1**) (Sugio et al., 1981; Ingledew, 1982; Elbehti et al., 1999, 2000; Yarzábal et al., 2002; Brasseur et al., 2004; Valdés et al., 2008; Quatrini et al., 2009; Bird et al., 2011; Shibanuma et al., 2011). Of particular note is that like *Shewanella* and *Geobacter* species known to have an ability for the direct extracellular electron transfer to and from an electrode, *A. ferrooxidans* also has *c*-type cytochromes (Cyc 2) on their outer-membrane compartments (Yarzábal et al., 2002). Electrons gained by Fe^{2+} oxidation at Cyc 2 are used for O_2 reduction via a down-hill pathway, which in turn generates proton motive force (PMF) that is used for pushing the electron to a bc1 complex via an up-hill pathway and/or triggering ATP synthesis (Sugio et al., 1981; Ingledew, 1982; Elbehti et al., 1999, 2000; Yarzábal et al., 2002; Brasseur et al., 2004; Valdés et al., 2008; Quatrini et al., 2009; Bird et al., 2011; Shibanuma et al., 2011). In the following experiments, *A. ferrooxidans* was inoculated in an electrochemical reactor without Fe^{2+} ions and examined if the PMF-dependent up-hill pathway is activated by the direct electron uptake from an electrode, instead of the oxidation of diffusible Fe^{2+} ions.

Direct Uptake of Electrons from an Electrode into Cells

Figure 1A shows current vs. time curves for *A. ferrooxidans* cultivated in the absence of Fe^{2+} ions. In the present system, a conducting glass electrode (FTO) poised at +0.4 V (vs. SHE) acts as a sole source of electrons, and dissolved O_2 and CO_2 are an electron acceptor and a carbon source, respectively. In the absence of bacteria, we detected no electrical current generation (broken line, **Figure 1A**). On the other hand, in

the reactors containing cells, the cathodic current gradually increased to approximately 7 μA after 20 h of cultivation (solid line, **Figure 1A**). The marked difference in current density depending on the presence of cells indicates that the cathodic current was derived from the metabolic activity of cells. Furthermore, *in-situ* sterilization of cells with the deep-UV (254 nm) irradiation immediately suppressed the cathodic current generation (**Figure 1B**). Almost no electrical response was observed after 6 h of sterilization, confirming the strong coupling of metabolic activity to electrical current generation.

It is noted that the cathodic current generation by *A. ferrooxidans* in **Figure 1A** is mostly derived from the cells attached on an electrode, rather than planktonic cells. This was confirmed by *in-situ* counting of cell number on the FTO electrode with simultaneous monitoring of electrical current generation (**Figures 1C,D**). Since an FTO electrode is optically transparent and placed on the bottom surface of the electrochemical reactor, optical microscope images of the electrode surface can be acquired during electrical current generation by *A. ferrooxidans*. **Figure 1C** shows the *in-situ* optical microscope observation of the FTO electrode surface at the indicated time in **Figure 1A** after the cell was added in the electrochemical reactor. We plotted current against cell number to quantify the contribution of the electrode-attached cells for the cathodic current generation. As shown in **Figure 1D**, the microbial current exhibited a negative correlation with the cell number, as a fitted line passed through the point of origin with a high correlation coefficient ($r^2 = 0.97$). This means that the current production was indeed dominated by the extracellular electron transfer of the cells directly attaching on the electrode surface. In other words, it appears that the gradual increase in
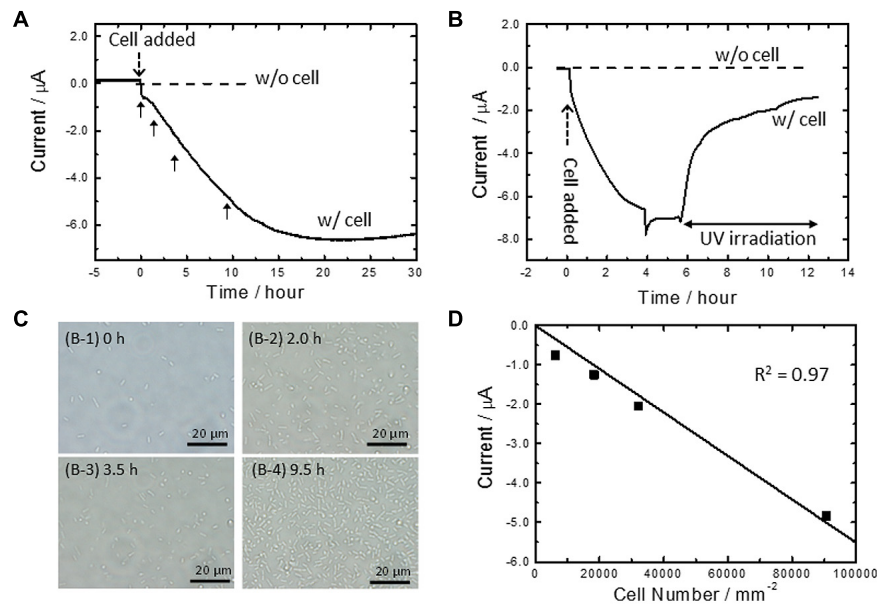

SCHEME 1 | Bifurcated electron and proton transfer model of Fe(II) oxidation in *Acidithiobacillus ferrooxidans* (Sugio et al., 1981; Ingledew, 1982; Elbehti et al., 1999, 2000; Brasseur et al., 2004; Valdés et al., 2008; Quatrini et al., 2009; Bird et al., 2011). A small periplasmic blue copper protein (rusticyanin, Rus) has been proposed as a branch point to switch an electron flow between NAD^+ and O_2. Proton circuit for a down-hill and an up-hill electron-transfer reaction is indicated by blue and red dotted line, respectively. Electron and energy delivery to the cells for carbon fixation is based on the diffusion and/or convection of soluble Fe^{2+} ions.

FIGURE 1 | (A) Current vs. time measurements for microbial current generation by *Acidithiobacillus ferrooxidans* cells on an fluorine-doped tin oxide (FTO) electrode in the absence of Fe^{2+} ions (solid line) at +0.4 V (vs. SHE). Current vs. time measurements without cells at +0.4 V was also depicted as a reference (broken line) **(B)** Effects of the deep-UV (254 nm) irradiation to the microbial current generation by the cells in the absence of Fe^{2+} ions at +0.4 V (solid line). Current vs. time measurements without cells at +0.4 V was also depicted as a reference (broken line). **(C)** *In-situ* optical microscope observation of an FTO electrode surface at the indicated time (panel A) after cell inoculation. **(D)** Plot of microbial current against cell number attached on an electrode surface obtained from *in-situ* optical microscope observation (panels A and B). The squares of the correlation coefficients were estimated by the addition of the point of origin to the obtained data. The geometric area of the FTO electrode was 3.14 cm^2. Initial OD_{500} was 0.02.

the cathodic current in **Figure 1A** correlates with the establishing process of the electrical conduits to the electrode poised at +0.4 V with the cells settled down to the bottom part of the reactor.

To evaluate the redox potential of electrical conduits established at the cell-electrode interface, electrodes covered with viable cells were examined by linear sweep (LS) voltammetry (solid line, **Figure 2**). As a reference, we also conducted LS voltammetry for cell cultures containing soluble Fe^{2+} ions, a system known as electrochemical cultivation of *A. ferrooxidans* (broken line, **Figure 2**) (Yunker and Radovich, 1986; Matsumoto et al., 1999, 2002; Ishii et al., 2012). In the presence of Fe^{2+} ions, the onset potential for cathodic current generation was estimated to be +0.65 V, as indicated in the peak in the logarithmic plot for current. This value is close to the redox potential of Fe^{3+}/Fe^{2+} couple and consistent well with the previously reported model for electrochemical cultivation of *A. ferrooxidans* (Yunker and Radovich, 1986; Matsumoto et al., 1999, 2002; Ishii et al., 2012). Namely, diffusible Fe^{2+} and Fe^{3+} ions serve as an electron shuttle which bridges electron transfer between planktonic cells and electrodes. Meanwhile, the LS voltammogram for the electrode-attaching cells provided one peak at +0.82 V, and no peak assignable to diffusible Fe^{3+}/Fe^{2+} redox couple was observed. This is the clear indication that the electrode-attaching cells established the different conduit of electrons to the FTO electrode rather than the Fe^{3+}/Fe^{2+} redox couple, which serves as an important information for understanding the bioenergetics of PMF-dependent electrolithoautotrophic carbon assimilation

(discuss later). Since the cathodic current generation was dominated by the cells directly attaching on an electrode surface (**Figure 1D**), the LS voltammetry results suggest the existence of outer-membrane-bound redox protein at a midpoint potential of +0.82 V, which bridges an electron donor of an FTO electrode to inner electron-trasnsfer chains responsible for carbon fixation.

In-Vivo Monitoring Down-Hill Electron-Transfer Pathway

To identify the inner electron-trasnsfer chains responsible for the cathodic current generation and to examine if the PMF-dependent up-hill pathway is activated by direct uptake of electrons from an electrode, we applied the artificial photochemical reaction to *A. ferrooxidans*. As previously reported (Shibanuma et al., 2011), the treatment of viable cells with CO allows for monitoring the electron-transfer reaction mediated by heme proteins under *in-vivo* conditions, since the redox activities of hemes are blocked upon CO binding and subsequently reactivated by photodissociation of CO. This technique enables us to identify the specific heme proteins involved in current generation by examining the wavelength dependency of photocurrent response. In this experiment, *A. ferrooxidans* cells inoculated in an Fe^{2+}-free electrochemical reactor were treated with CO and irradiated by the monochromic light with a band width of 10 nm in a course of microbial current generation.
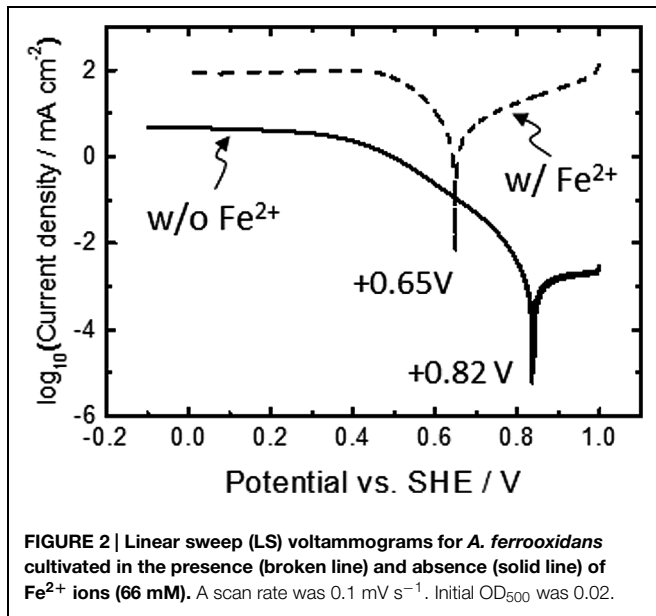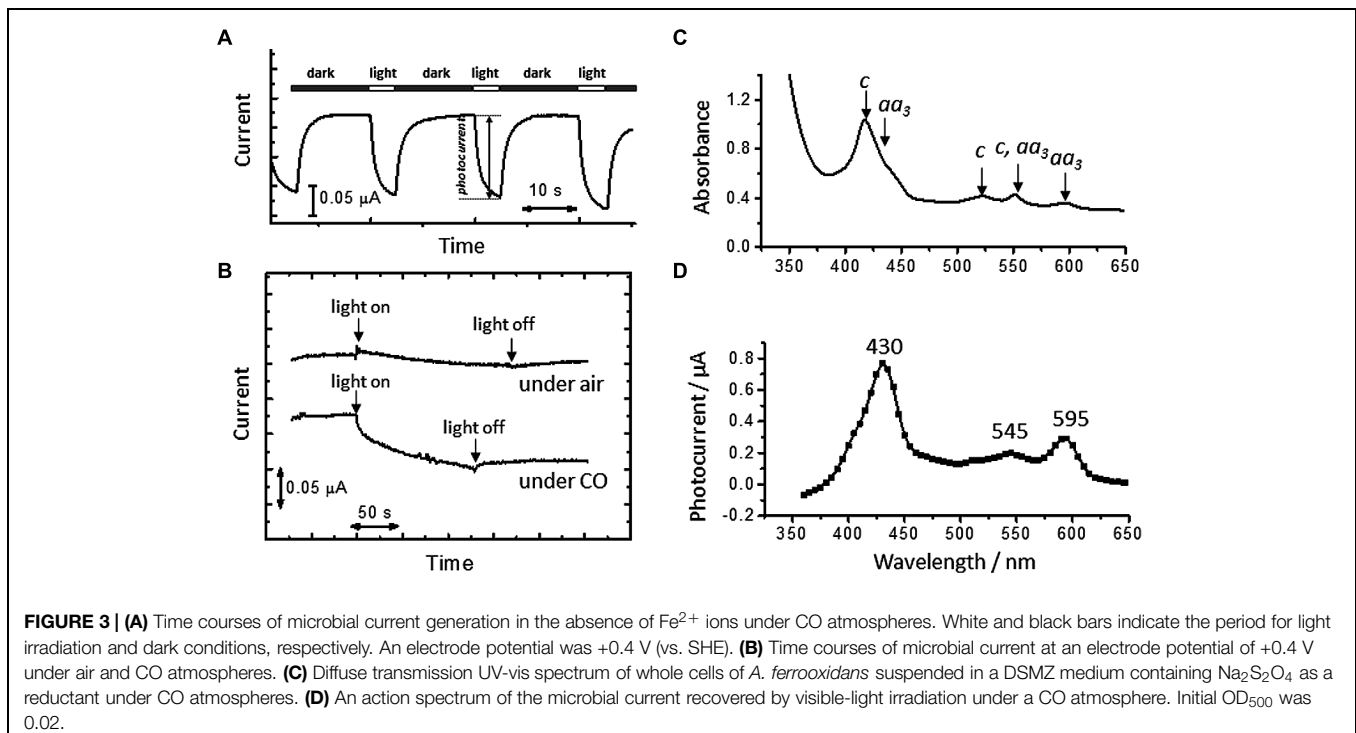
Figure 3A shows time courses of microbial current at an electrode potential of +0.4 V under CO atmospheres. Upon the treatment of the cells with CO, the microbial current decreased, suggesting that the formation of CO-ligated heme in living cells inhibited the extracellular electron-transfer reactions of *A. ferrooxidans*. The drop in the microbial current caused by CO was recovered upon visible-light irradiation; in contrast, visible-light irradiation induced little change in the current generation under N$_2$ atmospheres (**Figure 3B**).

A whole cell of *A. ferrooxidans* has multiple kinds of heme proteins, as indicated by UV-visible spectra of cell suspensions under CO atmospheres in the presence of Na$_2$S$_2$O$_4$ (50 mM) as a reductant (**Figure 3C**). It is seen from the spectral region of Q bands that the cell has *a*-type (∼550 and ∼600 nm) and *c*-type (∼525 and ∼550 nm) cytochromes. To clarify the origin of the light-induced current recovery, excitation wavelength dependency was investigated. The action spectrum of CO-treated cells resolved the three bands peaked at 430, 545, and 595 nm, which are well-correlated with the Soret (429 nm) and Q (546 and 590 nm) bands of a CO-ligated aa3 complex, respectively (**Figure 3D**) (Horie et al., 1983). This indicates that the current recovery due to visible-light irradiation is predominantly derived from the photodissociation of the CO ligand of an aa3 complex. Namely, the photodissociation generates redox-active hemes and revives the cellular respiratory electron transport reactions. The suppression of microbial current observed immediately after stopping visible-light irradiation (**Figure 3A**) is due to the recombination of CO with an aa3 complex.
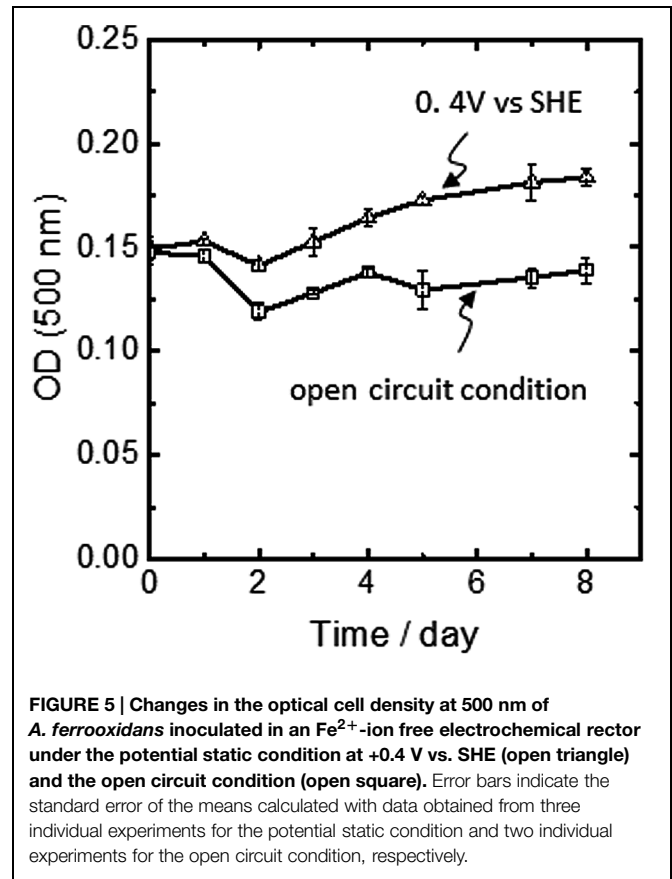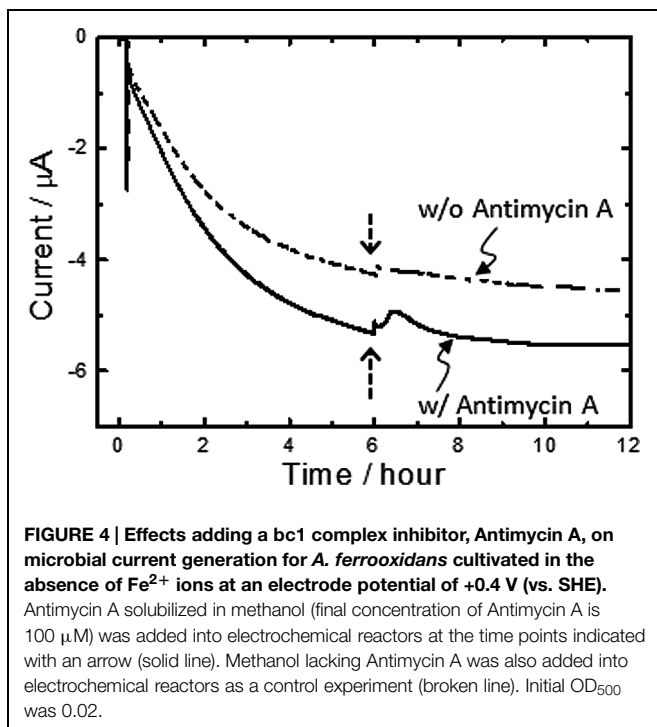
In-Vivo Monitoring of up-Hill Electron Transfer Pathway

It is worth noting here that the aa3 complex of *A. ferrooxidans* is expressed under Fe^{2+}-grown conditions and positioned at a terminal of the down-hill pathway (**Scheme 1**) (Sugio et al., 1981; Ingledew, 1982; Elbehti et al., 1999, 2000; Yarzábal et al., 2002; Brasseur et al., 2004; Valdés et al., 2008; Quatrini et al., 2009; Bird et al., 2011). Given that an aa3 complex is responsible for the generation of PMF for up-hill pumping of electrons and/or initiating ATP synthesis, it can be deduced that a portion of electrons directly taken from an electrode are pushed up-hill
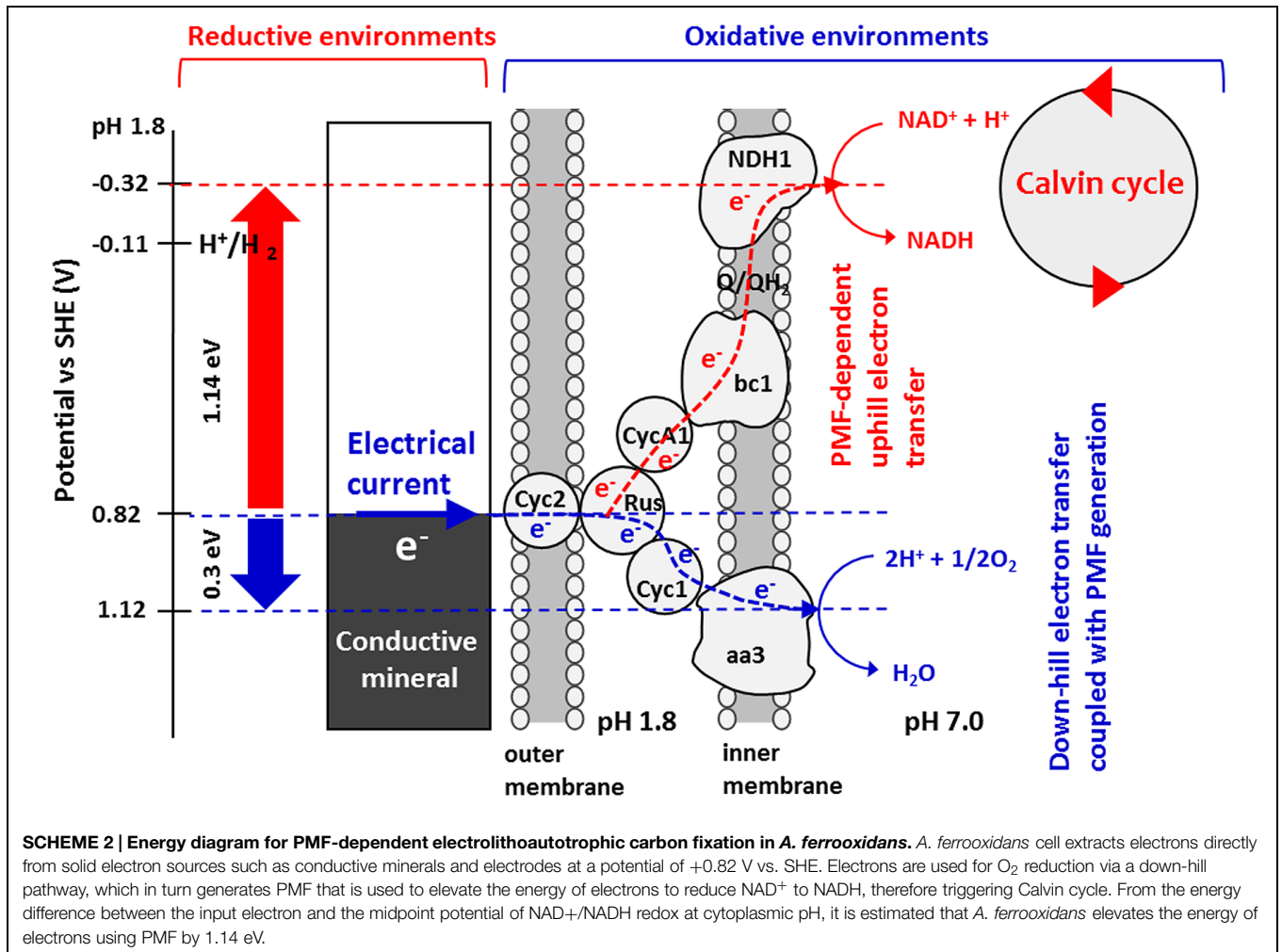

FIGURE 3 | (A) Time courses of microbial current generation in the absence of Fe^{2+} ions under CO atmospheres. White and black bars indicate the period for light irradiation and dark conditions, respectively. An electrode potential was +0.4 V (vs. SHE). **(B)** Time courses of microbial current at an electrode potential of +0.4 V under air and CO atmospheres. **(C)** Diffuse transmission UV-vis spectrum of whole cells of *A. ferrooxidans* suspended in a DSMZ medium containing Na$_2$S$_2$O$_4$ as a reductant under CO atmospheres. **(D)** An action spectrum of the microbial current recovered by visible-light irradiation under a CO atmosphere. Initial OD$_{500}$ was 0.02.

to NAD^+ through a bc1 complex. To assure the occurrence of PMF-dependent reverse electron transfer, we added a bc1 complex inhibitor, Antimycin A (Elbehti et al., 2000), to the electrode-attaching cells in the course of microbial current generation. As expected, upon addition of 1v/v % Antimycin A solubilized in methanol (final concentration of Antimycin A is 100 μM), the transient, but clear suppression of the microbial current generation by approx. 6% was observed (solid line, **Figure 4**). In contrast, the addition of 1 v/v % methanol lacking Antimycin A caused subtle change in the microbial current (broken line, **Figure 4**), confirming that the current suppression was due to the inhibition of the bc1 complex.

In *A. ferrooxidans*, the PMF-dependent up-hill electron transfer is a physiologically important phenomenon, since carbon dioxide fixation via the Calvin cycle is coupled to this process. **Figure 5** shows the time course of optical cell density at 500 nm (OD_{500}) obtained for *A. ferrooxidans* cells inoculated in an Fe^{2+}-ion-free electrochemical reactor for 8 days. Under the condition that the electrode potential was poised at +0.4 V, OD_{500} increased with incubation time. In contrast, when the cell was incubated under the same condition with the exception that no external potential was applied to the FTO electrode (open circuit condition), no growth of the cells was observed. Here, we should emphasize that under the open circuit condition, the electron flow from the FTO electrode to the cells was fully ceased and thus the electrode no longer functioned as an electron source for microbial growth. Therefore, the clear potential dependency of the cell growth indicates that the cathodic current was being used not only for PMF generation, but also for carbon dioxide fixation and cellular maintenance via an endergonic electron-transfer reaction.

FIGURE 5 | Changes in the optical cell density at 500 nm of *A. ferrooxidans* **inoculated in an Fe^{2+}-ion free electrochemical rector under the potential static condition at +0.4 V vs. SHE (open triangle) and the open circuit condition (open square).** Error bars indicate the standard error of the means calculated with data obtained from three individual experiments for the potential static condition and two individual experiments for the open circuit condition, respectively.

FIGURE 4 | Effects adding a bc1 complex inhibitor, Antimycin A, on microbial current generation for *A. ferrooxidans* **cultivated in the absence of Fe^{2+} ions at an electrode potential of +0.4 V (vs. SHE).** Antimycin A solubilized in methanol (final concentration of Antimycin A is 100 μM) was added into electrochemical reactors at the time points indicated with an arrow (solid line). Methanol lacking Antimycin A was also added into electrochemical reactors as a control experiment (broken line). Initial OD_{500} was 0.02.

Taken together, the results obtained by *in-vivo* electrochemistry with site-specific chemical marking suggest the bioenergetic pathway illustrated in **Scheme 2** as a model for PMF-dependent electrolithoautotrophic carbon assimilation of *A. ferrooxidans*. As estimated from LS voltammetry (**Figure 2**), *A. ferrooxidans* cells establish the direct electrical conduit to a solid electron donor at the potential of +0.82 V, which is 0.17 V more positive than the diffusible redox couple of Fe^{3+}/Fe^{2+} for chemolithoautotrophic carbon assimilation. Although Cyc 2 is located at the outer-cell surface of *A. ferooxidance*, we cannot exclude the possibility that self-secreted redox molecules are involved in the direct extracellular electron transfer, as recent studies demonstrated that self-secreted flavin acts as a bound-cofactor of outer-membrane *c*-type cytochromes of *Shewanella oneidensis* (Okamoto et al., 2013) and *Geobacter sulfurreducens* (Okamoto et al., 2014) for initiating the direct electron transfer from cells to electrodes. The involvement of H_2 as an electron carrier for the direct extracellular electron transfer and cell growth of *A. ferooxidance* can be excluded, since the onset potential of direct extracellular electron transfer is approximately 900 mV more positive than the redox potential of hydrogen evolution [$E(H^+/H_2) = -0.11$ V vs. SHE at pH1.8]. Even in the presence of extracellular enzymes suggested by *Methanococcus maripaludis* (Deutzmann et al., 2015), H_2 production by proton reduction is thermodynamically unfeasible in our experimental conditions.

SCHEME 2 | Energy diagram for PMF-dependent electrolithoautotrophic carbon fixation in *A. ferrooxidans*. *A. ferrooxidans* cell extracts electrons directly from solid electron sources such as conductive minerals and electrodes at a potential of +0.82 V vs. SHE. Electrons are used for O_2 reduction via a down-hill pathway, which in turn generates PMF that is used to elevate the energy of electrons to reduce NAD^+ to NADH, therefore triggering Calvin cycle. From the energy difference between the input electron and the midpoint potential of NAD+/NADH redox at cytoplasmic pH, it is estimated that *A. ferrooxidans* elevates the energy of electrons using PMF by 1.14 eV.

For initiating the carbon fixation by Rubisco enzymes, *A. ferrooxydans* cells require sufficient reductive energy to convert NAD^+ to NADH in the cytoplasm through a bc1 complex. As the reversible potential of the NAD^+/NADH redox couple is -0.32 V at cytoplasmic pH, we can estimate that *A. ferrooxydans* cells are capable of elevating the energy of electrons by 1.14 V using PMF through exergonic electron flow to O_2 (**Scheme 2**). Although how the electron flow switches between NAD^+ and O_2 is not known, a small periplasmic blue copper protein (rusticyanin, Rus) has been proposed as a branch point (Valdés et al., 2008; Quatrini et al., 2009). From the inhibition rate of cathodic current generation by Antimycin A (**Figure 4**), we can estimate that electrons gained from an FTO electrode split to an up-hill and a down-hill pathway with a ratio of approximately 1 to 15 under the condition of the present experiments. The presence of two functional bc1 complexes are known in *A. ferrooxidans*. One (PetA1B1C1) functions only in up-hill direction in iron-grown cells (Elbehti et al., 2000), whereas the other (PetA2B2C2) has been shown to function only in down-hill mode in sulfur-grown cells (Brasseur et al., 2004). Considering that the PMF-dependent up-hill pathway is activated for the cells attached

on the electrode surface, it is assumable that the former one is responsible in the observed electrolithoautotrophic carbon assimilation.

Summary

In the present study, we demonstrated for the first time that the chemolithoautotrophic Fe(II)-oxidizing bacterium, *A. ferrooxidans*, is capable of using electrical current as the energy source for carbon assimilation. The finding of the metabolism switched from chemolithoautotrophy to electrolithoautotrophy demonstrates a previously unknown bioenergetic versatility of energy yielding metabolisms in Fe(II)-oxidizing bacteria, which in turn supports our hypothesis (Nakamura et al., 2010; Yamamoto et al., 2013) highlighting the possibility of electrons to be a primary energy source for deep-sea hydrothermal ecosystems. Although recent studies have postulated that several microorganisms are capable of conducting a direct uptake of electrons from solid electron donors at highly negative redox potential ranging from -400 to -800 mV (vs. SHE; reviewed in Rabaey and Rozendal,

2010; Lovley and Nevin, 2013; Deng et al., 2015; Tremblay and Zhang, 2015), these potentials are too negative to be generated by natural environments, even at the highly reducing environments such as deep-sea alkaline hydrothermal vents (Martin et al., 2008). Accordingly, further investigation on PMF-dependent electrolithoautotrophy at geochemically relevant potential regions presented in this work will help understanding carbon assimilation of microbial components living around electronically conductive chimney walls. On-site electrochemical experiments at deep-sea hydrothermal vents are currently underway using a remotely operated vehicle equipped with the potentiostat and potential programmer system (Yamamoto et al., 2013), which will bring our understanding of electricity-dependent microbial habitats to a new realm.

References

Baaske, P., Weinert, F. M., Duhr, S., Lemke, K. H., Russell, M. J., and Braun, D. (2007). Extreme accumulation of nucleotides in simulated hydrothermal pore systems. *Proc. Natl. Acad. Sci. U.S.A.* 104, 9346–9351. doi: 10.1073/pnas.0609592104

Bird, L. J., Bonnefoy, V., and Newman, D. K. (2011). Bioenergetic challenges of microbial iron metabolisms. *Trends Microbiol.* 19, 330–340. doi: 10.1016/j.tim.2011.05.001

Bose, A., Gardel, E. J., Vidoudez, C., Parra, E. A., and Girguis, P. R. (2014). Electron uptake by iron-oxidizing phototrophic bacteria. *Nat. Commun.* 5, 3391. doi: 10.1038/ncomms4391

Brasseur, G., Levicán, G., Bonnefoy, V., Holmes, D., Jedlicki, E., and Lemesle-Meunier, D. (2004). Apparent redundancy of electron transfer pathways via bc 1 complexes and terminal oxidases in the extremophilic chemolithoautotrophic *Acidithiobacillus ferrooxidans*. *Biochim. Biophys. Acta* 1656, 114–126. doi: 10.1016/j.bbabio.2004.02.008

Coursolle, D., Baron, D. B., Bond, D. R., and Gralnick, J. A. (2010). The Mtr respiratory pathway is essential for reducing flavins and electrodes in *Shewanella oneidensis*. *J. Bacteriol.* 192, 467–474. doi: 10.1128/JB.00925-09

Deng, X., Nakamura, R., Hashimoto, K., and Okamoto, A. (2015). Electron extraction from an extracellular electrode by *Desulfovibrio ferrophilus* strain IS5 without using hydrogen as an electron carrier. *Electrochemistry* 83, 529–531. doi: 10.5796/electrochemistry.83.529

Deutzmann, J. S., Sahin, M., and Spormann, A. M. (2015). Extracellular enzymes facilitate electron uptake in biocorrosion and bioelectrosynthesis. *MBio* 6, e00496–e00515. doi: 10.1128/mBio.00496-15

Elbehti, A., Brasseur, G., and Lemesle-Meunier, D. (2000). First evidence for existence of an uphill electron transfer through the bc1 and NADH-Q oxidoreductase complexes of the acidophilic obligate chemolithotrophic ferrous ion-oxidizing bacterium *Thiobacillus ferrooxidans*. *J. Bacteriol.* 182, 3602–3606. doi: 10.1128/JB.182.12.3602-3606.2000

Elbehti, A., Nitschke, W., Tron, P., Michel, C., and Lemesle-Meunier, D. (1999). Redox components of cytochrome bc-type enzymes in acidophilic prokaryotes I. Characterization of the cytochrome bc 1-type complex of the acidophilic ferrous ion-oxidizing bacterium *Thiobacillus ferrooxidans*. *J. Biol. Chem.* 274, 16760–16765.

Fredrickson, J. K., Romine, M. F., Beliaev, A. S., Auchtung, J. M., Driscoll, M. E., Gardner, T. S., et al. (2008). Towards environmental systems biology of *Shewanella*. *Nat. Rev. Microbiol.* 6, 592–603. doi: 10.1038/nrmicro1947

Girguis, P. R., and Holden, J. F. (2012). On the potential for bioenergy and biofuels from hydrothermal vent microbes. *Oceanography* 25, 213–217. doi: 10.5670/oceanog.2012.20

Gorby, Y. A., Yanina, S., Mclean, J. S., Rosso, K. M., Moyles, D., Dohnalkova, A., et al. (2006). Electrically conductive bacterial nanowires produced by *Shewanella oneidensis* strain MR-1 and other microorganisms. *Proc. Natl. Acad. Sci. U.S.A.* 103, 11358–11363. doi: 10.1073/pnas.0604517103

Horie, S., Watanabe, T., and Kumiko, A. (1983). Studies on the ferricytochrome a-ferrocytochrome a3-carbon monoxide complex of mammalian cytochrome

Acknowledgments

oxidase. Conditions for preparation and some properties. *J. Biochem.* 93, 997–1010.

Ingledew, W. J. (1982). *Thiobacillus ferrooxidans* the bioenergetics of an acidophilic chemolithotroph. *Biochim. Biophys. Acta* 683, 89–117. doi: 10.1016/0304-4173(82)90007-6

Ishii, T., Nakagawa, H., Hashimoto, K., and Nakamura, R. (2012). *Acidithiobacillus ferrooxidans* as a bioelectrocatalyst for conversion of atmospheric CO2 into extracellular pyruvic acid. *Electrochemistry* 80, 327–329. doi: 10.5796/electrochemistry.80.327

Lovley, D. R. (2012). Electromicrobiology. *Annu. Rev. Microbiol.* 66, 391–409. doi: 10.1146/annurev-micro-092611-150104

Lovley, D. R., and Nevin, K. P. (2013). Electrobiocommodities: powering microbial production of fuels and commodity chemicals from carbon dioxide with electricity. *Curr. Opin. Biotechnol.* 24, 385–390. doi: 10.1016/j.copbio.2013.02.012

Marsili, E., Baron, D. B., Shikhare, I. D., Coursolle, D., Gralnick, J. A., and Bond, D. R. (2008). Shewanella secretes flavins that mediate extracellular electron transfer. *Proc. Natl. Acad. Sci. U.S.A.* 105, 3968–3973. doi: 10.1073/pnas.0710525105

Martin, W., Baross, J., Kelley, D., and Russell, M. J. (2008). Hydrothermal vents and the origin of life. *Nat. Rev. Microbiol.* 6, 805–814. doi: 10.1038/nrmicro1991

Matsumoto, N., Nakasono, S., Ohmura, N., and Saiki, H. (1999). Extension of logarithmic growth of *Thiobacillus ferrooxidans* by potential controlled electrochemical reduction of Fe (III). *Biotechnol. Bioeng.* 64, 716–721. doi: 10.1002/(SICI)1097-0290(19990920)64:6<716::AID-BIT11>3.3.CO;2-0

Matsumoto, N., Yoshinaga, H., Ohmura, N., Ando, A., and Saiki, H. (2002). Numerical simulation for electrochemical cultivation of iron oxidizing bacteria. *Biotechnol. Bioeng.* 78, 17–23. doi: 10.1002/bit.10173

Meierhenrich, U. J., Filippi, J. J., Meinert, C., Vierling, P., and Dworkin, J. P. (2010). On the origin of primitive cells: from nutrient intake to elongation of encapsulated nucleotides. *Angew. Chem. Int. Ed. Engl.* 49, 3738–3750. doi: 10.1002/anie.200905465

Mogi, T., Ishii, T., Hashimoto, K., and Nakamura, R. (2013). Low-voltage electrochemical CO2 reduction by bacterial voltage-multiplier circuits. *Chem. Commun.* 49, 3967–3969. doi: 10.1039/c2cc37986d

Myers, C. R., and Myers, J. M. (1997). Outer membrane cytochromes of *Shewanella putrefaciens* MR-1: spectral analysis, and purification of the 83-kDa c-type cytochrome. *Biochim. Biophys. Acta* 1326, 307–318. doi: 10.1016/S0005-2736(97)00034-5

Nakamura, R., Kai, F., Okamoto, A., and Hashimoto, K. (2013). Mechanisms of long-distance extracellular electron transfer of metal-reducing bacteria mediated by nanocolloidal semiconductive iron oxides. *J. Mater. Chem. A* 1, 5148–5157. doi: 10.1021/acs.langmuir.5b01033

Nakamura, R., Kai, F., Okamoto, A., Newton, G. J., and Hashimoto, K. (2009). Self-constructed electrically conductive bacterial networks. *Angew. Chem. Int. Ed. Engl.* 48, 508–511. doi: 10.1002/anie.200804750

Nakamura, R., Takashima, T., Kato, S., Takai, K., Yamamoto, M., and Hashimoto, K. (2010). Electrical current generation across a black smoker chimney. *Angew. Chem. Int. Ed. Engl.* 49, 7692–7694. doi: 10.1002/anie.201003311

Nealson, K. H., and Saffarini, D. (1994). Iron and manganese in anaerobic respiration: environmental significance, physiology, and regulation. *Annu. Rev. Microbiol.* 48, 311–343. doi: 10.1146/annurev.mi.48.100194.001523

Newman, D. K., and Kolter, R. (2000). A role for excreted quinones in extracellular electron transfer. *Nature* 405, 94–97. doi: 10.1038/35013189

Okamoto, A., Hashimoto, K., Nealson, K. H., and Nakamura, R. (2013). Rate enhancement of bacterial extracellular electron transport involves bound flavin semiquinones. *Proc. Natl. Acad. Sci. U.S.A.* 110, 7856–7861. doi: 10.1073/pnas.1220823110

Okamoto, A., Saito, K., Inoue, K., Nealson, K. H., Hashimoto, K., and Nakamura, R. (2014). Uptake of self-secreted flavins as bound cofactors for extracellular electron transfer in *Geobacter* species. *Energy Environ. Sci.* 7, 1357–1361. doi: 10.1039/c3ee43674h

Quatrini, R., Appia-Ayme, C., Denis, Y., Jedlicki, E., Holmes, D. S., and Bonnefoy, V. (2009). Extending the models for iron and sulfur oxidation in the extreme acidophile *Acidithiobacillus ferrooxidans*. *BMC Genomics* 10:394. doi: 10.1186/1471-2164-10-394

Rabaey, K., and Rozendal, R. A. (2010). Microbial electrosynthesis – revisiting the electrical route for microbial production. *Nat. Rev. Microbiol.* 8, 706–716. doi: 10.1038/nrmicro2422

Reysenbach, A. L., and Shock, E. (2002). Merging genomes with geochemistry in hydrothermal ecosystems. *Science* 296, 1077–1082. doi: 10.1126/science.1072483

Sander, S. G., and Koschinsky, A. (2011). Metal flux from hydrothermal vents increased by organic complexation. *Nat. Geosci.* 4, 145–150. doi: 10.1038/ngeo1088

Shibanuma, T., Nakamura, R., Hirakawa, Y., Hashimoto, K., and Ishii, K. (2011). Observation of in vivo cytochrome-based electron-transport dynamics using time-resolved evanescent wave electroabsorption spectroscopy. *Angew. Chem. Int. Ed. Engl.* 50, 9137–9140. doi: 10.1002/anie.201101810

Sievert, S., and Vetriani, C. (2012). Chemoautotrophy at deep-sea vents: past, present, and future. *Oceanography* 25, 218–233. doi: 10.5670/oceanog.2012.21

Sugio, T., Tano, T., and Imai, K. (1981). Isolation and some properties of silver ion-resistant iron-oxidizing bacterium *Thiobacillus ferrooxidans*. *Agric. Biol. Chem.* 45, 2037–2051. doi: 10.1271/bbb1961.45.1791

Takai, K., and Horikoshi, K. (1999). Genetic diversity of archaea in deep-sea hydrothermal vent environments. *Genetics* 152, 1285–1297.

Takai, K., Nakagawa, S., Reysenbach, A.-L., and Hoek, J. (2013). "Microbial ecology of Mid-ocean ridges and back-arc basins," in *Back-Arc Spreading Systems: Geological, Biological, Chemical, and Physical Interactions*, eds D. M. Christie,

C. R. Fisher, S.-M. Lee, and S. Givens (Washington, DC: American Geophysical Union), 185–213.

Takai, K., Nakamura, K., Suzuki, K., Inagaki, F., Nealson, K. H., and Kumagai, H. (2006). Ultramafics-Hydrothermalism-Hydrogenesis-HyperSLiME (UltraH3) linkage: a key insight into early microbial ecosystem in the Archean deep-sea hydrothermal systems. *Paleontol. Res.* 10, 269–282. doi: 10.2517/prpsj.10.269

Tremblay, P. L., and Zhang, T. (2015). Electrifying microbes for the production of chemicals. *Front. Microbiol.* 6:201. doi: 10.3389/fmicb.2015.00201

Valdés, J., Pedroso, I., Quatrini, R., Dodson, R. J., Tettelin, H., Blake, R., et al. (2008). *Acidithiobacillus ferrooxidans* metabolism: from genome sequence to industrial applications. *BMC Genomics* 9:597. doi: 10.1186/1471-2164-9-597

Yamaguchi, A., Yamamoto, M., Takai, K., Ishii, T., Hashimoto, K., and Nakamura, R. (2014). Electrochemical CO2 reduction by Ni-containing iron sulfides: how is CO2 electrochemically reduced at bisulfide-bearing deep-sea hydrothermal precipitates? *Electrochim. Acta* 141, 311–318. doi: 10.1016/j.electacta.2014.07.078

Yamamoto, M., Nakamura, R., Oguri, K., Kawagucci, S., Suzuki, K., Hashimoto, K., et al. (2013). Generation of electricity and illumination by an environmental fuel cell in deep-sea hydrothermal vents. *Angew. Chem. Int. Ed. Engl.* 52, 10758–10761. doi: 10.1002/anie.201302704

Yarzábal, A., Brasseur, G., Ratouchniak, J., Lund, K., Lemesle-Meunier, D., Demoss, J. A., et al. (2002). The high-molecular-weight cytochrome c Cyc2 of *Acidithiobacillus ferrooxidans* is an outer membrane protein. *J. Bacteriol.* 184, 313–317. doi: 10.1128/JB.184.1.313-317.2002

Yunker, S., and Radovich, J. (1986). Enhancement of growth and ferrous iron oxidation rates of *T. ferrooxidans* by electrochemical reduction of ferric iron. *Biotechnol. Bioeng.* 28, 1867–1875. doi: 10.1002/bit.260281214

Methane Emission in a Specific Riparian-Zone Sediment Decreased with Bioelectrochemical Manipulation and Corresponded to the Microbial Community Dynamics

Elliot S. Friedman[1][†], Lauren E. McPhillips[1], Jeffrey J. Werner[1,2], Angela C. Poole[3], Ruth E. Ley[3], M. Todd Walter[1] and Largus T. Angenent[1]*

[1] Department of Biological and Environmental Engineering, Cornell University, Ithaca, NY, USA, [2] Department of Chemistry, State University of New York College at Cortland, Cortland, NY, USA, [3] Department of Molecular Biology and Genetics, Cornell University, Ithaca, NY, USA

Dissimilatory metal-reducing bacteria are widespread in terrestrial ecosystems, especially in anaerobic soils and sediments. Thermodynamically, dissimilatory metal reduction is more favorable than sulfate reduction and methanogenesis but less favorable than denitrification and aerobic respiration. It is critical to understand the complex relationships, including the absence or presence of terminal electron acceptors, that govern microbial competition and coexistence in anaerobic soils and sediments, because subsurface microbial processes can effect greenhouse gas emissions from soils, possibly resulting in impacts at the global scale. Here, we elucidated the effect of an inexhaustible, ferrous-iron and humic-substance mimicking terminal electron acceptor by deploying potentiostatically poised electrodes in the sediment of a very specific stream riparian zone in Upstate New York state. At two sites within the same stream riparian zone during the course of 6 weeks in the spring of 2013, we measured CH_4 and N_2/N_2O emissions from soil chambers containing either poised or unpoised electrodes, and we harvested biofilms from the electrodes to quantify microbial community dynamics. At the upstream site, which had a lower vegetation cover and highest soil temperatures, the poised electrodes inhibited CH_4 emissions by ~45% (when normalized to remove temporal effects). CH_4 emissions were not significantly impacted at the downstream site. N_2/N_2O emissions were generally low at both sites and were not impacted by poised electrodes. We did not find a direct link between bioelectrochemical treatment and microbial community membership; however, we did find a correspondence between environment/function and microbial community dynamics.

Keywords: microbial iron reduction, riparian zones, methanogenesis, microbial food web, bioelectrochemical systems, microbial electrochemistry

INTRODUCTION

Riparian zones, which are the areas of land adjacent to streams, are often hotspots for biogeochemical transformations (Vidon et al., 2010). These ecosystems provide valuable services by acting as buffers between land and stream to prevent nutrients and pollutants from entering aquatic environments. Within riparian zones, subsurface microbial communities play a major role

in biogeochemical cycling, impacting carbon and nitrogen availability, and, by extension, plant productivity (Groffman et al., 1992; Burgin et al., 2010). Past work has examined denitrification processes in riparian zones, because these zones typically provide the last opportunity to mitigate excess nitrate in groundwater before it reaches the stream. Studies have found that the main regulators of denitrification (e.g., nitrate, anaerobic conditions, availability of other terminal electron acceptors and carbon sources) are spatially and temporally heterogeneous, which makes modeling these landscape-level processes particularly difficult (McClain et al., 2003; Groffman et al., 2009; Ranalli and Macalady, 2010; Vidon et al., 2010). Therefore, it is essential to have a full understanding of the underlying biogeochemistry to inform landscape level models, determine best management practices, and guide regulatory policies.

Bioelectrochemical systems (BESs) are engineered systems that utilize a biocatalyst, such as bacteria or enzymes, at electrodes. Microbial BESs capitalize on the ability of, for example, dissimilatory metal-reducing bacteria to respire with solid-state electrodes via extracellular electron transfer (Logan et al., 2006; Lovley, 2008; Franks and Nevin, 2010; Hamelers et al., 2010). These BESs produce power in microbial fuel cells (MFCs; He et al., 2005; Fornero et al., 2010a,b; Rosenbaum et al., 2011b); produce chemical products in microbial electrolysis cells (Rozendal et al., 2009; Villano et al., 2010; Cheng and Logan, 2011; Cusick et al., 2011; Rosenbaum et al., 2011a); remediate pollutants (Gregory and Lovley, 2005; Strycharz et al., 2010; Morris and Jin, 2012); sense environmental and chemical parameters (Chang et al., 2005; Kumlanghan et al., 2007); and produce logic gates in biocomputing devices (Li et al., 2011; TerAvest et al., 2011). In the environment, potentiostatically poised electrodes (i.e., electrodes held at a constant electrical potential using an electrical device called a potentiostat), can mimic iron(III)- and humic substance-compounds and act as the terminal electron acceptor for dissimilatory metal-reducing bacteria (Williams et al., 2010; Zhang et al., 2010; Friedman et al., 2012, 2013). The advantage of using an electrode instead of, for example, iron(III) is that the electrode can act as an inexhaustible terminal electron acceptor, which can be set precisely to the potential of interest without any other chemical interactions with the community. Thus, BESs can be a powerful tool for precise manipulation of environmental conditions for *in situ* experimentation. Here, we utilized a BES to study the interactions between microbial communities and the presence of iron(III) and humic substances as potential terminal electron acceptors under anaerobic conditions in a riparian zone.

Dissimilatory metal reduction has been shown to dominate a wide variety of anaerobic soils and sediments from the tropics to the poles (Weber et al., 2006; Dubinsky et al., 2010; Lipson et al., 2010, 2013; Keller and Takagi, 2013). Thermodynamically, iron- and manganese-reduction yield less energy than denitrification but more than sulfate reduction and methanogenesis (Bethke et al., 2011; Regnier et al., 2011). Therefore, in the presence of, for example, iron(III) [or electrodes mimicking iron[III]](Friedman et al., 2012, 2013)] under anaerobic conditions, methane emissions should decrease. Indeed, at least one study has clearly observed that the presence of electrodes in a MFC decreased

methane production (Ishii et al., 2008), although this was conducted in the laboratory and not in natural soil environments. Thermodynamic calculations are made under ideal conditions and do not take into account the ecological and physiological factors encountered *in situ*. For example, our recent work in Arctic peat soils has shown that bioelectrochemical manipulation designed to enrich for dissimilatory metal reduction actually increased methane emissions from soils. In this case, there was likely a bottleneck in the degradation of plant organic matter, which was widened by bioelectrochemical manipulation and stimulated the production of fermentation-like products (Friedman et al., 2013).

Modeling efforts are generally concerned with landscape-level function, such as pollutant removal or greenhouse gas emissions, but the parameters used in the model are dependent on the microbial-scale processes within the ecosystem and can vary by several orders of magnitude (Schmidt et al., 2011; Palmer and Febria, 2012; Wood et al., 2012). Therefore, it is critical to elucidate the links between microbial community structure and ecosystem processes (Raes and Bork, 2008; Morales and Holben, 2011). Here, we focused on the microbial scale within a riparian zone and we combined *in situ* bioelectrochemical manipulation with quantitative measurements of community structure (assessed by 16S rRNA gene sequences), environmental parameters (i.e., soil temperature, pH), and ecosystem function (rates of CH_4 and N_2/N_2O emissions). The objective of this work is to provide a foundation for elucidating the complex relationships between microbial community structure, community function, and ecosystem function (i.e., biogeochemical cycles); ultimately, the goal is to better inform modeling efforts through a more complete understanding of these complex relationships. One of our main objectives was to find correlations between changes of the environment, the community structure, and microbial function during the experimental period for several different experimental systems at two sites, rather than to describe the microbial community (α diversity) as a snapshot measurement, which does not inform about its function (Prosser, 2015).

At two distinct sites adjacent to an agricultural field within the riparian zone of Fall Creek in Freeville, NY, we measured CH_4 and N_2/N_2O emissions from soil chambers with either potentiostatically poised electrodes (mimicking inexhaustible iron[III] or humic substances) or unpoised electrodes (control) during a sampling period of 6 weeks in the spring of 2013. We also gathered environmental data during the experiment, including: soil temperature, pH, dissolved oxygen concentration, conductivity, iron concentrations and speciation, and anion concentrations. Once per week, bacterial biofilms were harvested from both poised and unpoised electrodes for 16S rRNA gene sequencing to determine microbial community structure. Here, we demonstrated the capability of small alterations to redox conditions to impact carbon release to the atmosphere, and provide a foundation for future examinations of biogeochemical cycling using *in situ* bioelectrochemical manipulations. Our hypothesis was that placement of iron(III)/humic substance-mimicking electrodes would reduce the emissions of methane in a very specific riparian zone of Fall Creek in Freeville, NY, USA.

MATERIALS AND METHODS

Field Location and Experimental Setup

This experiment was conducted within Fall Creek, which is a third order stream in Central New York that passes through the Homer C. Thompson Vegetable Research Farm and a Cornell University facility in Freeville, NY (42°31′N, 76°20′W; McPhillips et al., 2015). Six soil chambers were installed at each of two sites that were separated by ∼50 m. These sites are further denoted in the text as "upstream" or "downstream." At each site, three of the chambers contained potentiostatically poised graphite electrodes (experimental), while the other three contained unpoised graphite electrodes (control). We installed both soil chambers and electrodes by first making small incisions in the sediment with a serrated knife and then by inserting the chambers/electrodes. We performed the experiment from April 25th through June 6th, 2013.

Soil Chamber Construction

Soil chambers were constructed from 3.79 L plastic buckets (#2860, U.S. Plastic Corp., Lima, OH, USA). To create the base of the chamber, the bottom 2-cm of the bucket was removed leaving a 17-cm-long cylinder; when placed in the soil, 11-cm of the soil chamber was below the surface and 6-cm extended above the soil surface (Supplementary Figures S1–S3). From each chamber, an 8.5-cm × 4.5-cm section of the plastic material that would be in the subsurface area was removed and replaced with an anion exchange membrane (AMI-7001S, Membranes International, Glen Rock, NJ). To create a cap for the soil chamber, the top 4-cm was removed from another 3.79 L plastic bucket. The bottom edge of the plastic bucket was reinforced with foam insulation tape and duct tape to ensure an airtight seal between the soil chamber and the chamber cap (the cap was only used during short measurement periods). Two 0.635-cm cylindrical septa (AT6526, Fisher Scientific, USA) were affixed to the top of the chamber cap and sealed with urethane adhesive. During measurements, the chamber was vented with a 21G needle (#305129, VWR, USA) through one of the septa to prevent induced pressure differentials in the soil chamber (Hutchinson and Mosier, 1981). We took gas samples through the other septum.

Bioelectrochemical Systems

The working and counter electrodes (CE) were manufactured from medium-extruded graphite plates (GT001135, Graphite Store, Buffalo Grove, IL, USA). The CE consisted of a 6-cm × 6-cm of 0.635-cm thick block (surface area = 87.24 cm^2), while each working electrode (WE) consisted of six 6-cm × 6-cm × 0.635-cm blocks connected in parallel (total surface area = 523.44 cm^2). Having multiple electrodes in parallel for the WEs allowed for the harvesting of biofilms during different stages of the experiment. The WE and reference electrode (RE) were placed inside the chamber, while the CE was placed outside the chamber on the opposite side of the membrane to maintain an electrical connection while preventing cathodic hydrogen or methane production inside the soil chamber. Electrodes were connected

to microcontroller-based potentiostats (Friedman et al., 2012) by inserting the exposed end of a 3-m length of 18-gage stranded copper wire into a 1.59-mm hole drilled in the top of each graphite block. A conductive carbon adhesive (#12664, Electron Microscopy Sciences, Hatfield, PA, USA) was used to ensure a good electrical connection (resistance < 0.5 Ω), and the junction was sealed with a urethane adhesive (#4024, Hardman, South Bend, IN, USA). The WEs in experimental chambers were poised at 0.1 V_{SHE} using a microcontroller-based potentiostat (Friedman et al., 2012) and an Ag/AgCl RE was made in house. Electrodes in unpoised chambers were left at open circuit. Current data fluctuated throughout the experimental period due to many different factors, including diurnal changes (Supplementary Figures S4 and S5), and our data was not corrected for background chemical currents, chemical interactions, noise from electric fields, and open circuit potential for the unpoised electrodes.

Measurements

Measurements were taken every Monday and Thursday during the 6-week experimental period. We measured denitrification rates using the acetylene inhibition method, where acetylene is added to the soil to inhibit reduction of N_2O to N_2 (Freney et al., 1992; Thompson, 1996; Groffman et al., 2006), allowing quantification of N_2 and N_2O emissions through the measurement of N_2O only. Even though this method evaluates the denitrification rates (N_2 production), we indicate this in the text as N_2/N_2O emissions. We prepared and used beeswax-coated calcium carbide tablets, which react with water to form acetylene gas, as described by Thompson (1996). Six beeswax-coated calcium carbide tablets were inserted into each soil collar 45 min prior to gas sampling at a depth of 7–15 cm. We measured acetylene concentrations in the gas samples to ensure that ample acetylene (>1% v/v) was being produced to inhibit N_2O reduction (Thompson, 1996). Gas emissions were measured from the chambers by placing the cap on the chamber and collecting 12 mL of the headspace gas at four time points (0, 10, 20, and 30 min). Gas chromatography analysis of N_2O, CH_4, and C_2H_2 was performed on an Agilent 6890N gas chromatograph equipped with a HP 7694 Headspace Autosampler (Hewlett-Packard Company, Palo Alto, CA, USA). N_2O separation was performed using a Supel-Q^{TM} PLOT capillary column (30 m × 0.32 mm; Supelco Inc., Bellafonte, PA, USA) with ultra-pure helium carrier gas (2.6 mL min^{-1}) and 95:5 Ar:CH_4 make-up gas (8.2 mL min^{-1}) and an electron capture detector set to 250°C. CH_4 and C_2H_2 separation was performed using a Carboxen 1006 PLOT capillary column (30 m × 0.32 mm; Supelco, Inc.) and a flame ionization detector set to 200°C with H_2 gas (30 mL min^{-1}), air (400 mL min^{-1}), and N_2 makeup gas (25 mL min^{-1}). The oven temperature was initially set to −22°C for 4.7 min, then increased to 30°C for 0.85 min and finally increased to 80°C for 2.5 min to allow for elution of all three gasses of interest. Calibration curves were made using serial dilutions of 1 ppm N_2O, 20 ppm CH_4, and 2.5% C_2H_2 (Airgas Inc.). Emissions were calculated as the slopes of the linear regression (concentration vs. time) curves ($R^2 > 0.9$) for each measurement period (flux).

Soil temperature, pH, dissolved oxygen, and conductivity were measured at 7-cm depth directly adjacent to each soil chamber using a portable multiparameter meter (Orion Star A329, Thermo Scientific, Pittsburgh PA, USA) and probes (ROSS Ultra Triode pH/ATC electrode, DuraProbe conductivity probe, Orion RDO probe, Thermo Scientific, Pittsburgh, PA, USA). Soil water was collected from within each soil chamber (2–7 cm below the soil surface) using porous soil moisture samplers (#220300, Rhizosphere, Wageningen, The Netherlands), vacutainers (VT6430, BD, Franklin Lakes, NJ, USA), and 21G needles (#305129, VWR, USA). These samples were analyzed for nitrate, nitrite, chloride, and sulfate concentrations using a Dionex ICS-2000 ion chromatograph with IonPac AS-18 analytical column and 25-µL sample loop. Immediately following the collection of soil water, 0.5 mL of each sample was transferred to another vacutainer containing 0.5 mL of 0.5 N HCl; these samples were analyzed for Fe^{2+} and total Fe using the ferrozine assay (Braunschweig et al., 2012).

Microbial Community Analysis

Biofilms from the WEs of both experimental and control soil chambers were collected weekly throughout the 6-week period of the experiment. Each of the six parallel WEs in every soil chamber was harvested once during the course of the experiment to obtain a time series of the microbial community. We harvested biofilms by removing the electrode from the soil and by scraping the biofilm into a 15-mL sterile centrifuge tube (#93000-026, VWR, USA) using a sterile blade. Samples were placed on wet ice immediately in the field, and then stored at $-20°C$ until the completion of the experiment. Following biofilm harvesting, the bare electrodes were returned to the soil to keep the WE surface area constant throughout the experiment. Genomic DNA was extracted using a PowerSoil® DNA Isolation Kit (MoBio, Carlsbad, CA, USA). Bacterial extraction product was then amplified in duplicate 50-µL polymerase chain reactions (PCRs) according to Gilbert et al. (2010) using 25 cycles. In short, duplicate 50-µL PCR reactions were conducted using: 28 µL molecular grade water, 20 µL mastermix (5Prime Hot MasterMix, Catalog # 2200110, 5Prime, Fischer Scientific, USA), 0.5 µL 515f forward primer (Caporaso et al., 2012), 0.5 µL 806r barcoded reverse primer (Caporaso et al., 2012), and 1 µL template DNA. Reactions were run under the following conditions: 94°C for 3 min; then 94°C for 45 s, 50°C for 60 s, and 72°C for 90 s (repeat 25 times); 72°C for 10 min, and

then hold at 4°C. Duplicate PCR products were then pooled, the presence of amplicons confirmed by gel electrophoresis, and products cleaned using the Mag-Bind® E-Z Pure Kit (Omega, Norcross, GA, USA). Cleaned product was again confirmed with gel electrophoresis and barcoded amplicons for each sample were pooled at equimolar ratios to a final concentration of 8 ng DNA $µL^{-1}$. The single, pooled amplicon mixture was sequenced at the Cornell University Biotechnology Resource Center using an Illumina MiSeq (2×250 bp, paired end). Data were quality filtered with the quantitative insights into microbial ecology (QIIME) platform (v 1.6; Caporaso et al., 2010). Forward and reverse reads were joined using fastqjoin and the data returned to the QIIME platform for operational taxonomic unit (OTU) picking, alpha diversity, beta diversity, and further analysis. We applied a machine learning approach to identify taxa that discriminated between poised and unpoised electrode communities using the pamR package in R (Tibshirani et al., 2002), and applied a constrained correspondence analysis using the vegan package in R (Oksanen et al., 2013; R Core Team, 2013).

RESULTS AND DISCUSSION

CH_4 and N_2/N_2O Emissions

We measured CH_4 emissions bi-weekly in each of 12 chambers split between two riparian zone sites over the 6-weeks experimental period and calculated the absolute average CH_4 emission (**Table 1**). We observed differences between the two riparian zone sites, which were 50 m apart, in regards to CH_4 emissions, showing that this specific riparian zone was heterogeneous. The absolute average CH_4 emissions at the upstream site were considerably higher compared to the downstream site; absolute average CH_4 emissions with the unpoised electrode (control) chambers were 1.96 ± 1.42 mg $CH_4*m^{-2}*h^{-1}$ at the upstream site compared to 0.79 ± 0.65 mg $CH_4*m^{-2}*h^{-1}$ at the downstream site (**Table 1**). On average, the absolute CH_4 emissions from the poised electrode chambers at the upstream site were $\sim$50% lower than those from the unpoised electrode chambers, but due to the large temporal error not significantly different ($p = 0.55$, two-tailed t-test). At, the downstream site the absolute average CH_4 emissions from the poised electrode chambers were similar compared to those from the unpoised electrode chambers ($p = 0.91$, two-tailed t-test; **Table 1**). However, there were large temporal trends throughout

TABLE 1 | Average CH_4 emissions, N_2/N_2O emissions, SO_4^{2-} concentrations, and Cl^- concentrations from chambers with poised and unpoised electrodes at both the upstream and downstream sites during the experimental period.

Function or environmental parameter	Upstream poised	Upstream unpoised	Downstream poised	Downstream unpoised
CH_4 emission (mg $CH_4*m^{-2}*h^{-1}$)	0.96 ± 0.86	1.96 ± 1.42	0.93 ± 1.1	0.79 ± 0.65
N_2/N_2O emission (µg $N_2O\text{-}N*m^{-2}*h^{-1}$)	1793 ± 1794	2138 ± 2136	2394 ± 3287	2179 ± 2873
SO_4^{2-} concentration (ppm)	15.1 ± 14.6	38.2 ± 31.2	41.4 ± 35.8	45.5 ± 32.8
Cl^- concentration (ppm)	88.5 ± 39.7	107 ± 41.2	103 ± 63.0	218 ± 142

Large error is due to temporal changes during the experimental time period; as such, in further data analysis the groups were considered as paired samples on each measurement day (i.e., poised vs. unpoised) to remove the impacts of temporal trends when determining the effects of electrode-based manipulation. Error indicates standard error. N = 54 for all measurements.

the experimental period. The CH_4 emissions for each chamber were highest at the beginning of the experiment (earlier in the spring) and decreased throughout the 6-week experimental period (data not shown).

To more precisely determine the effects of potentiostatic manipulation, we normalized average CH_4 emissions (mg $CH_4*m^{-2}*h^{-1}$) from chambers with poised electrodes against the CH_4 emissions from chambers with unpoised electrodes at each site for each measurement day, resulting in an average percentage change in CH_4 emission ratios of poised vs. unpoised electrode chambers (**Figure 1A**). At the upstream site, we observed a 44% reduction in normalized CH_4 emission ($p = 0.017$, two-tailed paired t-test) for the poised vs. unpoised electrode chambers (**Figure 1A**). This is in agreement with our hypothesis: placement of iron(III)/humic substance-mimicking electrodes will reduce the emission rate methane compared to the control in a riparian zone, since it is thermodynamically more attractive to sustain iron/humic substance reduction (i.e., iron(III)/humic substances as the terminal electron acceptor) than methanogenesis (i.e., CO_2 as the terminal electron acceptor). However, for the downstream site for which we observed lower soil temperatures (Supplementary Figure S6), lower pH (Supplementary Figure S7), more vegetation cover, and less direct sunlight, we did not observe a significantly average change in normalized CH_4 emissions between the poised vs. unpoised chambers ($p = 0.61$, two-tailed paired t-test; **Figure 1A**). Noteworthy is that the temperature difference between the upstream and downstream sites may have caused for a small error in our data ($\sim$1%). Based on our hypotheses, we anticipated lower CH_4 emissions for the poised electrode chambers. It remains, however, unclear why the normalized CH_4 emissions were indeed lower at the upstream site and not at the downstream site with poised electrodes. This could be due to environmental differences between sites (e.g., soil temperature, pH), but further work is required to determine the precise reason(s).

There were no differences in the absolute average N_2/N_2O emissions (μg N_2O-$N*m^{-2}*h^{-1}$) between sites or treatments (**Table 1**). These data were also compared using percent change based on paired sample analysis in the same manner as the normalized CH_4 emissions, and there were no significant changes between groups at either site (upstream: $p = 0.051$; downstream: $p = 0.521$, two-tailed paired t-test, **Figure 1B**). Regardless, the discrepancies with our CH_4 emission results from adjacent field sites show the heterogeneous character of field research, and the importance to test results in the field rather than only at the bench.
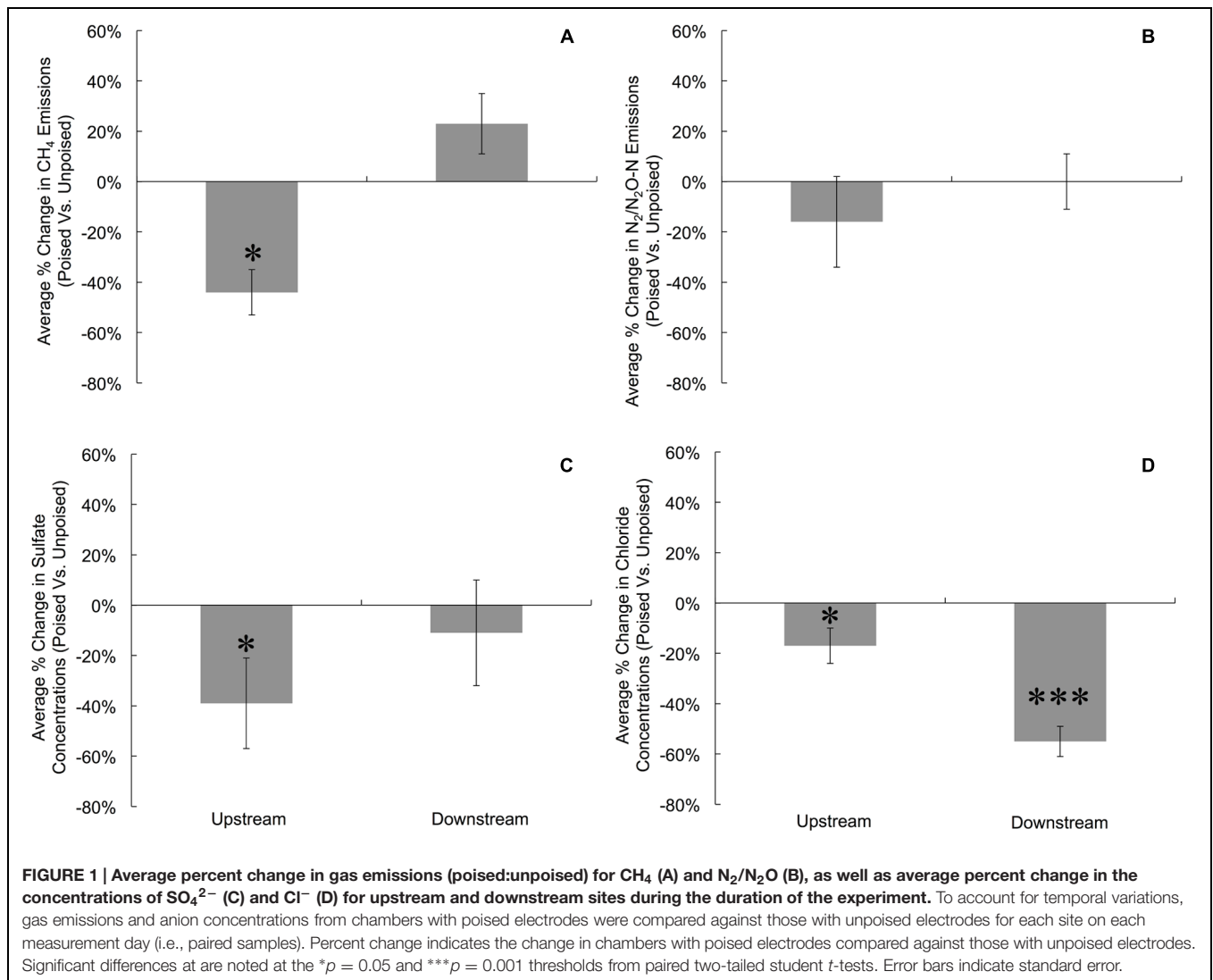
Environmental Parameters

We compared several environmental parameters that we measured for upstream and downstream sites during the study period. Soil temperature generally increased during the experimental period (and thus throughout the spring season), and ranged between 6.8 and 19.1°C (Supplementary Figure S6). On a daily basis throughout the 6-week period, the average soil temperatures at the upstream site were 1.5°C higher than that of the downstream site ($p < 0.001$, two-tailed t-test). The pH values across both sites were close to each other and

near neutral, with the upstream site averaging at 7.3 $\pm$ 0.2 and the downstream site at 7.2 $\pm$ 0.2 (Supplementary Figure S7). There were no differences in soil electrical conductivity between sites or control and treatment collars (Supplementary Figure S8); the average soil conductivity across both sites was 403 $\pm$ 165 μS/cm.

Dissolved oxygen was low across both sites due to water tables at or near the soil surface (for more than 75% of the experimental period), and both sites showed average concentrations of less than 1 mg L^{-1} dissolved oxygen (Supplementary Figure S9). Both NO_3^- and NO_2^- were low (<1 ppm) across sites and treatments, and were below detection limit (0.1 ppm) for most samples (consistent with the relatively low N_2/N_2O emissions rates). We did not observe a difference between sites and treatments for total iron concentrations from soil pore water, which averaged 10.97 $\pm$ 9.0 μM. Approximately 95% of this iron was in the reduced form (Fe^{2+}), and there were no differences between sites or treatments in iron speciation. At the upstream site, SO_4^{2-} concentrations were lower in chambers with poised electrodes than those with unpoised electrodes, however, there was not a significant difference in absolute SO_4^{2-} concentrations at the downstream site (**Table 1**). These values were corrected in the same manner as the normalized CH_4 emission rates, visualizing an average reduction in normalized SO_4^{2-} concentration of 39% with poised vs. unpoised electrodes ($p = 0.02$, two-tailed paired t-test; **Figure 1C**). It is unclear whether the difference in SO_4^{2-} concentrations at the upstream site was related to the reduction in CH_4 emissions, although sulfate reduction is more energetically favorable than methanogenesis, but less favorable than iron reduction (Regnier et al., 2011). Based on energetics, we would have anticipated a higher concentration of sulfate (less sulfate reduction) with a poised electrode. A conclusive explanation is elusive, but we can speculate: in some cases, microbial iron-reducing bacteria have been found to coincide with sulfate-reducing microbes (*Desulfovibrio* sp.; Lentini et al., 2012), and it is possible that a synergistic relationship between iron- and sulfate-reducers is responsible for the decreased sulfate concentrations in the chambers with poised electrodes at the upstream site. This co-occurrence is supported by the simultaneous normalized CH_4 emission reduction (via mimicked iron reduction with electrodes) and decreased normalized SO_4^{2-} concentration (via increased sulfate reduction) at the upstream site, while neither decrease occurred at the downstream site.

Absolute Cl^- concentrations were lower in pore water collected from chambers containing poised electrodes at both sampling sites (**Table 1**); these values were corrected in the same manner as normalized CH_4 emission rates. At the upstream sites, chambers with poised electrodes had normalized Cl^- concentrations that were 17% lower than those with unpoised electrodes ($p = 0.007$, two-tailed paired t-test); at the downstream site, normalized Cl^- concentrations were, on average, 55% lower than in chambers with unpoised electrodes ($p < 0.0005$, two-tailed paired t-test; **Figure 1D**). These lower Cl^- concentrations were a result of Cl^- transport from the inside to the outside chamber through the anion exchange membrane because of ion imbalances due to the electrochemical activity (Rozendal et al., 2006; Fornero et al., 2010b).

FIGURE 1 | Average percent change in gas emissions (poised:unpoised) for CH$_4$ (A) and N$_2$/N$_2$O (B), as well as average percent change in the concentrations of SO$_4^{2-}$ (C) and Cl$^-$ (D) for upstream and downstream sites during the duration of the experiment. To account for temporal variations, gas emissions and anion concentrations from chambers with poised electrodes were compared against those with unpoised electrodes for each site on each measurement day (i.e., paired samples). Percent change indicates the change in chambers with poised electrodes compared against those with unpoised electrodes. Significant differences at are noted at the *$p = 0.05$ and ***$p = 0.001$ thresholds from paired two-tailed student t-tests. Error bars indicate standard error.

Microbial Community Dynamics

We obtained a total of 72 samples (69 of which were sequenced; 3 samples had too low of a DNA yield to be sequenced) from the 12 chambers during 6 weeks and achieved an average sequencing coverage of 29,782 sequences (16S rRNA gene) per sample with an average length of 251 bp. We first analyzed the beta diversity, which quantifies the differentiation between sample communities, using UniFrac distances (Lozupone and Knight, 2005). Based on the differences in CH$_4$ emissions and environmental parameters, we had expected microbial communities to be similar to each other if they came from the same site or treatment. However, principal coordinate analysis of both unweighted UniFrac distances and weighted UniFrac distances (weighted takes into account relative abundances of OTUs within samples) did not reveal any clustering of samples by site or treatment (**Figures 2A,B**). However, there was a clear clustering of samples with time, which was highlighted by UniFrac distances between the first 2 weeks (weeks 1–2) and last 2 weeks (weeks 5–6) of the experimental period (**Figure 3**). This

result likely suggests that most of the broad differences in the microbial community phylogenetic structure were based simply on changing environmental parameters and community function with time, rather than experimental treatment.

In each of the electrode samples, over 80% of the 16S rRNA gene sequences were classified in the phyla Proteobacteria and Bacteroidetes, with a remaining 1–6% of sequences falling in the phyla Firmicutes, Acidobacteria, Actinobacteria, Verrucomicrobia, Cyanobacteria, Chloroflexi, Planctomycetes, and Gemmatimonadetes (**Figure 4**). Similar to the beta diversity data analysis, we grouped the taxonomy data for weeks 1–2 and weeks 5–6 with the objective to identify phyla that changed during the experimental period of 6 weeks. At the upstream site, the community composition at the poised electrodes between weeks 1–2 and 5–6 showed a 10% increase in Proteobacteria ($p = 0.19$, two-tailed t-test) and a 35% decrease in Bacteroidetes ($p = 0.04$, two-tailed t-test) during the experimental period. Proteobacteria and Bacteroidetes populations were not different at the unpoised electrodes between weeks 1–2 and 5–6
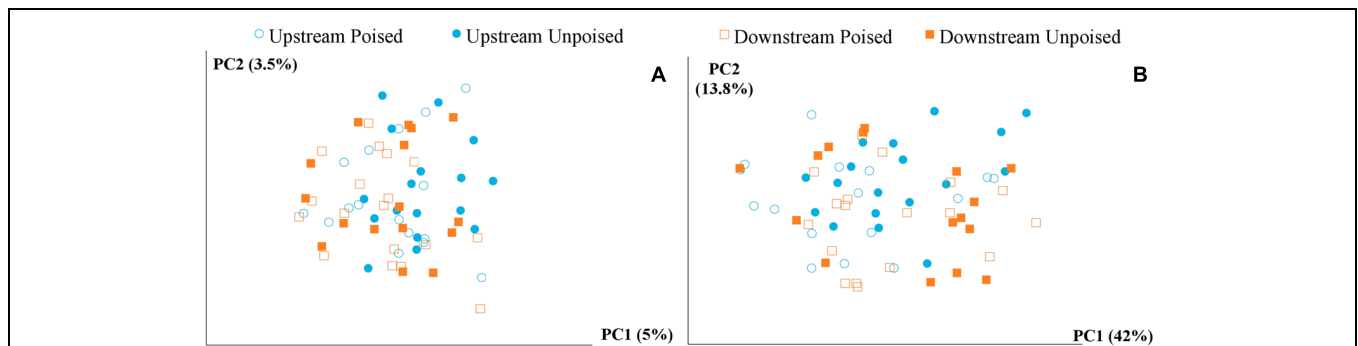
FIGURE 2 | Principal coordinate analysis of the beta diversity of microbial communities shown using unweighted (A) and weighted (B) UniFrac distances. The weighted **(B)** method explains more variation (55.8%) in the first two principal coordinates than the unweighted **(A)** method (8.5%); however, in both cases there are no clear clusters differentiating between sites (upstream or downstream) or treatment (poised or unpoised electrodes).
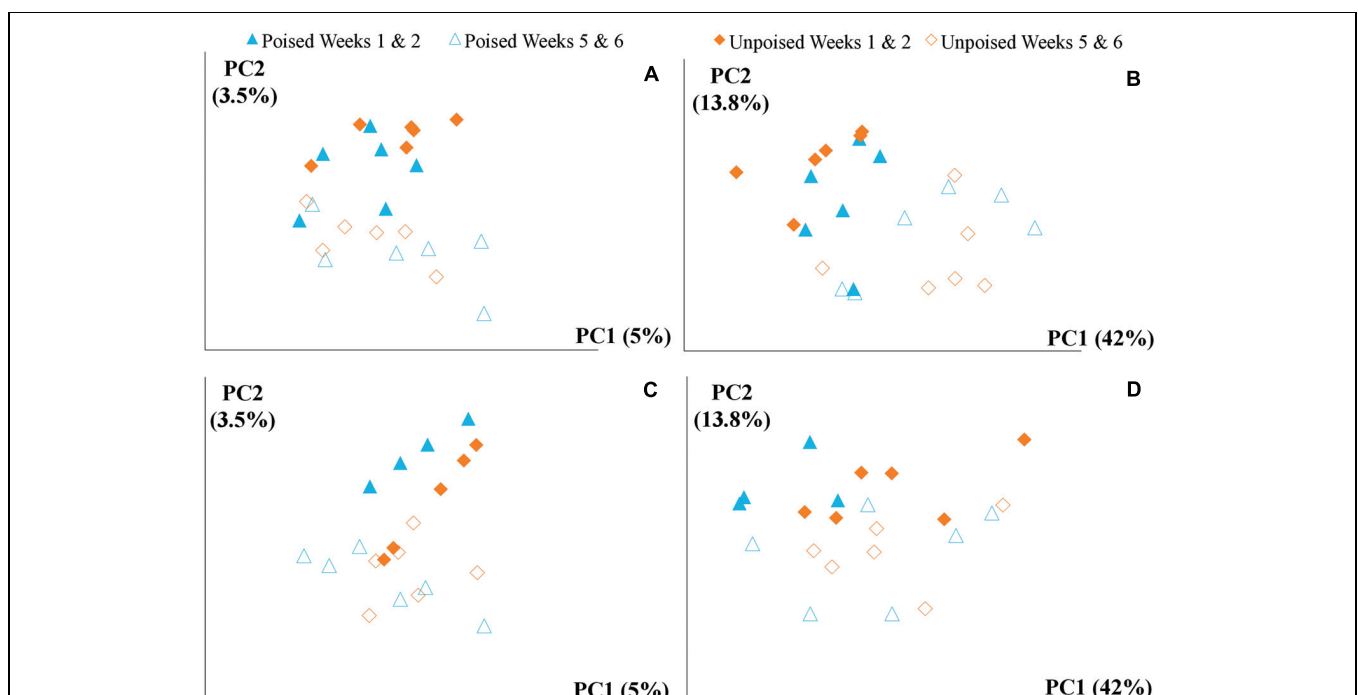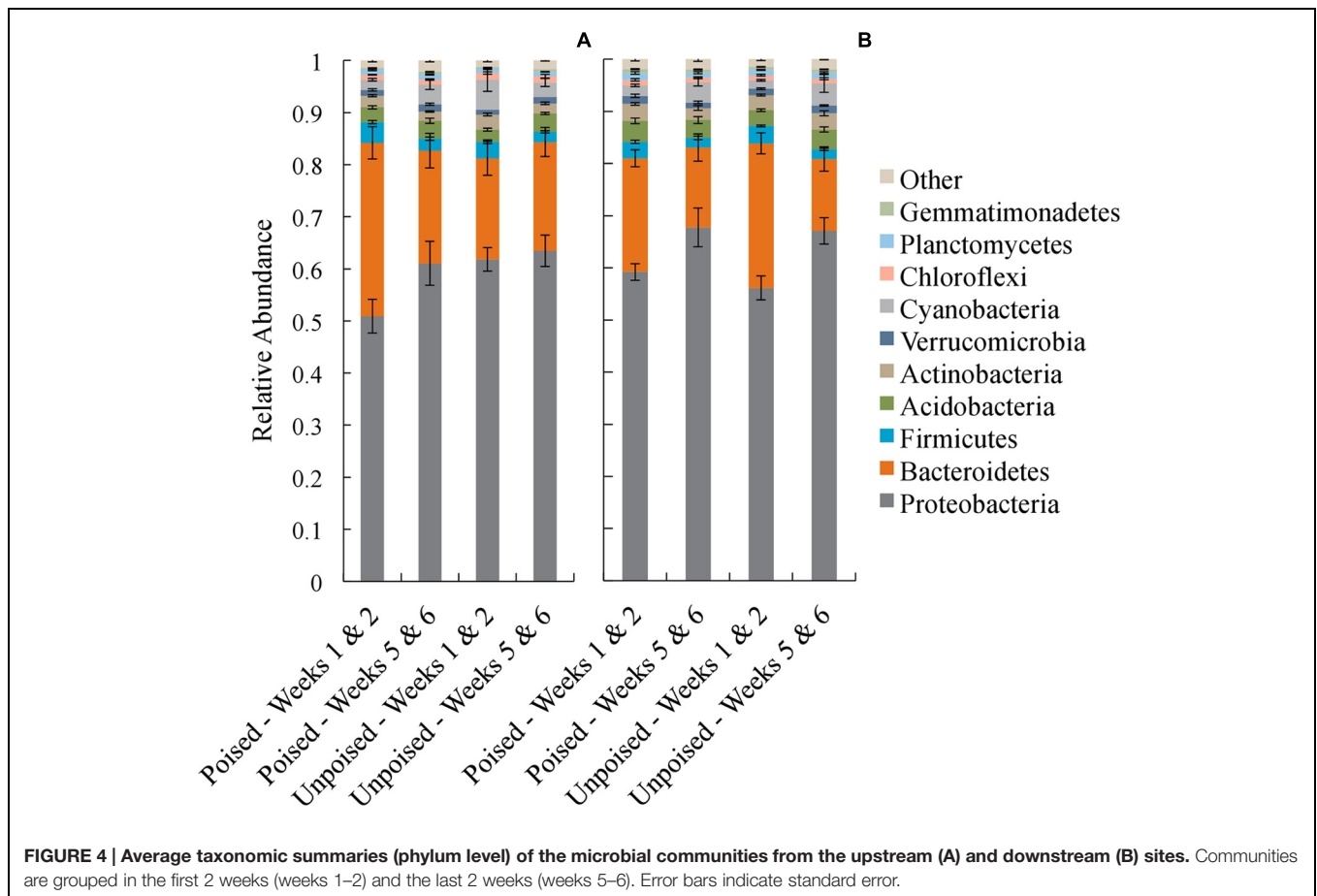

FIGURE 3 | Principal coordinate analysis of beta diversity at upstream and the downstream sites using unweighted and weighted UniFrac distances: (A) upstream site, unweighted UniFrac; (B) upstream site, weighted UniFrac; (C) downstream site, unweighted UniFrac; and (D) downstream site, weighted UniFrac. The weighted **(B,D)** method explains more variation (55.8%) in the first two principal coordinates than the unweighted **(A,B)** method (8.5%); however, in both cases there are no clear clusters differentiating between sites (upstream or downstream) or treatment (poised or unpoised electrodes). There was some clustering between time points (weeks 1 and 2 or weeks 5 and 6), suggesting that shifts in community were primarily driven by environmental conditions rather than manipulation.

(**Figure 4A**). At the downstream site, both poised and unpoised electrodes enriched for Proteobacteria between weeks 1–2 and 5–6, which was accompanied by a decrease in relative abundance of Bacteroidetes (**Figure 4B**). Specifically, the poised electrodes resulted in a 14% increase in Proteobacteria and a 30% decrease in Bacteroidetes ($p = 0.06$ for both phyla, two-tailed t-test) while the unpoised electrodes caused a 20% increase in Proteobacteria and a 50% decrease in Bacteroidetes ($p < 0.01$ for both phyla, two-tailed t-test) between weeks 1–2 and 5–6. The increase in Proteobacteria in both poised and unpoised treatments could be

due to the presence of the graphite electrodes, which provide a conductive surface that promotes both biofilm growth and long-range electron transport through soil microenvironments (even when unpoised; Erable et al., 2011; Kato et al., 2012; Friedman et al., 2013). Thus, with this phyla richness analysis we found that three out of four comparisons of week 1–2 and week 5–6 binned data showed a similar trend of increasing Proteobacteria, but this included the poised *and* unpoised electrodes at one site.

We used a machine learning approach to find OTUs that are predictive of samples taken from either poised or unpoised

FIGURE 4 | Average taxonomic summaries (phylum level) of the microbial communities from the upstream (A) and downstream (B) sites. Communities are grouped in the first 2 weeks (weeks 1–2) and the last 2 weeks (weeks 5–6). Error bars indicate standard error.

electrodes (**Figure 5**). We applied this to OTU abundance profiles from all samples (**Figure 5A**) as well as data from only the upstream site samples (**Figure 5B**). Upon cross-validation, the machine-learning algorithm returned a relatively high error rate (0.392 and 0.346 for both sites, and the upstream site, respectively), indicating that there were no indicator OTUs that could differentiate poised from unpoised electrode conditions. This machine learning approach confirmed our other findings from the principal coordinate analysis of UniFrac-based beta diversity (**Figures 2** and **3**) and the other taxonomic classification analysis (**Figure 4**) that the bioelectrochemical manipulation did not cause systematic, or reproducible, changes in the microbial membership.

Linking Microbial Community Dynamics to Gas Emissions and Environmental Parameters

Next, we investigated whether community function (e.g., gas emission) or environmental parameters were associated with microbial community membership. We performed correspondence analysis to compare OTU abundance profiles with gas emission and environmental metadata (rarified with 500 sequences per sample; **Figure 6**). First, we performed principal component analysis with our OTU tables, and second

we performed correspondence analysis to map environmental metadata onto the principal component results as vectors. The resulting direction of the vector (arrow) indicates that the specific variable corresponded strongly with community structure, while the resulting length of the vector indicates the magnitude of the association (i.e., longer arrows indicate a more significant weighting of the given variable in the overall ordination). When we used data from across all sites and treatments, the variables of strongest correspondence with the OTU tables were: N_2/N_2O emissions, pH, and Cl^- concentrations (**Figure 6A**). When limiting the analysis to the upstream site (where unpoised electrode chambers had higher CH_4 emissions), however, the CH_4 emissions were the most strongly weighted variable, with N_2/N_2O emissions, pH, Cl^- concentrations, and temperature being other variables (**Figure 6B**). Noteworthy is that temperature and time as a vector cannot be distinguished in our work because of slowly rising soil temperatures during our experimental period (Supplementary Figure S6).

Future Work Critical to Elucidate Microbial Community Dynamics in Riparian Zones

Riparian zones have the capability to buffer aquatic ecosystems from the adjacent land and are important ecosystems for

FIGURE 5 | Machine learning analysis using phylum level taxonomy shows the phyla that are most indicative of poised or unpoised electrode communities across: (A) both sites; and (B) just the upstream site. Machine learning classifier is a nearest shrunken centroid classifier calculated using the pamR package in R.
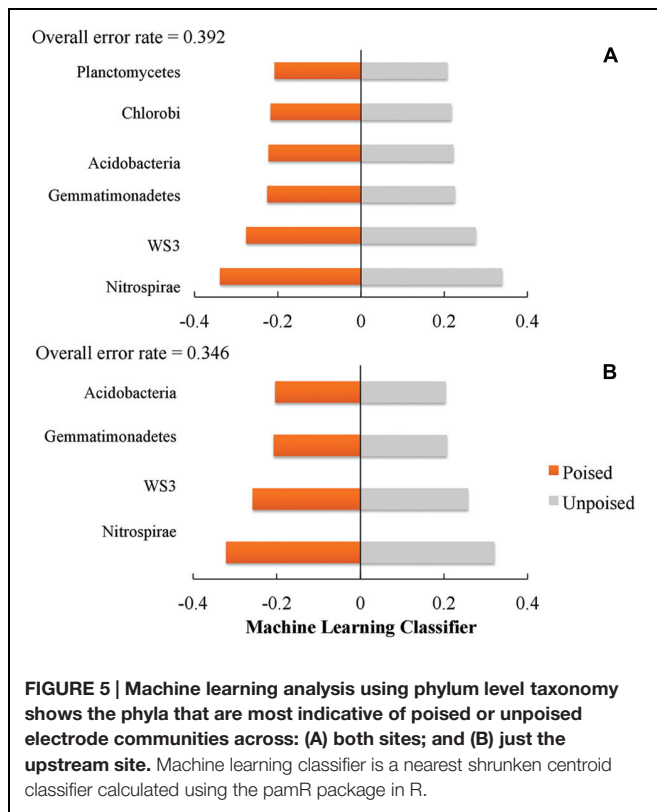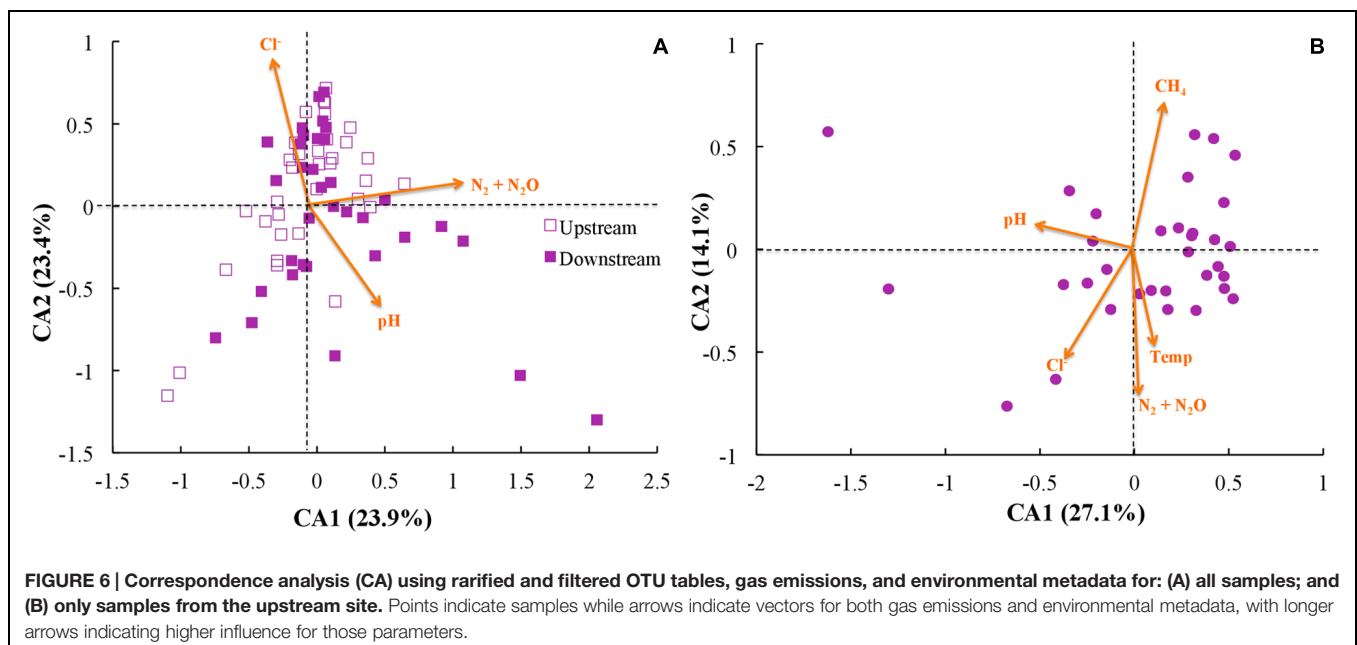
watershed management, especially in agricultural areas (McClain et al., 2003; Burt et al., 2010). Many studies have attempted to directly link hydrologic parameters (e.g., water table depth, groundwater flow patterns) to both denitrification rates and greenhouse gas emissions (Vidon and Hill, 2004; Aronson et al., 2012; Audet et al., 2013; McPhillips et al., 2015).

However, microbial communities are the drivers of subsurface biogeochemical transformations, and as such it is critical to quantitatively link microbial community dynamics to ecosystem level parameters and functions (Raes and Bork, 2008; Burt et al., 2010; Morales and Holben, 2011). There are often chemical or biological links (or both) between different ecosystem processes, such as temperature, groundwater flow, plant growth, and denitrification (Teh et al., 2008; Liptzin and Silver, 2009; Dubinsky et al., 2010; Vidon et al., 2010; Frei et al., 2012).

When we manipulated the soil redox environment using poised electrodes mimicking iron(III), there was a significant decrease in CH_4 emissions from the upstream site (**Figure 1A**), which we anticipated because the presence of a terminal electron acceptor with the redox potential of iron(III) for iron reduction is thermodynamically more favorable compared to carbon dioxide for methanogenesis. Furthermore, manipulation resulted in a decrease in SO_4^{2-} and Cl^- concentrations in soil porewater (**Figures 1C,D**). However, at the downstream site, which had a lower magnitude of emissions (nearly 50%) from the chambers with unpoised electrodes (i.e., controls), poised electrodes had no effect on CH_4 emissions. This is likely due to the lower overall CH_4 emission rates at this site, which would preclude inhibition via bioelectrochemical manipulation since methanogenic activity was already low.

We also observed, together with the reduction in CH_4 emission from the upstream site, an increase in the relative abundance of Proteobacteria and a decrease in Bacteroidetes (**Figure 4A**). However, we found no systematic link between community structure and experimental treatment (poised vs. unpoised electrodes; **Figures 2** and **3**). Further quantitative analysis showed that these microbial community changes corresponded with differences in the environmental parameters (pH and Cl^- concentrations) and CH_4 and N_2/N_2O emissions (**Figure 6**).

FIGURE 6 | Correspondence analysis (CA) using rarified and filtered OTU tables, gas emissions, and environmental metadata for: (A) all samples; and (B) only samples from the upstream site. Points indicate samples while arrows indicate vectors for both gas emissions and environmental metadata, with longer arrows indicating higher influence for those parameters.

The indirect alteration of microbial community structure and suppression of CH_4 emissions at the upstream site in conjunction with bioelectrochemical manipulation (using soil-based electrodes) demonstrates the fragile balance that governs biogeochemical cycles in these soils, and highlights the measurable impact that microbial competition has on ecosystem-scale processes. It is clear that microbial community structure and function is subject to influence from a wide array of biological, chemical, and physical factors, which in turn can have a measurable impact on the landscape level. Accurate modeling of biogeochemical processes is important for predicting responses to climate change, determining regulatory limits for anthropogenic pollutants, and designing effective best management practices (Vidon et al., 2010; Meng et al., 2011; Riley et al., 2011). As such, a deeper comprehension of subsurface microbial ecosystems, their responses to environmental conditions across spatial and temporal gradients, and their impacts on larger-scale function, is critical for improving model accuracy, and further studies are certainly warranted.

In summary, we manipulated the sediment redox environment by poising electrodes capable of being used as electron acceptors for iron(III)-reducing microbes and observed a response in ecosystem function (in this case, CH_4 emissions) at one riparian zone site. Poised electrodes provided an inexhaustible source of electron acceptor for iron reducers, and, at our upstream riparian zone site, resulted in reduced CH_4 emissions that could be a result of iron- or humic substance-reducers outcompeting methanogens for carbon sources and nutrients. However, we did not see such changes in CH_4 emissions at the downstream site. Furthermore, we showed that bioelectrochemical manipulation had minimal effects on the microbial community structure. This was confirmed by machine learning analysis, which was unable to develop an algorithm to predict sample grouping with an error rate below 30%. We did, however, find a correspondence between the community composition and the function of the microbiota (CH_4 emissions). Despite the lack of direct changes in microbial community structure at the upstream site with poised electrodes, the reduction ($\sim$45%) of CH_4 emissions together with its correspondence to the composition of microbiota suggests that the balance between competing anaerobic microbial processes can have a major impact on landscape-level processes.

Key Points:

- Potentiostatic manipulation was used to change redox dynamics in riparian soils.
- Manipulation inhibited CH_4 emissions but did not change the microbial community.
- Microbial community dynamics corresponded to environment and ecosystem function.

AUTHOR CONTRIBUTIONS

EF, LM, MW, and LA designed the study; EF and LM performed the field research; EF, LM, and AP performed the sample analysis; EF, LM, JW, AP, RL, MW, and LA analyzed the data, EF, LM, JW, AP, RL, MW, and LA wrote the manuscript.

ACKNOWLEDGMENTS

SUPPLEMENTARY MATERIAL

The Supplementary Material for this article can be found online at: http://journal.frontiersin.org/article/10.3389/fmicb.2015.01523

REFERENCES

Aronson, E. L., Vann, D. R., and Helliker, B. R. (2012). Methane flux response to nitrogen amendment in an upland pine forest soil and riparian zone. *J. Geophys. Res. Biogeosci.* 117, G03012. doi: 10.1029/2012jg001962

Audet, J., Johansen, J. R., Andersen, P. M., Baattrup-Pedersen, A., Brask-Jensen, K. M., Elsgaard, L., et al. (2013). Methane emissions in Danish riparian wetlands: ecosystem comparison and pursuit of vegetation indexes as predictive tools. *Ecol. Indic.* 34, 548–559. doi: 10.1016/j.ecolind.2013.06.016

Bethke, C. M., Sanford, R. A., Kirk, M. F., Jin, Q. S., and Flynn, T. M. (2011). The thermodynamic ladder in geomicrobiology. *Am. J. Sci.* 311, 183–210. doi: 10.2475/03.2011.01

Braunschweig, J., Bosch, J., Heister, K., Kuebeck, C., and Meckenstock, R. U. (2012). Reevaluation of colorimetric iron determination methods commonly used in geomicrobiology. *J. Microbiol. Methods* 89, 41–48. doi: 10.1016/j.mimet.2012.01.021

Burgin, A. J., Groffman, P. M., and Lewis, D. N. (2010). Factors regulating denitrification in a riparian wetland. *Soil Sci. Soc. Am. J.* 74, 1826–1833. doi: 10.2136/sssaj2009.0463

Burt, T., Pinay, G., and Sabater, S. (2010). What do we still need to know about the ecohydrology of riparian zones? *Ecohydrology* 3, 373–377. doi: 10.1002/eco.140

Caporaso, J. G., Kuczynski, J., Stombaugh, J., Bittinger, K., Bushman, F. D., Costello, E. K., et al. (2010). QIIME allows analysis of high-throughput community sequencing data. *Nat. Methods* 7, 335–336. doi: 10.1038/Nmeth.F.303

Caporaso, J. G., Lauber, C. L., Walters, W. A., Berg-Lyons, D., Huntley, J., Fierer, N., et al. (2012). Ultra-high-throughput microbial community analysis on the Illumina HiSeq and MiSeq platforms. *ISME J.* 6, 1621–1624. doi: 10.1038/Ismej.2012.8

Chang, I. S., Moon, H., Jang, J. K., and Kim, B. H. (2005). Improvement of a microbial fuel cell performance as a BOD sensor using respiratory inhibitors. *Biosens. Bioelectron.* 20, 1856–1859. doi: 10.1016/j.bios.2004.06.003

Cheng, S. A., and Logan, B. E. (2011). High hydrogen production rate of microbial electrolysis cell (MEC) with reduced electrode spacing. *Bioresour. Technol.* 102, 3571–3574. doi: 10.1016/j.biortech.2010.10.025

Cusick, R. D., Bryan, B., Parker, D. S., Merrill, M. D., Mehanna, M., Kiely, P. D., et al. (2011). Performance of a pilot-scale continuous flow microbial electrolysis

cell fed winery wastewater. *Appl. Microbiol. Biotechnol.* 89, 2053–2063. doi: 10.1007/s00253-011-3130-9

Dubinsky, E. A., Silver, W. L., and Firestone, M. K. (2010). Tropical forest soil microbial communities couple iron and carbon biogeochemistry. *Ecology* 91, 2604–2612. doi: 10.1890/09-1365.1

Erable, B., Etcheverry, L., and Bergel, A. (2011). From microbial fuel cell (MFC) to microbial electrochemical snorkel (MES): maximizing chemical oxygen demand (COD) removal from wastewater. *Biofouling* 27, 319–326. doi: 10.1080/08927014.2011.564615

Fornero, J. J., Rosenbaum, M., and Angenent, L. T. (2010a). Electric power generation from municipal, food, and animal wastewaters using microbial fuel cells. *Electroanalysis* 22, 832–843. doi: 10.1002/elan.2009 80011

Fornero, J. J., Rosenbaum, M., Cotta, M. A., and Angenent, L. T. (2010b). Carbon dioxide addition to microbial fuel cell cathodes maintains sustainable catholyte pH and improves anolyte pH, alkalinity, and conductivity. *Environ. Sci. Technol.* 44, 2728–2734. doi: 10.1021/Es9031985

Franks, A. E., and Nevin, K. P. (2010). Microbial fuel cells, a current review. *Energies* 3, 899–919. doi: 10.3390/En3050899

Frei, S., Knorr, K. H., Peiffer, S., and Fleckenstein, J. H. (2012). Surface micro-topography causes hot spots of biogeochemical activity in wetland systems: a virtual modeling experiment. *J. Geophys. Res.* 117, G00N12. doi: 10.1029/2012jg002012

Freney, J. R., Smith, C. J., and Mosier, A. R. (1992). Effect of a new nitrification inhibitor (wax coated calcium carbide) on transformations and recovery of fertilizer nitrogen by irrigated wheat. *Fertil. Res.* 32, 1–11. doi: 10.1007/BF01054388

Friedman, E. S., Miller, K. E., Lipson, D. A., and Angenent, L. T. (2013). Potentiostatically-poised electrodes mimic iron oxides and interact with soil microbial communities to alter the biogeochemistry of Arctic peat soils. *Minerals* 3, 318–336. doi: 10.3390/min3030318

Friedman, E. S., Rosenbaum, M. A., Lee, A. W., Lipson, D. A., Land, B. R., and Angenent, L. T. (2012). A cost-effective and field-ready potentiostat that poises subsurface electrodes to monitor bacterial respiration. *Biosens. Bioelectron.* 32, 309–313. doi: 10.1016/j.bios.2011.12.013

Gilbert, J. A., Meyer, F., Jansson, J., Gordon, J., Pace, N., Tiedje, J., et al. (2010). The Earth Microbiome Project: meeting report of the "1st EMP meeting on sample selection and acquisition" at Argonne National Laboratory October 6(th) 2010. *Stand. Genomic Sci.* 3, 249–253. doi: 10.4056/Sigs.1443528

Gregory, K. B., and Lovley, D. R. (2005). Remediation and recovery of uranium from contaminated subsurface environments with electrodes. *Environ. Sci. Technol.* 39, 8943–8947. doi: 10.1021/Es050457e

Groffman, P. M., Altabet, M. A., Bohlke, J. K., Butterbach-Bahl, K., David, M. B., Firestone, M. K., et al. (2006). Methods for measuring denitrification: diverse approaches to a difficult problem. *Ecol. Appl.* 16, 2091–2122. doi: 10.1890/1051-0761(2006)016[2091:MFMDDA]2.0.CO;2

Groffman, P. M., Butterbach-Bahl, K., Fulweiler, R. W., Gold, A. J., Morse, J. L., Stander, E. K., et al. (2009). Challenges to incorporating spatially and temporally explicit phenomena (hotspots and hot moments) in denitrification models. *Biogeochemistry* 93, 49–77. doi: 10.1007/s10533-008-9277-5

Groffman, P. M., Gold, A. J., and Simmons, R. C. (1992). Nitrate dynamics in riparian forests – microbial studies. *J. Environ. Qual.* 21, 666–671. doi: 10.2134/jeq1992.214666x

Hamelers, H. V. M., Ter Heijne, A., Sleutels, T. H. J. A., Jeremiasse, A. W., Strik, D. P. B. T. B., and Buisman, C. J. N. (2010). New applications and performance of bioelectrochemical systems. *Appl. Microbiol. Biotechnol.* 85, 1673–1685. doi: 10.1007/s00253-009-2357-1

He, Z., Minteer, S. D., and Angenent, L. T. (2005). Electricity generation from artificial wastewater using an upflow microbial fuel cell. *Environ. Sci. Technol.* 39, 5262–5267. doi: 10.1021/es0502876

Hutchinson, G. L., and Mosier, A. R. (1981). Improved soil cover method for field measurement of nitrous-oxide fluxes. *Soil Sci. Soc. Am. J.* 45, 311–316. doi: 10.2136/sssaj1981.03615995004500020017x

Ishii, S. I., Hotta, Y., and Watanabe, K. (2008). Methanogenesis versus electrogenesis: morphological and phylogenetic comparisons of microbial communities. *Biosci. Biotechnol. Biochem.* 72, 286–294. doi: 10.1271/bbb. 70179

Kato, S., Hashimoto, K., and Watanabe, K. (2012). Microbial interspecies electron transfer via electric currents through conductive minerals. *Proc. Natl. Acad. Sci. U.S.A.* 109, 10042–10046. doi: 10.1073/pnas.1117592109

Keller, J. K., and Takagi, K. K. (2013). Solid-phase organic matter reduction regulates anaerobic decomposition in bog soil. *Ecosphere* 4, art54. doi: 10.1890/ES12-00382.1

Kumlanghan, A., Liu, J., Thavarungkul, P., Kanatharana, P., and Mattiasson, B. (2007). Microbial fuel cell-based biosensor for fast analysis of biodegradable organic matter. *Biosens. Bioelectron.* 22, 2939–2944. doi: 10.1016/j.bios.2006.12.014

Lentini, C. J., Wankel, S. D., and Hansel, C. M. (2012). Enriched iron(III)-reducing bacterial communities are shaped by carbon substrate and iron oxide mineralogy. *Front. Microbiol.* 3:404. doi: 10.3389/fmicb.2012.00404

Li, Z. J., Rosenbaum, M. A., Venkataraman, A., Tam, T. K., Katz, E., and Angenent, L. T. (2011). Bacteria-based AND logic gate: a decision-making and self-powered biosensor. *Chem. Commun.* 47, 3060–3062. doi: 10.1039/C0cc05037g

Lipson, D. A., Jha, M., Raab, T. K., and Oechel, W. C. (2010). Reduction of iron (III) and humic substances plays a major role in anaerobic respiration in an Arctic peat soil. *J. Geophys. Res.* 115, G00I06. doi: 10.1029/2009jg001147

Lipson, D. A., Raab, T. K., Goria, D., and Zlamal, J. (2013). The contribution of Fe(III) and humic acid reduction to ecosystem respiration in drained thaw lake basins of the Arctic Coastal Plain. *Global Biogeochem. Cycles* 27, 399–409. doi: 10.1002/gbc.20038

Liptzin, D., and Silver, W. L. (2009). Effects of carbon additions on iron reduction and phosphorus availability in a humid tropical forest soil. *Soil Biol. Biochem.* 41, 1696–1702. doi: 10.1016/j.soilbio.2009.05.013

Logan, B. E., Hamelers, B., Rozendal, R., Schroder, U., Keller, J., Freguia, S., et al. (2006). Microbial fuel cells: methodology and technology. *Environ. Sci. Technol.* 40, 5181–5192. doi: 10.1021/es0605016

Lovley, D. R. (2008). The microbe electric: conversion of organic matter to electricity. *Curr. Opin. Biotechnol.* 19, 564–571. doi: 10.1016/j.copbio.2008.10.005

Lozupone, C., and Knight, R. (2005). UniFrac: a new phylogenetic method for comparing microbial communities. *Appl. Environ. Microbiol.* 71, 8228–8235. doi: 10.1128/Aem.71.12.8228-8235.2005

McClain, M. E., Boyer, E. W., Dent, C. L., Gergel, S. E., Grimm, N. B., Groffman, P. M., et al. (2003). Biogeochemical hot spots and hot moments at the interface of terrestrial and aquatic ecosystems. *Ecosystems* 6, 301–312. doi: 10.1007/s10021-003-0161-9

McPhillips, L. E., Groffman, P. M., Goodale, C. L., and Walter, M. T. (2015). Hydrologic and biogeochemical drivers of riparian denitrification in an agricultural watershed. *Water Air Soil Pollut.* 226:169. doi: 10.1007/s11270-015-2434-2

Meng, L., Hess, P. G. M., Mahowald, N. M., Yavitt, J. B., Riley, W. J., Subin, Z. M., et al. (2011). Sensitivity of wetland methane emissions to model assumptions: application and model testing against site observations. *Biogeosci. Discuss.* 8, 6095–6160. doi: 10.5194/bgd-8-6095-2011

Morales, S. E., and Holben, W. E. (2011). Linking bacterial identities and ecosystem processes: can 'omic' analyses be more than the sum of their parts? *FEMS Microbiol. Ecol.* 75, 2–16. doi: 10.1111/j.1574-6941.2010.00938.x

Morris, J. M., and Jin, S. (2012). Enhanced biodegradation of hydrocarbon-contaminated sediments using microbial fuel cells. *J. Hazard. Mater.* 213, 474–477. doi: 10.1016/j.jhazmat.2012.02.029

Oksanen, J., Blanchet, F. G., Kindt, R., Legendre, P., Stevens, H. H., and Wagner, H. (2013). *vegan: Community Ecology Package. R Package Version 2.0–8*. Available at: http://cran.r-project.org

Palmer, M. A., and Febria, C. M. (2012). The heartbeat of ecosystems. *Science* 336, 1393–1394. doi: 10.1126/science.1223250

Prosser, J. I. (2015). Dispersing misconceptions and identifying opportunities for the use of 'omics' in soil microbial ecology. *Nat. Rev. Microbiol.* 13, 439–446. doi: 10.1038/nrmicro3468

Raes, J., and Bork, P. (2008). Molecular eco-systems biology: towards an understanding of community function. *Nat. Rev. Microbiol.* 6, 693–699. doi: 10.1038/Nrmicro1935

Ranalli, A. J., and Macalady, D. L. (2010). The importance of the riparian zone and in-stream processes in nitrate attenuation in undisturbed and agricultural watersheds – a review of the scientific literature. *J. Hydrol.* 389, 406–415. doi: 10.1016/j.jhydrol.2010.05.045

R Core Team (2013). *R: A Language and Environment for Statistical Computing. Vienna, Austria. 2013.* Available at: http://www.R-project.org

Regnier, P., Dale, A. W., Arndt, S., Larowe, D. E., Mogollon, J., and Van Cappellen, P. (2011). Quantitative analysis of anaerobic oxidation of methane (AOM) in marine sediments: a modeling perspective. *Earth Sci. Rev.* 106, 105–130. doi: 10.1016/j.earscirev.2011.01.002

Riley, W. J., Subin, Z. M., Lawrence, D. M., Swenson, S. C., Torn, M. S., Meng, L., et al. (2011). Barriers to predicting changes in global terrestrial methane fluxes: analyses using CLM4Me, a methane biogeochemistry model integrated in CESM. *Biogeosciences* 8, 1925–1953. doi: 10.5194/bg-8-1925-2011

Rosenbaum, M., Aulenta, F., Villano, M., and Angenent, L. T. (2011a). Cathodes as electron donors for microbial metabolism: which extracellular electron transfer mechanisms are involved? *Bioresour. Technol.* 102, 324–333. doi: 10.1016/j.biortech.2010.07.008

Rosenbaum, M. A., Bar, H. Y., Beg, Q. K., Segre, D., Booth, J., Cotta, M. A., et al. (2011b). Shewanella oneidensis in a lactate-fed pure-culture and a glucose-fed co-culture with *Lactococcus lactis* with an electrode as electron acceptor. *Bioresour. Technol.* 102, 2623–2628. doi: 10.1016/j.biortech.2010.10.033

Rozendal, R. A., Hamelers, H. V., and Buisman, C. J. (2006). Effects of membrane cation transport on pH and microbial fuel cell performance. *Environ. Sci. Technol.* 40, 5206–5211. doi: 10.1021/es060387r

Rozendal, R. A., Leone, E., Keller, J., and Rabaey, K. (2009). Efficient hydrogen peroxide generation from organic matter in a bioelectrochemical system. *Electrochem. Commun.* 11, 1752–1755. doi: 10.1016/j.elecom.2009.07.008

Schmidt, M. W. I., Torn, M. S., Abiven, S., Dittmar, T., Guggenberger, G., Janssens, I. A., et al. (2011). Persistence of soil organic matter as an ecosystem property. *Nature* 478, 49–56. doi: 10.1038/nature10386

Strycharz, S. M., Gannon, S. M., Boles, A. R., Franks, A. E., Nevin, K. P., and Lovley, D. R. (2010). Reductive dechlorination of 2-chlorophenol by Anaeromyxobacter dehalogenans with an electrode serving as the electron donor. *Environ. Microbiol. Rep.* 2, 289–294. doi: 10.1111/j.1758-2229.2009.00118.x

Teh, Y. A., Dubinsky, E. A., Silver, W. L., and Carlson, C. M. (2008). Suppression of methanogenesis by dissimilatory Fe(III)-reducing bacteria in tropical rain forest soils: implications for ecosystem methane flux. *Glob. Chang. Biol.* 14, 413–422. doi: 10.1111/j.1365-2486.2007.01487.x

TerAvest, M. A., Li, Z. J., and Angenent, L. T. (2011). Bacteria-based biocomputing with Cellular Computing Circuits to sense, decide, signal, and act. *Energy Environ. Sci.* 4, 4907–4916. doi: 10.1039/C1ee02455h

Thompson, R. B. (1996). Using calcium carbide with the acetylene inhibition technique to measure denitrification from a sprinkler irrigated vegetable crop. *Plant Soil* 179, 9–16. doi: 10.1007/BF00011637

Tibshirani, R., Hastie, T., Narasimhan, B., and Chu, G. (2002). Diagnosis of multiple cancer types by shrunken centroids of gene expression. *Proc. Natl. Acad. Sci. U.S.A.* 99, 6567–6572. doi: 10.1073/pnas.082099299

Vidon, P., Allan, C., Burns, D., Duval, T. P., Gurwick, N., Inamdar, S., et al. (2010). Hot spots and hot moments in riparian zones: potential for improved water quality management1. *J. Am. Water Resour. Assoc.* 46, 278–298. doi: 10.1111/j.1752-1688.2010.00420.x

Vidon, P., and Hill, A. R. (2004). Denitrification and patterns of electron donors and acceptors in eight riparian zones with contrasting hydrogeology. *Biogeochemistry* 71, 259–283. doi: 10.1007/s10533-004-9684-1

Villano, M., Aulenta, F., Beccaru, M., and Majone, M. (2010). Microbial generation of H_2 or CH_4 coupled to wastewater treatment in bioelectrochemical systems. *Chem. Eng. Trans.* 20, 163–168.

Weber, K. A., Achenbach, L. A., and Coates, J. D. (2006). Microorganisms pumping iron: anaerobic microbial iron oxidation and reduction. *Nat. Rev. Microbiol.* 4, 752–764. doi: 10.1038/Nrmicro1490

Williams, K. H., Nevin, K. P., Franks, A., Englert, A., Long, P. E., and Lovley, D. R. (2010). Electrode-based approach for monitoring in situ microbial activity during subsurface bioremediation. *Environ. Sci. Technol.* 44, 47–54. doi: 10.1021/Es9017464

Wood, T. E., Cavaleri, M. A., and Reed, S. C. (2012). Tropical forest carbon balance in a warmer world: a critical review spanning microbial– to ecosystem-scale processes. *Biol. Rev.* 87, 912–927. doi: 10.1111/j.1469-185X.2012.00232.x

Zhang, T., Gannon, S. M., Nevin, K. P., Franks, A. E., and Lovley, D. R. (2010). Stimulating the anaerobic degradation of aromatic hydrocarbons in contaminated sediments by providing an electrode as the electron acceptor. *Environ. Microbiol.* 12, 1011–1020. doi: 10.1111/j.1462-2920.2009.02145.x

Simplifying microbial electrosynthesis reactor design

Cloelle G. S. Giddings[1], Kelly P. Nevin[2], Trevor Woodward[2], Derek R. Lovley[2] and Caitlyn S. Butler[1]*

[1] Department of Civil and Environmental Engineering, University of Massachusetts at Amherst, Amherst, MA, USA,
[2] Department of Microbiology, University of Massachusetts at Amherst, Amherst, MA, USA

Microbial electrosynthesis, an artificial form of photosynthesis, can efficiently convert carbon dioxide into organic commodities; however, this process has only previously been demonstrated in reactors that have features likely to be a barrier to scale-up. Therefore, the possibility of simplifying reactor design by both eliminating potentiostatic control of the cathode and removing the membrane separating the anode and cathode was investigated with biofilms of *Sporomusa ovata*. *S. ovata* reduces carbon dioxide to acetate and acts as the microbial catalyst for plain graphite stick cathodes as the electron donor. In traditional 'H-cell' reactors, where the anode and cathode chambers were separated with a proton-selective membrane, the rates and columbic efficiencies of microbial electrosynthesis remained high when electron delivery at the cathode was powered with a direct current power source rather than with a potentiostat-poised cathode utilized in previous studies. A membrane-less reactor with a direct-current power source with the cathode and anode positioned to avoid oxygen exposure at the cathode, retained high rates of acetate production as well as high columbic and energetic efficiencies. The finding that microbial electrosynthesis is feasible without a membrane separating the anode from the cathode, coupled with a direct current power source supplying the energy for electron delivery, is expected to greatly simplify future reactor design and lower construction costs.

Keywords: microbial electrosynthesis, bioelectrochemical system, *Sporomusa ovata*, renewable energy storage, artificial photosynthesis, CO_2 sequestration

Introduction

Microbial electrosynthesis shows promise as a strategy for the production of transportation fuels and other organic commodities from carbon dioxide with renewable electricity as the energy source (Leang et al., 2012; LaBelle et al., 2014; Rosenbaum and Henrich, 2014). In microbial electrosynthesis, microorganisms accept electrons from a cathode for the reduction of carbon dioxide to organic compounds that are excreted from the cell (Nevin et al., 2010, 2011; Lovley and Nevin, 2011, 2013; Marshall et al., 2013b; Rosenbaum and Henrich, 2014). When electrical energy is derived from solar technologies, microbial electrosynthesis is an artificial form of photosynthesis that has much higher potential energetic efficiencies and avoids many of the environmental and societal concerns associated with large-scale biomass cultivation and conversion to fuels (Nevin et al., 2011; Pant et al., 2011; Desloover et al., 2012; Lovley and Nevin, 2013).

One challenge for commercialization of microbial electrosynthesis is that pure cultures will likely be required in order to directly produce high-value fuels or other organic commodities.

Initiating microbial electrosynthesis with mixed cultures yields systems that produce primarily acetate (Marshall et al., 2012, 2013a,b) and likely can be attributed to the metabolism of acetogenic microorganisms. Pure culture studies have demonstrated that a diversity of acetogens can accept electrons from negatively poised electrodes for the reduction of carbon dioxide to acetate with high columbic efficiencies (Nevin et al., 2010, 2011). In order to produce higher value products via electrosynthesis, it will be necessary to genetically modify acetogens to divert carbon and electron flow to the generation of other products (Lovley and Nevin, 2013). The development of a genetic tool box for the acetogen *Clostridium ljungdahlii*, and the use of these tools to redirect carbon and electron flow, suggest that this necessary step in the development of commercially competitive microbial electrosynthesis can be met (Leang et al., 2012; Tremblay et al., 2013; Banerjee et al., 2014; Ueki et al., 2014).

Another major challenge is the design of a robust reactor for microbial electrosynthesis. To date, microbial electrosynthesis has relied on cathodes that have a potential that is carefully controlled with a potentiostat. Potentiostat control was employed in initial studies (Lovley and Nevin, 2013; Zhang et al., 2013) to maintain cathode potentials that would prevent production of H_2, and to avoid cathode potential fluctuations that might damage cells. Potentiostat control over large electrode systems is impractical because it is energy intensive to maintain a fixed potential and the potentiostat has limited control in large-scale systems (Rosenbaum et al., 2011).

Another concern is that the anode chamber and cathode chamber in previous microbial electrosynthesis reactors were separated with a membrane designed to permit ion flux between the chambers, while restricting oxygen diffusion. Oxygen produced at the anode and reaching the cathode will abiotically consume electrons, reducing reactor efficiency. Furthermore, the acetogenic microorganisms that serve as the catalysts for microbial electrosynthesis are among the most oxygen-sensitive of microorganisms. Finally, membranes add substantial cost, and designing large-scale reactors with two chambers separated by a membrane will be challenging.

The purpose of the study described here was to determine if microbial electrosynthesis reactors could be simplified by removing potentiostat control of the cathode and reconfiguring the anode and cathode to make it possible to avoid a separator membrane. The results suggest that microbial electrosynthesis reactors can be simplified in this manner while maintaining high energetic efficiencies.

Materials and Methods

Culturing Techniques in Microbial Electrosynthesis Reactors

The acetogen *Sporomusa ovata* was grown on electrons from an electrode in the cathode chamber of an H-cell reactor. Unmodified or control reactors contained graphite stick anodes and cathodes ($65\ cm^2$; Mersen, Greenville, MI, USA) suspended in two chambers, each containing 200 ml of modified DSMZ 311 defined growth medium (betaine, casitone, resazurin, and yeast extract omitted) media, that were separated with a Nafion 117 cation-exchange membrane (Electrolytica, Amherst, NY, USA), which had an effective working area of $6.25\ cm^2$. Reactor modifications are described below.

Sporomusa ovata for all experiments was initially grown in 50 mL of modified DSMZ 311 defined growth medium (yeast extract omitted) with hydrogen as the electron donor [H_2–CO_2 (80:20)] in 156 mL serum bottles, as described previously (Nevin et al., 2011). After the reactors were inoculated (40% v/v, unless otherwise stated; in same medium), the culture was bubbled with a gas mixture containing 7% hydrogen [N_2–CO_2–H_2 (80:13:7)] to help establish a biofilm on the cathode. Fifty percent of the medium was replaced once acetate concentrations were above 10 mM.

After three media-exchanges in each reactor configuration, the culture was switched to a different gas mixture [N_2–CO_2 (80:20)] that contained no hydrogen. After 2 days, the system was changed from a batch to flow-through process, where fresh medium was continuously added at 0.02 mL/min. A direct current power source provided a potential difference between the anode and cathode. Cathode potential, current, and total applied voltage was measured using a digital voltmeter. The total voltage applied was between 1.9 to 5 V, depending on the reactor system. Approximately 0.2 mL of liquid was regularly sampled for acetate measurement and the headspace of the reactors were sampled periodically to test for hydrogen production. All reactors were incubated at 25°C.

Reactor Schemes
Microbial Electrosynthesis Reactors

Unmodified reactors were run as controls to compare to the reactors studied with poised cathode potentials and were constructed as described in Section "Culturing Techniques in Microbial Electrosynthesis Reactors." Additionally, two H-cells were run with an increased applied voltage over the system to boost current density and to encourage acetate production (**Table 1**).

TABLE 1 | Summary of reactor designs and experimental program.

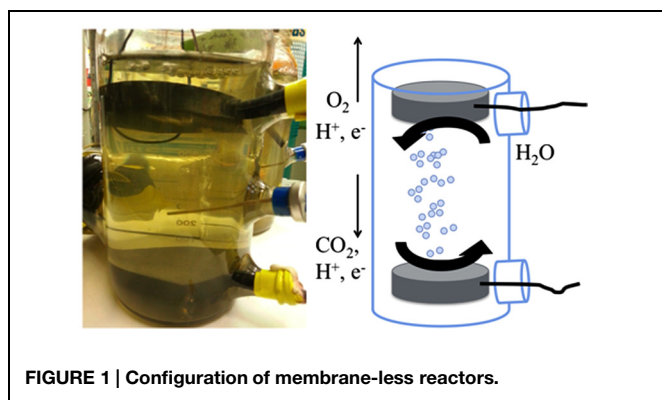| Configuration	Objective	Voltage delivered (V)	Cathode potential [V vs. standard hydrogen electrode (SHE)]
H-cells	H-cells poised at different cell potentials	3.0, 3.5, 5.0	−0.65, −0.71, −0.74
Abiotic	Measure hydrogen production in the absence of microbes	3.5	−0.79
Membrane-less	Decrease resistance of the reactors to increase energy efficiency	1.9 to 2.5	−0.70 to −0.81

FIGURE 1 | Configuration of membrane-less reactors.

Abiotic Reactors

Abiotic reactors were constructed identically to the unmodified H-cell reactors. A voltage was applied, and the working side of the reactor was sampled daily for hydrogen to explore hydrogen production in the absence of microorganisms (**Table 1**).

Membrane-Less Reactors

To decrease the internal resistance of our reactors, we constructed a reactor without a proton exchange membrane. The reactor was housed in a modified 1-L pyrex glass media bottle (Corning) that had three 20 mm serum ports (**Figure 1**). The cathode and anode were circular graphite disks, each with a surface area of 1.2×10^{-2} m^2 (diameter of 7.6 cm, height of 1.3 cm). A blunt-end cannula for gassing was placed between the electrodes to help keep oxygen generated at the anode from diffusing down to the cathode. Initially, the applied voltage to the reactor was 2.5 V, however, this was lowered over the course of the experiment to limit hydrogen production (**Table 1**). *S. ovata* culturing for the membrane-less reactors was as described above, but the initial inoculation level was lower ($\sim$15% v/v) as there was limited culture for these larger volume reactors because we maintained pure culture for inoculum in small volumes (50 mL). During operation, fresh media was supplied at a flow rate of 0.01 mL/min. An abiotic control of the membrane-less reactor was performed but a stable voltage could not be sustained and no acetate was produced.

Analytical Methods

Acetate was measured via high performance liquid chromatography (HPLC). Organic acids were separated on an Aminex NPX-87H column with 8 mM H_2SO_4 as the eluent and detected at 210 nm. Hydrogen was measured by running headspace samples on an Agilent 6890 gas chromatograph [Carbonex-1010 PLOT capillary column (Supelco); He carrier gas at 12 ml min^{-1} total flow; oven temperature 40°C; thermal-conductivity detector (TCD) temperature 225°C]. Aqueous phase hydrogen concentrations were assumed to be negligible due to stripping by the continuous gassing and because of the low solubility of H_2 gas. Cathode potentials were measured *in situ* vs. an Ag/AgCl reference electrode [+0.197 V vs. standard hydrogen electrode (SHE)]. All potentials have been adjusted and reported versus SHE.

Electron Recovery and Reactor Efficiency

The columbic efficiency (CE) was found by comparing the number of electrons appearing in acetate, based on Eq. 1, to electrons consumed as current (Eq. 2).

$$2CO_2 + 8e^- + 8H^+ + 2H_2O \rightarrow CH_3COOH + 2O_2 \quad (1)$$
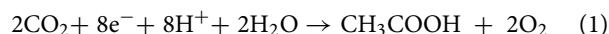
$$CE\,(\%) = \frac{n \mathrm{F} m_{acetate}}{\int_0^t I dt} \times 100\% \quad (2)$$

Where, n is the moles of electrons required to reduce carbon dioxide to one mole of acetate (i.e., eight electrons), F is Faraday's constant (96485 C mol^{-1}), m is the mass of acetate produced from t_0 to t. I is the current delivered to the reactor, which when integrated over time t_0 to t yields the total Coulombs transferred to the system to produce the measured acetate.

The reactor efficiency, η_{ME}, was found by comparing the energy content of the product (per mol of acetate) to the energy delivered to the reactor (Eq. 3),

$$\eta_{ME} = \frac{E_{out}}{E_{in}} \times 100\% = \frac{E_{acetate}}{E_{potential}} \times 100\% \quad (3)$$

where $E_{acetate}$ is the theoretical energy produced from acetate based on oxidation with oxygen as an electron acceptor (848 kJ mol^{-1}), and $E_{potential}$ is the sum of Gibb's energy of formation of acetate and the energy required to apply the voltage to the system based on microbial kinetic parameters which are assumed to be similar to hydrogen-oxidizing acetogenesis (Rittmann and McCarty, 2001), and varied depending on the voltage delivered. For example, at an applied voltage of 1 V, the total $E_{potential}$ is 991 kJ mol^{-1}.

Results and Discussion

Delivery of Electrons with a DC Power Source

Previous studies of electrosynthesis have poised the cathode at a fixed potential with a potentiostat. However, such a poised system would be difficult to control at a large scale. Therefore, the possibility of delivering electrons to the cathode with a DC power source was evaluated in 'H-cell' reactors similar to those used in previous studies with potentiostat-poised cathodes (Nevin et al., 2010, 2011).

The H-cell reactor required that a voltage of 3.0 V or higher be applied in order to maintain a stable cathode voltage. Applied voltages less than 3.0 V yielded a more positive cathode potential that was closer to the −0.4 V of previous studies (Nevin et al., 2010, 2011), but at applied voltages less than 3.0 V made it difficult to maintain a stable cathode potential.

With applied voltages of 3.0 or 3.5 V (1), *S. ovata* produced 0.45 and 0.54 mmoles of acetate per day, respectively (**Table 2**). These rates are nearly threefold higher than the rates previously

reported in the same reactors with the cathodes poised at -0.4 V with a potentiostat (Nevin et al., 2010, 2011). This improvement in performance may be attributed in part to the fact that the cathode potentials in the DC power source systems (**Table 2**) were lower than the -0.4 V potential of the potentiostat-poised system (Nevin et al., 2010).

In fact, the cathode potentials (-0.65 to -0.73 V) were theoretically low enough to produce H_2. However, no H_2 was detected during microbial electrosynthesis with *S. ovata* biofilms. In contrast, in abiotic controls at an applied voltage of 3.5 V, H_2 concentrations measured in the headspace ranged from 200 to 800 ppmv over the 2 weeks trial and the current density was only slightly less than the current density with *S. ovata* biofilms (**Figure 2**). Therefore, it is possible that *S. ovata* was using H_2 abiotically produced at the cathode as an electron donor rather than the direct cathode to microbe electron transfer that has been experimentally demonstrated in previous studies with *Geobacter* species (Gregory et al., 2004) and inferred in previous studies of microbial electrosynthesis with acetogenic bacteria (Nevin et al., 2010, 2011). However, the recovery of electrons consumed in acetate produced with the DC power source systems (**Table 2**) was comparable with the previously reported (Nevin et al., 2010) recovery of $86 \pm 21\%$ in the potentiostat-poised system with more positive cathode potentials. Therefore, even if H_2 was the ultimate electron donor for electrosynthesis in the DC power source systems, this was of little practical consequence as the *S. ovata* biofilms were highly effective in scavenging H_2 before it was lost to the gas stream passing through the reactor.

In order to determine if even higher applied voltages would be effective in yielding greater rates of acetate production, microbial electrosynthesis in an H-cell reactor with an applied voltage of 5.0 V was evaluated. As with the lower applied voltages, there was a steady production of acetate over time (**Figure 3**) with rates of acetate production that were approximately double those obtained with an applied voltage of 3.5 V (**Table 2**). Recovery of electrons consumed in acetate was slightly better than with the lower voltages, demonstrating effective cathode-to-microbe electron transfer whether or not H_2 was an intermediary electron carrier.

However, the reactor efficiency, which is the ratio of the energy delivered to the reactor to the energy content of the product (per mol of acetate), decreased as the applied voltage was increased (**Table 2**), reflecting the greater power requirement needed to run reactors at higher voltage. For example, the power to provide 5 V was almost three times higher than for the reactors at 3.0 V. Running reactors at higher voltage may be acceptable if there is an excess of electricity to be stored, such as with intermittent renewable energy sources. Otherwise, more conservative voltage schemes might be desirable.

Membrane-Less Reactor

In order to further simply microbial electrosynthesis reactor design, the possibility of designing a reactor without a membrane separating the anode and cathode was considered.

TABLE 2 | Performance of reactors varying voltage delivery.

Configuration*	Voltage delivered (V)	Current density (A/m²)	Power (mW)	Cathode potential (V vs. SHE)	Acetate production (mmole/day)	(mmole/day/m² cathode)	(g/kWh)	CE(%)	η_{ME} (%)
H-cell (1)	3.0	0.71 ± 0.06	13.8 ± 1.1	−0.65	0.45 ± 0.17	69 ± 26	81.4 ± 31.5	82 ± 19%	33%
H-cell (2)	3.5	0.87 ± 0.08	19.8 ± 1.8	−0.73	0.54 ± 0.08	83 ± 12	68.3 ± 11.9	83 ± 11%	29%
H-cell (3)	5.0	1.70 ± 0.19	55.2 ± 6.2	−0.74	1.07 ± 0.29	164 ± 45	48.5 ± 14.2	89 ± 12%	21%
Abiotic H-cell	3.5	0.77 ± 0.05	15.1 ± 3.3	−0.79	–	–	–	–	–
Membrane-less	1.9	0.17 ± 0.04	3.9 ± 0.6	−0.66	0.34 ± 0.05	28 ± 4	218.6 ± 64.3	105 ± 5%	50%
	2.2	0.25 ± 0.06	6.9 ± 1.9	−0.68	0.45 ± 0.02	38 ± 2	167.4 ± 37.1	79 ± 6%	44%
	2.5	0.46 ± 0.03	14.4 ± 0.7	−0.81	0.43 ± 0.14	36 ± 12	77.6 ± 25.6	54 ± 10%	39%

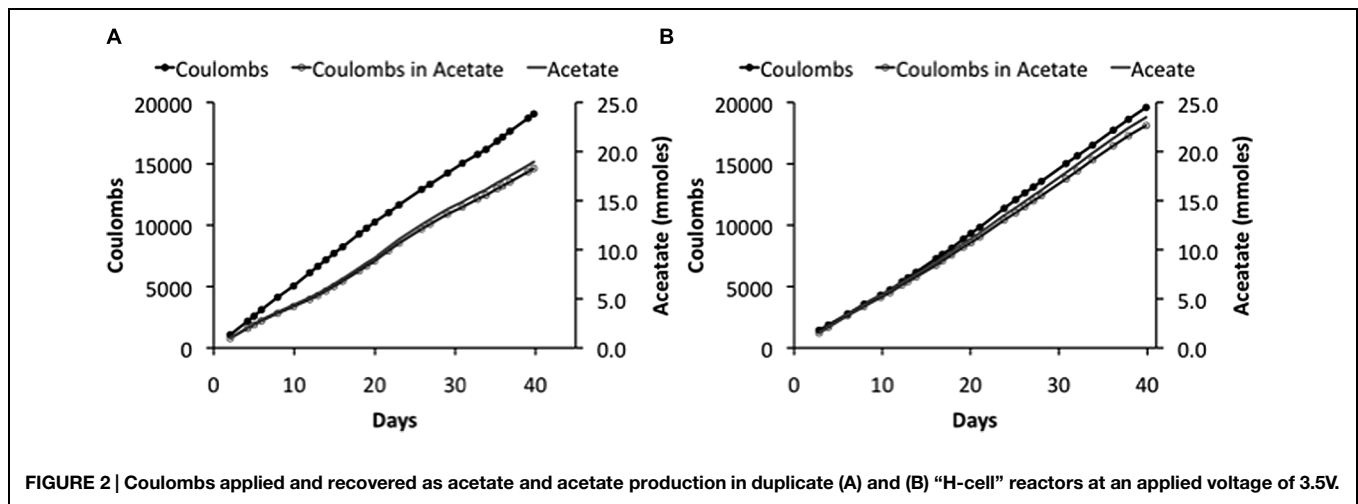*All reactors were run in duplicate.

FIGURE 2 | Coulombs applied and recovered as acetate and acetate production in duplicate (A) and (B) "H-cell" reactors at an applied voltage of 3.5V.
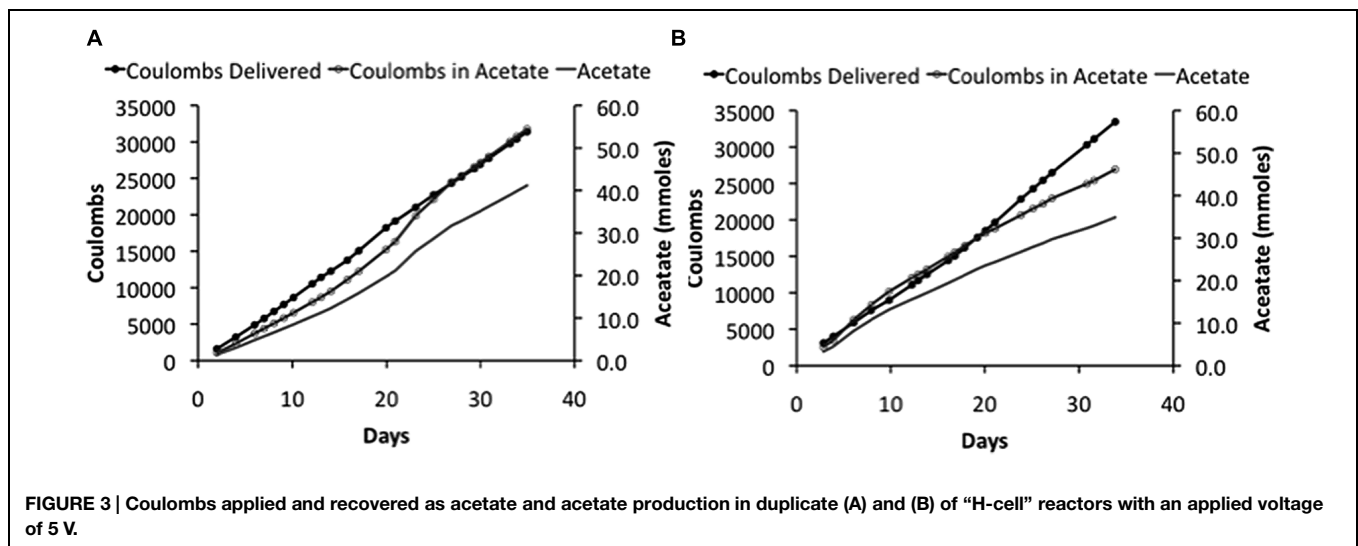

FIGURE 3 | Coulombs applied and recovered as acetate and acetate production in duplicate (A) and (B) of "H-cell" reactors with an applied voltage of 5 V.

The primary reason for including a membrane in previous microbial electrosynthesis reactor design was to prevent oxygen produced at the anode from coming into contact with the cathode biofilm of *S. ovata*, which is a strict anaerobe. In order to diminish the possibility of oxygen flux to the cathode, the anode was placed at the top of the reactor where the gas flushing through the reactor would remove oxygen produced, reducing downward flux of oxygen toward the cathode (**Figure 1**).

Sporomusa ovata thrived in the membrane-less reactor, steadily producing acetate over time (**Figure 4**). However, at the initial applied voltage of 2.5 V, 200–400 ppm H_2 was detected in the effluent gas, indicating that *S. ovata* was not effectively removing all of the H_2 produced at the cathode. This loss of H_2 resulted in a low recovery of electrons in acetate (~50%), which is unlikely to be cost effective. When the applied voltage was lowered to 2.2 V concentrations of H_2 were lower (around 150 ppm), but with a comparable acetate production rate, yielding a better electron recovery in acetate (**Table 2**). Further lowering the applied voltage to 1.9 V eliminated detectable H_2 and further
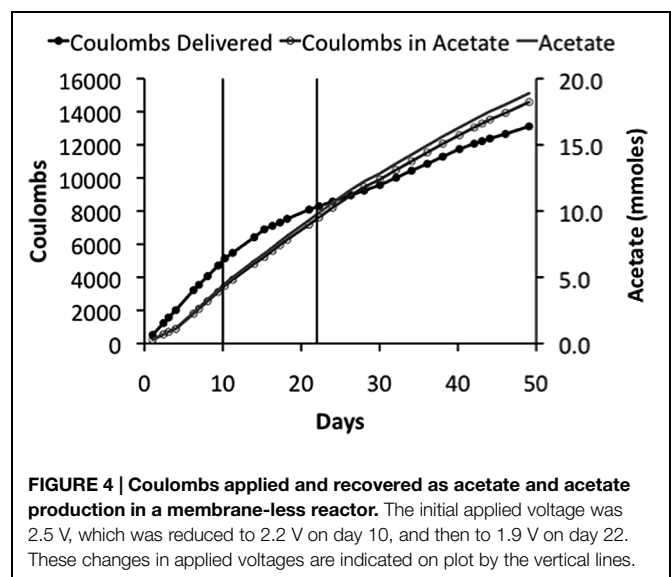

FIGURE 4 | Coulombs applied and recovered as acetate and acetate production in a membrane-less reactor. The initial applied voltage was 2.5 V, which was reduced to 2.2 V on day 10, and then to 1.9 V on day 22. These changes in applied voltages are indicated on plot by the vertical lines.

increased the efficiency of electron recovery in acetate (**Table 2**). Furthermore, this high CE was accomplished with a very good recovery of input energy in product (**Table 2**).

Implications

These results demonstrate that microbial electrosynthesis can be powered with DC power sources at high columbic efficiencies with good recovery of electrical energy supplied in organic product with a membrane-less reactor design. DC power sources are much simpler and inexpensive than poising cathodes with potentiostat-controlled systems, which are unlikely to function effectively with the large cathode surfaces that will be required in commercial-scale reactors. The ability to effectively shield microbial catalyst and the cathode from oxygen produced at the anode in the membrane-less system described here eliminates the substantial costs of effective membranes, and the technical difficulties of designing large reactors with membranes.

The simplification of microbial electrosynthesis with improved energetic efficiency with membrane-less reactors is expected to provide a foundation for the design of larger-scale reactors. Next-generation reactor designs should focus on maximizing cathode surface area with cathode materials optimized to support maximal rates of electrosynthesis (Zhang et al., 2013).

Acknowledgment

References

Banerjee, A., Leang, C., Ueki, T., Nevin, K. P., and Lovley, D. R. (2014). Lactose-inducible system for metabolic engineering of *Clostridium ljungdahlii*. *Appl. Environ. Microbiol.* 80, 2410–2416. doi: 10.1128/AEM.03666-13

Desloover, J., Arends, J. B. A., Hennebel, T., and Rabaey, K. (2012). Operational and technical considerations for microbial electrosynthesis. *Biochem. Soc. Trans.* 40, 1233–1238. doi: 10.1042/BST20120111

Gregory, K. B., Bond, D. R., and Lovley, D. R. (2004). Graphite electrodes as electron donors for anaerobic respiration. *Environ. Microbiol.* 6, 596–604. doi: 10.1111/j.1462-2920.2004.00593.x

LaBelle, E. V., Marshall, C. W., Gilbert, J. A., and May, H. D. (2014). Influence of acidic pH on hydrogen and acetate production by an electrosynthetic microbiome. *PLoS ONE* 9:e109935. doi: 10.1371/journal.pone.0109935

Leang, C., Ueki, T., Nevin, K. P., and Lovley, D. R. (2012). A genetic system for *Clostridium ljungdahlii*: a chassis for autotrophic production of biocommodities and a model homoacetogen. *Appl. Environ. Microbiol.* 79, 1102–1109. doi: 10.1128/aem.02891-12

Lovley, D. R., and Nevin, K. P. (2011). A shift in the current: new applications and concepts for microbe-electrode electron exchange. *Curr. Opin. Biotechnol.* 22, 441–448. doi: 10.1016/j.copbio.2011.01.009

Lovley, D. R., and Nevin, K. P. (2013). Electrobiocommodities: powering microbial production of fuels and commodity chemicals from carbon dioxide with electricity. *Curr. Opin. Biotechnol.* 24, 385–390. doi: 10.1016/j.copbio.2013.02.012

Marshall, C. W., LaBelle, E. V., and May, H. D. (2013a). Production of fuels and chemicals from waste by microbiomes. *Curr. Opin. Biotechnol.* 24, 391–397. doi: 10.1016/j.copbio.2013.03.016.

Marshall, C. W., Ross, D. E., Fichot, E. B., Norman, R. S., and May, H. D. (2013b). Long-term operation of microbial electrosynthesis systems improves acetate production by autotrophic microbiomes. *Environ. Sci. Technol.* 47, 6023–6029. doi: 10.1021/es400341b

Marshall, C. W., Ross, D. E., Fichot, E. B., Norman, R. S., and May, H. D. (2012). Electrosynthesis of commodity chemicals by an autotrophic microbial community. *Appl. Environ. Microbiol.* 78, 8412–8420. doi: 10.1128/aem.02401-12

Nevin, K. P., Hensley, S. A., Franks, A. E., Summers, Z. M., Ou, J., Woodard, T. L., et al. (2011). Electrosynthesis of organic compounds from carbon dioxide is catalyzed by a diversity of acetogenic microorganisms. *Appl. Environ. Microbiol.* 77, 2882–2886. doi: 10.1128/AEM.02642-10

Nevin, K. P., Woodard, T. L., Franks, A. E., Summers, Z. M., and Lovley, D. R. (2010). Microbial electrosynthesis: feeding microbes electricity to convert carbon dioxide and water to multicarbon extracellular organic compounds. *mBio* 1, e00103–e00110. doi: 10.1128/mBio.00103-10

Pant, D., Singh, A., Van Bogaert, G., Gallego, Y. A., Diels, L., and Vanbroekhoven, K. (2011). An introduction to the life cycle assessment (LCA) of bioelectrochemical systems (BES) for sustainable energy and product generation: relevance and key aspects. *Renew. Sust. Energ. Rev.* 15, 1305–1313. doi: 10.1016/j.rser.2010.10.005

Rittmann, B. E., and McCarty, P. (2001). *Environmental Biotechnology: Principles and Applications*. New York: McGraw-Hill.

Rosenbaum, M., Aulenta, F., Villano, M., and Angenent, L. T. (2011). Cathodes as electron donors for microbial metabolism: which extracellular electron transfer mechanisms are involved? *Bioresour. Technol.* 102, 324–333. doi: 10.1016/j.biortech.2010.07.008

Rosenbaum, M. E., and Henrich, A. W. (2014). Engineering microbial electrocatalysis for chemical and fuel production. *Curr. Opin. Biotechnol.* 29, 93–98. doi: 10.1016/j.copbio.2014.03.003

Tremblay, P.-L., Zhang, T., Dar, S. A., Leang, C., and Lovley, D. R. (2013). The Rnf complex of *Clostridium ljungdahlii* is a proton-translocating ferredoxin:NAD+ oxidoreductase essential for autotrophic growth. *mBio* 4, e00406–e00412. doi: 10.1128/mBio.00406-12

Ueki, T., Nevin, K. P., Woodard, T. L., and Lovley, D. R. (2014). Converting carbon dioxide to butyrate with an engineered strain of *Clostridium ljungdahlii*. *mBio* 5, e01636–e01614. doi: 10.1128/mBio.01636-14

Zhang, T., Nie, H., Bain, T. S., Lu, H., Cui, M., Snoeyenbos-West, O. L., et al. (2013). Improved cathode materials for microbial electrosynthesis. *Energy Environ. Sci.* 6, 217–224. doi: 10.1039/C2EE23350A

High rate copper and energy recovery in microbial fuel cells

Pau Rodenas Motos[1,2]*, Annemiek ter Heijne[2], Renata van der Weijden[1,2], Michel Saakes[1], Cees J. N. Buisman[1,2] and Tom H. J. A. Sleutels[1]

[1] Wetsus, European Centre of Excellence for Sustainable Water Technology, Leeuwarden, Netherlands, [2] Sub-department of Environmental Technology, Wageningen University, Wageningen, Netherlands

Bioelectrochemical systems (BESs) are a novel, promising technology for the recovery of metals. The prerequisite for upscaling from laboratory to industrial size is that high current and high power densities can be produced. In this study we report the recovery of copper from a copper sulfate stream (2 g L^{-1} Cu^{2+}) using a laboratory scale BES at high rate. To achieve this, we used a novel cell configuration to reduce the internal voltage losses of the system. At the anode, electroactive microorganisms produce electrons at the surface of an electrode, which generates a stable cell voltage of 485 mV when combined with a cathode where copper is reduced. In this system, a maximum current density of 23 A m^{-2} in combination with a power density of 5.5 W m^{-2} was produced. XRD analysis confirmed 99% purity in copper of copper deposited onto cathode surface. Analysis of voltage losses showed that at the highest current, most voltage losses occurred at the cathode, and membrane, while anode losses had the lowest contribution to the total voltage loss. These results encourage further development of BESs for bioelectrochemical metal recovery.

Keywords: microbial fuel cells, bioelectrochemical systems, metal recovery, copper

Introduction

Heavy metals pose a serious problem when they are released into the environment due to their toxicity for humans and its negative effect on biodiversity (Norgate and Rankin, 2002). Therefore, removal, and recovery of heavy metals, remediation of polluted sites, and decontamination of waste streams is needed in heavy metal and mining industries. Today, the conventional method to recover metals, such as copper, is by electrowinning, which uses electric power to electrochemically reduce dissolved metals to their metallic form. As metals are becoming more scarce and expensive (Watkins and McAleer, 2006; Geman and Smith, 2013), the revenues compensate for the electricity costs. However, considerable amounts of electrical energy are still required in electrolysis cells (2.23 kW h kg^{-1} of Copper; Vegliò et al., 2003). In comparison, bioelectrochemical systems (BESs) can provide the energy by the bioelectrochemical degradation of organic compounds present in waste waters, for instance, acetate (electron donor), at a so called bioanode. By coupling this bioanode to a metal reducing cathode, waste water treatment can be coupled to the recovery of heavy metals in a clean and sustainable way. When additional energy is harvested from these two reactions, the system is known as a microbial fuel cell (MFC). It is also possible to add extra electrical energy to drive and accelerate a reduction reaction at the cathode, in that case, the system is known as a microbial electrolysis cell (MEC) (Logan et al., 2008). The anode and the cathode compartment are generally separated by a membrane to simultaneously avoid mixing of the

electrolytes and in theory, these membranes allow ions to pass selectively, so charge neutrality is maintained.

ter Heijne et al. (2010) showed the proof of principle of this concept where they combined bioelectrochemical oxidation of acetate with the reduction of copper. In their system, electricity was produced while copper was removed and plated onto a solid electrode. A maximum current density of 3.2 A m^{-2} was achieved in a setup with a flat plate graphite electrodes and a bipolar membrane (BPM). Since then, other studies have reported MFCs in which copper was reduced at the cathode, reaching current densities ranging from 0.9 to 7 A m^{-2} with, for example, an increased surface area of the anode compared to the cathode (Modin et al., 2012; Zhang et al., 2012).

To make BESs practical and economically suitable to replace existing technologies, higher current densities are required. To reach high current densities, it is essential to reduce the voltage losses by reducing the internal resistance. Sleutels et al. (2012) analyzed the effect of the internal resistance on the practical applicability of BES. A resistance below 40 mΩ m^2 was considered acceptable for BES applications to achieve sufficiently high current and power densities to make BESs economic. Besides economic studies based on internal resistance, other attempts have been done to estimate feasibility of BESs using life-cycle assessment (LCA) analysis (Foley et al., 2010; Pant et al., 2011; Sleutels et al., 2012).

On the other hand, copper recovery is a highly valuable application for BES research. The recovery of valuable products allows for higher internal resistances compared to the recovery of energy alone (Sleutels et al., 2012). Copper recovery as a cathode reaction can potentially lead to high current densities due to its low overpotential. It is therefore, a suitable cathode reaction to demonstrate that MFCs can be operated at high current densities.

The main objective of this study was to increase the current and power density of a copper reducing MFC. Our approach was to reduce the internal resistance compared to previous studies by four changes: (i) decreasing the distance between electrodes, (ii) use an anion exchange membrane (AEM), (iii) use a copper plate as cathode, and (iv) use carbon felt as anode material.

First, the distance between anode and cathode was reduced from 3 to 0.5 cm (ter Heijne et al., 2010). Second, an AEM is known to have lower internal resistance than other membranes when applied in MEC (Rozendal et al., 2007; Sleutels et al., 2009a). As the BPM resulted in high energy losses; the internal resistance was expected to be reduced by using an AEM. Third, cathode material was changed from graphite paper to copper, which is a material conventionally used in copper electroplating. Fourth, anode material was replaced from graphite paper to carbon felt to achieve high specific surface area for electroactive biofilm growth. To make this anode material available for microbial activity, the solution was forced via a perpendicular flow through this felt as shown by Sleutels et al. (2009b, 2011).

We operated this new cell design at different current densities and analyzed its performance in terms of power production and voltage losses.
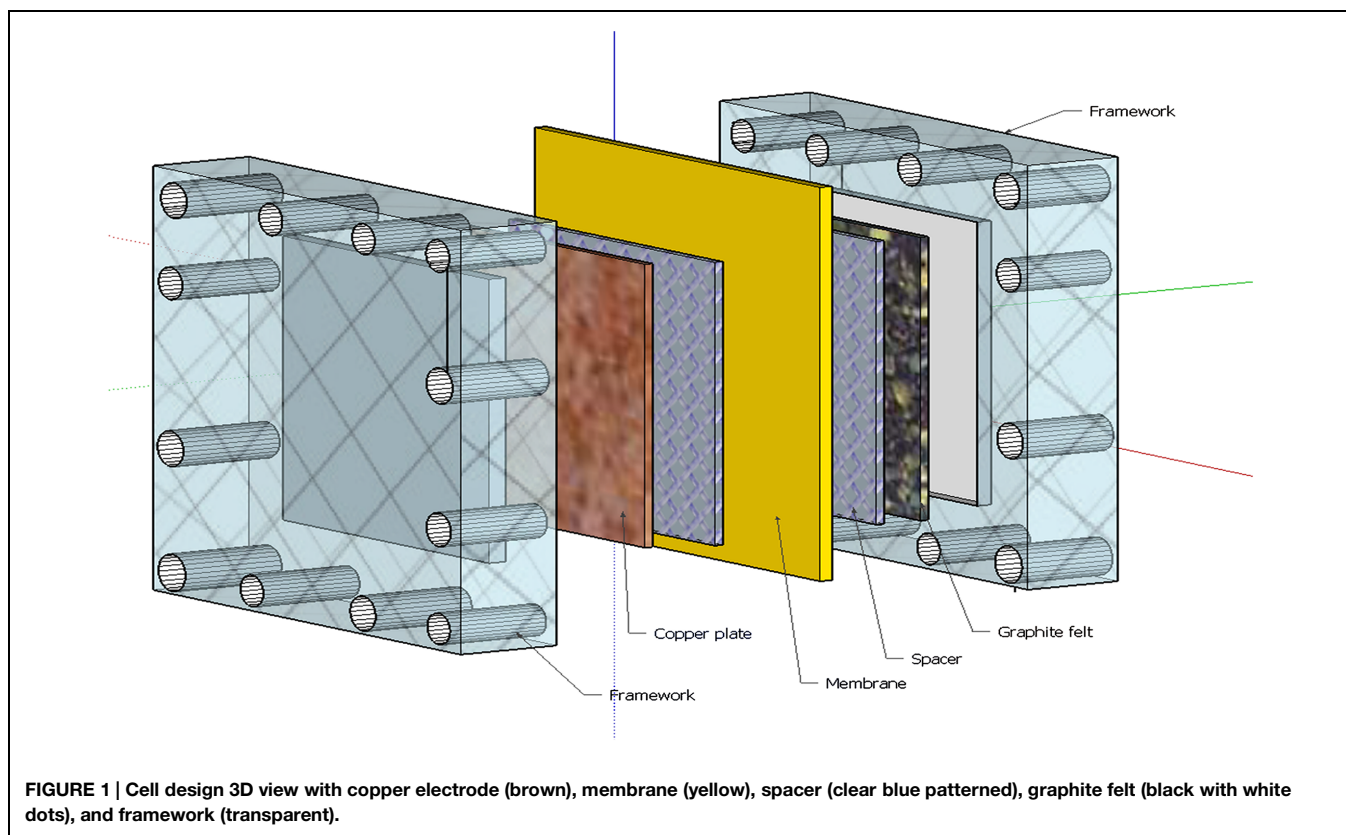
Materials and Methods

Research Set Up

The cell used in these experiments was similar to the one used by Kuntke et al. (2014). This cell was built using 10 cm × 10 cm metallic copper plates as cathode and 10 cm × 10 cm carbon felt of 1.5 mm thickness as anode. A Ralex®AEM (MEGA a.s., Stráž pod Ralskem, Czech Republic) was placed in between the anode and cathode compartment. To force the electrolyte to flow perpendicular through the electrodes, 1.2 mm spacer (64% open; PETEX 07-4000/64, Sefar BV, Goor, Netherlands) was placed between the membrane and the electrodes in both compartments (**Figure 1**). The anolyte was forced to flow toward the membrane through the electrode (Sleutels et al., 2011). The anode, cathode, spacer material, and membrane were kept in place by bolting them in between two PMMA endplates.

The anode compartment was controlled at 30°C via a water flow through the outer wall in the anode recirculation bottle. Only the cathode temperature was measured and it oscillated between 20 and 23°C. Nitrogen was flushed continuously through anolyte and catholyte to keep anaerobic conditions in anode and cathode compartments. Anode and cathode potentials were measured against Ag/AgCl 3 M reference electrode (ProSense, Oosterhout, Netherlands; 201 mV vs. Standard Hydrogen Electrode). Voltage losses across the membrane were measured as the voltage difference between the two reference electrodes placed in catholyte and anolyte. Cell voltage and potentials of cathode, anode, and membrane were continuously recorded together with pH and temperature in both compartments using a data logger (Endress+Hauser Messtechnik GmbH+Co., Rhein, Germany).

Start-Up and Operation

At the beginning of the experiment a 2 g L^{-1} Cu^{2+} solution was prepared dissolving CuSO$_4$ 5·H$_2$O as catholyte. The anode influent (2mL min^{-1}) consisted of synthetic waste water solution containing 20 mM acetate, phosphate buffer (10 mM, pH 7), nutrients, and vitamins as described in ter Heijne et al. (2008). The anode was fed with an excess of acetate to make sure the current production was not limited by substrate availability. Acetate was measured over time to ensure an excess of electron donor in the anode to produce current. Any competing processes at the anode for example methanogens were taken into consideration. Anolyte and catholyte had a constant recirculation rate of 200 ml min^{-1}. The total catholyte volume was 10 L. Cathode and anode pH were controlled at pH 3 and pH 7, respectively, with two dose pumps (STEPDOS 08, KNF, Germany) with 0.1 M H$_2$SO$_4$ and 0.1 M KOH. No supporting electrolyte was used. The conductivity of the solution was not measured during the experiment, only at the beginning of the experiment, and the values are 9.2 mS/cm for the catholyte and 6.2 mS/cm for the anolyte. The presence of an excess of acetate and sulfate (transported from the cathode) in the anolyte resulted in sulfate reduction (due to sulfate reducing bacteria; Hamilton, 1985) and consequently, in a consumption of protons. Hence, acid addition was required in the anode compartment. It should be noted that addition of chemicals to control the pH is not a sustainable solution for practical applications but it was used here

FIGURE 1 | Cell design 3D view with copper electrode (brown), membrane (yellow), spacer (clear blue patterned), graphite felt (black with white dots), and framework (transparent).

to be able to study the maximum performance of the system for copper removal. The cell started up at a constant resistance of 1 kΩ. The resistor was switched to a lower value (stepwise using 1 kΩ, 500 Ω, 250 Ω, and 100 Ω) after the anode potential had stabilized at a value of −450 mV vs Ag/AgCl. During this growing period of 2 weeks stable conditions were ensured using buffer solution as catholyte for oxygen reduction and measuring stable voltages over the entire cell. During the measurements that are reported in the results section below, the resistances were lowered sequentially from 1000 Ω to 0.5 Ω and catholyte was changed to copper sulfate solution. For each resistance steady state values over a period of 24 h were used to calculate the polarization curve.

Analyses

Copper concentration was measured using inductively coupled plasma optical emission spectrometry (ICP-OES) Perkin Elmer Optima 5300 (Perkin Elmer, Groningen, Netherlands). The consumed acetate during the experiment was tracked every 24 h measuring TOC (Total Organic Carbon) and IC (Inorganic Carbon) that was correlated with the concentration of acetate and bicarbonate using Shimadzu TOC-L CPH combustion TOC analyzer (Shimadzu Benelux, 's-Hertogenbosch, Netherlands). The gas composition in the headspace of the cells was also examined with a gas chromatograph [Varian Inc. (Part A) – CP-4900 Micro-GC].

The deposited copper on the electrode was scratched with a knife from the surface, weighed in a test tube and dissolved in 5 ml of 33% HNO_3. Then, 5 ml of Mili-Q water was added to dilute

the solution. Then the solution obtained was diluted 1000 times again and measured by ICP–OES Perkin Elmer Optima 5300 to determine the amount of copper plated on the electrode.

Calculation

The theoretical cell voltage (E_{emf} in V) can be calculated from the Gibbs free energy change of the overall reaction occurring at the cathode and anode, while the practical value can be directly measured at open cell conditions

$$E_{emf} = \frac{-\Delta G_r}{nF} \qquad (1)$$

Where, ΔG_r is the Gibbs free energy of the overall reaction (kJ mol^{-1}), n is the number of electrons transferred in the reaction, F is Faraday constant (96485 C mol^{-1}).

The contribution of the partial voltage losses to the total voltage loss inside the cell can be calculated according to

$$E_{CELL} = E_{emf} - \eta_{Cath} - \eta_{Anod} - \eta_{mem} \qquad (2)$$

Where E_{CELL} is the voltage measured during cell operation (V), η_{Cath} is the measured cathode overpotential (theoretical cathode potential-measured cathode potential; V), η_{Anod} is the measured anode overpotential (theoretical anode potential-measured anode potential; V), and η_{mem} is the voltage lost across the membrane (cathode ref potential-anode ref potential; V).

Results and Discussion

Current and Power Output

Figure 2 shows the current and power density generated over the entire experimental period. The arrows indicate the moment at which the value of the external resistance was lowered. The current density increased from 0.5 A m^{-2} at an external resistance of 100 Ω up to a stable value of 19 A m^{-2} at an external resistance of 1 Ω. The peak current density was 23 A m^{-2} and at this maximum current density, the peak power density was 5.5 W m^{-2}. When the resistor was further decreased to 0.5 Ω, the current density did not increase further, and the power output dropped from 4.0 to 2.0 W m^{-2}. **Figure 3** shows the polarization curve of the MFC, summarizing the whole experimental period, using the average values for cell voltage, current, and power density at each external resistor. The open circuit voltage (OCV) measured the first day was 485 mV, which is lower than the theoretical value of 575 mV.

During the whole period only 60% of the total amount of acetate was consumed by the biofilm, from this amount only the 26% was used to produce electricity. The detection of methane and sulfide in the head space of the recirculation bottle let us conclude that acetate was used for methane production and sulfate reduction by methanogens and sulfate reducers competing for the substrate with the electrogenic bacteria. The oxidation of acetate coupled to the reduction of sulfate by sulfate reducing bacteria was described by Muyzer and Stams (2008) via:

$$\text{Acetate}^- + \text{SO}_4^{2-} \rightarrow 2\text{HCO}_3^- + \text{HS}^- \qquad (3)$$

Analysis of the Performance

To analyze the reason for the drop in power production in more detail, we have analyzed the separate contributions of anode, cathode, and voltage losses across the membrane throughout the experimental period in line with a previous study from ter Heijne et al. (2006). **Figure 4** shows the relative contribution of the voltage losses for these three main components of the system: at every external resistance. The voltage loss over
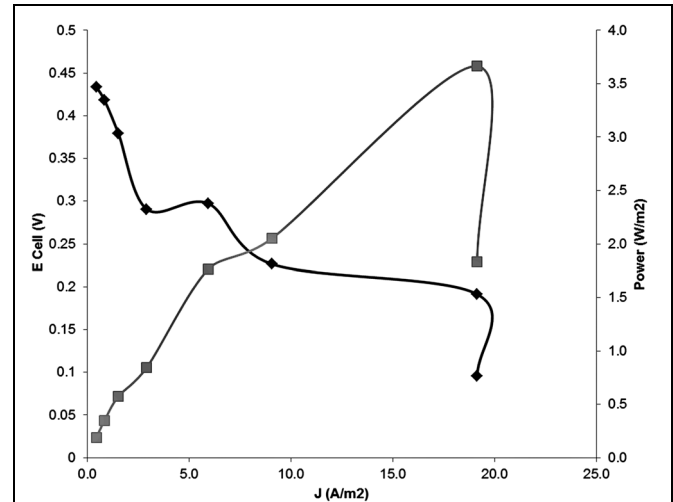
FIGURE 3 | Polarization curve of the copper reducing microbial fuel cell (MFC). The potential is represented vs. current density (black) and the power is shown versus current density (grey).
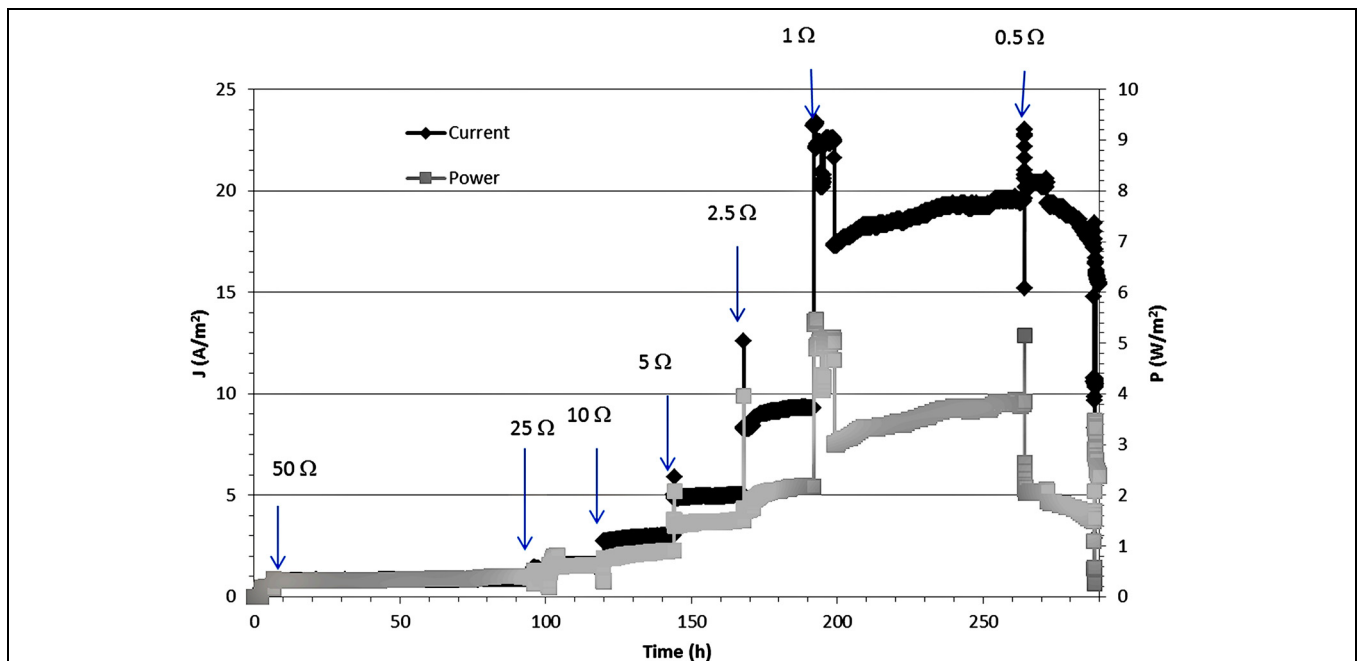
FIGURE 2 | Evolution of current density (black) and the power density (grey) shown vs. time during the entire range of the experiment. The arrows indicate when resistances were changed.
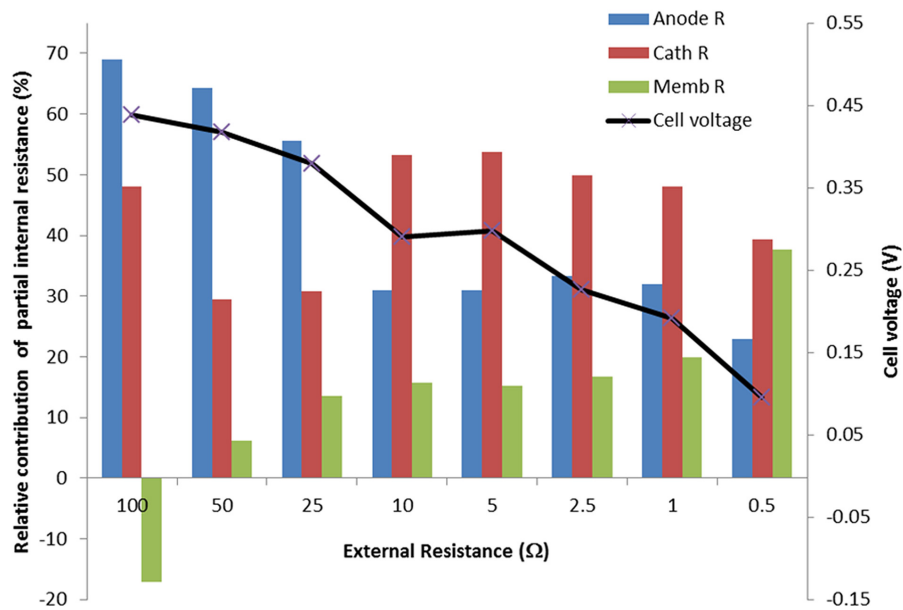
FIGURE 4 | Contribution of the cell components (anode, cathode, and membrane) to the total voltage loss in the system at different external resistors. Also the cell voltage is shown for each external resistor.

the membrane was measured using the reference electrode inserted in the anode and cathode compartment. Then, the ionic resistance of the electrolyte (anode and cathode) is measured as part of the membrane voltage loss. Note that **Figure 4** shows the contribution of the three components, the three of them summing up to 100%. This was done to illustrate the differences with time more clearly. Obviously, at a high external resistance the produced current was lowest while at a decreasing external resistor the produced current increased (**Figure 2**). So overall, the internal resistance of the system decreased with time.

With an increase in current density, the contribution of anode overpotential to the total voltage losses decreased considerably from 68 to 23%. We observed an increase in anode voltage from −450 to −400 mV vs Ag/AgCl for the first steps with high external resistances. However, when current reached its maximum values, the anode potential raised only to −350 mV vs Ag/AgCl. Apparently the biofilm was not affected by the high protons production rate that is associated with the current production. Instead an increase in the voltage loss over the membrane was observed. At increasing current densities voltage losses across the membrane increased from −50 mV on first day to 180 mV on ninth day. This value of −50 mV was result of the difference in chemical potential between anolyte and catholyte due to the difference in composition of these electrolytes. Sulfate was transported through the membrane from catholyte to anolyte. This chemical potential contributes positively to the cell potential. At the highest current reached, the dominant losses occurred at the cathode, approximately around 50% of total losses contribution between 10 Ω external resistance and 1 Ω external resistance. The increase in current density at

lower external resistance was also reflected in an increase of the cathode overpotential. Cathode potential went down from 50 mV during first day to −60 mV vs Ag/AgCl at the end of the experiment due to the decrease in Copper concentration.

An increase in the membrane voltage losses is likely at higher current densities since more ions need to be transported in the same time period. Additionally, the increase in membrane voltage losses can also be related to scaling. At the end of the experiment, when the cell was disassembled, precipitates were found in the catholyte and on the membrane surface. **Figures 5A,B** show the scanning electron microscope (SEM) image of scaling and biofouling in the cathode and in the anode side respectively on top of the membrane. Analysis of these structures with electron diffraction X-ray (EDX) shows the presence of copper, sulfur, and phosphor, which lead us to believe that the precipitates are copper sulfates, copper sulfides, and copper phosphates. Scaling is more likely to occur when divalent ions (like Copper and sulfate in this system) are present. Scaling is a serious issue that may limit the transport of ionic species from one compartment to the other, and thereby limiting performance of these systems. Prevention of this scaling is an important aspect of further study.

Performance Comparison to Previous Studies

To improve MFC performance the cell design was improved compared to previous study (ter Heijne et al., 2010) by modifying the electrode materials, the membrane, and the distance between electrodes and mass transport within the system. **Table 1** compares the performance of the MFC described in this study to other studies that used copper reduction as cathode reaction. Main differences between this and other studies are:
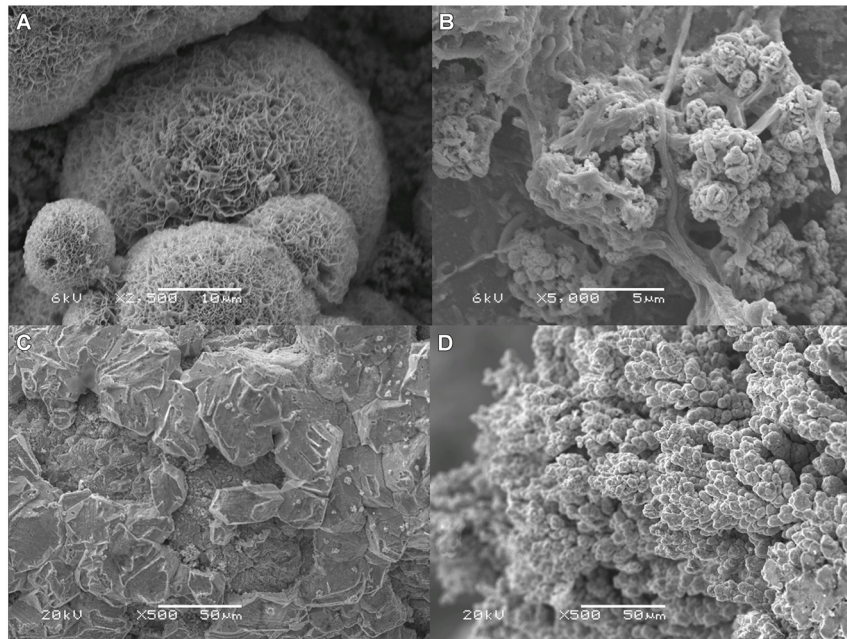
FIGURE 5 | (A) SEM image of crystalline scaling from cathode side on anion exchange membrane (AEM), **(B)** SEM image of biofilm on anode side of AEM. **(C)** SEM image of smooth copper deposited on flat copper surface **(D)** SEM image of the dendrites formed on cathode surface.

TABLE 1 | Microbial fuel cell (MFC) comparison between different authors and cathode configurations.

Anode material and surface area	Cathode material and surface area	Membrane used	Voc (V)	Jpeak (A m^{-2})	Pmax (W m^{-2})	Reference
Graphite felt of 100 cm^2	Copper plate of 100 cm^2	AEM	0.485	23.0	5.50	This study
Graphite paper of 20 cm^2	Graphite paper of 20 cm^2	BPM	0.600	3.20	0.80	ter Heijne et al. (2010)
Carbon fiber brush	Carbon rod of 4.7 cm^2	AEM	0.590	1.20	0.28	Cheng et al. (2013)
Graphite plate/graphite felt of 147 cm^2	Graphite plate of 27 cm^2	PEM	0.480	2.00*	0.24*	Tao et al. (2011)
2 × Graphite felt of 29.6 cm^2	Titanium Wire of 1.02 cm^2	AEM	–	7.00	–	Modin et al. (2012)
4 × Graphite felt of 22.5 cm^2	Graphite plate of 22.5 cm^2	AEM	0.550	0.90	0.20	Zhang et al. (2012)

The measurements of Tao et al. (2011) are expressed in A m^{-3} and W m^{-3} for current and power densities.

cell configuration, type of membrane, and different electrode materials. For example, all studies list in **Table 1** except Modin et al. (2012) and present study used carbon electrodes as cathode instead metal electrodes. The maximum current density in short circuit conditions produced by Modin et al. (2012) cell, was 7 A m^{-2} for 128 cm^2 of anode felt surface using a small cathode surface of 1 cm^{2,}, and using also an AEM. Even though, ter Heijne et al. (2010) achieved 3.2 A m^{-2} using graphite paper electrodes with a surface of 20 cm^2 and a BPM. Cheng et al. (2013) achieved 1.2 A m^{-2} using a carbon fiber brush anode and a carbon rod cathode. On the other hand, this study achieved a current density of 23 A m^{-2} for 100 cm^2 of anode graphite felt surface and 100 cm^2 copper cathode and using AEM.

Although previous studies reported considerable current densities, the power production was not always equivalent due to, either short circuit conditions or high internal resistance.

However, in this study the produced power density was 5.5 W m^{-2}, which is considerably higher than the reported before with power densities ranging between 0.2 and 0.8 W m^{-2}. This achievement is explained as a result of the low voltage losses of this MFC compared to other MFC configurations.

Copper Removal and Analysis of the Deposited Copper

Samples from catholyte were taken and analyzed five times per week. Interestingly, during the first 100 h, we found out a slight increase in copper concentration from 2.0 g/L to 2.2 g/L. In this time period, the current density was still low, below 1 A m^{-2}. Only when current density exceeds 1.0 A m^{-2}, copper concentration started to drop and showed a steady decrease to 0.2 g/L after 24 h. A reasonable explanation for the increase in copper concentration may be that

the copper electrode itself was oxidized to copper (II) under acidic conditions (pH 3). In order to check that copper oxidation occurs at acidic pH, a parallel experiment at open circuit in the same acidic conditions and copper concentration was performed. Here, a loss in weight of the electrode of 1.72 g of copper was observed after 24 h. This confirmed that the copper electrode can be oxidized under acidic conditions and explains the increase in copper concentration at low current densities (below 1 A m^{-2}). Finally, it is important to mention that no copper was detected in the anode during any of the experiments.

After 1 month of operation, the cell was disassembled and the copper layer on the cathode was analyzed for purity. **Figures 5C,D** show the SEM images of the copper deposited on top of the copper cathode. Copper exhibited dendritic formations, which are likely a result of the high current densities. These dendrites crossed the spacer and touched the membrane surface. This is a point of attention because these structures might damage the membrane. Analysis of the Copper electrode by nitric acid leaching showed that the composition of the deposited copper on the cathode has a copper purity of 99.4 ± 1.0% with 0.3% in zinc. XRD analysis confirmed the copper purity of the copper deposited onto the electrode.

Implications

High current density and power production were achieved in this improved cell design compared to the proof of principle by ter Heijne et al. (2010). The current was enhanced from 3.2 to 23 A m^{-2} while the power density increased from 0.8 to 5.5 W m^{-2}.

State of the art technologies like solvent extraction and electrowinning SX/EW consume 2.716 kWh Kg^{-1} of Cu (Alvarado, 2002). On the contrary, this study produced a constant power of 3.7 W m^{-2} equivalent to an energy production of 0.081 kWh Kg^{-1} of Cu. It should be mentioned that, the energy required to operate the system was not taken into account here. Also, 2.056 kg of acetate is required per kilogram of copper, which can be considered as a waste product.

The current density can be improved even further by supplying an external voltage to the system. Although the produced current and removed amount of copper will be higher, this would go at the expense of energy input.

Analysis of the voltage losses showed that anode was the main contribution to the voltage losses in the system at low current densities, but when currents were higher the cathode and the membrane started to limit the system. Consequently, the transport of ionic species through the system and membrane should be studied in more detail, as well as the scaling on the membrane surface related to the ion transport are an important aspect that needs attention in the future. However, to improve the bioanode performance further, many strategies have been considered for future research like Inhibition of methanogens and sulfate reducers to improve coulombic efficiency. Recently also some studies had improved the bioanode by improving electrode material by organic and inorganic coatings on top, that improves the amount of bacteria that can be attached onto the electrode (Zhang et al., 2011, 2015).

Several challenges remain to be solved before this technology becomes practically applicable. The use of a copper electrode, which is normally used in electro-winning, may pose difficulties in MFCs. Those difficulties are typically the slow reaction rates and the fact that copper actually dissolves. Further research on copper deposition at low current densities with other metallic electrodes, such as stainless steel or titanium, would give more insights on this system performance.

Acknowledgments

References

Alvarado, S. (2002). Long term energy-related environmental issues of copper production. *Energy* 27, 183–196. doi: 10.1016/S0360-5442(01)00067-6

Cheng, S.-A., Wang, B.-S., and Wang, Y.-H. (2013). Increasing efficiencies of microbial fuel cells for collaborative treatment of copper and organic wastewater by designing reactor and selecting operating parameters. *Bioresour. Technol.* 147, 332–337. doi: 10.1016/j.biortech.2013.08.040

Foley, J. M., Rozendal, R. A., Hertle, C. K., Lant, P. A., and Rabaey, K. (2010). *Life Cycle Assessment of High-Rate Anaerobic Treatment, Microbial Fuel Cells, and Microbial Electrolysis Cells.* Available at: http://pubs.acs.org.ezproxy.library.wur.nl/doi/full/10.1021/es100125h [accessed March 26, 2015].

Geman, H., and Smith, W. O. (2013). Theory of storage, inventory and volatility in the LME base metals. *Resour. Policy* 38, 18–28. doi: 10.1016/j.resourpol.2012.06.014

Hamilton, W. A. (1985). Sulphate-reducing bacteria and anaerobic corrosion. *Annu. Rev. Microbiol.* 39, 195–217. doi: 10.1146/annurev.mi.39.100185.001211

Kuntke, P., Sleutels, T., Saakes, M., and Buisman, C. J. N. (2014). Hydrogen production and ammonium recovery from urine by a Microbial Electrolysis Cell. *Int. J. Hydrogen Energy* 39, 4771–4778. doi: 10.1016/j.ijhydene.2013.10.089

Logan, B. E., Call, D., Cheng, S., Hamelers, H. V. M., Sleutels, T. H. J. A., Jeremiasse, A. W., et al. (2008). Microbial electrolysis cells for high yield hydrogen gas production from organic matter. *Environ. Sci. Technol.* 42, 8630–8640. doi: 10.1021/es801553z

Modin, O., Wang, X., Wu, X., Rauch, S., and Fedje, K. K. (2012). Bioelectrochemical recovery of Cu, Pb, Cd, and Zn from dilute solutions. *J. Hazard. Mater.* 235–236, 291–297. doi: 10.1016/j.jhazmat.2012.07.058

Muyzer, G., and Stams, A. J. M. (2008). The ecology and biotechnology of sulphate-reducing bacteria. *Nat. Rev. Microbiol.* 6, 441–454. doi: 10.1038/nrmicro1892

Norgate, T. E., and Rankin, W. J. (2002). *The Role of Metals in Sustainable Development,* 49–55. Available at: http://www.scopus.

com/inward/record.url?eid=2-s2.0-2342565850&partnerID=40&
md5=87a444cdfc05a408550a2a5b33804b

Pant, D., Singh, A., Van Bogaert, G., Gallego, Y. A., Diels, L., and
Vanbroekhoven, K. (2011). An introduction to the life cycle assessment
(LCA) of bioelectrochemical systems (BES) for sustainable energy and
product generation: relevance and key aspects. *Renew. Sustain. Energy Rev.* 15,
1305–1313. doi: 10.1016/j.rser.2010.10.005

Rozendal, R. A., Hamelers, H. V. M., Molenkamp, R. J., and Buisman,
C. J. N. (2007). Performance of single chamber biocatalyzed electrolysis with
different types of ion exchange membranes. *Water Res.* 41, 1984–1994. doi:
10.1016/j.watres.2007.01.019

Sleutels, T. H., Hamelers, H. V., and Buisman, C. J. (2011). Effect of
mass and charge transport speed and direction in porous anodes on
microbial electrolysis cell performance. *Bioresour. Technol.* 102, 399–403. doi:
10.1016/j.biortech.2010.06.018

Sleutels, T. H. J. A., Hamelers, H. V. M., Rozendal, R. A., and Buisman, C. J. N.
(2009a). Ion transport resistance in Microbial Electrolysis Cells with anion
and cation exchange membranes. *Int. J. Hydrogen Energy* 34, 3612–3620. doi:
10.1016/j.ijhydene.2009.03.004

Sleutels, T. H. J., Lodder, R., Hamelers, H. V. M., and Buisman, C. J. N. (2009b).
Improved performance of porous bio-anodes in microbial electrolysis cells by
enhancing mass and charge transport. *Int. J. Hydrogen Energy* 34, 9655–9661.
doi: 10.1016/j.ijhydene.2009.09.089

Sleutels, T. H. J. A., Ter Heijne, A., Buisman, C. J. N., and Hamelers, H. V. M.
(2012). Bioelectrochemical systems: an outlook for practical applications.
ChemSusChem 5, 1012–1019. doi: 10.1002/cssc.201100732

Tao, H. C., Liang, M., Li, W., Zhang, L. J., Ni, J. R., and Wu, W. M.
(2011). Removal of copper from aqueous solution by electrodeposition in
cathode chamber of microbial fuel cell. *J. Hazard. Mater.* 189, 186–192. doi:
10.1016/j.jhazmat.2011.02.018

ter Heijne, A., Hamelers, H. V. M., de Wilde, V., Rozendal, R. A., and Buisman,
C. J. N. (2006). A bipolar membrane combined with ferric iron reduction as
an efficient cathode system in microbial fuel cells. *Environ. Sci. Technol.* 40,
5200–5205. doi: 10.1021/es0608545

ter Heijne, A., Hamelers, H. V. M., Saakes, M., and Buisman, C. J. N. (2008).
Performance of non-porous graphite and titanium-based anodes in microbial

fuel cells. *Electrochim. Acta* 53, 5697–5703. doi: 10.1016/j.electacta.2008.
03.032

ter Heijne, A., Liu, F., Weijden, R. V., Weijma, J., Buisman, C. J., and Hamelers,
H. V. (2010). Copper recovery combined with electricity production in
a microbial fuel cell. *Environ. Sci. Technol.* 44, 4376–4381. doi: 10.1021/
es100526g

Vegliò, F., Quaresima, R., Fornari, P., and Ubaldini, S. (2003). Recovery
of valuable metals from electronic and galvanic industrial wastes by
leaching and electrowinning. *Waste Manag.* 23, 245–252. doi: 10.1016/S0956-
053X(02)00157-5

Watkins, C., and McAleer, M. J. (2006). Pricing of non-ferrous metals futures
on the London Metal Exchange. *Appl. Finan. Econ.* 16, 853–880. doi:
10.1080/09603100600756514

Zhang, C., Liang, P., Jiang, Y., and Huang, X. (2015). Enhanced power generation
of microbial fuel cell using manganese dioxide-coated anode in flow-through
mode. *J. Power Sources* 273, 580–583. doi: 10.1016/j.jpowsour.2014.09.129

Zhang, L. J., Tao, H. C., Wei, X. Y., Lei, T., Li, J. B., Wang, A. J., et al.
(2012). Bioelectrochemical recovery of ammonia-copper(II) complexes from
wastewater using a dual chamber microbial fuel cell. *Chemosphere* 89, 1177–
1182. doi: 10.1016/j.chemosphere.2012.08.011

Zhang, Y., Hu, Y., Li, S., Sun, J., and Hou, B. (2011). Manganese dioxide-
coated carbon nanotubes as an improved cathodic catalyst for oxygen
reduction in a microbial fuel cell. *J. Power Sources* 196, 9284–9289. doi:
10.1016/j.jpowsour.2011.07.069

The "Oil-Spill Snorkel": an innovative bioelectrochemical approach to accelerate hydrocarbons biodegradation in marine sediments

Carolina Cruz Viggi[1], Enrica Presta[1], Marco Bellagamba[1], Saulius Kaciulis[2], Santosh K. Balijepalli[2], Giulio Zanaroli[3], Marco Petrangeli Papini[4], Simona Rossetti[1] and Federico Aulenta[1]*

[1] Water Research Institute, National Research Council, Rome, Italy, [2] Institute for the Study of Nanostructured Materials, National Research Council, Rome, Italy, [3] Department of Civil, Chemical, Environmental and Materials Engineering, University of Bologna, Bologna, Italy, [4] Department of Chemistry, Sapienza University of Rome, Rome, Italy

This study presents the proof-of-concept of the "Oil-Spill Snorkel": a novel bioelectrochemical approach to stimulate the oxidative biodegradation of petroleum hydrocarbons in sediments. The "Oil-Spill Snorkel" consists of a single conductive material (the snorkel) positioned suitably to create an electrochemical connection between the anoxic zone (the contaminated sediment) and the oxic zone (the overlying O_2-containing water). The segment of the electrode buried within the sediment plays a role of anode, accepting electrons deriving from the oxidation of contaminants. Electrons flow through the snorkel up to the part exposed to the aerobic environment (the cathode), where they reduce oxygen to form water. Here we report the results of lab-scale microcosms setup with marine sediments and spiked with crude oil. Microcosms containing one or three graphite snorkels and controls (snorkel-free and autoclaved) were monitored for over 400 days. Collectively, the results of this study confirmed that the snorkels accelerate oxidative reactions taking place within the sediment, as documented by a significant 1.7-fold increase ($p = 0.023$, two-tailed t-test) in the cumulative oxygen uptake and 1.4-fold increase ($p = 0.040$) in the cumulative CO_2 evolution in the microcosms containing three snorkels compared to snorkel-free controls. Accordingly, the initial rate of total petroleum hydrocarbons (TPH) degradation was also substantially enhanced. Indeed, while after 200 days of incubation a negligible degradation of TPH was noticed in snorkel-free controls, a significant reduction of $12 \pm 1\%$ ($p = 0.004$) and $21 \pm 1\%$ ($p = 0.001$) was observed in microcosms containing one and three snorkels, respectively. Although, the "Oil-Spill Snorkel" potentially represents a groundbreaking alternative to more expensive remediation options, further research efforts are needed to clarify factors and conditions affecting the snorkel-driven biodegradation processes and to identify suitable configurations for field applications.

Keywords: anoxic marine sediments, bioelectrochemical systems, crude oil pollution, *in situ* bioremediation, Oil-Spill Snorkel

Introduction

Petroleum hydrocarbons are released into the marine environment both from natural seeps and from anthropogenic activities involved in the drilling, manufacturing, storing, and transporting of crude oil and oil products (Gong et al., 2014).

Application of oil dispersants has been a critical response measure to mitigate impacts of marine oil spill for decades (Prince, 2015). This approach makes the oil spill less visible by reducing the size of oil droplets, changing the oil surface physicochemical properties and increasing oil dispersion in the water column (Gong et al., 2014). Nevertheless, dispersants and dispersed oil under the ocean surface are hazardous for marine life (Kirby and Law, 2008). Particularly, once the dispersed oil reaches the sediments it tends to persist there for a very long time due to the prevailing anoxic conditions which drastically limit the occurrence of oxidative biodegradation processes. Both physical–chemical and biological treatment methods (i.e., bioremediation) have been proposed for the cleanup of oil polluted sediments, with the latter receiving a greater attention due to the lower costs, lower environmental impact, and wide applicability to a range of contamination scenarios (Fodelianakis et al., 2015). So far, a number of strategies have been proposed to enhance the *in situ* biodegradation of petroleum hydrocarbons, including the addition of nutrients, (bio)surfactants, electron acceptors and even oil-degrading bacteria (Nikolopoulou et al., 2013; Singh et al., 2014). The interplay between the (bio)availability of electron acceptors (e.g., oxygen, sulfate, nitrate) and hydrocarbons, as the electron donors and carbon sources for microorganisms, is certainly one of the most important factors influencing the performance of sediment bioremediation systems (Lu et al., 2014a).

Leading to faster rates of hydrocarbons activation and biodegradation, aerobic bioremediation is frequently preferred over its anaerobic counterpart. In this context, a number of engineered approaches have been proposed to effectively deliver oxygen to contaminated sediments. Among them, a modular slurry system which performs *in situ* aeration of the contaminated sediments, while minimizing the risk of spreading the contamination away from the treatment zone, has been recently developed (Genovese et al., 2014). Although the system turned out to be highly effective in stimulating the metabolism of aerobic hydrocarbon-degrading bacteria and in reducing sediment toxicity, its application is highly labor-, and energy-intensive. Other methods include the addition of oxygen-releasing compounds (e.g., calcium peroxide-based chemicals) to the contaminated sediment (Abdallah et al., 2009). However, the rapid abiotic oxygen consumption by reactions with reduced species (e.g., Fe^{2+}, S^{2-}) and the difficulties in controlling the rate of oxygen release over time make these approaches often poorly effective (Borden et al., 1997).

Recently, bioelectrochemical systems employing solid-state (graphite) electrodes as electron donors or acceptors have been proposed to stimulate biodegradation processes in subsurface environments (Aulenta et al., 2011a,b; Lovley, 2011; Lu et al., 2014b; Li and Yu, 2015). As an example, *Geobacter*
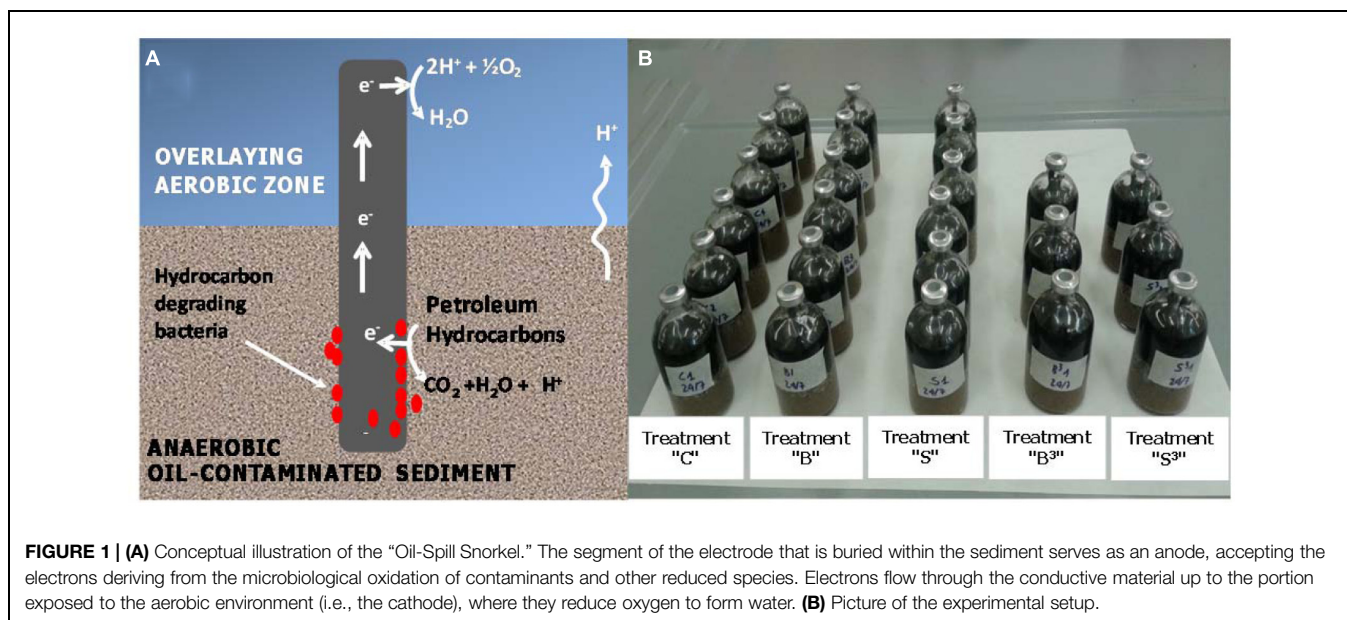
metallireducens was shown to be capable of oxidizing toluene with a graphite electrode (polarized at +500 mV vs. the standard hydrogen electrode with a potentiostat) serving as a direct electron acceptor (Zhang et al., 2010). Other recent studies have shown that lab-scale microbial fuel cells, typically using carbon-based anodes and catalyzed cathodes exposed to air, can be used to accelerate the biodegradation of oil hydrocarbons in contaminated soil and sediment (Morris and Jin, 2012; Lu et al., 2014a,b). In principle, the use of electrodes to stimulate the microbiological oxidation of hydrocarbons in subsurface environments is extremely appealing since they can potentially serve as permanent, low-cost, low maintenance source of electron acceptor capacity (Zhang et al., 2010).

The aim of this study is to present the proof-of-concept of a novel bioelectrochemical approach to accelerate hydrocarbons biodegradation in anoxic marine sediment. The system, hereafter named "Oil-Spill Snorkel" is based on the "Microbial Electrochemical Snorkel" (MES) concept originally developed for the treatment of urban wastewaters (MFCs; Erable et al., 2011). The "Oil-Spill Snorkel" consists of a single conductive material (i.e., an electrode) positioned so as to create an electrochemical connection between an anoxic zone (e.g., the contaminated sediment) and an oxic zone (i.e., the overlying O_2-containing water). The lower segment of the electrode, buried within the contaminated sediment, serves as the anode accepting the electrons deriving from the microbiological oxidation of contaminants and other reduced species. Electrons flow through the conductive material to the portion exposed to the aerobic environment (i.e., the cathode) where they reduce oxygen to form water (**Figure 1A**; Erable et al., 2011). In principle, this configuration virtually eliminates the electric resistances resulting from electrode separation in conventional microbial fuel cells and other engineered bioelectrochemical systems. Overall, the "Oil-Spill Snorkel" aims at providing bacteria within the sediment access to a high redox potential electron acceptor (oxygen) and by so doing accelerating oxidative biodegradation processes. To our knowledge, this is the first time that a MES is applied for bioremediation purposes and specifically for the treatment of marine sediments contaminated by petroleum hydrocarbons.

Materials and Methods

Experimental Setup

The hereafter described microcosm experiments were carried out using sandy marine sediments from Messina Harbour (Italy; Bargiela et al., 2015). The sediment was artificially contaminated in the laboratory with crude oil (Intermediate Fuel Oil, IFO 180). To this aim, the available sediment was firstly divided into four parts (i.e., quartering); one part was thoroughly mixed with oil that was pre-dissolved in hexane. Then, the hexane was evaporated through the air-drying of the sediment. Finally, the contaminated sediment was mixed, under nitrogen atmosphere, with the remaining three parts of the sediment. This procedure has been used in order to achieve a homogenous contamination

FIGURE 1 | (A) Conceptual illustration of the "Oil-Spill Snorkel." The segment of the electrode that is buried within the sediment serves as an anode, accepting the electrons deriving from the microbiological oxidation of contaminants and other reduced species. Electrons flow through the conductive material up to the portion exposed to the aerobic environment (i.e., the cathode), where they reduce oxygen to form water. **(B)** Picture of the experimental setup.

of the sediment while preserving a large fraction of the sediment microbial communities.

The so-prepared contaminated sediment was used to setup sacrificial microcosms in 120-mL serum bottles. Each bottle was filled (starting from the bottom) with 50 g of contaminated sediment, 40 g of clean sand, 10 g of Norit granular activated carbon (serving as oxygen reduction catalyst; Zhang et al., 2009, 2011; Watson et al., 2013), and 40 mL of oxygenated seawater from the site. Graphite rods, one or three depending on the treatment (7.5 cm length, 0.6 cm diameter, Sigma–Aldrich, Italy) were also inserted vertically through the layers of the different materials to create the electrochemical connection between the anoxic sediment and the oxygenated overlaying water (**Figures 1A,B**). Five different treatments were setup, namely: treatment "S³" which contained three graphite rods, treatment "S" which contained one graphite rod, treatment "C" (biotic control) which contained no graphite rods, treatment "B³" (autoclaved control) which contained three graphite rods and was autoclaved (120°C for 1 h) on three successive days and treatment "B" (autoclaved control) which contained one graphite rod and was also autoclaved (120°C for 1 h) on three successive days (**Figure 1B**).

Once prepared all the microcosms were statically incubated in the dark in a temperature-controlled room at 20 ± 1°C. Weekly, the headspace of the bottles was analyzed for oxygen consumption and carbon dioxide evolution by gas-chromatography (GC) with thermal conductivity detector (TCD), as described in the following "Analytical Methods" section. Every time the analyses indicated that oxygen concentration was below 5% (v/v), it was re-added by flushing the headspace with air. At fixed times, one bottle from each treatment was sacrificed: the sediment was analyzed (upon liquid–solid extraction) by GC and flame ionization detector (FID) for quantification of hydrocarbons; the liquid phase was analyzed by ion chromatography (IC)

for quantification of seawater anions. The abundance and composition of the biomass in the sediment and attached to the graphite rods was also analyzed by *in situ* hybridization techniques.

Analytical Methods

Concentration of oxygen and carbon dioxide in the headspace of the microcosms was analyzed by injecting 50 μL of gaseous samples, taken with a gastight syringe (Hamilton, Reno, NV, USA), into a Perkin–Elmer Auto System GC (stationary phase: stainless-steel column packed with molecular sieve (Supelco, USA); carrier gas: N_2 at 20 mL/min; oven temperature: 225°C; injector temperature: 200°C; thermal conductivity detector (TCD) temperature: 200°C).

The anions in the liquid phase were determined by injecting a filtered sample (0.22 μm porosity) into an IC (IonPac AS14 analytical column, Dionex DX-100 system, Dionex Corp., Sunnyvale, CA, USA).

Quantification of total petroleum hydrocarbons (TPH) in the sediment was performed by GC-FID, upon liquid–solid extraction. In brief, sediment samples (∼5 g) were air dried and extracted with a Dionex ASE 200 (Dionex Corp., Sunnyvale, CA, USA) using an acetone:hexane (1:1 v/v) mixture at 100°C and a system pressure of 1500 psi. The obtained extract was evaporated under nitrogen flow and then re-dissolved in 10 mL of an n-heptane solution containing n-dodecane (n-C_{12}) and n-tetracontane (n-C_{40}), each at 10 mg/L, as integration markers for the GC analysis. Subsequently, the heptane solution was purified using solid phase extraction cartridges filled with Florisil® and anhydrous sodium sulfate (Chromabond® Na_2SO_4/Florisil®, 6 mL polypropylene columns, 2g/2g) to remove polar components and non-petroleum compounds.

A sample (1 μL) of the purified solution was injected (in pulsed splitless mode) into a GC-FID (Perkin Elmer Clarus 480; column: HP-5 (Agilent) 30 m, ID 0.25 mm, d_f 0.25 μm; carrier

gas: helium at 20 psi; injector temperature: 270°C; detector temperature: 320°C; oven temperature program: initial 40°C, hold for 1 min, 10°C/min to 200°C, 20°C/min to 320°C, hold for 10 min).

The TPH amount was determined by summing up both the unresolved and resolved components eluted from the GC capillary column between the retention times of n-C_{12} and of n-C_{40}, using solutions of diesel motor oil and diesel mineral oil in hexane as calibration standards (concentration range 0.15–2 g/L).

Molecular Analysis of the Microbial Communities

Sediment samples and biofilms growing on the surface of the graphite rods (i.e., the snorkels) were taken for microbiological analysis. In brief, approximately 1 g of sediment was immediately fixed in formaldehyde (2% v/v final concentration) and processed to extract cells from sediment particles as elsewhere described (Barra Caracciolo et al., 2005). The detached cells were filtered through 0.2 μm polycarbonate filters (Ø 47 mm, Millipore) by gentle vacuum (<0.2 bar) and stored at –20°C until use. To fix the biomass from the biofilm formed at the graphite rods, the surface of the electrode was gently scraped with a sterile spatula. The detached biomass was initially collected in PBS buffer containing 2% v/v formaldehyde, and then filtered as described above.

Catalyzed Reporter Deposition-Fluorescence *In Situ* Hybridization (CARD-FISH) was carried out following previously published protocol (Fazi et al., 2008) using probes targeting *Bacteria* (EUB338 I,II,III), *Archaea* (ARCH915), *alphaproteobacteria* (ALF968), *betaproteobacteria* (BET42A), *gammaproteobacteria* (GAM42A), *deltaproteobacteria* (DELTA495a,b,c), *Firmicutes* (LGC354a,b,c), *Actinomycetes* (HGC69a), *Cytophaga/Bacteroidetes* (CF319), and *Chloroflexi* (GNSB941 and CFX1223).

Probes, labeled with horseradish peroxidase (HRP), were purchased from BIOMERS[1]. Probe details and conditions are reported in probeBase[2]. DAPI (4′,6-diamidino-2-phenylindole) staining was performed for determining total cell numbers, from which the relative abundances of each targeted bacterial population was calculated. Total cells count was performed at the end of the hybridization assay by using Vectashield Mounting Medium with DAPI (Vector Labs, Italy). At least 20 randomly selected microscopic fields for each sample were analyzed to enumerate the cells by microscopic analysis. Slides were examined by epifluorescence microscopy (Olympus, BX51) and the images were captured with Olympus F-View CCD camera and handled with Cell^F software (Olympus, Germany).

X-Ray Photoelectron Spectroscopy of Graphite Electrodes

The surface chemical composition of the graphite rods was determined by using the X-ray photoelectron spectroscopy (XPS). XPS measurements were performed in an Escalab 250Xi spectrometer (Thermo Fisher Scientific, UK) equipped with a monochromatic Al Kα source and a 6-channeltron detection

system. The photoemission spectra were collected at the base pressure of 5×10^{-8} Pa, by using 40 eV pass energy of the analyzer and standard electromagnetic lens mode with about 1 mm diameter of analyzed area. Spectroscopic data were processed by the Avantage v.5 software. Shirley background and mixed Lorentzian/Gaussian peak shape (30%) with linked peak widths were used for the peak fitting.

Results

Oxygen Consumption and Carbon Dioxide Evolution

The working hypothesis of the "Oil-Spill Snorkel" is that the graphite electrode (i.e., the snorkel) creates an electrochemical connection between the anoxic sediment and the overlying aerobic seawater and, by so doing, provides sediment microorganisms with the opportunity to "respire" a spatially distant electron acceptor (i.e., oxygen).

To verify this exciting hypothesis, oxygen consumption and carbon dioxide evolution were monitored, via headspace analysis of the different microcosms, throughout the whole experimental period (**Figure 2**). Live microcosms containing one (treatment "S") and three (treatment "S³") graphite rods displayed a higher cumulative oxygen consumption compared to the corresponding (live) control microcosms (treatment "C") lacking the graphite rod(s) (i.e., 61.2 ± 1.0 mL and 88.3 ± 4.3 mL, respectively, versus 50.6 ± 4.0 mL). However, a statistical analysis (two-tailed *t*-test) indicated that only treatment "S³" was statistically different ($p = 0.023$) from treatment "C."

Collectively, these findings indicate that the presence of the graphite electrode(s) within the sediment enhance oxygen uptake from the headspace of the microcosms. Since the graphite rods do not alter the physical–chemical properties of the water–sediment interface and therefore are not expected to modify the rate of oxygen transport from the headspace to the sediment, the observed enhancement of oxygen consumption was likely driven by the electrons released to the graphite rods (from the oxidation of reduced organic and inorganic species in the sediment) which reacted with oxygen forming water as a byproduct.

Unexpectedly, a substantial respiratory activity was observed also in autoclaved controls (treatments "B" and "B³"; **Figure 2A**), suggesting the occurrence of non-biological (abiotic) oxidation reactions in the sediment driven by the graphite rod(s) and/or the presence of microorganisms resistant to thermal treatment.

In all incubations, the rate of oxygen consumption (i.e., the slope of the oxygen consumption curve) steadily decreased over time possibly suggesting a gradual loss of biological and/or electrochemical activity of the systems under consideration.

Figure 2B shows the cumulative production of carbon dioxide in the different microcosms. In agreement with oxygen consumption data, at the end of the incubation the highest CO_2 production was observed in the treatment "S³" (1.4-fold higher than in treatment "C," $p = 0.04$ based on two-tailed *t*-test), whereas a lower (and statistically indistinguishable, $p = 0.49$) production was observed in treatments "S" and "C" (**Figure 2B**). Notably, a substantial CO_2 production was also

FIGURE 2 | Cumulative oxygen consumption (A) and carbon dioxide evolution (B) in the different treatments. Error bars represent the SE of replicate incubations.
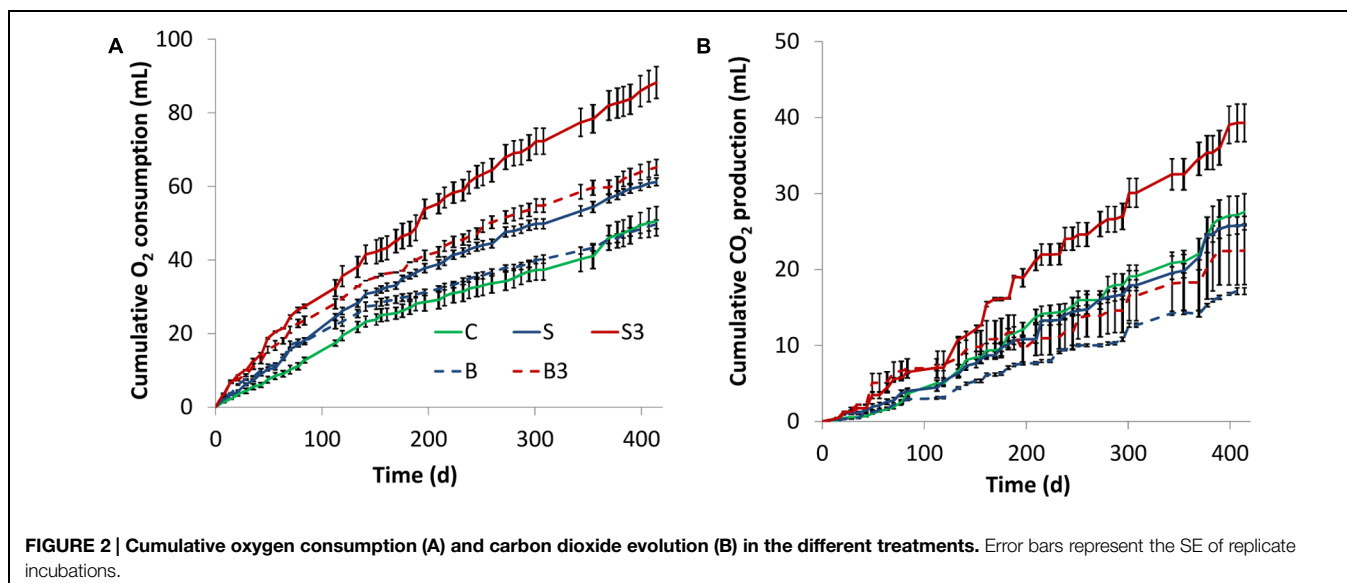
observed in autoclaved treatments (i.e., "B[3]," "B"), hence proving an additional line of evidence of the inefficiency of the thermal treatment for microcosm sterilization. Finally, throughout the incubation negligible methane formation was observed in all treatments.
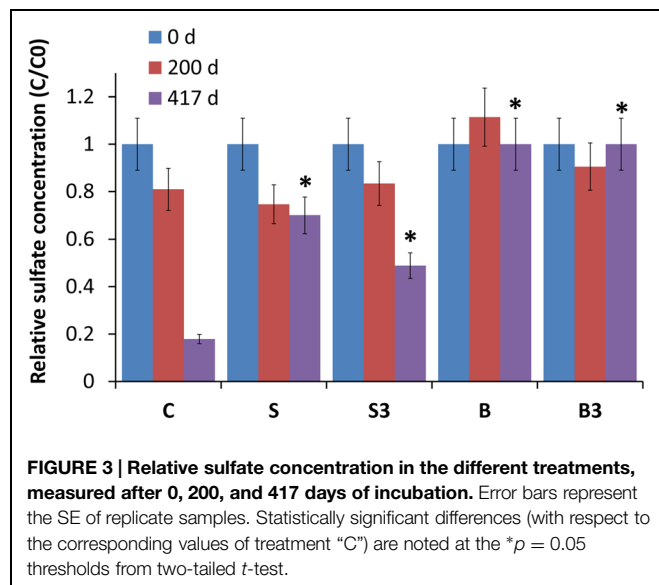
Sulfate Consumption

At fixed times (i.e., day 0; day 200; day 417), one bottle from each treatment was sacrificed and the liquid phase was analyzed by IC for determination of seawater anions, with main attention being paid at sulfate which is a key respiratory electron acceptor in marine environments.

Analyses revealed the occurrence of sulfate reduction in all the biotic treatments ("C," "S[3]," "S"), but not in the autoclaved ones ("B" and "B[3]"; **Figure 3**). Notably, sulfate reduction in treatment "C" was substantially higher ($p < 0.05$; two-tailed t-test) than in the "snorkels," with $82 \pm 9\%$ of sulfate removal in 417 days compared with 51 ± 6 and $30 \pm 3\%$ of sulfate removal in treatment "S[3]" and treatment "S," respectively. On day 417, the observed difference between treatment "S" and treatment "S[3]" was found to be not statistically significant ($p = 0.16$, two-tailed t-test).

Total Petroleum Hydrocarbons (TPH) Degradation

On day 0, 200, and 417, the different treatments were also analyzed to determine (by GC-FID following accelerated solvent extraction with an acetone:hexane mixture) the concentration of TPH in the sediments. The initial (day 0) concentration of TPH in the different microcosms was the following (in mg/g of dry sediment): treatment "C" = 12.3 ± 0.20; treatment "S" = 11.8 ± 1.01; treatment "S[3]" = 11.9 ± 0.12; treatment "B" = 12.1 ± 0.14; treatment "B[3]" = 11.3 ± 0.11.
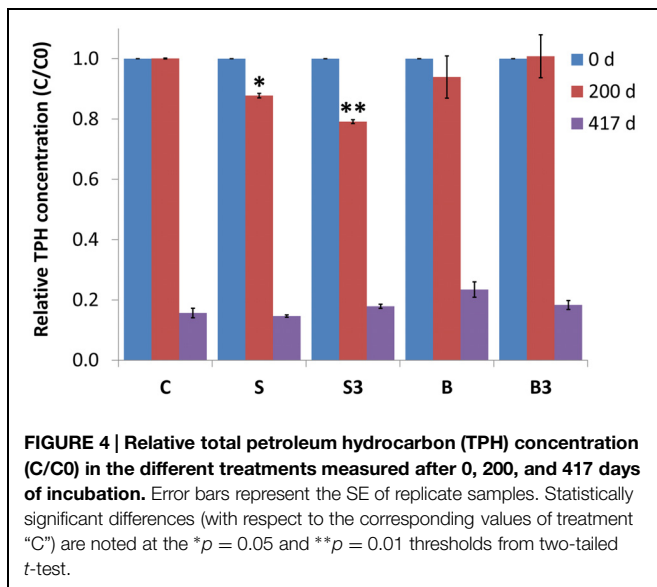
After 200 days of incubation, while a negligible degradation of TPH was noticed in snorkel-free biotic and autoclaved controls, a significant reduction of $12 \pm 1\%$ ($p = 0.004$) and $21 \pm 1\%$

FIGURE 3 | Relative sulfate concentration in the different treatments, measured after 0, 200, and 417 days of incubation. Error bars represent the SE of replicate samples. Statistically significant differences (with respect to the corresponding values of treatment "C") are noted at the *$p = 0.05$ thresholds from two-tailed t-test.

($p = 0.001$) was observed in microcosms containing one and three snorkels, respectively (**Figure 4**). This important finding provides a straightforward confirmation of the effectiveness of the proposed approach to accelerate hydrocarbons biodegradation in contaminated sediments.

Following a more prolonged incubation (day 417), an extensive degradation of TPH occurred in all treatments, including the autoclaved controls (i.e., treatment "B" and "B[3]"), with removals exceeding 80% in most treatments (**Figure 4**). In correspondence to this last sampling time, the beneficial effect of the "snorkels" was no longer evident (**Figure 4**).

Most probably, over time the rate of microbiological reactions taking place in the bulk of the sediment, driven by sulfate and/or the oxygen steadily dissolving from the headspace of the bottles, exceeded the rate of electrode-driven reactions. This was likely

FIGURE 4 | Relative total petroleum hydrocarbon (TPH) concentration (C/C0) in the different treatments measured after 0, 200, and 417 days of incubation. Error bars represent the SE of replicate samples. Statistically significant differences (with respect to the corresponding values of treatment "C") are noted at the *p* = 0.05 and **p* = 0.01 thresholds from two-tailed *t*-test.

due to a number of factors such as the relatively low surface area of electrodes compared to the amount of sediment used and the batchwise type of incubation which limited the possibility to consistently maintain a spatial separation between the oxic and the anoxic zones. On the other hand, it cannot be excluded that the rate of electrodic reactions also decreased over time due to a gradual passivation of the electrodic surfaces induced by deposition of non-conductive minerals such as sulfides.

Microbiological Characterization by CARD-FISH

A whole-cell detection method was applied for the characterization of the microbial communities growing in the sediment and at the surface of the graphite rods (i.e., "the snorkels") in the different microcosms. As shown in **Figure 5A**, near the totality of the microbial population in the sediment was composed of Bacteria, with a ratio Bacteria/total DAPI stained cells ranging between 83 and 99%. The abundance of total microbial cells and Bacteria in the sediment samples from the live control (treatment "C") and from the microcosms containing the "snorkel(s)" (treatment "S" and "S3") increased over time, ultimately reaching a similar value of around 5×10^7 cells per gram of sediment at the end of the incubation (i.e., day 417; **Figure 5A**). A statistically relevant difference among the treatments was observed on day 200 whereby the concentration of total cells in the microcosms containing the snorkel(s) was higher than in the corresponding control ($4.4 \pm 0.4 \times 10^7$ and $4.5 \pm 0.4 \times 10^7$ cells per gram of sediment in treatment "S" and "S3," respectively, versus $3.1 \pm 0.3 \times 10^7$ cells per gram of sediment in treatment "C"; $p < 0.001$ for both "S" and "S3" treatments, two-tailed *t*-test; **Figure 5A**).

In accordance with oxygen consumption, CO_2 evolution, and TPH degradation data, an increase in total cells and Bacteria was observed also in the autoclaved controls (treatment "B" and "B3") confirming the occurrence of growth of microorganisms resistant to the thermal sterilization treatment. However, the total cell

concentration was substantially lower than in the non-autoclaved treatments ($p < 0.001$, two-tailed *t*-test; **Figure 5A**). This finding is in line with previous studies which showed microbial activity in sediment samples also after several serial sterilization treatments (O'Sullivan et al., 2015). Consistent with the lack of methanogenic activity in the microcosms, no archaeal cells were detected by CARD-FISH.
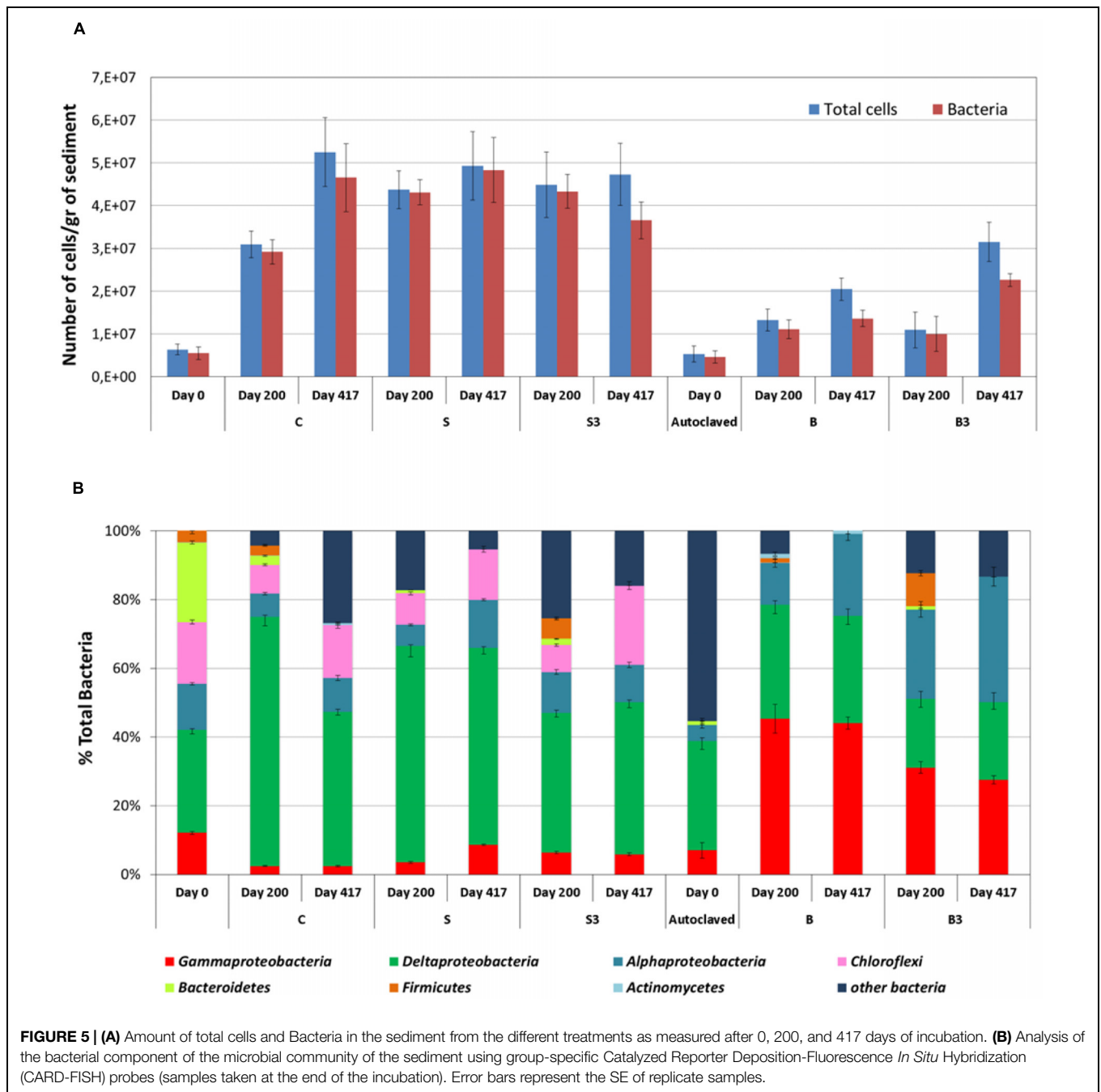
The structure of the sediment biomass was further detailed by using group specific probes (**Figure 5B**). *Deltaproteobacteria* were the main component in the live microcosms ("C," "S," and "S3"), accounting from 44 to 57% of total Bacteria at the end of the incubation (**Figure 5B**). Since many sulfate-reducing bacteria (SRB) are affiliated to *deltaproteobacteria*, this finding is consistent with the occurrence of active sulfate reduction in the live microcosms. SRBs include a variety of different families like *Desulfovibrionaceae, Desulfobacteriaceae,* and *Syntrophobacteraceae* often found responsible of oil degradation in contaminated sediments (Miyatake et al., 2009; Sherry et al., 2013; Cravo-Laureau and Duran, 2014; Genovese et al., 2014).

Differently from live microcosms, *gammaproteobacteria* (up to 45.3% of total bacteria) and *alphaproteobacteria* (up to 53%) were the main bacterial components in the autoclaved treatments "B" and "B3." Several aerobic marine hydrocarbon-degrading bacteria, affiliated to *gammaproteobacteria* have been described in the literature (Yakimov et al., 2007). Accordingly, the extensive TPH degradation observed in autoclaved treatments (at least after 417 days of incubation) can probably be attributed to these microorganisms, which likely used the oxygen slowing diffusing into the sediment from the headspace of the microcosms.

Deltaproteobacteria were the main bacterial component soon after the autoclaving together with a large portion of bacteria not identified with the group specific probes applied in this study. Autoclave-surviving SRB were recently described in sediment slurries due to the widespread occurrence of bacterial spores in marine sediment (O'Sullivan et al., 2015). The thermal treatment negatively impacted on the survival of some of the groups originally present in the untreated sediment (t0) such as *Chloroflexi* and *Bacteroidetes* which almost disappeared in the sediment after autoclaving (**Figure 5B**).
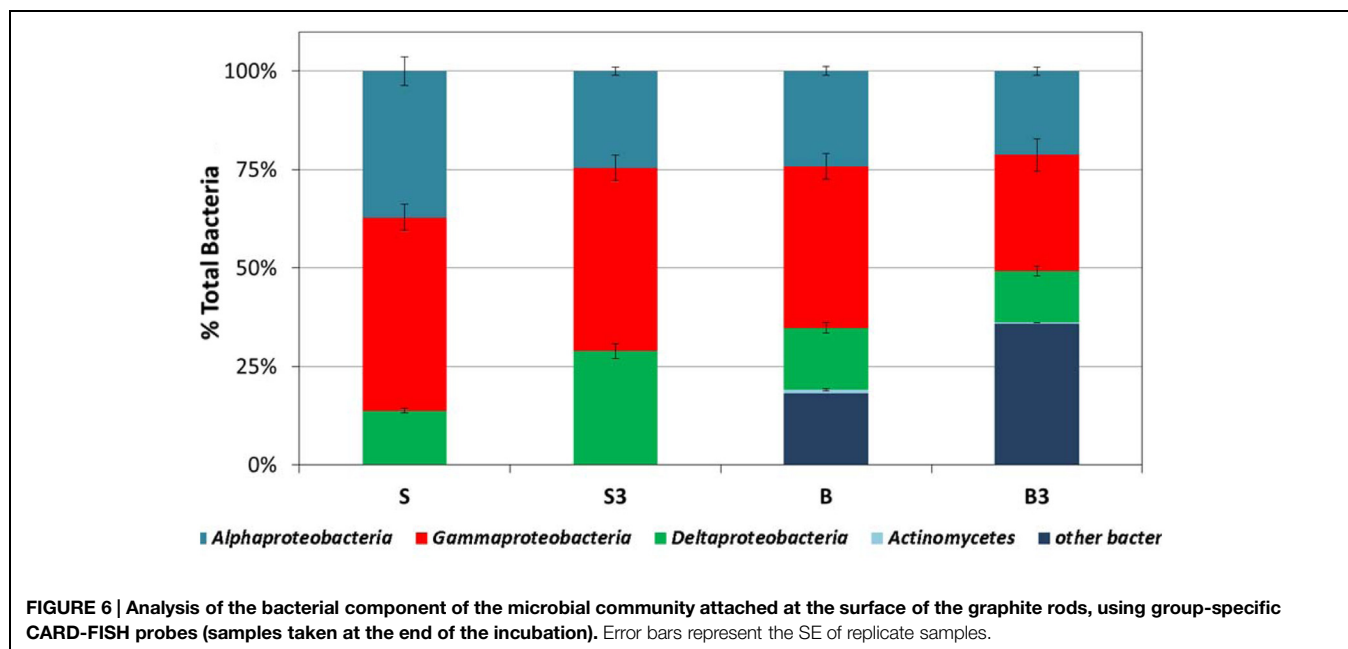
The biofilm growing attached to the surface of the graphite rods (the segment buried within the sediment) also primarily consisted of Bacteria. Overall, the total amount of cells detached from the surface of the graphite rods in treatment "S" and "S3" was over four-times higher ($p < 0.05$, two-tailed *t*-test) than that detached from the graphite rods in the autoclaved treatments "B" and "B3" (e.g., 8.0×10^7 cells from treatment "S" vs. 2.0×10^7 cells from treatment "B").

At the end of the incubation, in all treatments the biofilm primarily consisted of *alphaproteobacteria* (accounting for around 25–35% of total Bacteria), *gammaproteobacteria* (accounting for around 30–50% of total Bacteria) and, although to a minor extent, *deltaproteobacteria* (accounting for around 15–30% of total Bacteria; **Figure 6**). In the autoclaved treatments ("B" and "B3") a significant fraction (up to 35%) of total Bacteria remained unidentified (**Figure 6**). Interestingly, the predominance of *alphaproteobacteria* and *gammaproteobacteria* at the surface of the graphite rods suggests

FIGURE 5 | (A) Amount of total cells and Bacteria in the sediment from the different treatments as measured after 0, 200, and 417 days of incubation. **(B)** Analysis of the bacterial component of the microbial community of the sediment using group-specific Catalyzed Reporter Deposition-Fluorescence *In Situ* Hybridization (CARD-FISH) probes (samples taken at the end of the incubation). Error bars represent the SE of replicate samples.

the existence of an ecological niche for these microorganisms. A wide diversity of chemoautotrophic *alphaproteobacteria* and *gammaproteobacteria* responsible for sulfur oxidation in marine sedimentary environments have been described in the literature (Meyer and Kuever, 2007; Meyer et al., 2007; Yamamoto and Takai, 2011; Lenk et al., 2012), hence raising the intriguing possibility that these microorganisms were responsible for the bioelectrochemical oxidation of sulfur, deriving from the abiotic electrochemical oxidation of sulfide, to sulfate with the graphite electrode serving as electron acceptor.

Notably, the capacity to oxidize sulfur to sulfate with an electrode serving as direct electron acceptor has been documented also in *deltaproteobacteria,* the other bacterial component identified at the surface of the graphite rods, such as *Desulfuromonas* strain TZ1 (Zhang et al., 2014). Furthermore, it should also be noted that the vast majority of Bacteria isolated so far with the capability to link the anaerobic oxidation of organic substrates to electrode reduction, such as *Geobacter, Shewanella, Geoalkalibacter*, also belong to the subclass of *deltaproteobacteria* (Bond and Lovley, 2003; Biffinger et al., 2011; Badalamenti et al., 2013). Hence, it cannot be excluded that their occurrence at

FIGURE 6 | Analysis of the bacterial component of the microbial community attached at the surface of the graphite rods, using group-specific CARD-FISH probes (samples taken at the end of the incubation). Error bars represent the SE of replicate samples.

the surface of the graphite rods can be associated to the direct oxidation of TPH and possibly other organic substrates contained in the sediment, with the electrode serving as direct electron acceptor. In spite of these considerations, the identity of the electrode-associated microbes needs to be further elucidated and efforts are certainly needed to unravel their specific function and electron transfer strategies.

Surface Characterization of the "Snorkels" by XPS

X-ray photoelectron spectroscopy was employed to identify the chemical species present on the surface of the graphite rods retrieved, at the end of the incubation, from the treatments "S" and "B." For comparative purposes, an identical (yet unused) graphite rod was also analyzed. Besides the trace amounts of impurities, mainly consisting of silicon (as SiO_2), oxygen (as OH^-), and chlorine (as Cl^-), photoemission spectra of the untreated graphite rod revealed only the presence of graphitic carbon (**Table 1**). The C 1s spectrum of carbon in the autoclaved treatment "B" was very similar to that of unused graphite, showing the presence of graphitic carbon only.

In contrast, the C 1s spectrum of the graphite rod deriving from the treatment "S" clearly revealed the presence of the second component at 287.7 eV due to the bonds of C = O and/or C-N, most likely attributable to the presence of adherent bacterial cells. Consistently, the nitrogen spectrum revealed the presence of N 1s peak with binding energy of 399.0 eV which is characteristic for C = NH, $C-NH_2$ bonds. Even though microbiological and chemical analyses indicated the presence of bacteria also in the autoclaved treatment "B," they could not be detected by XPS probably due to their much lower abundance compared to the treatment "S." As far as the sulfur spectrum S 2p is concerned, XPS analyses did not reveal the presence of elemental sulfur but only sulfides (about 164 eV) and sulfates (about 169 eV; Gusmano

et al., 2004), particularly after the treatment "S," hence providing an additional line of evidence of the involvement of the "Snorkel" in the redox cycling of sulfur species.

Another interesting result of the XPS analysis is the relatively high abundance (2.1 atomic %) of iron ions Fe^{3+} (710.2 eV; Mari et al., 2009) on the surface of graphite rods deriving from the treatment "S," whereas it was undetectable in the other samples. The presence of iron was also visually confirmed by the fact that when the graphite rod from the treatment "S" was removed from the serum bottle and briefly exposed to the atmospheric oxygen before introducing into XPS apparatus, its surface immediately turned reddish. Interestingly, the reddish color is typical of "electro-active" biofilm harboring high amounts of Fe-bearing *c*-type cytochromes which are key redox protein involved in the electron transfer processes between the microbial cells and the electrodes.

Discussion

This study presented the proof of concept of the "Oil-Spill Snorkel," a novel bioelectrochemical approach to accelerate *in situ* the biodegradation of petroleum hydrocarbons in anoxic marine sediments. Collectively, the results of this study which are based on a comprehensive set of chemical, microbiological, and spectroscopic data have pointed out that the introduction of a conductive graphite rod in the sediment allows creating a bioelectrochemical connection between two spatially separated redox zones (i.e., the anoxic sediment and the overlying oxic water) and, by so doing, affecting a number of microbiological and chemical reactions occurring within the sediment (**Figure 7**). The snorkel accelerated the rate of oxidative reactions taking place within the sediment, as documented by the enhancement of the rate of oxygen uptake and carbon dioxide evolution.

TABLE 1 | Results of X-ray photoelectron spectroscopy (XPS) analysis of untreated graphite rod and snorkels from the treatments "S" and "B."

	Carbon (1s)		Oxygen (1s)	Nitrogen (1s)		Sulfur (2p)		Iron (2p)
Chemical bond	Graphitic	C = O,C-N	Oxides	C = NH C-NH$_2$	NH$_3$ NH$_2$OH	Sulfide	Sulfate	Fe^{3+}
Untreated graphite rod (atomic %)	100.0	–	–	–	–	–	–	–
Snorkel treatment "S" (atomic %)	68.0	7.4	15.5	3.3	2.9	0.2	0.6	2.1
Snorkel treatment "B" (atomic %)	98.3	–	–	–	1.3	0.1	0.3	–
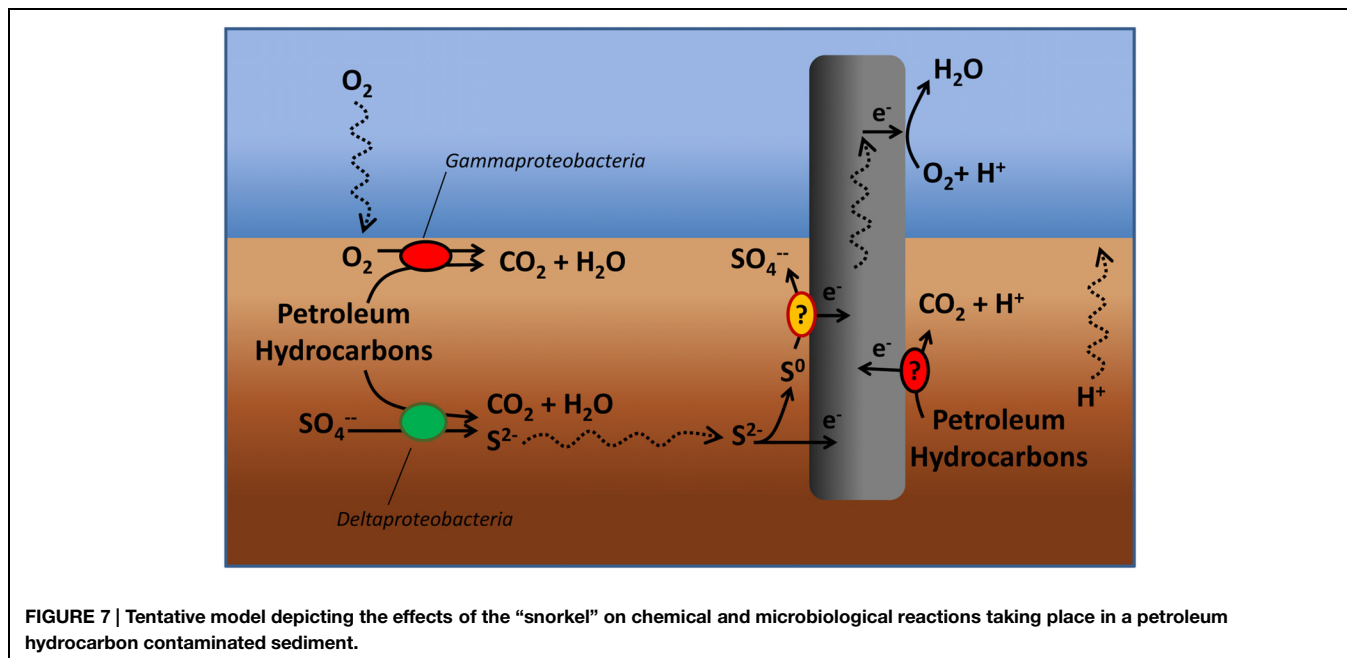
FIGURE 7 | Tentative model depicting the effects of the "snorkel" on chemical and microbiological reactions taking place in a petroleum hydrocarbon contaminated sediment.

Consistently, also the initial rate of petroleum hydrocarbons biodegradation was substantially increased, even though upon extended incubation (over 400 days) the final hydrocarbons removal was similar among treatments. Probably, a greater beneficial effect of the snorkel could be obtained in larger-scale and continuous-flow systems in which the spatial separation between the oxic and anoxic redox zones can be stably maintained over time.

A striking effect of the snorkel was also noticed on sulfate reduction which proceeded at slower rates in treatments containing the electrode(s). A possible explanation for this finding is the preferential use of the "snorkel" over sulfate as respiratory electron acceptor for the oxidation of organic substrates in the sediment. In principle, this hypothesis is consistent with the higher redox potential of oxygen (E°' O$_2$/H$_2$O = +0.82 V), which is the ultimate sink for electrons released to the snorkel, compared to sulfate (E°' SO$_4$$^{2-}$/HS$^-$ = −0.217 V).

On the other hand, another possible explanation is that the "snorkels" facilitate the back-oxidation (to sulfate) of the sulfide generated in the sediment from the activity of sulfate-reducing microorganisms, hence resulting in an apparently lower sulfate reduction. However, under abiotic (purely electrochemical) conditions sulfide is only partially oxidized to elemental sulfur (Rabaey et al., 2006; Dutta et al., 2008; Sun et al., 2009); hence,

the complete conversion of sulfide to sulfate requires the initial abiotic step (from sulfide to elemental sulfur) to be followed by the microbiological oxidation of elemental sulfur to sulfate (Gong et al., 2013). Recently, a number of microorganisms such as *Desulfobulbus propionicus* (Holmes et al., 2004a,b) and *Desulfuromonas* strain TZ1(Zhang et al., 2014) with the capability to oxidize elemental sulfur using a graphite electrode as direct electron acceptor have been described in the literature.

At present, it is unclear whether the effect of the snorkel on hydrocarbons biodegradation was direct (e.g., the graphite electrode served as a direct electron acceptor for hydrocarbons oxidation), indirect (e.g., the electrode somehow stimulated the activity of hydrocarbon-oxidizing sulfate-reducing bacteria) or both. To specifically address this issue, future research efforts will have to focus on the identification of involved biochemical pathways of hydrocarbons activation and biodegradation, through for instance the detection of signature metabolites.

An interesting finding of the study was the formation on the surface of the snorkels of a Fe^{3+}-rich, reddish biofilm dominated (among the others) by *deltaproteobacteria* which could be an indirect indication that the biofilm was capable to engage in extracellular electron transfer processes with the electrode. More specific (bio)electrochemical investigations are, however, needed to confirm this intriguing hypothesis.

From an applicative standpoint, the oil-spill snorkel could potentially represent a groundbreaking *in situ* alternative to more expensive remediation options relying on dredging or on often ineffective practices of oxygen delivery to the sediment. The oil-spill snorkel is indeed a fully passive bioelectrochemical system which, upon installation does not necessitate the input of external energy and requires little to no maintenance, employing corrosion-resistant materials (i.e., carbon based electrodes) suitable for use in marine environments. Also compared to other bioelectrochemical systems previously applied to the treatment of petroleum hydrocarbons in contaminated soil and sediments, the oil-spill snorkel has several potential advantages such as the fact that it does not necessitate the presence of expensive electrode materials and catalysts as well as the use of membranes, thereby suggesting a greater potential for practical application (Morris and Jin, 2012; Lu et al., 2014a,b).

However, a number of factors possibly influencing its long-term operation still need to be evaluated, including the possible formation of non-conductive precipitates (e.g., sulfides) on the surface of the snorkel which may eventually lead to a gradual passivation of the electrode.

Clearly, it is important to mention that the geometry and setup of the electrodes employed in this study may not reflect the optimal configuration for full-scale "real world" applications. Most probably, in order to treat extended surface, a horizontal positioning of the electrodes (rather than the vertical one used in this study) would be preferable. Furthermore, crucial to the scaling up of the technology is also the radius of influence of the snorkel which will require an experimental study at a larger scale to be precisely identified.

Acknowledgments

References

Abdallah, E., Goncalves, A. A., and Gagnon, G. A. (2009). Oxygen release compound as a chemical treatment for nutrient rich estuary sediments and water. *J. Environ. Sci. Health A Tox. Hazard. Subst. Environ. Eng.* 44, 707–713. doi: 10.1080/10934520902847844

Aulenta, F., Ferri, T., Nicastro, D., Majone, M., and Papini, M. P. (2011a). Improved electrical wiring of microbes: anthraquinone-modified electrodes for biosensing of chlorinated hydrocarbons. *N. Biotechnol.* 29, 126–131. doi: 10.1016/j.nbt.2011.04.001

Aulenta, F., Tocca, L., Verdini, R., Reale, P., and Majone, M. (2011b). Dechlorination of trichloroethene in a continuous-flow bioelectrochemical reactor: effect of cathode potential on rate, selectivity, and electron transfer mechanisms. *Environ. Sci. Technol.* 45, 8444–8451. doi: 10.1021/es202262y

Badalamenti, J. P., Krajmalnik-Brown, R., and Torres, C. I. (2013). Generation of high current densities by pure cultures of anode-respiring *Geoalkalibacter* spp. under alkaline and saline conditions in microbial electrochemical cells. *MBio* 4, e00144–13. doi: 10.1128/mBio.00144-13

Bargiela, R., Mapelli, F., Rojo, D., Chouaia, B., Tornés, J., Borin, S., et al. (2015). Bacterial population and biodegradation potential in chronically crude oil-contaminated marine sediments are strongly linked to temperature. *Sci. Rep.* 5, 11651. doi: 10.1038/srep11651

Barra Caracciolo, A., Grenni, P., Cupo, C., and Rossetti, S. (2005). In situ analysis of native microbial communities in complex samples with high particulate loads. *FEMS Microbiol. Lett.* 253, 55–58. doi: 10.1016/j.femsle.2005.09.018

Biffinger, J. C., Fitzgerald, L. A., Ray, R., Little, B. J., Lizewski, S. E., Petersen, E. R., et al. (2011). The utility of Shewanella japonica for microbial fuel cells. *Bioresour. Technol.* 102, 290–297. doi: 10.1016/j.biortech.2010.06.078

Bond, D. R., and Lovley, D. R. (2003). Electricity production by *Geobacter sulfurreducens* attached to electrodes. *Appl. Environ. Microbiol.* 69, 1548–1555. doi: 10.1128/AEM.69.3.1548-1555.2003

Borden, R. C., Goin, R. T., and Kao, C. M. (1997). Control of BTEX migration using a biologically enhanced permeable barrier. *Ground Water Monit. Remediat.* 17, 70–80. doi: 10.1111/j.1745-6592.1997.tb01186.x

Cravo-Laureau, C., and Duran, R. (2014). Marine coastal sediments microbial hydrocarbon degradation processes: contribution of experimental ecology in the omics'era. *Front. Microbiol.* 5:39. doi: 10.3389/fmicb.2014.00039

Dutta, P. K., Rabaey, K., Yuan, Z. G., and Keller, J. (2008). Spontaneous electrochemical removal of aqueous sulfide. *Water Res.* 42, 4965–4975. doi: 10.1016/j.watres.2008.09.007

Erable, B., Etcheverry, L., and Bergel, A. (2011). From microbial fuel cell (MFC) to microbial electrochemical snorkel (MES): maximizing chemical oxygen demand (COD) removal from wastewater. *Biofouling* 27, 319–326. doi: 10.1080/08927014.2011.564615

Fazi, S., Aulenta, F., Majone, M., and Rossetti, S. (2008). Improved quantification of *Dehalococcoides* species by fluorescence in situ hybridization and catalyzed reporter deposition. *Syst. Appl. Microbiol.* 31, 62–67. doi: 10.1016/j.syapm.2007.11.001

Fodelianakis, S., Antoniou, E., Mapelli, F., Magagnini, M., Nikolopoulou, M., Marasco, R., et al. (2015). Allochthonous bioaugmentation in ex situ treatment of crude oil-polluted sediments in the presence of an effective degrading indigenous microbiome. *J. Hazard. Mater.* 287, 78–86. doi: 10.1016/j.jhazmat.2015.01.038

Genovese, M., Crisafi, F., Denaro, R., Cappello, S., Russo, D., Calogero, R., et al. (2014). Effective bioremediation strategy for rapid in situ cleanup of anoxic marine sediments in mesocosm oil spill simulation. *Front. Microbiol.* 5:162. doi: 10.3389/fmicb.2014.00162

Gong, Y. M., Ebrahim, A., Feist, A. M., Embree, M., Zhang, T., Lovley, D., et al. (2013). Sulfide-driven microbial electrosynthesis. *Environ. Sci. Technol.* 47, 568–573. doi: 10.1021/es303837j

Gong, Y. Y., Zhao, X., Cai, Z. Q., O'reilly, S. E., Hao, X. D., and Zhao, D. Y. (2014). A review of oil, dispersed oil and sediment interactions in the aquatic environment: influence on the fate, transport and remediation of oil spills. *Mar. Pollut. Bull.* 79, 16–33. doi: 10.1016/j.marpolbul.2013.12.024

Gusmano, G., Montanari, R., Kaciulis, S., Montesperelli, G., and Denk, R. (2004). "Gold corrosion": red stains on a gold Austrian Ducat. *Appl. Phys. A Mater. Sci. Process.* 79, 205–211. doi: 10.1007/s00339-004-2534-0

Holmes, D. E., Bond, D. R., and Lovley, D. R. (2004a). Electron transfer by *Desulfobulbus propionicus* to Fe(III) and graphite electrodes. *Appl. Environ. Microbiol.* 70, 1234–1237. doi: 10.1128/AEM.70.2.1234-1237.2004

Holmes, D. E., Bond, D. R., O'neill, R. A., Reimers, C. E., Tender, L. R., and Lovley, D. R. (2004b). Microbial communities associated with electrodes harvesting electricity from a variety of aquatic sediments. *Microb. Ecol.* 48, 178–190. doi: 10.1007/s00248-003-0004-4

Kirby, M. F., and Law, R. J. (2008). Oil spill treatment products approval: the UK approach and potential application to the Gulf region. *Mar. Pollut. Bull.* 56, 1243–1247. doi: 10.1016/j.marpolbul.2008.03.002

Lenk, S., Moraru, C., Hahnke, S., Arnds, J., Richter, M., Kube, M., et al. (2012). Roseobacter clade bacteria are abundant in coastal sediments and encode a novel combination of sulfur oxidation genes. *ISME J.* 6, 2178–2187. doi: 10.1038/ismej.2012.66

Li, W. W., and Yu, H. Q. (2015). Stimulating sediment bioremediation with benthic microbial fuel cells. *Biotechnol. Adv.* 33, 1–12. doi: 10.1016/j.biotechadv.2014.12.011

Lovley, D. R. (2011). Live wires: direct extracellular electron exchange for bioenergy and the bioremediation of energy-related contamination. *Energy Environ. Sci.* 4, 4896–4906. doi: 10.1039/c1ee02229f

Lu, L., Huggins, T., Jin, S., Zuo, Y., and Ren, Z. J. (2014a). Microbial metabolism and community structure in response to bioelectrochemically enhanced remediation of petroleum hydrocarbon-contaminated soil. *Environ. Sci. Technol.* 48, 4021–4029. doi: 10.1021/es4057906

Lu, L., Yazdi, H., Jin, S., Zuo, Y., Fallgren, P. H., and Ren, Z. J. (2014b). Enhanced bioremediation of hydrocarbon-contaminated soil using pilot-scale bioelectrochemical systems. *J. Hazard. Mater.* 274, 8–15. doi: 10.1016/j.jhazmat.2014.03.060

Mari, A., Agostinelli, E., Fiorani, D., Flamini, A., Laureti, S., Peddis, D., et al. (2009). Ordered arrays of FePt nanoparticles on unoxidized silicon surface by wet chemistry. *Superlattices Microstruct.* 46, 95–100. doi: 10.1016/j.spmi.2009.02.001

Meyer, B., Imhoff, J. F., and Kuever, J. (2007). Molecular analysis of the distribution and phylogeny of the soxB gene among sulfur-oxidizing bacteria - evolution of the Sox sulfur oxidation enzyme system. *Environ. Microbiol.* 9, 2957–2977. doi: 10.1111/j.1462-2920.2007.01407.x

Meyer, B., and Kuever, J. (2007). Molecular analysis of the diversity of sulfate-reducing and sulfur-oxidizing prokaryotes in the environment, using aprA as functional marker gene. *Appl. Environ. Microbiol.* 73, 7664–7679. doi: 10.1128/AEM.01272-07

Miyatake, T., Macgregor, B. J., and Boschker, H. T. S. (2009). Linking microbial community function to phylogeny of sulfate-reducing Deltaproteobacteria in marine sediments by combining stable isotope probing with magnetic-bead capture hybridization of 16s rrna. *Appl. Environ. Microbiol.* 75, 4927–4935. doi: 10.1128/AEM.00652-09

Morris, J. M., and Jin, S. (2012). Enhanced biodegradation of hydrocarbon-contaminated sediments using microbial fuel cells. *J. Hazard. Mater.* 213, 474–477. doi: 10.1016/j.jhazmat.2012.02.029

Nikolopoulou, M., Eickenbusch, P., Pasadakis, N., Venieri, D., and Kalogerakis, N. (2013). Microcosm evaluation of autochthonous bioaugmentation to combat marine oil spills. *N. Biotechnol.* 30, 734–742. doi: 10.1016/j.nbt.2013.06.005

O'Sullivan, L. A., Roussel, E. G., Weightman, A. J., Webster, G., Hubert, C. R. J., Bell, E., et al. (2015). Survival of *Desulfotomaculum* spores from estuarine sediments after serial autoclaving and high-temperature exposure. *ISME J.* 9, 922–933. doi: 10.1038/ismej.2014.190

Prince, R. C. (2015). Oil spill dispersants: boon or bane? *Environ. Sci. Technol.* 49, 6376–6384. doi: 10.1021/acs.est.5b00961

Rabaey, K., Van De Sompel, K., Maignien, L., Boon, N., Aelterman, P., Clauwaert, P., et al. (2006). Microbial fuel cells for sulfide removal. *Environ. Sci. Technol.* 40, 5218–5224. doi: 10.1021/es060382u

Sherry, A., Gray, N. D., Ditchfield, A. K., Aitken, C. M., Jones, D. M., Roling, W. F. M., et al. (2013). Anaerobic biodegradation of crude oil under sulphate-reducing conditions leads to only modest enrichment of recognized sulphate-reducing taxa. *Int. Biodeterior. Biodegradation* 81, 105–113. doi: 10.1016/j.ibiod.2012.04.009

Singh, A. K., Sherry, A., Gray, N. D., Jones, D. M., Bowler, B. F. J., and Head, I. M. (2014). Kinetic parameters for nutrient enhanced crude oil biodegradation in intertidal marine sediments. *Front. Microbiol.* 5:160. doi: 10.3389/fmicb.2014.00160

Sun, M., Mu, Z. X., Chen, Y. P., Sheng, G. P., Liu, X. W., Chen, Y. Z., et al. (2009). Microbe-assisted sulfide oxidation in the anode of a microbial fuel cell. *Environ. Sci. Technol.* 43, 3372–3377. doi: 10.1021/es802809m

Watson, V. J., Delgado, C. N., and Logan, B. E. (2013). Improvement of activated carbons as oxygen reduction catalysts in neutral solutions by ammonia gas treatment and their performance in microbial fuel cells. *J. Power Sources* 242, 756–761. doi: 10.1016/j.jpowsour.2013.05.135

Yakimov, M. M., La Cono, V., Denaro, R., D'auria, G., Decembrini, F., Timmis, K. N., et al. (2007). Primary producing prokaryotic communities of brine, interface and seawater above the halocline of deep anoxic lake L'Atalante, Eastern Mediterranean Sea. *ISME J.* 1, 743–755.

Yamamoto, M., and Takai, K. (2011). Sulfur metabolisms in epsilon– and gamma-Proteobacteria in deep-sea hydrothermal fields. *Front. Microbiol.* 2:192. doi: 10.3389/fmicb.2011.00192

Zhang, F., Cheng, S. A., Pant, D., Van Bogaert, G., and Logan, B. E. (2009). Power generation using an activated carbon and metal mesh cathode in a microbial fuel cell. *Electrochem. Commun.* 11, 2177–2179. doi: 10.1016/j.elecom.2009.09.024

Zhang, F., Pant, D., and Logan, B. E. (2011). Long-term performance of activated carbon air cathodes with different diffusion layer porosities in microbial fuel cells. *Biosens. Bioelectron.* 30, 49–55. doi: 10.1016/j.bios.2011.08.025

Zhang, T., Bain, T. S., Barlett, M. A., Dar, S. A., Snoeyenbos-West, O. L., Nevin, K. P., et al. (2014). Sulfur oxidation to sulfate coupled with electron transfer to electrodes by *Desulfuromonas* strain TZ1. *Microbiology* 160, 123–129. doi: 10.1099/mic.0.069930-0

Zhang, T., Gannon, S. M., Nevin, K. P., Franks, A. E., and Lovley, D. R. (2010). Stimulating the anaerobic degradation of aromatic hydrocarbons in contaminated sediments by providing an electrode as the electron acceptor. *Environ. Microbiol.* 12, 1011–1020. doi: 10.1111/j.1462-2920.2009.02145.x

Advantages of publishing in Frontiers

OPEN ACCESS

Articles are free to read, for greatest visibility

COLLABORATIVE PEER-REVIEW

Designed to be rigorous – yet also collaborative, fair and constructive

FAST PUBLICATION

Average 85 days from submission to publication (across all journals)

COPYRIGHT TO AUTHORS

No limit to article distribution and re-use

TRANSPARENT

Editors and reviewers acknowledged by name on published articles

SUPPORT

By our Swiss-based editorial team

IMPACT METRICS

Advanced metrics track your article's impact

GLOBAL SPREAD

5'100'000+ monthly article views and downloads

LOOP RESEARCH NETWORK

Our network increases readership for your article

Find us on